METEOR PHENOMENA AND BODIES

ZDENĚK CEPLECHA and JIŘÍ BOROVIČKA
Ondřejov Observatory, Astronomical Insitute, Academy of Sciences, Czech Republic

W. GRAHAM ELFORD
Department of Physics and Mathematical Physics, University of Adelaide, Australia

DOUGLAS O. REVELLE
Los Alamos National Laboratories, U.S.A.

ROBERT L. HAWKES
Department of Physics, Engineering, and Geology, Mount Allison University, Sackville, Canada

VLADIMÍR PORUBČAN
Astronomical Institute, Slovak Academy of Sciences, Slovakia

MILOŠ ŠIMEK
Ondřejov Observatory, Astronomical Insitute, Academy of Sciences, Czech Republic

(Received 31 January, 1998)

Abstract. Meteoroids can be observed at collision with the Earth's atmosphere as meteors. Different methods of observing meteors are presented: besides the traditional counts of individual events, exact methods yield also data on the geometry of the atmospheric trajectory; on the dynamics and ablation of the body in the atmosphere; on radiation; on the spectral distribution of radiation; on ionization; on accompanying sounds; and also data on orbits. Theoretical models of meteoroid interaction with the atmosphere are given and applied to observational data. Attention is paid to radar observations; to spectroscopic observations; to experiments with artificial meteors and to different types of meteor sounds. The proposed composition and structure of meteoroids as well as their orbits link them to meteorites, asteroids and comets. Meteor streams can be observed as meteor showers and storms. The rate of influx of meteoroids of different sizes onto Earth is presented and potential hazards discussed.

1. Introduction

Solid particles of the solar system that are large enough produce light during their collisions with the Earth's atmosphere. The phenomenon is traditionally termed a *meteor*. This word is also sometimes used for the particle. Folowing the IAU (International Astronomical Union) nomenclature, we will rather call the particle *meteoroid*. The smallest meteoroid size able to produce meteors depends on their velocities; 0.01 mm can be taken as a rough limit. (Size $\equiv$ bulk dimension, i.e., in analogy to 'diameter of a sphere'.) Toward large sizes, there is no cut-off: we may also call an impacting interplanetary body of km-size a meteoroid. However, the upper sizes of interplanetary bodies in this review will be limited to the largest

Space Science Reviews **84:** 327–471, 1998.

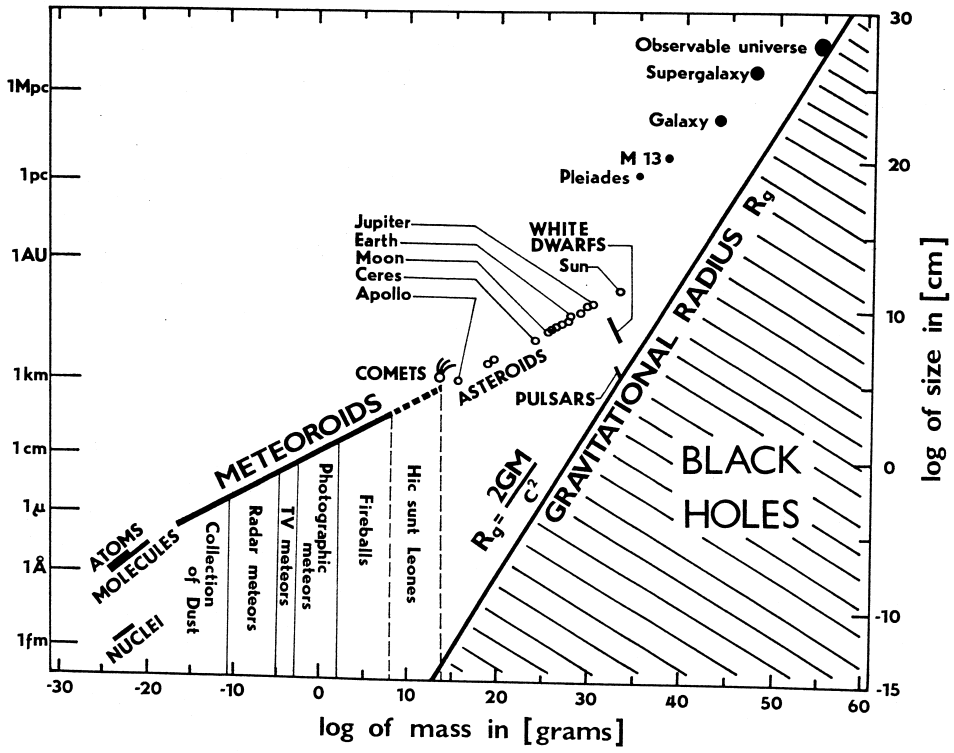

Figure 1. Diagram of size versus mass contains some known objects of the observable universe and shows the significance of the meteoroid complex. Meteoroids with sizes of tens and hundreds of meters are the least known bodies of the solar system.

meteoroids recorded by scientific instruments as meteors during their interaction with the atmosphere, which are about 10-m-size bodies.

Meteoroids will be viewed in different sections from different viewpoints: observational, theoretical, in the atmosphere, in interplanetary space as individual bodies and also as meteor streams producing showers. The importance of the entire meteoroid complex can be demonstrated by their multitude, by the wide range of their sizes, and also by the large diversity in their composition and structure (Figure 1).

Part of the meteoroid population is clearly linked to comets as *shower* meteors derived from cometary meteoroid *streams*. Another part is linked to asteroids, and we can study some of these bodies in our laboratories as *meteorites*. Some meteoroids may be left directly from the process of formation of larger planetary bodies or as the disintegration of a large presumably cometary body coming occasionally (intervals of few hundred thousand years or so) into the inner solar system from the Oort cloud.

1.1. METEOROIDS

Majority of our knowledge on meteoroids comes from an extremely short interval of their atmospheric penetration. Our knowledge is biased by the condition that the meteoroid orbit must intersect the Earth's orbit. Our atmosphere is actually a large sensor recording the meteoroid impacts upon the Earth. The penetration through the atmosphere may then give rise, for certain sizes and velocities, to a luminous phenomenon known as a *meteor*, or if brighter, as a *meteoric fireball*, eventually called also a *bolide* (originally used only for detonating fireballs). Figure 2 contains a survey of the basic terminology used for meteoroids interacting with the Earth.

We should bear in mind that the encounter of a meteoroid particle with the Earth is actually a collision. Except for extremely low velocities, only a minor part is due to gravity. Velocities of solar-system meteoroids at their encounter with the Earth's atmosphere are within the following limits: the lower one 11.2 km s^{-1} (only gravity of the Earth), the upper one 72.8 km s^{-1} (42.5 parabolic at Earth's perihelion plus 30.3 km s^{-1} the velocity of the Earth at perihelion). The direction where the meteoroid comes from is traditionally called the *radiant*, a term originating from the observation of near parallel trails of meteoroids belonging to one *stream*: the apperent trails of meteors then belong to the same meteor *shower* and are seemingly *radiating* from one point on the sky, from the *radiant* of the shower and stream. Meteors not belonging to any specific shower (meteoroid stream) are called *sporadic meteors*.

The ability to penetrate into the atmosphere depends strongly on the meteoroid velocity. Especially the mass loss due to severe *ablation* causes a practical upper velocity limit of about 30 km s^{-1} for the occurence of a meteorite fall (the terminal mass varies as about v_∞^{-6}, where v_∞ is the initial velocity before entering the atmosphere). Thus, at higher velocities only a huge body can produce some small fragments on the Earth's surface. The term *ablation* has the meaning of mass loss of a meteoroid in any form and phase: solid as fragments, fluid as droplets and loss of hot gas, which forms always the final stage and is responsible for the observed meteor phenomenon.

1.2. THE METEOR PHENOMENON

The penetration of a meteoroid into the Earth's atmosphere at hypersonic velocity gives rise to 4 different phenomena, depending mostly on mass and partly on velocity. All the quantitative data are presented here for a velocity of 15 km s^{-1}, for a meteoroid of bulk density of 3500 kg m^{-3} (meteoric stones: ordinary chondrites) and for a vertical flight, i.e., for a radiant in zenith.

In all four types of interaction, ions and free electrons are produced during the atmospheric flight, an ionized column is formed, and forwarding with the meteoroid velocity. This yields a possibility to observe meteor phenomena by radar echoing. Especially meteors, meteoric dust particles, and the border sizes between these two regimes are the domain of the radar observations (see Section 2.4).

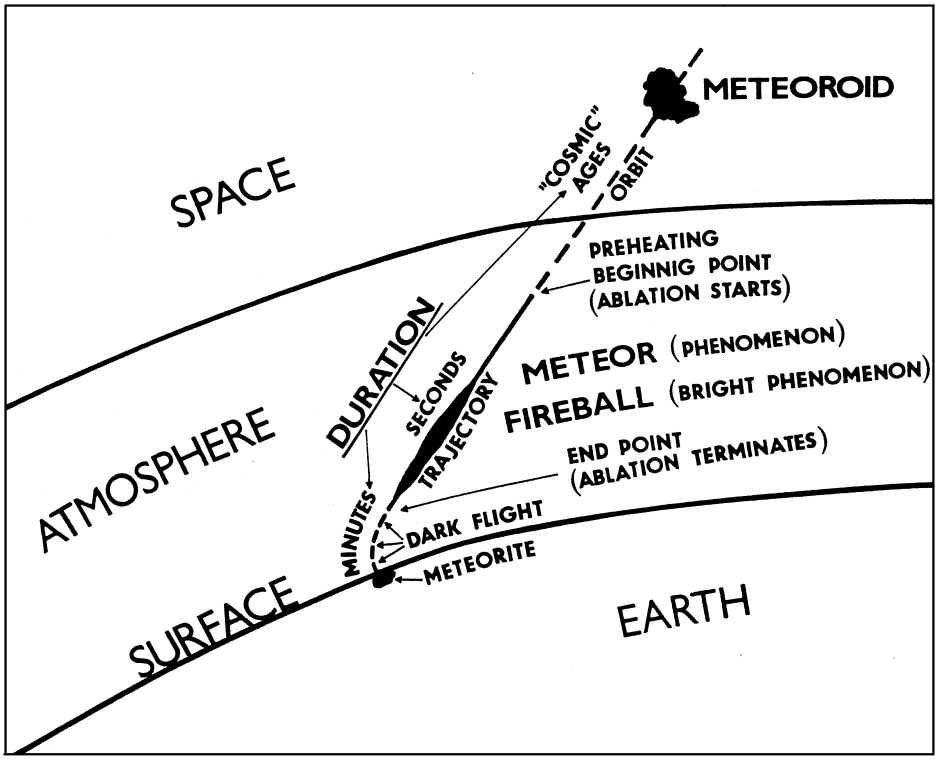

Figure 2. Basic terminology for meteors.

1.2.1. *Meteors*

'Typical' meteors seen by naked eye, recorded by a television camera or by a telescope, are caused by meteoroids larger than about 0.01 mm. The exact size limit depends on velocity. A zero magnitude meteor is caused by the body of 2-cm size at a velocity of 15 km s^{-1}, of 1-cm size at 30 km s^{-1} and of 0.5-cm size at 60 km s^{-1}. 'Typical' meteors are associated with meteoroid sizes between 0.05 mm and 20 cm. Entering the denser parts of the atmosphere they are heated up very quickly. If the sizes are between 0.05 mm and 0.5 mm, the body is heated throughout; in the case of a meteoroid larger than 0.5 mm, only a surface layer down to a few tenths of a millimeter is heated. When the surface temperature reaches about 2200 K – this usually occurs somewhere between heights of 80 and 90 km – the meteoroid material starts to sublimate from the surface and fills the surroundings of the body by its hot vapors. Excited states of atoms of these vapors are gradually de-excited by radiation. Meteor light consists mostly of radiation of discrete emission spectral lines belonging for the most part to metals and mainly to iron. More than 90% of the meteor light originates from radiation of single low-excited atoms of meteoroid material (several eV; temperatures 3000 to 5000 K). During this ablation part of the trajectory, the meteoroid is increasingly slowing down. After traveling a distance

of several kilometers up to few tens of kilometers, *the meteor terminates its light, because it has lost all of its mass*, though not radically changed its velocity (the velocity changes several percent to a few tens of percent).

1.2.2. *Fireballs, Bolides, Meteorite Falls*

This type of meteoroid interaction with the atmosphere happens, when the size of the body is larger than about 20 cm (for 15 km s^{-1}, etc., as mentioned above). In this case there is not enough time to ablate the entire meteoroid mass, before the body slows down to a critical limit of about 3 km s^{-1}. At such a small velocity there is not enough energy transported to the surface of the meteoroid for keeping the surface temperature above 2200 K. However, there is still a significant remnant flying with continuously lower velocity. The meteoroid starts to be cooled on its surface. The thin melted layer on the meteoroid surface solidifies and forms a *crust* that is typical for *meteorites*. The term meteorite should be exclusively used only for meteoric bodies recovered on the Earth's surface. In this case, *meteor*, or better to say *meteoric fireball* (it is a fireball of -8 mag or brighter), *terminates its light due to small velocity of the meteoroid remnant*. The remnant mass (10 g or more in this example) falls down to the Earth's surface in a *dark-flight* and its velocity approaches gradually the free fall velocity in a resisting medium. This free fall velocity is a velocity limit, which is being approached by slowing down from higher velocities. The dark-flight lasts typically several minutes in contrast to the fireball luminous trajectory, which lasts for several seconds.

1.2.3. *Explosive Impacts*

The third type of meteoroid interaction with the atmosphere is a very rare phenomenon due to the small probability of Earth's encounter with a very large body. If the body is larger than several meters and sufficiently strong, the deceleration is small and *the body hits the Earth's surface before it is slowed down below hypersonic velocity*. Such a big mass is not much evaporated and decelerated during the atmospheric penetration, and hits the Earth's surface with a velocity of few kilometers per second, at least. In this case the meteoroid vapors emit light down to the very contact with the Earth's surface, where an explosive crater forms.

1.2.4. *Meteoric Dust Particles*

The fourth type of encounter cannot be observed as a luminous phenomenon. If the size of *the meteoroid* is less than several hundredths of a millimeter, *it is slowed down* to less than a few kilometers per second *very high in an extremely rare atmosphere before its temperature can rise to the evaporation point*. Meteoroid with 15 km s^{-1} reaches the maximum temperature higher than 90 km and the temperature then decreases. Thus the evaporation regime is not reached at all and the hot vapors are not present, i.e., there is no meteor phenomenon. Such a meteoroid dust particle sediments slowly and unchanged through the atmosphere to reach the Earth's surface.

1.3. METEOROID INTERACTION WITH THE ATMOSPHERE

Let us now discuss a meteorite fall in more details (it is the most complete case of a meteoroid interaction with the atmosphere). We distinguish then the following 5 regimes of meteoroid motion including the orbital motion. The 4 regimes of the atmospheric motion are: preheating, ablation, dark-flight and impact. Ionization is an important phenomenon of the preheating and of the ablation part of the trajectory. Even if certainly present, it has not been observed yet for a dark flight.

Table I summarizes all possible meteoroid interactions with the atmosphere and the regimes of the meteoroid atmospheric trajectory to which they correspond.

1.3.1. *Orbital Motion*

Orbital motion of a meteoroid is dominated by the gravity of our Sun perturbed by close approaches to bigger bodies. The meteoroid is affected by collisions, irradiation from cosmic rays and other forces. It is usually a long time since separation from a parent body. For several meteor streams we are reasonably sure of the individual parent comet. For sporadic meteoroids we handle the problem of parental bodies only statistical way so far, i.e., we associate populations of meteoroids with systems of bodies.

1.3.2. *Preheating*

Preheating is caused by the impacting molecules of the individual constituents of the air gas, when the body approaches the Earth at heights of 300 to 100 km (depending on energy of encounter that in turn depends on v^3). The surface temperature of the meteoroid rises quite rapidly (by the same rate as the ambient air density, i.e., proportionally to e^t). There is no time for bodies of even millimeter dimensions to be heated throughout. The inside of most meteoroids (except very small grains) remains practically unheated. The preheating is a very quick phenomenon lasting only seconds or tens of seconds. For bodies larger than 1 mm the process is governed by heat conductivity, while radiation transfer becomes very important for smaller bodies. When the surface tension (tangential compression) reaches the strength of the material, spallation starts; this coincides with heating to about 900 K for a homogeneous solid stone of centimeter and larger sizes. The internal compression is important for smaller bodies and surface temperatures as low as 500 K can disrupt a homogeneous body (through the temperature gradient inside the meteoroid).

1.3.3. *Ablation*

Ablation is the next stage of atmospheric penetration of the meteoroid. It starts as fragmentation (or spallation) at the lower temperatures. After melting the final stage of ablation is the evaporation from the body and from its fragments. Temperatures are then close to 2500 K when evaporation starts. After reaching this temperature, further increase is then small because most of the kinetic energy is spent in

the ablation (including fragmentation) process itself. We know that the evaporation is the final stage of majority of the ablated material, because we observe the meteor spectra as atomic line emissions of hot metalic gases. The fragmentation process has not been well understood until recently and mostly *single body theory* has been used. Only large values of ablation coefficients as derived from observations speak for continuous fragmentation as the main ablation process. Recently modifications of the single-body theory due to gross-fragmentation process at discrete trajectory points was successfully applied to observations. Once ablation starts, it is a severe process and consumes the majority of the kinetic energy. Deceleration can compete with the ablation in consuming kinetic energy only for larger bodies (the meteorite dropping) and when they move lower down in the atmosphere. If 3 km s^{-1} is reached somewhere high above the surface and there still remains a significant mass, this mass continues to move without emitting light in a dark flight: there are not enough hot gases round the body any more to emit visible light.

1.3.4. *Dark Flight*

Ablation ceases during this part of trajectory. There is not enough kinetic energy to either evaporate, or to provide heating. The process is now just the opposite: it is a quick cooling (exponential with time). The solidification of the crust takes place. The crust is thin because the melted layer is also thin. Without wind and being decelerated to several hundreds of m s^{-1} very soon, the body motion changes to vertical trajectory quite quickly and a free fall follows with velocity decreasing proportionally to square root of the air density. If the air density were constant, the velocity would be soon also constant. The impact velocities on the Earth' surface are of the order of several 10 m s^{-1} for smaller meteorites and several 100 m s^{-1} for larger meteorites. Different wind directions and speeds at different heights perturb the trajectory and complicate the situation, but knowing the wind field, the dark flight trajectory can be computed by numerical integration of the equations of motion and the impact point predicted with about 1 km precision for 1 kg meteorite. This statement is based on experience with 3 photographic meteorite falls. The biggest unknown in this problem always remains; the shape of the body, and thus also the unknown aerodynamic lift.

1.3.5. *Impact*

Impact velocities are 10 to 100 m s^{-1} for 10 g to 10 kg terminal masses, respectively. The impact forms a small pit on the surface, which is somewhat larger than the size of the body itself. Even for a meteorite of several hundreds of kilograms, the shape of such a pit *does not convey* any information on the initial motion of a meteoroid before entering the atmosphere, but shows overwhelming direction of winds during the last few kilometers of the dark-flight (which is just the free fall in the wind field). The depth of a meteorite pit is about the size of the body on an average soft surface (dry soil of a farmed field). If ablation continues to the Earth's

TABLE I
Survey of meteor phenomena and flight regimes

	Preheating	Ablation	Dark-flight	Impact
Dust	yes	no	no	no
Meteor	yes	yes	no	no
Meteorite-dropping fireball	yes	yes	yes	yes
Crater-forming event	yes	yes	no	yes

surface, a much bigger impact crater is formed due to sudden explosive release of the enormous kinetic energy.

1.4. Some more phenomena connected with meteors

1.4.1. *Meteor Flares*

The meteor flare is a sudden increase in meteor brightness usually by more than one magnitude. It is typical for high velocity meteors. A flare at the terminal point may be due to a real explosion and a terminal disintegration into many small fragments. Two usual reasons for flares are:

- sudden fragmentation (gross or discrete fragmentation in contrast to continuous fragmentation),
- sudden change in physical circumstances giving rise to more evaporation, excitation and ionization.

1.4.2. *Meteor Wakes*

Meteor wake is a special term for radiation which is emitted just behind the meteoroid, whereas the radiation surrounding the body is sometimes called *head radiation*. Typical dimensions of the wake are several hundred meters to several kilometers behind the body and a typical duration is of the order of several tenths of seconds. There are two types of wakes depending on the origin of the radiation: (a) gaseous, (b) particulate. Spectral records of wakes show lines of the same elements as in the head radiation, but the excitation energy is significantly lower.

1.4.3. *Meteor Trains*

The meteor train is a radiation emitted behind the body for seconds or more. A substantial part of train radiation comes from forbidden lines of neutral and ionized oxygen. Some shower meteors exhibit an excess of meteors with trains, as compared with the sporadic meteors, e.g., Perseids. Occasionally such trains may last for hours.

2. Observational Methods

Different observational methods are capable of getting various data on meteoroids and their interactions with the atmosphere, e.g., ionization at different points of the trajectory can be obtained from radar and spectral observations, etc. As an ideal we would like to have a 'complete' set of data on an individual meteor, i.e., geometrical data (position of the trajectory in the atmosphere), dynamical data (height and distance along the trajectory as function of time; velocity; deceleration; 'dynamical' mass), photometric data (integrated light intensity in the complete pass-band as function of time, 'photometric' mass), spectral data (intensity radiated in individual spectral lines and molecular bands as function of time), ionizational data (density of ions and free electrons as function of time), and orbital data (elements of the Keplerian orbit at encounter with Earth). If a meteorite fall was to be recovered after such a complete recording, we would have an ideal case for testing our theories. This has never been achieved, but combining observational methods as they are individually described in the following sections, may eventually serve us with all these important data on meteoroid interaction with the atmosphere.

Besides complete studies of an individual meteoroid during its interaction with the atmosphere, meteors can also be studied in a statistical way. Visual observation with a simple counting of meteors seen per hour may serve as an example of a method, which can be used only statistical way.

2.1. PHOTOGRAPHIC OBSERVATIONS

Meteor photography has been used since November 1885, when L. Weinek took the first known photograph of a meteor in Prague. During the first 50 years, the photographic meteor programs gave rather scanty results. The major breakthrough occured in 1936, when the Harvard patrol cameras were equipped with rotating shutters for making time marks (Whipple, 1938, 1954); this program was terminated 1951. 'Classical' photographic cameras used for photographing meteors are usually called small cameras to distinguish them from Super-Schmidt cameras capable of recording meteors as faint as +3rd stellar magnitude. Small cameras can reach to 0 mag. These cameras are equipped with rotating shutters breaking the image and thus making time marks, which can be used for determining velocities.

The second largest program of double-station meteor photography started at the Ondřejov Observatory in Czechoslovakia in 1951 using 30 cameras of 180 mm focal length with panchromatic photographic plates (Ceplecha, 1957); this program was in operation until 1977. After the first 8 years of this program with 2500 hours of operation, a very bright fireball of −19 maximum absolute magnitude was photographed on April 7, 1959. Four meteorites were found near Příbram in western parts of the Czechlands in an area predicted from the double-station photographic records of the fireball (Ceplecha, 1961a). This was the first ever photographed bolide with associated meteorite fall, and it initiated systematic observational pro-

grams for photographing such rare events like fireballs are, and eventually also for photographing more meteorite-dropping fireballs. Photographic fireball networks started: they are systems covering relatively large regions of the Earth's surface by many stations equipped with photographic cameras.

Practically at the same time, in the fall of 1963, the first stations of two networks were put into operation, in Czechoslovakia and in the USA. The Czechoslovak network (Ceplecha and Rajchl, 1965) after the addition of more stations in other European countries became the European Fireball Network (EN): it is still in operation with 50 stations spaced by about 100 km, one all-sky camera (fish-eye lens) at each station, and covering about a million km^2 (Spurný, 1997). The US project is known as Prairie Network (PN), with 16 stations spaced about by 250 km, 4 cameras with 90° field of view, and covering also about a million km^2. The second meteorite dropping fireball was photographed within the Prairie Network in 1970 (McCrosky et al., 1971) and the Network was closed in 1973. Another fireball network in Canada (known as MORP) was in operation from 1971 to 1985 obtaining data on one meteorite fall, Innisfree in 1977 (Halliday et al., 1981). More details on the fireball networks and references to original papers can be found in Ceplecha (1986).

Fainter meteors were systematically photographed from 1952 to 1954 using Super-Schmidt cameras (Jacchia and Whipple, 1961; McCrosky and Posen, 1961). Trajectory and orbital data on more than 2000 faint meteors are available from this project. These remain the most important data set on meteors from many aspects. The precision for the 413 meteors published by Jacchia and Whipple (1961) is exellent. One disadvantage of the system was the use of blue sensitive films, since most of the faint meteor radiation takes place in the red part of the spectrum (Ceplecha, 1959).

An unusual system for photographing meteors was applied in Dushanbe, Tajik Republic (and at several more places in the previous USSR) (Babadzhanov and Getman, 1980). It consisted of cameras with a rotating shutter having a very narrow slit located close to the focal plane, which made the exposure of the meteor trail very short, almost 'instantaneous', while the usually used systems smear the image of a meteor and superpose wake radiation on the head (leading) radiation.

In recent years several programs of meteor photography operated by serious amateur astronomers have become increasingly active, especially in Europe and Japan, and their results are regularly published (WGN, the Journal of the IMO; Radiant, the Journal of the Dutch Meteor Society; Memoirs of the Nippon Meteor Society, Japan).

Examples of mathematical procedures used in reducing photographic observations of meteors can be found in Ceplecha (1987a,b). If older procedures described, e.g., in Whipple and Jacchia (1957) are used, one should be aware of non-adequate values of some constants, namely those, which depend on the kilometer content of 1 AU and on the Earth's mass. These values were very much improved since the year 1957. Also the quite artificial definition of initial velocity should be taken

into account, when correcting an observed velocity in order to compute the orbit (Ceplecha, 1987a).

Most of our detailed knowledge of meteor radiation, motion, and ablation in the atmosphere originates from meteor photographs. Because of random time and position of a meteor phenomenon, cameras with wide field of view have to be used, yet requiring enough precision over this field. Because of extremely short exposure time (≈ 0.0001 s) of a fast-moving meteor-image in this large field of view, existing CCD technology cannot be used.

2.2. TELEVISION AND VIDEO OBSERVATIONS

Now serious amateur meteor astronomers and professional groups are employing low light level television (LLLTV) methods for the study of meteors. Reviews of television as a technique for the study of meteors have been written by Hawkes and Jones (1986) and Hawkes (1993). In terms of sensitivity, typical LLLTV systems are intermediate between photographic and sensitive radio techniques, with limiting apparent magnitudes down to about $+9$. They are also intermediate in accuracy (on individual meteor trajectories), being less accurate than photographic and more accurate than radio methods. Hawkes et al. (1993) have shown that typical two station television meteor systems result in errors of the order of 0.4 deg in radiant, 0.3 km in heights, and 2 km s^{-1} in velocities. These optical techniques are less prone to potential biases inherent in radio methods (such as the bias against high meteors because of the rapid diffusion of the ionization trail). However, this is not to say that the methods are without bias. The small fields of view (typical television systems employ lenses resulting in about 15 deg fields of view) result in many partial trails, and the poor signal to noise (for faint meteors) hampers precise studies of the light curves. Even with advanced video frame grabbing and digital image processing software, LLLTV analysis procedures are still somewhat time consumming, and observations are restricted to dark, clear nights. As a consequence most LLLTV studies have been restricted to a relatively small number of meteors. At the moment, it is important for those using LLLTV data to realize that only a small fraction of the year is represented in currently published summaries, and some of the major showers are not represented at all.

Meteor showers which have been studied using television techniques include the Perseids (Hapgood et al., 1982; Hawkes and Fleming, 1995), the Geminids (de Lignie et al., 1993; Ueda and Fujiwara, 1993) and the eta Aquarids (Suzuki et al., 1993). The three largest published samplings of multistation largely sporadic meteors are those of Hawkes et al. (1984), Sarma and Jones (1985), and Ueda and Fujiwara (1995). There is some indication that meteor shower radiants are more diffuse at these fainter magnitudes, although it is not clear whether this is a real effect (due to greater ejection velocities from the parent comet) or are simply the consequence of larger measurement errors.

Much of the emphasis in the past number of years has been centred upon using television techniques to determine the physical and chemical makeup of meteoroids which produce faint optical meteors. Recent published contributions in the area of television meteor spectra include a detailed study of three faint meteors (Mukhamednazarov and Mal'tseva, 1989), the results suggesting a very similar chemical composition for all three. Two observational searches for wake in faint television meteors (Robertson and Hawkes, 1992; Shadbolt and Hawkes, 1995) have yielded the surprising result that very few LLLTV meteors exhibit wake within the spatial and sensitivity limits of the equipment. It is not clear whether this is because of a single body structure for most meteoroids in this size range, or whether it is due to a remarkable consistency in constituent grain size in fragmented meteoroid clusters. Piers and Hawkes (1993) directly observed one clustered dust-ball meteor using television techniques. Methods for video photometry have been developed and applied to an analysis of light curves of faint, double station, sporadic meteors (Fleming et al., 1993). The light curves were on average symmetric about the point of maximum luminosity.

While there have, over the past several decades, been occasional simultaneous television-radar and television-visual meteor observations, LLLTV has not been as effectively employed as possible for calibration of different meteor observing methods as possible. Although recent excellent work has used LLLTV to estimate the errors in telescopic meteor observations (Pravec, 1992; Pravec and Boček, 1992).

While it is usual to consider the faint television meteors, with increasing availability of camcorders there will be serendipity observation of bright fireballs using television techniques. The most spectacular video meteor records are, without a doubt, the 15 videotapes obtained from various locations in the eastern United States of the fireball associated with the Peekskill meteorite fall (October 9, 1992). These are the first ever motion picture recordings of a fireball with an associated meteorite fall. There is a wealth of dynamic detail with a complex and rapidly changing fragmentation (Brown et al., 1994). The meteoroid of 1 to 2 m size flew in an extremely shallow trajectory (the would-be perigee at a height of 22 km), with a tremendous fragmentation (at least 70 fragments separated by more than 20 km) starting at a height of 42 km under dynamic pressure of 0.7 MPa. The dark flight of a presumably largest remnant started at 30 km height and a meteorite of 12.4 kg landed on a parked car in Peekskill, NY, USA (Graf et al., 1994).

2.3. SPECTRAL OBSERVATIONS

The history of meteor spectral observations has been described by Millman and McKinley (1963) and Millman (1980). In the second half of the nineteenth century, meteor spectra were observed visually by A. S. Herschel, J. Browning, N. von Konkoly, and others, using binocular prism spectroscopes. It was found that the most prominent features in meteor spectra are emission lines. The two common-

est and brightest lines were positively identified with the yellow neutral sodium doublet and the green neutral magnesium triplet.

The first photograph of a meteor spectrum was taken by chance on a Harvard objective prism plate in 1897. The first successful program of meteor spectroscopy was organized by S. Blajko in Moscow in 1904. However, the next program was started only in 1931 by P. M. Millman in Canada. By 1940 a total of 60 meteor spectra had been recorded photographically. Starting from 1950, good replica transmission gratings became available and largely replaced prisms in meteor spectrographs. Extensive spectroscopic programs were carried on in Canada, USA, former USSR, and former Czechoslovakia. The use of special emulsions and optics enabled the extention of the spectral window to 3100–9000 Å. Fireball spectra with dispersion better than 50 Å mm^{-1} were obtained. Special programs were also devoted for recording spectra of fainter meteors. By 1970, the world list of photographic meteor spectra contained about 1500 different meteors. However, during the seventies, the programs in Canada and the USA were closed.

Television techniques have also been used for meteor spectroscopy starting in 1969, making it possible to record meteors down to a magnitude of +4. The high frame-frequency enables one to study the time and spatial evolution of the spectra without confusion. Originally, it was necessary to film the TV monitor with a motion picture camera to analyse the spectra. Later it became possible to transform the video image to a hard copy. Now, the video record can be digitized and analyzed by a computer system. Though, the spectral resolution of the TV systems is much lower than in photographic spectra.

Classical meteor spectrographs were described, e.g., by Halliday (1958), and by Ceplecha and Rajchl (1963). The spectra of faint meteors were photographed by the system described in Harvey (1973b). Babadzhanov and Getman (1980) used the method of instantaneous photographs. Different TV techniques and the TV data reduction methods are presented in Hemenway et al. (1971), Millman and Clifton (1975, 1979), Mukhamednazarov and Maltseva (1989), and Borovička and Boček (1996). Spectra of two fireballs were recorded fortuitously by electronic spectrographs mounted on large telescopes (Stauffer and Spinard, 1978; Borovička and Zamorano, 1995). A small segment of fireball spectrum was obtained with an imaging spectrometer by Meisel et al. (1995).

The analysis of a meteor spectrum consists of three steps: the determination of a wavelength scale and line identification, the absolute calibration of intensities, and the physical interpretation of the spectrum. The method of wavelength determination from a grating spectrogram without any additional assumptions was developed by Ceplecha (1961b). In most cases, however, the identification of some lines is immediately apparent and interpolation or regression is sufficient for the computation of other wavelengths. In the case of a prism spectrogram, the Hartmann formula, $\lambda = \lambda_0 + C/(d_0 - d)$, is to be used. Here λ is the wavelength, d is the measured coordinate and λ_0, C, d_0 are constants to be determined. The photometric calibration includes the construction of the characteristic curve (for

photographic observation), the reduction for sensitivity versus wavelength and the conversion of relative sensitivities to absolute fluxes. The full calibration of meteor spectra is given e.g., in Ceplecha and Rajchl (1963), Ceplecha (1971), Cook et al. (1971), Nagasawa (1978), and Borovička (1993).

As meteor spectrographs are slitless, the individual emission lines represent a monochromatic image of the meteor. The profiles of spectral lines cannot be therefore studied. In most cases, however, the resolution is insufficient to resolve even the meteor image and only the total line intensity has a physical meaning. The spatial resolution in the direction of meteor flight is degraded by the superposition of different parts in course of the meteor motion. The separation of the head and the wake is possible to some extent at the beginnings and the ends of shutter breaks, on instantaneous photographs and on TV frames.

2.4. RADAR OBSERVATIONS

The existence of a meteor ionized trail was recognized by Skellett (1931, 1935) and his collaborators at the Bell Telephone Laboratories, and by Schafer and Goodall (1932) who used a pulsed ionospheric transmitter operating in the wavelength range of 47 m$< \lambda <$ 190 m during the activity period of the Leonid 1931 meteor shower. Early applications of radio methods in meteor science were described among others, by Hey and Stewart (1947), Lovell (1954), McKinley (1961), and by Millman and McKinley (1963). Technological progress led to the introduction of the defence radar during World War II. Their operating wavelengths around $\lambda = 10$ m made them a powerful tool for the investigation of meteor phenomena. Several wartime radars were adapted for meteor investigations and operated in the USA, Great Britain and Canada during 1946–1947.

Rapid development of meteor radio-astronomy started at Jodrell Bank near Manchester under the leadership of Sir A. C. B. Lovell. Radar observations are not limited by weather conditions (except thunderstorms) and by sunlit hours. This enabled detection of day-time meteor showers. The sensitivity of the radar depending on transmitted pulse power and antenna parameters allowed detection of meteors bellow the visual limit. Therefore, the number of recorded meteors increased enormously.

A new phenomenon, a head-echo was first recognized and used in England by Hey et al. (1947) for determining the meteoroid velocity during the Giacobinids of 1946. The nature of head-echoes is not yet fully explained: it is characterized by faint radio signals reflected from targets close to some of the meteoroids in their atmospheric flight. McKinley and Millman (1949) in Canada used three-station observations of head echoes for the determination of the meteor orbits. Application of head echoes for velocity and orbital calculations suffered by extremely low head echo rates and by the low precision.

Suggestions by Herlofson (1948) for use of Fresnel diffraction patterns formed during the passage of a meteoroid through a radar beam stimulated C. D. Ellyett

and J. G. Davies (1948) to introduce a new method of meteor velocity determination. Manning (1948) proposed a method of three closely separated stations for determining of orbital elements of individual meteors. The method was refined by J. G. Davies and successfully used by Gill and Davies (1956). Unmodulated continuous wave systems were also used for tracking meteor trails (Manning et al., 1949).

Not only radar (back-scatter) systems, which transmit the rf-signals toward the meteor ionized trail, but also a forward-scatter method in which the receiver detects electromagnetic energy reflected from a distant transmitter yields information on meteoric ionization. This principle was successfully applied in the JANET system of long-distance communication, first implemented by Forsyth et al. (1957) in Canada.

Pioneering theoretical works were made by Herlofson (1948), Clegg (1948), Greenhow (1952), Kaiser and Closs (1952), Weiss (1955), Kaiser (1955a,b), Davis et al. (1959) and others, and led to a dynamic development of radar meteor science.

New meteor radars were build in the fifties and sixties in Australia (Adelaide and Newcastle), Canada (Ottawa), Czechoslovakia (Ondřejov), England (Sheffield), Germany (Kühlungsborn), Italy (Firenze), New Zealand (Christchurch), Sweden (Onsala), USA (Havana), and USSR (Khar'khov, Dushanbe, Kazan, and Kiev) with the new generation of researchers contributing significantly to further progress of radar meteor methods and their full-value application in meteor science. (See Sections 3.5 and 4.)

2.5. Acoustic, infrasonic, and seismic observations

Audible observations of the blast/explosion wave effects from bright meteor-fireballs have been known for a very long time (ReVelle, 1976, 1997). Clearly, the detection of the 10 Mt, June 30, 1908 Tunguska bolide event on barographs as far away as Great Britain was a great impetus for further study of the blast effects of very energetic bolides and other large atmospheric explosions. Starting about 1960, infrasound from bolides had been used as a tool to detect, locate and to estimate the kinetic energy of these airborne sources. These and other ancillary data, collected by the US Air Force, allowed ReVelle and Wetherill (1978) and ReVelle (1997) to estimate the global influx rate of these deep penetrating bodies which are capable of producing blast effects due to their great hypersonic velocity. Subsequent observational and theoretical research programs were initiated by the University of Michigan at their infrasound field station near Sioux Falls, South Dakota and at the National Research Council of Canada near Ottawa (Springhill Meteor Observatory) and at another field station near Saskatoon, Saskatchewan. Current programs now exist at the Los Alamos National Laboratory in New Mexico. Great success has been made in the last three years with infrasonic detections having been made by the network of four Los Alamos arrays of three large bolides that were also detected by US DoD satellites as well, etc. This technique offers much promise

for gaining an understanding of the detailed source mechanisms of bolides and certainly deserves much further attention by meteor and infrasound researchers. Seismic blast effects have also been measured from bolides and from the Space Shuttle reentry as well (ReVelle, 1997), etc. This technique offers a complimentary approach to the infrasonic detection method and should also be pursued as another method of monitoring bolide activity in the atmosphere.

2.6. VISUAL OBSERVATIONS

This is the oldest method using the naked eye or sometimes equipped with a telescope of wide field of view. Simple counting of meteors seen within a traditional 1 hour interval, so called *hourly rate* of meteors, is the main purpose of such observations. These observations became a main objective of many amateur groups. Serious amateurs are well organized in IMO (International Meteor Organization) and in regional organizations. Their observations are of indispensable value for recording the changing activity of meteors (showers and sporadic meteors) and have been used by many professional meteor astronomers for deriving significant results on the meteoroid complex. Recording stellar magnitudes and other data of individual meteors may give additional information, namely the population index in the narrow mass-range of visual meteors. Statistical procedures of how to bring the observed hourly rates to ideal conditions of the radiant in the zenith, to an average field of view, and to weather and seeing conditions, etc., are a prime interest of serious amateur groups and organizations. Moreover, observations of meteors from the past are solely visual. Thus calibration of visual observations by direct comparison (the same meteor observed visually and by other methods, e.g., radar, TV, photographic) became very important for better relating present results to observations made in the past.

Sometimes meteors are plotted onto a stellar map. Because of the very short duration of the phenomenon, such plots contain information very much limited by low precision induced by insufficient human capacity. Such plots may help in the recognition of shower meteors with very low hourly rates. Prolongation of the plotted trails should intersect in the apparent radiant of a shower. Such plots are important when a new unknown radiant becomes active during the night of observation. More and more serious amateurs are using sensitive video cameras for recording meteors. Recognition of meteors turns from the fun of suddenly facing a meteor appearance to the PC-software searching of videorecords.

The extension of amateur observational work, namely for showers, is evident from the fact that the published meteor papers on visual observations, namely hourly rates, form the largest proportion of published material on meteors, exceeding the number of professional papers on meteors. These observations are published mainly in WGN (International Meteor Organization), Radiant (Dutch Meteor Society), Meteor News (Callahan Astronomical Society), Memoirs of the Nippon Meteor Society (Japan), etc.

There is another important field: casual visual sightings of very bright meteors (fireballs, bolides). Collecting them after a passage of a very bright object, sometimes accompanied by a meteorite fall, is an important task for estimating a fireball trajectory and orbit. This is mostly the only one possibility so far, except the photographic fireball networks (now working only in a part of Europe). However, one should be warned that casual observers (including experienced ones – the amateur meteor observers) tend to place the trajectory too low in the sky (a casual observer perhaps subconsciously wants to 'help to bring it down'). Ploting on a star map is not much help, because during the flight of such a bright object there are no stars visible (because of physiological effects) for a while. By comparing photographic trajectories with casual observations of the same fireball, this effect proved to be systematic, but very different for different observers; the deviation is the largest at 45° elevation of the real path.

2.7. Artificial meteors

We denote by the term 'artificial meteors' meteor phenomena produced by man-made bodies fired down to the atmosphere. Artificial meteors are the best known way to test and calibrate theoretical models of meteoroid penetration through the atmosphere. There has been little done in this respect in free atmosphere and all for rather low velocities and small masses. The first experiments were realized by McCrosky and Soberman (1963). Ayers et al. (1970) published results on 10 artificial meteors originating from projectiles fired down from heights of 80 to 280 km using shaped charge accelerators. Projectile velocities from 8 to 16 km s^{-1} were realized for masses from 0.6 to 5.7 g. Material of the artificial meteoroids was limited to iron, steel and nickel, because of technological problems of firing materials at these high velocities. These experiments gave results on luminous efficiencies for objects in a mass-range of grams with low velocities. These are the only directly-derived luminous efficiencies so far available for interpreting light curves of meteors in terms of mass loss of their meteoroids. They have to be compared with laboratory experiments on luminous efficiency for smaller masses and higher velocities (Friichtenicht et al., 1968), and with luminous efficiencies derived for larger masses and velocities below 20 km s^{-1} derived from photographic observations of bolides accompanied by meteorite falls (Halliday et al., 1978, 1981; Ceplecha, 1996a).

Additional work on artificial meteors especially for higher velocities and larger bodies is highly desirable as well as a continuation of laboratory experiments related to meteor phenomenona.

2.8. Combined observational methods

It would be highly desirable to observe one meteor by many observational methods and to combine the results of these methods (eventually combine the observations directly) in order to obtain as much data as possible on the body and on its interaction with the atmosphere (and also perhaps data on the atmosphere itself). In this

respect the observational methods described in the preceding sections were never carried out all simultaneously.

Recent data on a -10 mag fireball (Meisel et al., 1995) were derived from a combination of many methods (visual, photographic, imaging radar, video camera, infrared CCD, narrow-band spectrometer), but basic data on the trajectory geometry from double station photographs are missing. A single fish-eye camera photograph was available and the authors used a rather too simple a methods for positional reductions, and also for analyzing the distance along the trajectory and heights as function of time (interpolation polynomial used!). Most of the reductions were done below the top possibilities available nowadays (citation of a paper on atmospheric corrections to meteor velocity from 1955, when there are advanced papers on the same question from the last five years!). This extensive paper contains then rather speculative results for the orbit of this body. It would be very useful to re-analyze this case by combining the best available knowledge and software for individual observational methods in order to get at better precision and to eliminate some of the speculations. Much better data are available on many fireballs just from multistation-photographic and spectral records than in this case of multi-method observation of bolide AIDA.

All systematic work in this region was done usually by combining two or three observational methods. Systematic observations made in 1972 and 1973, and published by Znojil et al. (1980, 1981, 1987) can serve as a good example of combining radar and visual (and visually telescopic) methods. A large proportion of combined observations happened just by chance (e.g., Park and McIntosh, 1967).

Well-equipped multi-method observations are highly desirable to bring a better understanding to meteor phenomena, to composition and structure of meteor bodies, and to the role of meteoroids in the solar system.

3. Meteoroid Interaction with the Atmosphere (Physical Theory of Meteors)

3.1. Aerodynamics of meteor entry: descriptions in terms of dimensionless numbers and relevant forces

During the hypersonic drag interaction of a meteoroid with the atmosphere, a number of very interesting phenomena can occur and are summarized in Table II. This table was generated physically on the basis of a modeling approach that unifies the study of meteor entry on all size scales, but neglects the gross fragmentation process. Despite the large range of values of all the parameters, only six discrete interaction regimes are possible (ReVelle, 1993).

As the drag interaction proceeds molecules initially directly impact the body and at sufficiently high altitudes these impacts are so infrequent that a molecule colliding with the meteoroid is more likely to hit the body again than it is to encounter another air molecule. This is due to the rarefied flow conditions at high altitudes

(low collision frequency and large neutral gas mean free path). The ballistic part of this interaction can be understood in terms of the ratio of the surface pressure of the atmosphere compared to the body's modified ballistic entry parameter (proportional to the mass to area ratio of the bolide) as can be seen in Table II. For small bodies this ratio is quite large indicating that a significant deceleration will occur during entry in the absence of ablation processes (in the thermospheric micrometeoroid regime, 1). Conversely, for large bolides, the values of this ratio will be quite small and the deceleration will be quite small in the absence of significant ablation effects (continuum flow regime 4, etc.).

During the free molecule flow regime, the collisions induce a preheating of the body which will subsequently raise its surface temperature sufficiently to initiate the ablation process. At lower heights a diffuse shock wave forms as the body begins to ablate and a protective air cap or viscous boundary layer forms around the front face of the meteoroid shielding it from further direct impacts. At still lower heights for sufficiently large bodies an intensely radiating fluid blast wave of nearly cylindrical shape forms (in the absence of gross fragmentation phenomena), which rapidly expands outward as a line source with mechanical energy radiating both forward from the meteoroid and at right angles to its trajectory. This intensely nonlinear zone surrounding the body is approximately the product of the meteoroid's Mach number and its diameter, as long as significant gross fragmentation effects have not occurred (see below). For very large fireballs this radius can be greater than 1 km. With still deeper penetration stagnation pressures can exceed the bodies mechanical strengths (tensile or compressive) and gross fragmentation and major disruption of the body will likely occur, except perhaps for very large iron bodies.

An analytical treatment of the entry interaction after this gross fragmentation process has been initiated is very difficult. There are some recent treatments that attempt to model this effect that invoke the formation of a greatly enhanced frontal drag area, i.e., the so-called pancake break-up model due to lateral spreading of the body which is supposedly applicable only for the very largest, most deeply penetrating bodies. This approach actually dates back to 1979 (Bronshten and Zotkin, 1995) and to the work of Grigoryan. It is the opinion of this author that the detailed modeling of bolide break-up using this effect is not very realistic. Although originally promoted by Hills and Goda (1993) and other authors, this pancake effect was later found to be hydrodynamically unstable and thus subject to severe oscillatory behavior after its onset (J. Hills, personal communication, 1995). A somewhat similar approach was also proposed by Baldwin and Sheaffer (1971) that produced an increase in the frontal drag area after the onset of break-up which was proportional to the number of fragments produced during the break-up to the $\frac{1}{3}$ power. This model also completely failed in its ability to successfully predict the observed detailed behavior of the US Prairie Network fireballs (Ceplecha, 1980).

The key forces affecting the interaction include that of drag, lift (depending on shape) and of the body weight component along the trajectory. In what follows

TABLE II

The meteoroid-atmosphere interaction spectrum

Interaction type		Kn	α	A_e
(1)	Thermosphere micro-meteoroid regime	$\gg 1$	$\gg 1$	$\ll 1$
(2)	Free molecule flow regime	$\gg 1$	$\gg 1$	$\gg 1$
(3)	Transition flow regime	O(1)	> 1	$\gg 1$
(4)	Continuum flow regime	$\ll 1$	O(1)	> 1
(5)	Impact cratering regime	$\ll 1$	< 1	O(1)
(6)	Explosive cratering regime	$\ll 1$	$\ll 1$	$\ll 1$

$Kn \equiv$ local Knudsen number.
$\alpha \equiv$ surface pressure/modified ballistic entry parameter.
$A_e \equiv$ changes in dimensionless ablation efficiency.
Associated phenomena for each regime:
(1) Negligible mass loss and light production.
(2) Extensive mass loss and concomitant light production.
(3) Moderate to extensive mass loss; diffuse shock wave formation and light curve flaring.
(4) Mass loss highly size and velocity dependent; strong blast wave formation and propagation – hypersonic booms.
(5) Low velocity and negligible mass loss with direct earth or oceanic impact. Bolide kinetic energy depletion height intersects the earth's surface. Blast wave interaction with the ocean/land interface; tektites; electrophonic noise through interaction with the geomagnetic field; mesoscale Rossby radius generated $> 10^5$ to 10^6 m.
(6) Climatic change effects, explosive cratering. Bolide kinetic energy exceeds the atmospheric potential energy (3.8×10^{23} J). Negligible mass loss with large atmospheric changes expected. Blast wave propagation; surface fires; tektites; tsunamis; electrophonic noise; synoptic scale Rossby radius generated ($> 10^6$ m).

we will assume that LTE (local thermodynamic equilibrium) applies, i.e., that the characteristic times for vibrational and chemical processes are sufficiently short compared to those for the emission and absorption of photons. Non-equilibrium processes may also apply however especially for very large entry velocities, but because of the limited space for this review, we will not pursue this subject further. The key dimensionless numbers that affect the meteoroid behavior include the Reynolds number, Re (= inertial fluid forces/viscous fluid forces), Mach number, Ma (= body speed with respect to the adiabatic phase velocity of sound waves, c_s), Knudsen number, Kn (= ratio of the neutral gas mean free path to a characteristic body dimension). Also, for very large and deeply penetrating bodies traveling at high Mach number, the Bouguer number, Bu, and the radiation-convection parameter of an adiabatic shock layer, Γ_{rc} (the ratio of the black body radiation losses to the convective free stream power input) are also fundamental to an understanding of the dynamics and energetics of the entry process. Γ_{rc} is used to determine

whether radiative or convective heat transfer will dominate the heat transfer to the body from the air. Often the Goulard number, Bo, is used as an alternative to Γ_{rc}. These three dimensionless numbers, Bo, Bu, and Γ_{rc} are all closely related however (Schneider, 1974), i.e., since $\Gamma_{rc} = f(Bu, Bo)$. The Bu is a means of estimating the global optical thickness of the shock-ablation layer (over all wave frequencies). It is found by computing the product of the volumetric absorption coefficient (averaged over all electromagnetic wave frequencies) and the boundary layer thickness on the front face of the bolide. Additional perspectives on this topic have recently been provided in Bronshten (1993a,b).

When radiative heating dominates over convection ($\Gamma_{rc} \gg 1$), strong shock wave radiation effects occur such as free stream absorption (also referred to as precursor ionization), ablation products absorption, etc. Also, for $Bu \gg 1$, the boundary layer is expected to be optically thick whereas for $Bu \ll 1$, the limiting case of an optically thin boundary layer is approached. The precursor ionization effects can be intense enough so that the ambient air density ahead of the body can even be modified by the ultraviolet radiation field from the shock wave. Finally, for the very largest and most energetic bodies, the blast wave interaction can become sufficiently nonlinear that the Rossby deformation radius will become of truly synoptic scale dimensions. Thus, large horizontal atmospheric regions, $> 10^6$ m in radius, can be affected by the blast wave interaction (Fleagle and Businger, 1980).

For substances with large thermal conductivity (such as iron meteoroids) that are small enough to allow complete melting during entry, the Weber number is also of key importance as well, which determines the effects of surface tension forces on the structural stability of any liquefied droplets. If significant rotational/tumbling effects occur then the consequences of significant centrifugal forces (Taylor number = centrifugal forces/viscous forces) must also be considered as well. If significant chemical reactions occur during the bolide-atmosphere interaction, then the Damkohler number also needs to be considered, etc.

The boundary separating the shock front from the free stream air ahead of the body is a viscous air/ablative products gas cap. For sufficiently energetic bodies this initially laminar flow becomes fully turbulent at the stagnation (no flow) point. ReVelle (1979) has given a zeroth order method for calculating this transition as a function of Re, but the transition is also likely to be a function of the drag coefficient, C_D, the body shape, and of the ablation processes that are occurring, etc. The wake itself can also be laminar or turbulent, but tends to become turbulent quite rapidly for large, energetic bodies. In the wake region the ablation products are the predominant species radiating light. This has been studied spectrally by Ceplecha and by Borovička, etc. In contrast to the viscous flow between the body and the shock, the flow in front of the shock is nearly inviscid.

For typical meteoroid entry velocities, Re for large bodies is $\gg 1$ (typically $> 10^6$), indicative of a turbulent fluid flow if Kn is also $\ll 1$. Except for the terminal portion of the atmospheric entry, Ma is quite large ($>$ 30–100). Also, Kn is a function of both Ma and Re and varies as body size and altitude changes. It can

vary from the limits of free molecular flow ($Kn > 10$), through transitional flow ($1 < Kn < 10$), through slip flow to continuum flow ($Kn \ll 1$).

3.2. ABLATION

For many decades theoretical models of the motion and ablation of a meteoroid were based on so called single body motion. Early history (starting with classical work by Öpik, 1933, 1937) and the inference of differential equations of meteoroid motion in the atmosphere can be found in the classical paper of Whipple (1938, on p. 526). Whipple used Hoppe's solution (1937) to the equations of motion and ablation with constant coefficients, the first such solution presented in a closed mathematical form. This single body theory has sometimes been called 'Hoppe's theory'. Significant work in 'meteor physics' (a traditional name for this branch of meteor science) was done by Levin (1961) and by Bronshten (1983); the later presented a more general solution with changing coefficients. ReVelle (1979) proposed a 'quasi-simple ablation model' and applied it also to photographically recorded meteorite falls. ReVelle used changing coefficients in the basic equations, derived from theoretical and empirical aerodynamics data and kept them constant only inside a small step of an integration interval. All these older solutions assumed schematic isothermal atmosphere and found closed mathematical expressions only for velocity as function of time.

A new solution to the differential equations of meteoroid motion and ablation in the atmosphere was presented by Pecina and Ceplecha (1983, 1984) in the form of $l = l(t)$, i.e., the distance, l, traveled by the body in its trajectory as function of time, t. This solution holds for any atmospheric density profile. Because the primary determined value in precise meteor observations (multi-station photographic and television records) is the distance, l_{obs}, traveled by the body along its trajectory, the theoretical distance, l, can be directly compared to l_{obs}. The disadvantage of keeping the coefficients of the differential equations constant can be circumvented by applying the solution to smaller time intervals following ReVelle. Moreover this solution is capable not only to account for continuous fragmentation (a common process), but can also include points of sudden gross fragmentation at discrete trajectory points (Ceplecha et al., 1993). This solution is described below.

The motion and ablation of a single non-fragmenting body through the atmosphere can be represented by three differential equations: the drag equation (1); the mass-loss equation (2); the height equation (3), which is purely geometrical and is written here for a spherical Earth's surface, i.e. with $\cos z$ as function of time. By the term 'ablation' we understand any removal of mass from a meteor body during its passage through the atmosphere, i.e., in form of gas, droplets, or solid fragments. This removal can be either continuous or sudden, i.e., at a discrete point. Masses determined from motion and ablation of the body are sometimes called 'dynamical' masses to distinguish them from masses computed from a light curve of a meteor ('photometric masses').

$$\frac{\mathrm{d}v}{\mathrm{d}t} = -\Gamma A \varrho_d^{-2/3} \varrho m^{-1/3} v^2 \,, \tag{1}$$

$$\frac{\mathrm{d}m}{\mathrm{d}t} = -\frac{\Lambda A}{2\xi} \varrho_d^{-2/3} \varrho m^{2/3} v^3 \,, \tag{2}$$

$$\frac{\mathrm{d}h}{\mathrm{d}t} = \frac{l - A/2}{B/2 + h}\, v \,, \tag{3}$$

$$\frac{A/2 - l}{B/2 + h} = \cos z(t) \,, \tag{4}$$

$$Al + Bh + C = l^2 - h^2 \,, \tag{5}$$

Equation (5) contains constant values A, B, C, which are given by the geometrical relation between distances along the meteoroid trajectory and heights measured from the spherical Earth's surface. Equation (5) can also be used as a good check of validity of any set of l and h values for meteors.

For a meteoroid at an arbitrary point of its trajectory, the notation has the following meaning: $v \equiv$ velocity; $t \equiv$ time (independent variable); $m \equiv$ mass; $h \equiv$ height; $l \equiv$ distance along the trajectory; $\varrho \equiv$ air density; $z \equiv$ zenith distance of the radiant (i.e., inclination of the trajectory to the vertical); $\Gamma \equiv$ drag coefficient; $\Lambda \equiv$ heat transfer coefficient; $A = Sm^{-2/3}\varrho_d^{2/3}$ is the shape factor; $S \equiv$ head cross-section; $\varrho_d \equiv$ bulk density; $\xi \equiv$ energy necessary for ablation of a unit mass. Two independent parameters of the problem can be expressed as the ablation coefficient

$$\sigma = \frac{\Lambda}{2\xi\Gamma} \tag{6}$$

and the shape-density coefficient

$$K = \Gamma A \varrho_d^{-2/3} \,. \tag{7}$$

By keeping σ and K constant, we can derive the following integrals of Equations (1)–(3):

$$m = m_\infty \exp(\tfrac{1}{2}\sigma[v^2 - v_\infty^2]) \tag{8}$$

where $m \to m_\infty$, $v \to v_\infty$, for $t \to -\infty$ (outside the atmosphere). By substitution of (8) into (1) and integrating we obtain the velocity integral:

$$\mathrm{Ei}(\tfrac{1}{6}\sigma v_\infty^2) - \mathrm{Ei}(\tfrac{1}{6}\sigma v^2) = \frac{2K \exp(\tfrac{1}{6}\sigma v_\infty^2)}{m_\infty^{1/3}} \int_h^\infty \frac{(B/2 + h)\varrho \,\mathrm{d}h}{(A^2/4 + C + h^2 + Bh)^{1/2}} \,. \tag{9}$$

The integral relating velocity to time is

$$t - t_0 = \int_{l_0}^{l} \frac{\mathrm{d}l}{v} \tag{10}$$

and the integral relating height and distance along the trajectory to time is

$$\frac{\mathrm{Ei}(\frac{1}{6}\sigma v_\infty^2) - \mathrm{Ei}(\frac{1}{6}\sigma v^2)}{\mathrm{Ei}(\frac{1}{6}\sigma v_\infty^2) - \mathrm{Ei}(\frac{1}{6}\sigma v_0^2)} = \frac{\int_{h}^{\infty} \frac{(B/2+h)\varrho\,\mathrm{d}h}{(A^2/4+C+h^2+Bh)^{1/2}}}{\int_{h_0}^{\infty} \frac{(B/2+h)\varrho\,\mathrm{d}h}{(A^2/4+C+h^2+Bh)^{1/2}}} , \tag{11}$$

where the relation of height to distance is given by

$$h = -B/2 + \sqrt{B^2/4 - C + l^2 - Al} . \tag{12}$$

Here $\mathrm{Ei}(x)$ is the exponential integral function, given by

$$\mathrm{Ei}(x) = \int_{-\infty}^{x} \frac{e^x}{x}\,\mathrm{d}x , \tag{13}$$

v is defined by (10) and $v = v_0$, $h = h_0$, $l = l_0$ holds for $t = t_0$. We can define $t_0 = 0$ at any point of a meteoroid trajectory: This only defines at what instant we start to count the relative time t.

These integrals hold for any air density profile. Equations (10) and (11) represent the complete solution of the problem of the single non-fragmenting body with constant coefficients σ and K, and express the distance along the trajectory and the height as function of time, if the four parameters, l_0, v_0, v_∞, σ, are known. We can consider velocity, v , as an intermediate parameter to be eliminated from Equations (10) and (11). The solution represented by Equations (10) and (11) is also equivalent to the condition $K =$ constant.

The problem contains 4 unknown parameters l_0, v_0, v_∞, σ, to be determined from observations. We can make the problem linear by writing it for small increments of the parameters. The partial derivatives of (10) and (11) with respect to all four unknown parameters are explicit analytical expressions, as follows. This makes the computation convenient and speedy, especially if we have some good estimates of the initial values of the parameters. We proceed by writing the total differential according to changing parameters, making thus the problem linear in computation of small increments of the unknown parameters.

$$l_{\mathrm{obs}} - l = \frac{\partial l}{\partial l_0}\Delta l_0 + \frac{\partial l}{\partial v_0}\Delta v_0 + \frac{\partial l}{\partial v_\infty}\Delta v_\infty + \frac{\partial l}{\partial \sigma}\Delta\sigma , \tag{14}$$

$$\frac{\partial l}{\partial l_0} = \frac{1}{v_0 D}\left\{2v\ \exp(\tfrac{1}{6}\sigma v^2)\int_{h_0}^{\infty}\frac{\varrho\,\mathrm{d}h}{\cos z}+\right.$$

$$\left.+v_0 v^2[\mathrm{Ei}(\tfrac{1}{6}\sigma v_\infty^2)-\mathrm{Ei}(\tfrac{1}{6}\sigma v^2)]\varrho(h_0)\int_{l_0}^{l}\frac{\mathrm{d}l}{v^2}\right\}\,, \tag{15}$$

$$\frac{\partial l}{\partial v_0} = \frac{2v^2}{v_0 D}\ \exp(\tfrac{1}{6}\sigma v_0^2)\int_{h}^{\infty}\frac{\varrho\,\mathrm{d}h}{\cos z}\int_{l_0}^{l}\frac{\mathrm{d}l}{v^2}\,, \tag{16}$$

$$\frac{\partial l}{\partial v_\infty} = -\frac{2v^2}{v_\infty D}\ \exp(\tfrac{1}{6}\sigma v_\infty^2)\left[\int_{h}^{\infty}\frac{\varrho\,\mathrm{d}h}{\cos z}-\int_{h_0}^{\infty}\frac{\varrho\,\mathrm{d}h}{\cos z}\right]\int_{l_0}^{l}\frac{\mathrm{d}l}{v^2}\,, \tag{17}$$

$$\frac{\partial l}{\partial \sigma} = \frac{v^2}{\sigma D}\int_{l_0}^{l}\frac{\mathrm{d}l}{v^2}\left[\exp(\tfrac{1}{6}\sigma v_0^2)\int_{h}^{\infty}\frac{\varrho\,\mathrm{d}h}{\cos z}-\right.$$

$$\left.-\exp(\tfrac{1}{6}\sigma v_\infty^2)\int_{h}^{h_0}\frac{\varrho\,\mathrm{d}h}{\cos z}-\exp(\tfrac{1}{6}\sigma v_0^2)\int_{h}^{\infty}\frac{\varrho\,\mathrm{d}h}{\cos z}\right]\,, \tag{18}$$

where the denominator D is given by

$$D = 2\ \exp(\tfrac{1}{6}\sigma v^2)\int_{h_0}^{\infty}\frac{\varrho\,\mathrm{d}h}{\cos z}+v^2[\mathrm{Ei}(\tfrac{1}{6}\sigma v_\infty^2)-\mathrm{Ei}(\tfrac{1}{6}\sigma v_0^2)]\varrho(h)\int_{l_0}^{l}\frac{\mathrm{d}l}{v^2}\,. \tag{19}$$

Continuous fragmentation can also be treated using this solution, because of the general definition of the ablation coefficient in the single-body model: ablation means just removal of mass in any form, either gas, or fluid and or solid fragments. If the body fragments suddenly at a point, the solution is no longer valid, but we can easy generalize the solution in this respect. The simplest model with only one point of gross-fragmentation during the entire atmospheric trajectory, is the same as given by Equations (10) and (11), except that we integrate in two steps (before respectively after the fragmentation point) and thus we have two additional parameters, i.e., altogether 6 parameters to be determined from observations. If the gross-fragmentation point is located at $t = t_0$ (we can chose this point, from where the relative time is counted), then

$$l_{\text{obs}} - l = \frac{\partial l}{\partial l_0}\Delta l_0 + \frac{\partial l}{\partial v_0}\Delta v_0 + \frac{\partial l}{\partial v_{\infty 1}}\Delta v_{\infty 1} + \frac{\partial l}{\partial \sigma_1}\Delta\sigma_1 + \\ + \frac{\partial l}{\partial v_{\infty 2}}\Delta v_{\infty 2} + \frac{\partial l}{\partial \sigma_2}\Delta\sigma_2 \,, \tag{20}$$

which is a linear equation analogical to (14), except it contains the following 6 unknown increments of parameters to be determined from observations

$\Delta v_{\infty 1}, \Delta\sigma_1$	$\Delta l_0, \Delta v_0$	$\Delta v_{\infty 2}, \Delta\sigma_2$
before fragmentation	at fragmentation	after fragmentation

Partial derivatives in (20) are again explicit analytical expressions as in the non-fragmentation case (14), in complete analogy. Equations (17) and (18) have to be now written with two subscripts, 1 and 2: subscript 1 is valid before the fragmentation point and subscript 2 is valid after the fragmentation point. The computational procedure is analogical to that described above Equation (14). Because the solution is again completely equivalent to keeping K constant, the relative change of mass at the fragmentation point forms also a part of the solution. The ratio of $Km^{-1/3}$ before and after the fragmentation point determines m_f, the ratio of mass after and before the fragmentation point, which is independent of the actual value of K. Once a gross-fragmentation point is fixed at a value determined from observations (the point, where sum of squared residuals has a minimum value), the complete solution has now 8 unknown parameters that are completely determinable from observations: the 6 unknowns directly contained in the equations, plus the amount of fragmentation (fraction of stripped-off mass) and the position of the fragmentation point.

In case of more fragmentation points, the situation is not so simple. Each additonal fragmentation point adds four parameters, if the relative amount of fragmented mass and the position of fragmentation points are also taken as unknowns.

Large meteor bodies, especially the meteorite dropping fireballs can reach a maximum deceleration point on their luminous trajectory. If suffix md is used for notation of this point, we have the following condition for the velocity v_{md} at the maximum deceleration point:

$$(\tfrac{1}{6}\sigma v_{md}^2 - 1)\exp(-\tfrac{1}{6}\sigma v_{md}^2)[\text{Ei}(\tfrac{1}{6}\sigma v_\infty^2) - \text{Ei}(\tfrac{1}{6}\sigma v_{md}^2)] + 1 = 0 \,. \tag{21}$$

The maximum deceleration is given by

$$\left(\frac{\mathrm{d}v}{\mathrm{d}t}\right)_{md} = -\tfrac{1}{2}b\cos z_R \frac{v_{md}^2}{1 - \tfrac{1}{6}\sigma v_{md}^2} \,. \tag{22}$$

This theoretical model was applied to photographic observations of meteors in order to be checked by several independent methods. Photographic records of meteors contain sometimes a visible split of the trajectory (Figure 3), which defines

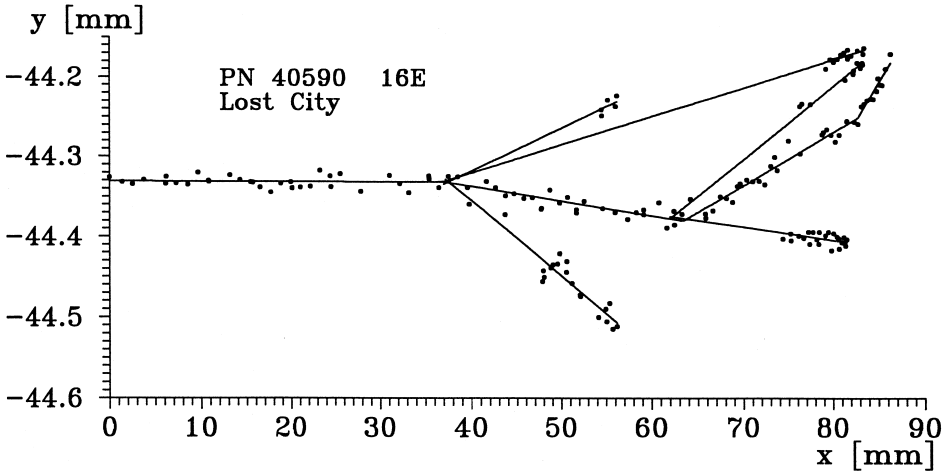

Figure 3. Splitting trails of fireball PN 40590 (Lost City). This is the direct image as seen on the film except the *y*-axis is greatly enlarged to visualize the separation of individual fragments. Dots are the individually measured points: least-squares fits of straight lines to these points define trails of individual fragments.

gross-fragmentation points geometrically from the intersection of the fragment trails. This can be compared with the dynamical solution from equations of this section. Independent solutions of the same meteor from different stations can also be used for this purpose. For details see Ceplecha et al. (1993).

When this model was applied to the photographic observations of PN and EN fireballs, it was evident that using of air densities from a simple isothermal atmosphere model or from a yearly averaged standard atmosphere is insufficient (Pecina and Ceplecha, 1984). Atmospheres with different air densities for each month of the year and for different latitudes have to be used (e.g., CIRA 72 or CIRA 86 atmosphere). In principle high quality observations of fireballs can be used to determine differences of instantaneous air densities from the CIRA atmospheres (Ceplecha and Borovička, 1992).

The gross-fragmentation model has been applied to photographic observations of almost 500 meteors, mostly PN and EN fireballs (McCrosky et al., 1976, 1977; Ceplecha and McCrosky, 1997). Sizes of the photographed fireball meteoroids were up to several meters with the highest observed dynamic pressure of slightly over 10 MPa. All analyzed meteors can be modeled as either the single-body or the single-body with a gross-fragmentation under dynamic pressures mostly in the range from 0.1 to 1.2 MPa (Ceplecha et al., 1993). Typical standard deviations of the distance l flown along the trajectory was found to be in the range of ± 10 to ± 30 m for one observed distance; this corresponds to the geometrical precision of the observations. *The gross-fragmentation model can explain all high quality observations of meteoroids up to initial sizes of several meters with high precision* (Borovička and Spurný, 1996). Also the three photographed meteorite falls fit this

model and the recovered meteorites and their properties are consistent with the solutions (Ceplecha, 1994a).

The video-recorded Peekskill fireball underwent a severe fragmentation between 0.7 and 1.0 MPa starting at a height of 42 km, while its ordinary chondrite (the one which hit the parked car in New York State) has a strength of some 30 MPa. The initial size of the Peekskill body was close to 2 m (Brown et al., 1994). Video-records of the Peekskill fireball are the fourth case of precisely observed atmospheric trajectory of Earth-grazing meteoroids (perigee above the Earth's surface: Ceplecha, 1979, 1994b).

3.3. SPECTRA OF METEORS

As already mentioned, meteor spectra consist primarily of atomic emission lines and molecular bands. The identifications have been done by many authors. The most extensive lists of identified lines are given by Halliday (1961) for Perseid meteors (velocity 60 km s^{-1}), by Ceplecha (1971) for a 32 km s^{-1} meteor and by Borovička (1994a) for a 19 km s^{-1} meteor. The near infrared spectra of Perseids (up to $\approx$ 9000 Å) are also described by Millman and Halliday (1961). Halliday (1969) and Harvey (1973a) observed lines in the ultraviolet to 3100 Å.

The survey of reliably identified atoms and ions is given in Table III. For each element, one or more lines suitable for the element detection are given. These are in most cases the brightest lines for a particular element in the spectral window covered by present observations. Alternatively, the lines less blended with lines of other elements are given. Additional lines are included in the table only when they are widely separated. If there are several suitable lines in the same spectral region, only the most suitable is given.

For each line, the wavelength, multiplet number according to Moore (1945), and the excitation potential of the upper level is given. The relative brightness in the scale 1–5 is presented for orientation. It expresses the strength the line can reach in some spectra, not the typical strength. Intensity 1 means faint line, 2 medium line, 3 strong line, 4 very strong line, and 5 the strongest line in the spectrum. In the sixth column, the spectral component (see below) to which the line belongs is given. The references are given in the last column. Maximally three references are included and the three above extensive lists are preferred. All identifications have recently been critically evaluated.

In Table IV likely but still uncertain identifications of atoms and ions are given. The certainly and possibly identified molecules are listed in Table V. No specific wavelengths are given for molecules because the appearance of molecular bands strongly depends on spectral resolution.

Meteor spectra were classified by Millman (see, e.g., Millman and McKinley, 1963) according to which lines are the brightest. The four main types were defined as follows:

TABLE III

Atoms and ions certainly identified in meteor spectra and the spectral lines most suitable for identification

Atom or ion	λ (Å)	Multiplet	E_2 (eV)	Intensity	Component	References
H I	6563	1	12.09	3	s	[1, 2, 4]
Li I	6708	1	1.85	2	m	[6, 9]
N I	8680	1	11.76	4	sa	[1, 4]
	6465	21	13.66	1	sa	[1, 2, 7]
	4110	10	13.70	1	sa	[1, 2, 7]
N II	5680	3	20.66	1	a	[1, 9]
O I	7772	1	10.74	5	sa	[1, 4]
	6158	10	12.75	3	sa	[1, 2, 7]
Na I	5890	1	2.11	5	m	[1, 2, 3]
Mg I	5184	2	5.11	5	m	[1, 2, 3]
	3838	3	5.94	5	m	[1, 2, 3]
Mg II	4481	4	11.63	4	s	[1, 2, 8]
Al I	3962	1	3.14	3	m	[2, 3, 9]
Si I	3906	3	5.08	3	m	[1, 3]
Si II	6347	2	10.07	3	s	[1, 2, 3]
	4131	3	12.83	2	s	[1]
Ca I	4227	2	2.93	4	m	[1, 2, 3]
	6162	3	3.91	3	m	[1,2,3]
Ca II	3934	1	3.15	5	s, m	[1, 2, 3]
	8542	2	3.15	4	s, m	[1, 4]
Ti I	4982	38	3.33	2	m	[2, 3, 9]
Ti II	3349	1	3.74	3	s, m	[5, 8]
Cr I	4254	1	2.91	4	m	[1, 2, 3]
	5208	7	3.32	3	m	[1, 2, 3]
	3593	4	3.44	3	m	[1, 5, 10]
Cr II	3125	5	6.42	2	s	[5]
Mn I	4031	2	3.08	3	m	[1, 2, 3]
Fe I	3860	4	3.21	5	m	[1, 2, 3]
	4384	41	4.31	4	m	[1, 2, 3]
	5270	15	3.21	4	m	[1, 2, 3]
Fe II	5018	42	5.36	2	s	[1, 2]
	3228	6	5.51	2	s	[5]
Co I	4813	158	5.79	1	m	[2]
	4121	28	3.93	1	m	[3]
	3506	21	4.05	1	m	[10]
Ni I	5477	59	4.09	2	m	[2, 3]
	3462	17	3.60	2	m	[5, 10]
Sr II	4078	1	3.04	2	s, m	[1]

Components: m – main, s – second, a – atmospheric line.

References: [1] Halliday (1961), [2] Ceplecha (1971), [3] Borovička (1994a), [4] Millman and Halliday (1961), [5] Halliday (1969), [6] Borovička and Zamorano (1995), [7] Harvey (1977), [8] Millman et al. (1971), [9] Borovička and Spurný (1996), [10] Harvey (1973a).

TABLE IV
Atoms and ions possibly identified in meteor spectra

Atom or ion	λ (Å)	Multiplet	E_2 (eV)	References
O II	4649	1	25.65	[1, 2]
	4676	1	25.64	[1, 2]
V I	5727	35	3.24	[3]
Cu I	5782	2	3.79	[3]
Sr I	4607	2	2.69	[1]
Ba II	4554	1	2.72	[1, 3]

For the code of the references see Table III.

TABLE V
Molecules identified in meteor spectra

Certainly:	N_2 [2,7,8], CN [2], C_2 [2,3], FeO [2,3,9], CaO [9], AlO [9], MgO [9]
Possibly:	N_2^+ [8], O_2^+ [8], OH [8], CH [2]

For the code of the references see Table III.

Type Y – H and K lines of Ca II (3968 and 3934 Å) are the strongest.
Type X – the Na I or Mg I lines are the strongest.
Type Z – the Fe I or Cr I are the strongest.
Type W – none of the above.

Most meteors (about 90%) are of either type Y or X. Type Y represents the spectra of higher excitation and predominates in fast meteors, while type X is typical for medium and slow velocities. However, fainter meteors exhibit lower excitation than bright meteors and type X is also found among faint fast meteors. Type Z represents meteors with different chemical composition and type W includes peculiar spectra, often weak and of low quality.

Harvey (1973b) presented statistics of spectra for meteors in the magnitude range from $+1$ to -3 (velocity data were not available). He concluded that the dominant radiation in about 60% of the spectra are the violet multiplets of iron, i.e., the spectra of type Z. This conclusion, however, may have been influenced by the better performance of his spectrographs in the violet and blue spectral region suppressing the sodium yellow line. In any case, only 2% of spectra in this magnitude interval were of type Y. Harvey (1971) and other authors therefore considered the dominant brightness of H and K lines in bright fast meteors as an anomaly.

Millman's classification has only descriptive characters. Physical interpretation was possible for bright meteors with many lines. The line spectrum is excited by the collisions between the atoms evaporated from the meteoroid and atmospheric

species. The simplest assumption is that level populations are given by the Boltzman distribution for thermal equilibrium:

$$n_i = \frac{n}{U} g_i e^{E_i/kT}, \tag{23}$$

where n is the concentration of all atoms of the given element, n_i is the concentration of atoms with level i populated, U is the partition function, g_i is the statistical weight of the level, E_i is the energy of the level above the ground level, k is Boltzman constant, and T is temperature.

Assuming the same temperature in the whole radiating volume and taking into account the self-absorption of radiation inside the volume, the solution of the equation of radiative transfer gives the resulting specific intensity at frequency ν,

$$I_\nu = B_\nu(T)(1 - e^{-\tau_\nu}), \tag{24}$$

where $B_\nu(T)$ is the Planck function for blackbody radiation and τ_ν is the optical depth at frequency ν. Only bound-bound transitions in atoms and ions are considered as the sources of opacity. The optical depth produced by a single line at frequency ν is

$$\tau_\nu = N \frac{\pi e^2}{mcU} g_1 f \, e^{-E_1/kT} \, (1 - e^{-h\nu/kT}) \, \Phi(\nu), \tag{25}$$

where N is the column density of the given element (cm^{-2}), i.e., the concentration integrated along the line of sight. Index 1 at g and E denotes the lower level of the transition; f is the oscillator strength, a quantity closely related to the transition probability (the values $\log gf$ for different spectral lines are tabulated). The factor $(1 - e^{-h\nu/kT})$ is a correction for stimulated emission and it is close to unity for lines in visual region. $\Phi(\nu)$ is the normalized line profile, $\int_0^\infty \Phi(\nu)\, \mathrm{d}\nu = 1$. Other quantities are physical constants: electron charge, e, electron mass, m, speed of light, c, and Planck constant, h. The frequency is related to wavelength by $\lambda = c/\nu$.

As the resolution of the observed spectra is insufficient to resolve line profiles, only the total line intensity can be compared with observations. This means that the specific intensity is to be integrated over the line profile and over the visible surface of the radiating volume.

Ceplecha (1964) constructed three models of the radiating volume and computed theoretical emission curves of growth. Applying theoretical curves to 70 lines of Fe I observed in a bright meteor flare, he was able to determine the Fe I excitation temperature of 2970 K as well as other parameters of the models. The abundances of atoms were computed under the assumption that temperature was the same for all of them. The same method was used by Ceplecha (1965, 1967b, 1971) for another three fireballs. In the last case, the excitation temperatures could be determined independently for four atoms, resulting in 4380 ± 100 K for Fe I, 5280 ± 60 K for Ca I, 4120 ± 200 K for Na I, and $14\,000 \pm 3000$ K for O I.

Babadzhanov and Getman (1980) determined the excitation temperature of 4040 K in their spectrum.

Although Ceplecha (1973) stressed the importance of self-absorption in meteor spectra, Harvey (1973a, c) and Nagasawa (1978) considered meteor spectra as a result of pure emission. In that case, the line intensity is given by

$$I = N \frac{2\pi e^2 h}{mU} \frac{g_1 f}{\lambda^3} e^{-E_2/kT}. \tag{26}$$

In fact, this is a limiting case for $\tau_\nu \ll 1$ and $I_\nu = B_\nu(T)\tau_\nu$. Excitation temperatures about 3000 K were derived but neglecting the self-absorption for meteors brighter than magnitude $+3$ is unsatisfactory, as confirmed again by Borovička (1993).

Borovička (1993) assumed that the profiles of spectral lines can be described by the usual Voigt function and that the meteor head can be approximated as a uniformly bright object, i.e., the integration over the meteor surface can be replaced by simple multiplication by the surface size, P. Under these assumptions he was able to compute meteor synthetic spectrum and to compare it with the observed spectrum. The free parameters of the synthetic spectrum are the excitation temperature, T (assumed the same for all elements), the column densities of different elements, N_j, the meteor size, P, and the damping constant, Γ. Adjusting the free parameters by the least squares method, most lines in the spectrum could be well explained. The spectrum of a bright fireball was analyzed at 43 points along the trajectory. The temperature was found to vary in the range 3500–4700 K and the variations of atomic abundances and the size of the radiating volume could be also studied.

Not all lines, however, could be explained using a single temperature. Borovička (1993) revealed that meteor spectra are composed of two distinct components with different temperatures. This was confirmed by detailed analyses of spectra of four other fireballs with different velocities (Borovička, 1994b).

The component with lower temperature has been called the main spectrum. The temperature lies usually in the range 3500–5000 K and does not depend on meteor velocity. The main spectrum contains several hundreds of lines in bright fireballs, mostly neutral lines of atoms of meteoric origin. Thermal equilibrium is nearly satisfied, although some lines may deviate. Chemical composition of the radiating gas can be computed from the main spectrum.

The high temperature component is called the second spectrum. It consists only of a few lines, the brightest belonging to ionized Ca, Mg, Si, neutral O, N, and the N_2 molecule. The temperature is nearly 10 000 K and is again independent of velocity. However, the temperature and other parameters can be only estimated in this case due to insufficient number of lines. In contrast to the main spectrum, the second spectrum is usually optically thin. Most metals are singly ionized under the conditions of the second spectrum.

The second spectrum is strong in fast meteors while it can be absent in slow meteors with velocity of about 15 km s^{-1}. The ratio of gas masses involved in the production of both components was found to be a steep function of velocity. Millman's classification of meteor spectra primarily reflects the strength of the second spectral component. Type Y represents meteors with strong second spectrum as the Ca II lines are the brightest lines of this component. The attribution of observed spectral lines to the components has been given in Table III. The low excitation transitions in singly ionized atoms can be present in both components. This is the case of Ca II, Ti II, and Sr II. No evidence has been found in meteor spectra for a source with an intermediate temperature, between 5000 and 10 000 K. Both components are therefore strictly distinct. The much higher temperature of O I in comparison with other three atoms as found by Ceplecha (1971) is simply due to O I radiation originating from the second spectrum.

An interesting question is the ratio of meteoric vapors to the atmospheric species in both components. No lines of nitrogen and oxygen are present in the main spectrum. However, this is due to the absence of allowed low excitation transitions in these atoms. The atoms simply do not radiate at 5000 K. An indirect evidence based on the pressure balance with surrounding atmosphere led Borovička (1993) to the conclusion that about 95% of atoms in the low temperature gas were the invisible atmospheric species. In the second spectrum, both meteoritic and atmospheric emissions are observable. Their ratio varies widely. This is evident from the changing ratio of infrared Ca II and O I lines (Millman and Halliday, 1961). In faint meteors of medium and high velocity the meteoritic emissions in the second spectrum are often absent, while the O I and N I lines and N_2 bands are still present and bright (Mukhamednazarov and Maltseva, 1989; Millman and Clifton, 1975). The N_2 bands sometimes appear very early on the trajectory (Cook et al., 1973). In a Perseid spectrum, Borovička and Boček (1996) showed that meteoritic emissions invisible at the start of the trajectory burst out later, while the atmospheric lines brighten only moderately. All these effects show that the atmospheric emissions are less dependent on the ablation rate, a finding that might be expected.

Thermal equilibrium proved to be a good first approximation for the main spectrum. This forms evidence that the spectrum is excited by thermal collisions in a region protected from direct impacts of incoming air molecules. The most often encountered deviation from thermal equilibrium is the larger strength of low-excitation low-transition-probability lines. These lines are typical for the radiation of meteor wakes (see below). Their enhanced brightness in the head is probably caused by the fact that they originate in larger volume than normal lines with high transition probabilities.

The second spectrum is nearly consistent with thermal equilibrium as well, although the limited number of lines of the same element prevents to verify this assumption in detail. The higher temperature and the distinct nature of this spectrum suggest its connection with the shock wave. However, also species radiating in this spectrum do not seem to be excited by direct impacts. Direct impacts can

be responsible for the N II and O II lines. N II and O II lines would require much higher temperature than 10 000 K, if they were excited by thermal processes. On the other hand, the kinetic energy necessary for dissociation, ionization and excitation of nitrogen in the N_2 molecule (45 eV) is achieved already at the velocity of 18 km s^{-1}. The fireballs Benešov and Kouřim (Borovička and Spurný, 1996) really exhibit short ($<10^{-3}$ s) flares of N II radiation, although the velocity of these fireballs was not particularly high (21 and 27 km s^{-1}, respectively). The presence of O II and even O III lines in spectra of Perseid meteor trains (Borovička et al., 1996) confirms the production of highly ionized atoms in fast meteors.

A theoretical understanding of the above observations is not very advanced yet. Nemtchinov et al. (1994, 1995) concluded on the basis of hydrodynamical calculations that the radiation of the air compressed and heated in the shock wave is the source of the meteor luminosity in the continuous flow regime. Later, meteoric vapors were incorporated into the model and theoretical spectra were simulated (Golub et al., 1996, 1997). The primary radiation of shock heated air was shown to be absorbed and re-radiated by the cooler vapors producing a continuous spectrum with superimposed vapor lines. Detailed comparison with the observed spectrum of the very bright Benešov bolide (Borovička et al., 1998) showed qualitative agreement, but the continuum level is lower in the observed spectrum, and significant differences in individual line intensities remain. The observation suggests that the vapor volume was much larger and density lower than predicted by the model. The continuum can be interpreted as due to thermal collisions in the vapor region (Borovička and Spurný, 1996), and the question whether the ablation is driven by the UV radiation of the shocked air (as predicted in the model) remains open.

3.3.1. *Spectra of Meteor Wakes and Trains*

The spectrum of a meteor wake is different from the spectrum of a meteor head. Thermal equilibrium cannot be used even as a first approximation for radiation of meteor wake. The dominant characteristic for wake spectrum are intercombination lines, i.e., lines with low excitation and small transition probability. These include Mg I – multiplet 1, Ca I – multiplet 1, and Fe I – multiplets 1, 2, 3. Intercombination lines have the slowest decay and are visible toward the very end of the wake. Besides them, low excitation lines (which are strong and optically thick in the head) are also strong in the first part of the wake (e.g., Na I – multiplet 1). The classification of multiplets according to their duration and intensity in the wake was presented by Halliday (1968).

A wake is formed by gas that is quickly decelerated relatively to the meteoroid. Thermal collisions are rare in this cooling gas and radiative processes are decisive for level populations which results in a non-equilibrium state. Wake is typical for the upper part of fireball trajectories. At lower heights, wake of another character (an apparent wake) can be formed by tiny droplets and solid fragments separated from the meteoroid and evaporating subsequently. In this case the spectrum is sim-

ilar to spectra of faint meteors. Faint television meteors seldom exhibit detectable wake (Shadbolt and Hawkes, 1995).

The radiation mechanism of meteor trains is less well understood. Trains with duration up to 3 s are produced by the forbidden auroral line of neutral oxygen at 5577 Å. This type of train is typical for faint and fast meteors such as Perseids (Halliday, 1960a; Millman et al., 1971), but has been observed also in faint Geminids (Millman and Clifton, 1975). The line starts to radiate with some delay after the meteor passage and reaches the maximal intensity at higher heights than the meteor. Occasionally, long enduring trains can be caused by bright meteors. Forbidden lines of ionized oxygen and sulphur were identified in their spectra together with lines of neutral atoms (Borovička et al., 1996).

3.3.2. *Summary*

We can summarize that meteor spectra in general do not exhibit large differences and can be described in terms of several parameters, at least to the first approximation. The main differences are the strength of the second spectrum relatively to the main spectrum, which depends on velocity and mass, and the relative strength of atmospheric and meteoric emissions in the second spectrum. Temperatures do not show dependence on velocity. The main spectrum is rich and optically thick in many lines in bright meteors and poorer in faint meteors. Exceptionally bright meteors can become optically thick also in thermal continuum and can produce continuous radiation. The enhancement of intercombination lines is another obvious effect in some spectra. The differences in chemical composition of the meteoroid and/or the radiating gas produce additional differences. These are discussed in Section 5.3. Up to now, no self-consistent model of meteoroid ablation and radiation explaining the observed spectra has been developed.

3.4. INTEGRAL LIGHT

3.4.1. *Traditional Differential Luminous Efficiency*

Most meteors are observed in integral light and their spectra are not available. Besides tracking the meteoroid's trajectory and dynamics, we like to use the light to obtain the meteoroid's initial mass and its mass loss along the trajectory. The use of light for these purposes is based on the fact that a fraction of the meteoroid kinetic energy is transformed into radiation during the meteor flight. We can therefore write

$$I = \tau \frac{\mathrm{d}E_k}{\mathrm{d}t}, \tag{27}$$

where I is the meteor luminosity, E_k is the meteoroid kinetic energy and τ is the luminous efficiency. In most cases, the energy loss is dominated by ablation

which leads to the classical luminous equation relating mass loss (ablation) and luminosity:

$$I = -\tau \frac{v^2}{2} \frac{\mathrm{d}m}{\mathrm{d}t}. \tag{28}$$

In general, however, the term of energy loss due to deceleration should be included:

$$I = -\tau \left(\frac{v^2}{2} \frac{\mathrm{d}m}{\mathrm{d}t} + mv \frac{\mathrm{d}v}{\mathrm{d}t} \right) = -\tau \left(1 + \frac{2}{\sigma v^2} \right) \frac{v^2}{2} \frac{\mathrm{d}m}{\mathrm{d}t}. \tag{29}$$

Here, the ratio of deceleration from Equation (1) and mass-loss from Equation (2) are used and σ is the ablation coefficient. The term $2/(\sigma v^2)$ is important for slow meteors with a small ablation coefficient. The precision of meteor photometry is usually of the order of 50% in I (± 0.4 mag). In this sense, the deceleration term is only significant for meteors with $v < 16$ km s^{-1} and $\sigma < 0.016$ s^2 km^{-2}. On the other hand, the possibility exists that the luminous efficiency is different for the ablation and deceleration term but both efficiencies could not be separated from observations (Pecina and Ceplecha, 1983). We will therefore consider one global τ as in Equation (27).

The luminous efficiency is by no means a constant, it depends on many parameters. From the discussion of meteor spectra in the previous section it is evident that a hypothetical slowly moving meteoroid composed only from elements like H, C, N, O would emit practically no visible light (perhaps except for some faint molecular bands), because these elements have no spectral lines in the main spectral component. However, the same meteoroid at higher velocity would emit near infra-red and visible lines of H, N, and O in the second spectrum. In this case, the N and O emissions of atmospheric origin could also appear, even in the absence of ablation. It is therefore clear that the luminous efficiency depends on the spectral region of observations, on chemical composition of the meteoroid and the atmosphere, on meteoroid velocity and probably also on the mass.

Before discussing the values of τ, we will discuss its units, a question that is also closely related to the spectral region of observation. In Equation (27), τ is dimensionless and I is given in energetic units (erg s^{-1}) $\equiv$ (10^{-7} W), i.e., the luminosity is taken to be the total energy emitted across the whole electromagnetic spectrum. In practice, meteors are observed in a limited spectral region (photographic, visual) and their brightness is usually expressed in absolute (100 km distance) magnitudes, M, as determined through comparison with stars. We can define the magnitude-based luminosity as

$$I_V^* = 10^{-0.4 M_V}. \tag{30}$$

For luminosity defined in this way, the system in which the magnitude is measured must be specified. Here we used the V-band magnitude. The corresponding luminous efficiency is τ_V^* in units (0 mag erg^{-1} s). If I_V^* and τ_V^* are known, the luminous

equation can be used with these quantities. However, for a theoretical considerations we need to know the conversion to the energetic units. The conversion factor generally depends on the meteor spectrum.

A meteor spectrum can be described by the function I_ν – the intensity of meteor radiation (erg s^{-1} cm^{-2} $ster^{-1}$ Hz^{-1}) at frequency ν. It is given by

$$I_\nu = B_\nu(T)\,(1 - e^{\eta_\nu}). \tag{31}$$

Here $B_\nu(T)$ is the Planck function at temperature T and η_ν is the optical depth at frequency ν (we use the notation η_ν instead of usual τ_ν to avoid misidentification with the luminous efficiency). Here we consider only the main spectral component. In the centers of bright lines $\eta_\nu \gg 1$ and $I_\nu = B_\nu$, where B_ν is the limiting intensity. The actual values of η_ν in spectral lines are given by Equation (25).

Assuming for simplicity that the meteor is of sperical shape of radius r, then its total luminosity is

$$I = 4\pi r^2 \int_0^\infty I_\nu \, \mathrm{d}\nu. \tag{32}$$

We define the filling factor $f_{\nu_1}^{\nu_2}$ between frequencies ν_1 and ν_2 as

$$f_{\nu_1}^{\nu_2} = \frac{\int_{\nu_1}^{\nu_2} I_\nu \, \mathrm{d}\nu}{\int_{\nu_1}^{\nu_2} B_\nu \, \mathrm{d}\nu}, \tag{33}$$

$f_{\nu_1}^{\nu_2}$ is always ≤ 1. It is clear that for small intervals $\langle \nu_1, \nu_2 \rangle$ the filling factors will be very different depending on which lines are present inside the interval. However, for wide passbands in case of bright meteors which contain a lot of randomly distributed lines, the filling factors will be very similar and will converge to the global filling factor f_0^∞ (further denoted simply as f).

Using the filling factor, the total luminosity can be rewritten as

$$I = 4\pi r^2 f \int_0^\infty B_\nu(T) \, \mathrm{d}\nu = r^2 f a c T^4, \tag{34}$$

where $a = 7.65 \times 10^{-15}$ erg cm^{-3} K^{-4} is the radiation constant. This equation could in principle be used, if we estimated T, r, and f from the meteor spectrum. However, in most cases, only the meteor magnitude is known.

If the meteor is observed from the distance R, the radiation flux is

$$F_\nu = \pi I_\nu \left(\frac{r}{R}\right)^2. \tag{35}$$

The magnitude M_V is given by (Allen, 1973):

$$M_V = -2.5 \log \left(\int_0^\infty V_\lambda F_\lambda \, \mathrm{d}\lambda \right) - 13.74, \tag{36}$$

where F_λ is given in erg cm^{-2} s^{-1} Å^{-1} and V_λ is the V filter passband (reaching unity near 5300 Å and dropping on both sides, see, e.g., Bessel (1990) for the function). Using Equations (35) and (36) we obtain for $R = 100$ km

$$I_V^* = 9.84 \times 10^{-9} \, r^2 f \int_0^\infty V_\lambda B_\lambda(T) \, \mathrm{d}\lambda \tag{37}$$

and the ratio of physical to magnitude-based intensities is

$$\frac{I}{I_V^*} = \frac{2.30 \times 10^4 T^4}{\int V_\lambda B_\lambda(T) \, \mathrm{d}\lambda}. \tag{38}$$

Analogical equation can be written also for B band based magnitudes – the constant will be 4.68×10^4. Numerical values of the conversion factors I/I_V^* and I/I_B^* for various temperatures are given in Table VI.

The conversion factors have been derived under the assumption that the local and global filling factors are nearly the same. This can be reasonably assumed only for the main spectrum in bright meteors. Both the second spectrum and the main spectrum in faint meteors contain too few lines for the extrapolation from the wavelength limited measurement to the total energy output to be done without really modeling the whole electromagnetic spectrum. So, only the values for temperatures around 4000 K in Table VI are useful in practice.

To determine the actual values of the luminous efficiency, we need to know the mass loss rate $\mathrm{d}m/\mathrm{d}t$ for some meteors independently of the photometry. From a good quality fireball spectrum, the total mass, m_G, of meteoric vapors in the radiating volume (of the main spectrum) can be derived. This is done by correcting the observed absolute abundances of atoms for ionization and adding the mass of unobservable elements using the known or assumed chemical composition of the meteoroid. However, this tells us nothing about the mass loss rate because we do not know the time the evaporated atoms spend in the radiating volume. This time was called the relaxation time, t_R, by Ceplecha (1973). The mass loss rate is then

$$\frac{\mathrm{d}m}{\mathrm{d}t} = \frac{m_G}{t_R}. \tag{39}$$

The upper limit of the relaxation time for a particular meteor can be estimated from the duration of meteor flares. This method was applied to two bright Perseids by Borovička and Betlem (1997) yielding $t_R \approx 0.011$ s, $\log \tau_V^* = -11.9$, and

TABLE VI

Radiative energetical output (erg s^{-1}) $\equiv$ (10^{-7} W) in whole electromagnetic spectrum and to all directions of a meteor of zero absolute V-band or B-band magnitude, assuming many-line spectrum produced at the temperature T

T	I/I_V^*	I/I_B^*
3000	5.37×10^{10}	2.77×10^{11}
4000	1.95×10^{10}	6.13×10^{10}
4500	1.50×10^{10}	4.00×10^{10}
5000	1.28×10^{10}	2.96×10^{10}
6000	1.10×10^{10}	2.06×10^{10}
8000	1.13×10^{10}	1.64×10^{10}
10000	1.38×10^{10}	1.71×10^{10}
15000	2.57×10^{10}	2.64×10^{10}

$\log \tau_P^* = -11.4$ (panchromatic). The higher luminous efficiency for the panchromatic magnitude is caused by the very bright Ca II lines. Transformation to the absolute units for the whole electromagnetic spectrum is not possible in this case due to the dominance of only few spectral lines.

In principle, the mass as a function of time can also be obtained from the solution of meteor motion (the dynamic mass). However, the solution depends on the assumed drag coefficient, shape factor and bulk density. Therefore, to estimate the mass changes we have to know either the initial or the terminal mass of the meteoroid. This has been possible only for artificial meteors and for photographed meteorite falls.

Thus the luminous efficiency is still not a well known quantity, even if it has been studied since the classical work of Öpik (1933, 1955, 1963). Luminous efficiency was usually taken to be a function of meteoroid velocity. Two different scales for luminous efficiencies were proposed for meteors photographed within photographic fireball networks. For small velocities, McCrosky used luminous efficiencies published by Ceplecha and McCrosky (1976) based on artificial meteor experiments with iron masses of the order of grams (Ayers et al., 1970). For higher velocities, he used direct proportionality of luminous-efficiency to velocity (proposed originally by Öpik) calibrated by Jacchia's results from Super-Schmidt meteor studies (Jacchia et al., 1965). Halliday et al. (1981, 1984) used the Innisfree meteorite fall and its fireball records to determine luminous efficiencies that are significantly higher than the ones for gram-mass bodies, and that also are depending on the mass of individual meteorite fragments.

A new analysis of the atmospheric motion and ablation of the Lost City fireball (with a recovered meteorite fall) has been performed quite recently (Ceplecha, 1996a) using its original photographic records re-measured at the Ondřejov Observatory by Keclíková. Continuous and discrete fragmentation of the body was taken into account using the gross-fragmentation model. From the residuals of this model, the initial rotation of the body was determined by Adolfsson (1998). These procedures explain the atmospheric motion and ablation of the Lost City fireball in a self-consistent way without any discrepancy remaining (Table VII). The initial dynamic mass $m = 163 \pm 5$ kg and the resulting change of mass with time (rate of ablation) were used for evaluation of the luminous efficiency yielding values of 6.1% at $v = 13$ km s^{-1} and 1.2% at 4 km s^{-1} for a temperature of the source 4500 K. These values are about 10× larger than the already mentioned values determined from artificial meteors produced by gram masses fired downward from high-altitude rockets by shaped-charges (Ayers et al., 1970). Note that these results apply only to low velocity meteors and of iron or stony composition.

3.4.2. *ReVelle's Differential (Instantaneous) Radiation Efficiency*

The differential power relation utilized in ReVelle (1980) was that developed earlier by ReVelle and Rajan (1979), with τ_{cfv}, the differential (instantaneous) luminous efficiency, P_L, the instantaneous light power produced over all wavelengths and E_k, the source kinetic energy, and M_p, the photographic stellar magnitude (with the traditional 'color' index $= -2$ assumed) in the form:

$$P_L = -\tau_{cfv}\frac{\mathrm{d}E_k}{\mathrm{d}t} = 10^{-0.4(M_p+2)+9.72}. \tag{40}$$

For many years this type of relationship was used to compute the so-called photometric mass of meteors using an empirically-based differential luminous efficiency value (Ceplecha and McCrosky, 1976), but with the power loss resulting solely from an entry with negligibly small deceleration ($\mathrm{d}v/\mathrm{d}t = 0$). ReVelle and Rajan (1979) used this relation in combination with the entry dynamics model of ReVelle (1979) to compute the differential luminous efficiency of the three photographed and recovered chondritic meteorites with available data at that time. It was this comparison that ultimately led later authors to use a revised photometric mass for fireballs some 20 times smaller than that suggested using the older, empirical differential value of the luminous efficiency.

Öpik suggested to ReVelle the name *radiation efficiency* rather than the more conventional term luminous efficiency in order to emphasize the very broad wavelength range considered so that a correct interpretation could still be made by the conventional observers of meteors and meteor-fireballs (a limited wavelength photographic passband approach).

TABLE VII

Model of continuous and gross fragmentation (Ceplecha et al., 1993), and of rotation of meteoroids (Adolfsson, 1998) applied to observed distances and heights as function of time

Precision of two independent least-squares fits on partly superposing time intervals (135 measured points):	
Standard deviation	
for one measured point	$\pm$ 21 m
including rotation	$\pm$ 18 m
Initial velocity	14.1485 $\pm$ 0.0012 km s^{-1}
Ablation coefficient from	0.0146 $\pm$ 0.0004 s^2 km^{-2}
to	0.0114 $\pm$ 0.0003 s^2 km^{-2}
Initial mass	163 $\pm$ 5 kg
Terminal mass	9.79 $\pm$ 0.86 kg
The largest recovered meteorite	9.83 kg
ΓA	1.10 $\pm$ 0.04 (c.g.s.)
Initial rotation period	1 rotation per 3.3 $\pm$ 0.3 s
Flatness	2.1 $\pm$ 0.4
Maximum head cross-section at	h = 40.7 $\pm$ 1.1 km
Drag coefficient Γ	0.7 $\pm$ 0.1
The first gross-fragmentation at	h = 40.74 $\pm$ 0.08 km
with stripped-off mass of	59.0% $\pm$ 1.9%
The second gross-fragmentation at	h = 21.89 $\pm$ 0.25 km
with stripped-off mass of	49.9% $\pm$ 2.3%
Luminous efficiency at v = 13 km s^{-1}	log τ = –11.4 $\pm$ 0.2
Luminous efficiency at v = 4 km s^{-1}	log τ = –12.1 $\pm$ 0.3
(c.g.s. units with $I = 1$ for 0 stellar magnitude)	
For 4500 K corresponds to:	
6.1% of total kinetic energy of mass loss at 13 km s^{-1}	
1.2% of total kinetic energy of mass loss at 4 km s^{-1}	

3.4.3. *Integral Radiation Efficiency*

ReVelle used the integral of the light produced over all wavelengths compared to the total power output of a bolide at its conventional end height (McIntosh, 1970; ReVelle, 1979, 1980), i.e., where the bolide is no longer luminous to the eye or to its photographic recording, in order to compute this quantity.

If the direct connection is made between power output from a bolide and the light produced by the interaction with the atmosphere over all possible radiative wavelengths, then the inverse of the ratio of these two components as evaluated over the entire flight that was defined by ReVelle (1980) to be the integral radiation

efficiency of the bolide. This was accomplished assuming that the decay of the meteoroid kinetic energy could be uniquely separated in the form:

$$E_k = E_{k\infty} \exp(-D) \; ; \qquad D = \alpha + \beta. \tag{41}$$

The term involving α accounts for kinetic energy depletion due to ablative processes, whereas the term involving β accounts for energy removal due to air drag processes. Although not proven in ReVelle (1980), this linear separation assumption is in fact easily and directly verifiable.

Using the definitions of the efficiencies of light, heat, ionization and of compressional (acoustical) waves, ReVelle was able to formulate an integral radiation efficiency of light production, τ_L, in terms of P_L, the light power radiated in a specified electromagnetic passband, E_∞, the initial kinetic energy and E_E, the terminal value of the kinetic energy and t is time along the trajectory as

$$\tau_L = \frac{\int P_L \, \mathrm{d}t}{E_\infty - E_E}. \tag{42}$$

The computed values of the light efficiency ranged over a factor of about 4 for the Přibram, Lost City and Innisfree meteorite observations depending on the absolute energy conversion (color index and scale factor relative to observations of the sun in the same passband), the nominal efficiency ranged from about 0.2–5% of the original kinetic energy of the body. No quantum mechanical calculations were performed as Öpik had done much earlier, but instead observations of the ratios of the other individual efficiencies were directly utilized (and assumed constant). Thus, ReVelle concluded that about 99% of the initial kinetic energy of the bolide was consumed during the entry process according to this approach. This approach led to other papers which culminated in the complete numerical solution to the problem in ReVelle (1993) and not the earlier analytic approach described above, which was only 'exact' in the limit of $\sigma v^2/2 <\approx 6.25$, with σ being the ablation coefficient.

ReVelle also subsequently applied the method to the US Prairie Network fireballs with good dynamic data so that a more reliable initial mass could be computed during the computation of the initial kinetic energy of the body (prior to entry into the atmosphere) as discussed in Ceplecha (1980). The analysis clearly showed two important facts in a way that had not previously been addressed. First the fireballs clearly separated into groupings as shown earlier by Ceplecha and McCrosky (1976). Group I and II were overlapping somewhat, but even statistically their end heights were only different by about 3 to 5 km even in the original discovery paper of Ceplecha and McCrosky. Secondly, the analysis clearly showed that the group III were quite anomalous in their light production behavior with computed efficiencies exceeding 100% in many cases. Part of this discrepancy was explained by the fact that the computed masses that were considered by Ceplecha (1980) were not the 'true' initial masses, but instead were only an approximate mass computed purely from the dynamic mass at the end height and scaled by simple ablation theory to

the 'top' of the atmosphere to be used for relative comparison purposes. ReVelle (1979) had earlier determined that these mass estimates were about 3 to 4 times smaller than those determined using his detailed height and velocity dependent entry model, i.e., a model of variable ablation coefficient, rather than the simple ablation theory with a constant (height-averaged) ablation coefficient. Thus, the predicted integral radiation efficiency for group III fireballs is actually only about 50 to 75% and not 200 to 300% as computed in Ceplecha (1980) and used as a demonstration of clearly wrong concept of theoretical description of meteor radiation.

Values of total luminous efficiencies in a panchromatic pass band (from ≈ 3600 – 6700 Å) for the brightest PN fireballs on record (brighter than absolute magnitude –10) are given in Table VIII (Ceplecha et al., 1996) together with more data on each fireball as they resulted from application of the gross-fragmentation model. Symbols used for classification (type) of each fireball is explained in Section 5.2. Note substantially smaller value for the Lost City fireball (PN 40590), if compared with its differential luminous efficiency for 13 km s^{-1} in Table VII. Averaging over the whole trajectory (smaller values of luminous efficiency for lower velocities), and definition of the differential luminous efficiency containing only the dm/dt part of the time change of the kinetic energy, are responsible for this. Units of energy in Table VIII are kT TNT (4.185×10^{12} J).

3.4.4. *The Integral Radiation Efficiency: Future Efforts*

Future efforts should be directed at defining the various conversion efficiency ratios (differential and integral values) as a function of mass and velocity of the body, both experimentally and using sophisticated hydrodynamic blast wave codes. This will allow an evaluation as a function of the flow regime encountered during entry. In addition, a method described in Cox (1958) and used by Brown et al., (1996) (for the analysis of the source energy of the St. Robert meteorite fall; see Equation (59)), utilizes the acoustic efficiency concept to make an estimate of the source energy of the event. Using the historical record of the infrasonic data presented in ReVelle (1995), where horizontal range, signal duration, signal amplitude as a function of time, etc. are well known, we can now calculate the acoustic efficiency ratio experimentally as well. An independent estimate of the source energy can be provided by the US Air Force Source energy-period at maximum amplitude relation mentioned earlier, which has been independently calibrated by seismic methods for meteorites that also impacted the earth. If this calculation proves to unify the range of probable values for the various fireball events, we will then be in a position to reverse the process and compute the source energies on the basis of knowledge of the acoustic efficiency, using period at maximum amplitude and using the wind normalized source energy range relation given by Equations (56) and (57).

TABLE VIII

43 PN bolides brighter than magnitude –10: No. ... number of the bolide, classification 'type' of the bolide, σ ... ablation coefficient, v_∞ ... initial velocity, m_∞ ... initial mass, E_∞ ... initial kinetic energy, $\int I\,\mathrm{d}t$ ... total radiated energy, $M_{\max}$ ... maximum absolute magnitude, τ_t ... total luminous efficiency

No.	Type	σ $s^2\ km^{-2}$	v_∞ $km\ s^{-1}$	$\log m_\infty$ kg	$\log E_\infty$ kT TNT	$\log \int I\,\mathrm{d}t$ kT TNT	$M_{\max}$ abs. mag.	τ_t %
39043	IIIA	0.084	23.769			–5.768	–10.80	
39048	IIIB	0.19	22.143	1.077	–3.156	–5.190	–12.65	0.92
39049	IIIA		31.8			–5.559	–10.60	
39080A	I	0.0128	32.53	0.468	–3.430	–4.449	–12.80	9.58
39085	II	0.023	28.51			–5.196	–11.40	
39093B	IIIA	0.074	18.415	0.887	–3.505	–5.527	–12.30	0.95
39113A	II	0.040	15.117	1.892	–2.672	–5.102	–11.05	0.37
39115B	II	0.043	29.72			–6.009	–10.94	
39122	I	0.0035	22.30			–4.677	–12.25	
39240	I	0.011	17.254	1.201	–3.248	–4.933	–11.40	2.06
39259	II	0.061	18.793	0.825	–3.550	–5.148	–10.60	2.52
39276	IIIB	0.16	25.71	–0.319	–4.421	–5.825	–10.65	3.95
39337A	IIIAi	0.123	38.56	0.076	–3.675	–4.814	–14.00	7.25
39363	I	0.0179	27.245	0.391	–3.661	–5.267	–10.35	2.48
39382	I	0.014	33.29	0.693	–3.185	–5.342	–10.65	0.70
39403	IIIB	0.13	25.89	0.348	–3.748	–4.890	–12.05	7.22
39404	I	0.012	15.436	0.344	–4.201	–5.237	–10.70	9.20
39406A	II	0.032	17.228	1.864	–2.586	–4.112	–15.70	2.98
39406B	IIIA	0.054	23.54	–0.678	–4.857	–5.934	–10.65	8.38
39423	I	0.0092	34.22			–5.340	–10.75	
39425	II	0.039	19.73	1.332	–3.001	–4.832	–11.25	1.47
39434	I	0.0137	14.307	3.463	–1.149	–3.446	–14.20	0.50
39450	I	0.002	24.51	0.679	–3.466	–5.129	–11.70	2.17
39457	II	0.051	21.39	0.179	–4.083	–5.856	–10.90	1.69
39535E	I	0.0108	43.01	0.130	–3.525	–5.124	–11.55	2.52
39708A	IIIAi		60.5			–6.190	–10.35	
39728	II		67.2			–5.805	–10.39	
39794B	II	0.051	21.83	1.363	–2.882	–5.380	–10.22	0.32
39874	II	0.031	20.28	1.671	–2.637	–5.155	–10.25	0.30
39893A	I	0.0153	33.086			–5.069	–11.22	
39907	II		60.95			–5.263	–11.66	
39910	I	0.019	21.95	0.348	–3.892	–5.090	–11.24	6.33
39911	I	0.0187	30.57	1.679	–2.274	–4.332	–13.22	0.87
39935	I	0.0013	17.75	1.348	–3.077	–4.683	–11.30	2.48
39988	II	0.026	34.80	–0.620	–4.459	–5.592	–10.88	7.37
40151	I	0.011	13.45	1.524	–3.142	–4.741	–11.21	2.52
40161	II	0.053	16.873	2.406	–2.063	–4.774	–10.29	0.19
40405	II	0.022	14.697	1.819	–2.769	–4.995	–10.31	0.59
40425	II	0.041	25.67	1.104	–2.999	–5.580	–10.49	0.26
40503	II	0.022	20.86	3.281	–1.004	–2.380	–20.00	4.20
40590	I	0.0142	14.149	2.212	–2.409	–4.219	–12.42	1.55
40660B	I	0.0079	26.336	1.015	–3.067	–5.164	–10.37	0.80
41157B	I	0.017	33.25	1.419	–2.460	–4.785	–12.12	0.47

3.5. IONIZATION

3.5.1. *The Ionized Trail Formation*

The ionization produced by inelastic collisions of the vaporized atoms of a meteoroid with air molecules can be described in terms of the rate of loss of mass of the meteoroid and the number of free electrons, β, produced per vaporized meteor atom. The number of electrons produced per meter from a meteoroid of mass m, moving with speed V, is

$$q = -\frac{\beta}{\mu V}\frac{\mathrm{d}m}{\mathrm{d}t}, \tag{43}$$

where μ is the average mass of an ablated meteoroid atom. The quantity β depends strongly on the relative speed in an atom – molecule collision (Massey and Sida, 1955; Sida, 1969; Massey, 1982) for $V > 35$ km s^{-1}, and can be written $\beta = \beta_0 V^n$, where n lies between 3 and 4. A comprehensive survey by Bronshten (1983) of the quantities involved in this expression, led to $\beta_0 = 3.02 \times 10^{-17}$, $n = 3.42$, when V is in m s^{-1}. For $V < 35$ km s^{-1}, Jones (1997) has developed the following expression for the ionization coefficient of faint radio meteors: $\beta = 9.4 \times 10^{-6}(v - 10)^2 v^{0.8}$, where the value of v is in km s^{-1}. Following Love and Brownlee (1991), the value of the mean atomic mass of the evaporated atoms is taken as 40.

The majority of meteor trails detected by radar are produced by meteoroids of mass smaller than 10^{-5} kg (radius $\sim$ 0.1 cm), and ablation studies show that such individual trails extend over a height range of 10–15 km. For radar studies of meteors distribution of the ionization density along the trail can be considered as a parabolic function of the density of the atmosphere about the height of maximum ionization. The maximum value of the line density of the ionization (electrons per meter) is proportional to the initial mass of the meteoroid and to cos χ where χ is the zenith angle of the trail.

From a comparison of simultaneous visual and radar observations of meteors Kaiser (1953) found that a trail with q electrons per meter is related to its visual magnitude M by the formula, $M = 40.0 - 2.5 \log q$. This formula is valid for trails formed by meteoroids with velocities of about 40 km s^{-1}. McKinley (1961) suggests that a more general expression is $M = 36 - 2.5(\log q - \log V)$ where V is the velocity in km s^{-1}.

The beginning heights of trails formed by small single particle stony meteoroids were calculated following methods developed by Jones and Kaiser (1996) and Love and Brownlee (1991). Extensive modeling of the ablation of meteoroids with masses $< 10^{-4}$ kg entering the Earth's atmosphere showed that significant mass loss occurs when the surface temperature reaches about 1850 K; this criterion was used to generate the beginning heights plotted in Figure 4. The lines marked $M = 15$ and $M = 10$ are the locus of trails with these approximate maximum magnitudes or the equivalent maximum line densities 10^{10} and 10^{12} electrons per meter respectively. Particles whose masses are less than 10^{-7} to 10^{-8} kg are sufficiently small that during heating their interior temperature is within a few degrees

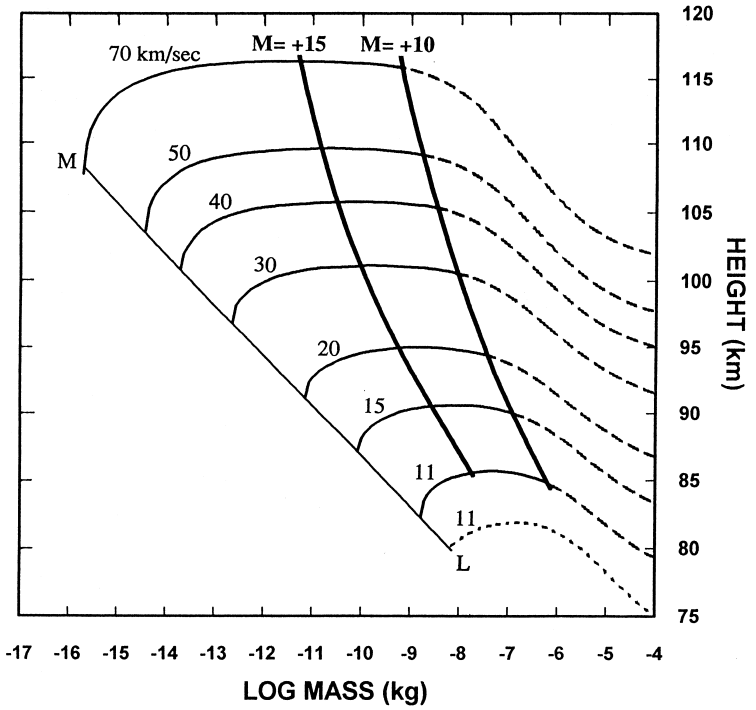

Figure 4. Plots of the theoretical heights of commencement of ablation of single stony particles entering the atmosphere at a zenith angle of 45°, as a function of mass and velocity. The heavy lines give the mass and velocity of particles that produce trails of maximum line density 10^{10} and 10^{12} electrons per meter (radio magnitudes $\sim$ +15 and +10). The line ML is the micrometeoroid limit. Values are calculated for the CIRA–86 atmosphere, June 45° N, except for the dotted curve for 11 km s^{-1} that applies in December. For discussion of dashed curves see text.

of their surface temperature and the energy loss due to radiation cannot be ignored. A balance between radiation and heating occurs for particles whose masses lie at the extreme edge of the plot, which thus defines the micrometeoroid limit.

The graphs to the right of $M = 10$ in Figure 4 are drawn as broken lines as the observed beginning heights of meteors brighter than magnitude +10 do not fall away with increasing mass as suggested by the plots, but tend to occur at heights similar to meteors fainter than magnitude +10 with the same velocity. This is attributed to continuous fragmentation or dustball nature of the meteoroid (Hawkes and Jones, 1975).

The height of maximum ionization for a faint meteor can be determined from ablation theory, and plots of the predicted heights as a function of velocity for meteors of line densities 10^{10} and 10^{12} electrons per meter are shown in Figure 5.

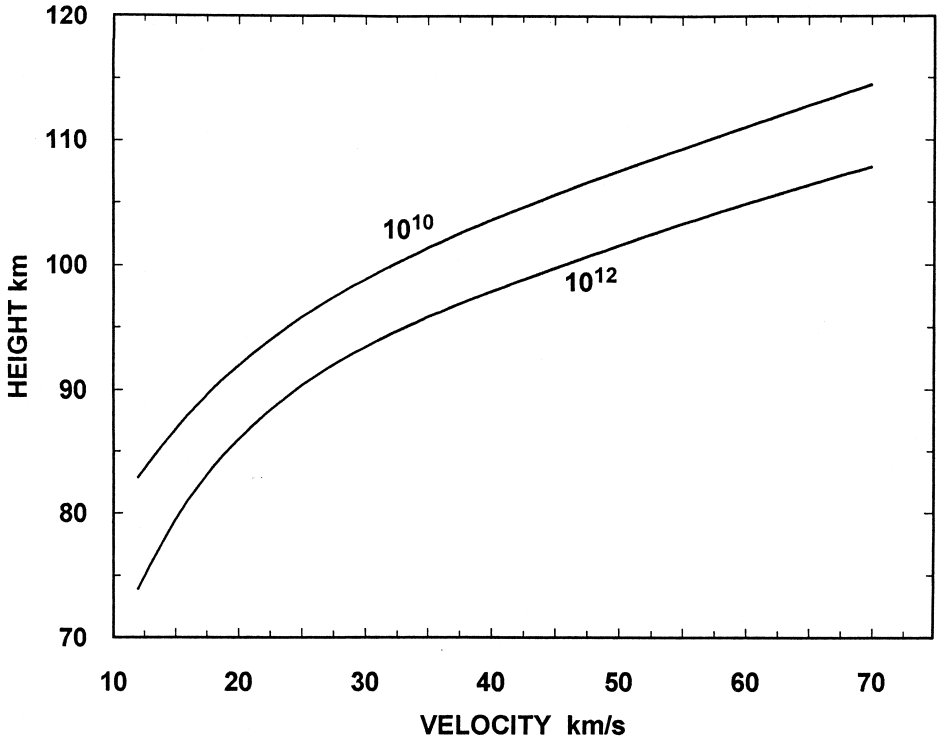

Figure 5. Height of point of maximum ionization as a function of velocity, plotted for two values of maximum line density of ionization, 10^{10} and 10^{12} electrons per meter (mag. +15 and +10, respectively, at 40 km s^{-1}).

3.5.2. *Initial Radius and Initial Temperature of the Ionized Trail*

Collisions reduce the thermal velocity of the ionized meteor atoms to ambient values in a time less than a millisecond at 100 km (Massey and Sida, 1955; Bronshten, 1983; Jones, 1995). Estimates of the initial radius of the plasma column have been determined both theoretically and experimentally. Theoretical analysis of collision cooling indicates that the initial radius, r_0 can be expressed as $\rho^a v^b$, where ρ is the density of the atmosphere, $a \sim -1$, and $b \sim 0.8$ (Bronshten, 1983). However, Öpik (1958) and Hawkes and Jones (1975) suggested that continuous fragmentation of rotating dust-ball type meteoroids will produce a lateral spread of ablating particles and hence increase the initial radius. This effect opposes the tendency for the radius to vary as ρ^{-1}.

Using a computer simulation based on collisions between elastic spheres, Jones (1995) showed that the ablated ions reach thermal equilibrium after about 10 collisions, and he defined the initial radius r_0 at this time as the r.m.s. value of the radial positions of the ions. He also found that the initial ionization distribution is not Gaussian but has a higher density core of radius of the order of $0.4\,r_0$ immersed in a more diffuse distribution. The value of r_0 varies as ρ^{-1}. In contrast, radio

TABLE IX
Values of initial radius in meters

Height	Experimental				$v = 40$ km s^{-1}	
km	$v = 20$ km s^{-1}	40 km s^{-1}	60 km s^{-1}	Bright	Theory ($1/\rho$)	$r_{0(\mathrm{eff})}$
75	0.22	0.33	0.42	0.35*	–	–
80	0.27	0.40	0.51	0.56*	–	–
85	0.33	0.49	0.63	0.93*	–	–
90	0.41	0.61	0.78	1.62*	0.72	0.72
95	0.51	0.77*	0.98	2.83*	1.53	1.38
100	0.63	0.96*	1.23*	5.00*	3.22	2.16
105	0.79	1.20*	1.53*	8.77	6.82	2.66
110	0.98	1.49*	1.90*	–	15.6	3.10
115	1.19	1.81*	2.30	–	30.6	3.63
120	1.41	2.13	2.72	–	64.4	4.30

measurements of the initial radius of meteors of magnitude $+5$ to $+10$, based upon the assumption of a Gaussian distribution, indicate a density exponent in the range -0.25 to -0.45, while brighter meteors ($M + 2.5$) have a significantly more rapid height variation (Baggaley, 1970; Baggaley and Fisher, 1980). Jones partially resolved the inconsistency between theory and experiment by estimating an 'effective initial radius', $r_{0(\mathrm{eff})}$, that is obtained when the theoretical non-Gaussian trail is assumed to scatter radio waves as if it had a Gaussian radial distribution of ionization. Experimental values of the initial radius given in Table IX reflect the single point observations and the observed height and velocity dependence. At heights above 95 km the theoretical values of the effective radius are about twice the experimentally determined values of the initial radii.

Experimental values in the table for faint meteors can be described using the empirical relation $r_0 \propto \rho^a v^b$, where $a = -0.25$, and $b = 0.6$. For bright meteors the value of a is –0.63. Asterisks indicate radio measurements (Baggaley, 1970, 1981; Baggaley and Fisher, 1980; Bayrachenko, 1965; Kashcheev and Lebedinets, 1963). The theoretical values and $r_{0(\mathrm{eff})}$ are taken from Jones (1995) for the CIRA–86 atmosphere at 45° N.

Since the plasma column must at all times be in a condition of charge neutrality the radial distribution of the electrons will be the same as that of the thermalized ions. However, in general the electrons cool much less rapidly than the ions and can remain 'hot' for periods ranging from $\sim$ 1 ms at 80 km to $\sim$ 150 ms at 115 km (Baggaley and Webb, 1977), as shown in Table X.

The presence of 'hot' electrons increases the rate of diffusion of the ionization during the early evolution of the trail. Electrons in trails with line densities $< 2.5 \times$

TABLE X
Thermalization times of electrons (ms) (time to reach 10% of ambient temperature)

Height	Line density (m^{-1})		
(km)	$< 2.5 \times 10^{14}$	2.5×10^{15}	2.5×10^{16}
80	0.6	0.6	0.5
90	4.0	3.3	1.8
100	21	16	7.5
110	85	66	45
120	240	240	240

10^{14} m^{-1} at 110 km remain 'hot' for over 80 ms after the trail has been formed, the 'electron temperature' at 25 ms after formation being about 600 K or 2.5 times the ambient value. This increases the coefficient of diffusion of the trail by 75% (see the next section).

3.5.3. *Dissipation of the Ionization*

After the trail is formed the electron concentration will decrease because of ambipolar diffusion, atmospheric turbulence, and loss of ionization through recombination and ionic reactions. The whole trail will also be subject to large scale wind shears that cause bending and twisting of the original highly linear column. Based on radio studies of meteors, the most important dissipation factor is ambipolar diffusion, which reduces the volume density without affecting the line density. At heights below 90 km, where the effect of the Earth's magnetic field on the diffusing plasma may be ignored, the volume density of electrons (and ions) at time t and distance r from the column axis is described by the radial diffusion equation,

$$\frac{\partial n(r)}{\partial t} = D\,\nabla^2 n(r), \tag{44}$$

where D is the effective diffusion coefficient in square meters per second. For a cylindrical column of ionization with initial radius r_0, Jones (1995) has shown that, provided $4Dt \gg r_0^2$, the appropriate solution of this equation is

$$n(r, t) = \frac{q}{\pi a^2} \exp\left(-\frac{r^2}{a^2}\right), \tag{45}$$

where q is the electron line density, and $a^2 = 4Dt + r_0^2$. Jones pointed out that the inequality $4Dt \gg r_0^2$ may not always be satisfied in the early stages of diffusion.

This fact, taken together with the non-Gaussian form of the initial distribution, indicates that Equation (45) should be applied with caution when t is small.

The effective diffusion coefficient for electrons in a meteor trail, (provided the geomagnetic field can be ignored) may be written as

$$D = D_i(1 + T_e/T_i), \tag{46}$$

where D_i is the diffusion coefficient for positive ions and T_e and T_i are the electron and ion temperatures respectively (Mason and McDaniel, 1988). The ions and electrons can be considered to be in thermal equilibrium with the ambient atmosphere except in the very early stages of the formation of a meteor trail, so that T_e can be equated to T_i, and $D = 2D_i$. The diffusion coefficient D_i can be described in terms of the zero field mobility K of a group of ions, using the Einstein relation

$$D_i = kT_i\ K/e, \tag{47}$$

where k is Boltzmann's constant and e is the electronic charge. Laboratory measurements have yielded values of K for a significant number of ions in a variety of common gases. For alkali ions in nitrogen at STP a typical value is $2.2 \times 10^{-4}\,\mathrm{m^2\,s^{-1}\,V^{-1}}$, and the value changes by less than 20% per 100 K change in ambient temperature. Since K is inversely proportional to the molecular concentration of the ambient gas, the expression for the ambipolar diffusion coefficient D ($\mathrm{m^2\ s^{-1}}$) becomes

$$D = 2D_i = 6.390 \times 10^{-2}\ KT^2/p = 1.41 \times 10^{-5}T^2/p, \tag{48}$$

where p is the atmospheric pressure in pascals. Table XI gives values of D in the meteor region for mid-summer and mid-winter at some representative latitudes. Above 95 km the effect of the Earth's magnetic field can no longer be ignored and the diffusion becomes anisotropic. The values of the ambipolar diffusion coefficient listed in Table XI for heights above 95 km are the maximum values and are limited to a particular radial direction, as described below.

For electrons moving parallel to the magnetic field in the absence of positive ions, the diffusion coefficient is $D_{e\parallel} = kT/m_e\nu$, where ν is the collision frequency and m_e is the electronic mass. The Earth's magnetic field has a marginal effect on the motion of the positive ions, the value of $D_{i\perp}$ showing a small reduction compared to $D_{i\parallel}$ at heights above 110 km (3% at 110 km, 12% at 115 km, and 34% at 120 km). As $D_i \ll D_{e\parallel}$, the rate of diffusion of the meteor trail in the direction of the magnetic field is clearly controlled by the positive ions at all heights.

On the other hand, for electrons moving transverse to the magnetic field, the diffusion coefficient is given by

$$D_{e\perp} = D_{e\parallel}\ \nu^2/(\nu^2 + \omega^2), \tag{49}$$

TABLE XI

Ambipolar diffusion coefficient [m^2 s^{-1}] (pressure and temperature data taken from CIRA–1986). Reduced mobility of typical ion = 2.2×10^{-4} m^2 s^{-1} V^{-1}

Height	June				December			
(km)	60S	40S	40N	60N	60S	40S	40N	60N
70	0.24	0.17	0.11	0.10	0.09	0.11	0.16	0.22
75	0.45	0.35	0.22	0.17	0.17	0.21	0.34	0.44
80	0.90	0.72	0.43	0.33	0.31	0.42	0.71	0.89
85	2.20	1.62	0.90	0.56	0.65	0.79	1.42	1.94
90	4.53	3.30	2.12	1.55	1.35	1.83	2.81	3.82
95	9.12	7.16	5.73	5.14	4.43	4.93	6.15	7.76
100	21.0	16.9	17.0	18.5	15.9	14.6	14.5	18.0
105	51.6	42.0	50.2	61.9	53.2	43.3	36.2	44.5
110	132.4	115.7	142.4	167.7	143.5	122.7	99.8	114.3
115	357.2	356.5	373.8	369.2	318.3	317.9	307.8	308.6
120	913.1	908.3	890.5	869.1	745.3	751.6	784.7	789.9

where ω is the angular gyro-frequency. The value of $D_{e\perp}$ becomes equal to D_i at a height of about 95 km, and at greater heights rapidly becomes much less than the value for the positive ions, so that the net diffusion is controlled by the electrons, thus causing the trails to become elliptical in cross-section. This situation, with a trail formed at any arbitrary angle to the magnetic field has been analysed by Jones (1991) and the results are summarised in Figure 6. Diffusion in the radial direction lying in the plane defined by the trail and magnetic field is unaffected by the field, and this direction delineates the major axis of the elliptical cross-section. The degree of inhibition of diffusion in the orthogonal radial direction decreases steadily as the angle to the field decreases from 90° to about 5° where the trail cross-section becomes almost circular at all heights and the coefficient of diffusion has its ambipolar value. As the angle is decreased still further the diffusion coefficient falls rapidly to the value given by $2\,(D_{e\perp}^{-1} + D_{i\perp}^{-1})^{-1}$ (Kaiser et al., 1969). Thus, lifetimes of trails formed above 95 km and aligned within about 2° of the direction of the magnetic field can be many times the typical lifetime of other trails at the same height.

Immediately after formation a meteor trail has a circular cross-section defined by the initial radius. Thus, the development of significant ellipticity at heights above 95 km will take more time than inferred from a simple comparison of D_x and D_y given in Figure 6. Nevertheless, it is likely that at heights above 110 km the initial cylindrical column of ionization becomes ribbon-like before being finally dissipated by processes other than diffusion.

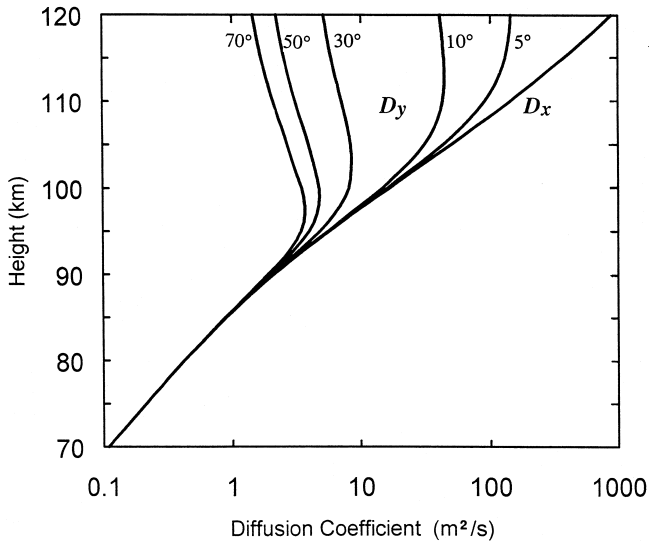

Figure 6. Diffusion coefficients plotted as a function of height. D_x applies to diffusion in the plane containing the trail and the Earth's magnetic field. D_y applies to diffusion in the orthogonal direction, and its value depends on the angle between the trail and the direction of the field, as indicated on the five curves for D_y.

The beginning and end heights of meteors detected by radar differ by 10 to 15 km, and over this height range the ambipolar diffusion coefficient changes by a factor of 4 to 10 (Table XI). This variation together with the change in initial radius with height (Table IX) causes a significant downward tapering of the trail, and earlier dissipation at the greater heights. Such effects modify the radio echoes from trails as is discussed in Section 4.

3.6. METEOR SOUNDS: UNDERSTANDING THE NATURE OF THE SOURCE AND SIMPLE ENERGY PROPAGATION CONCEPTS

Acoustic reports from the observers of large bolides have been available for a long time. They are generally of two distinct types, 'ordinary' hypersonic booms (including multiple booms) heard after a delay of one to several minutes depending on the position of the observer and electrophonic (ethaerial) sounds heard simultaneously with the flight of the body. The latter sounds have only been accepted as scientifically meaningful for about 20 years (Keay, 1980, 1993). Here we will not discuss the smaller sounds heard near the place of fall itself, so-called hissing or whistling noises as the meteorites land nearby with a thud on the ground or in a small crater, etc. (Wylie, 1932).

3.6.1. *Hypersonic Booms: 'Normal' Meteor Sounds*

Any material object moving at a speed, $V(z)$, at height z faster than the adiabatic phase speed of acoustical waves, $c_s(z)$, in a gas will generate a sonic boom wave whose energy propagates at roughly the speed of sound away from its source and which is confined to a so-called Mach cone whose half angle is $\sin^{-1}(V(z)/c_s(z))$. This description is only true for continuum and slip flow where the mean free path of the neutral gas is sufficiently small with respect to the size of the body. For meteoroids large enough to generate such effects (see Table II), typical entry speeds are from 35 to 100 times the local sound speed or even greater. Thus, in such cases the half angle of the Mach cone is so small that in reality a moving point source can be modeled as a line source of initially, nonlinear blast waves whose wavefronts are essentially perpendicular to the entry trajectory. The geometry of such waves was analyzed by ReVelle (1976) who showed that refractive effects can be very important if the angle of entry is quite steep as is typically observed. If terminal gross fragmentation occurs during entry, a point source-like type explosion can also occur and generate nearly spherical wavefronts close to the end of the trajectory.

For the point and line source cases respectively there are characteristic blast wave relaxation radii, R_0, whose magnitudes depend on the energy deposited into the fluid at the height of the source. The relaxation radii denote the extent of the explosive zone of strongly nonlinear wave behavior about the source for each specific type of source geometry. The spherical blast wave radius is proportional to the cube root of the energy deposited by the explosion, $E_s(z)$ divided by the air pressure at the source altitude, $p_s(z)$, namely:

$$R_0 = (E_s(z)/(4\pi/3)\, p_s(z))^{1/3}. \tag{50}$$

Similarly, the cylindrical blast wave radius is proportional to the square root of the energy deposited per unit length, $E_l(z)$, of the trajectory divided by the air pressure at the source altitude, namely:

$$R_0 = (E_l(z)/p_s(z))^{1/2} \approx M\, d_m \quad \text{for a non-fragmenting body} \tag{51}$$

when a single-body, hypersonic drag law ($= 0.5\,\rho(z)\, V^2(z)\, C_D A$) is substituted for E_l, with M denoting the Mach number and d_m denoting the meteor diameter (ReVelle, 1976). We have also assumed that for hypersonic flow the wave drag due to the normal stresses (also called form or pressure drag at lower Reynolds numbers in continuum flows) dominates completely over the so-called skin friction drag due to the tangential stresses. For hypersonic flows of a blunt body, the drag coefficient, C_D, has been assigned a standard value of 0.92 in (51) and γ, the ratio of the specific heat of air at constant pressure to that at constant volume has been set = 1.40, the value for a perfect diatomic gas. In addition, $\rho(z)$, is the static atmospheric density and $A(z)$, is the front cross-sectional area of the body. The shape of the body is assumed to be constant and spherical. This usage of the hypersonic drag law is an acceptable substitution in the absence of significant ablation or gross

fragmentation effects. The expectation is that the effective source 'size', d_m, will become greater with break-up than that deduced for a composite single body, but probably not exceeding twice this value, except in rare instances. For R_0 to be strictly applicable to the moving point source meteor sound problem, the meteor velocity must also be nearly constant since only flows with very small deceleration meet the dynamic flow similarity criteria for a line source explosion. For meteor-fireballs that attain continuum flow conditions, these nonlinear relaxation radii can range from a few meters to a few km (for associated sources from about 10^{10} to 10^{18} J or from about 10^{-3} kt to 100 Mt, where 1 kt $= 4.185 \times 10^{12}$ J).

The fraction of the original kinetic energy of the source converted into the acoustical energy of the remnant shock wave is called the acoustic efficiency ratio. This percentage has been determined from conventional blast wave measurements to depend slightly on range (Cox, 1958) and has also been estimated for meteor-fireballs (ReVelle, 1980; ReVelle and Whitaker, 1996a). It will be discussed briefly later with regard to modeling of the luminous efficiency of meteor-fireballs, but its numerical value is essential to an understanding of the total energy budget of the interaction.

As shown by ReVelle (1976) the frequency of the associated acoustic wave far from the trajectory is proportional to $c_s(z)/R_0(z)$. Thus, for smaller meteor sources, as discussed by Öpik (1958), the fundamental wave frequency is so large that atmospheric absorption due to molecular viscosity and heat conduction processes, etc. completely dominate the energy removal of the acoustic signal before it can propagate very far away from the source region. ReVelle (1976) has related the continuum regime blast wave radius to both the amplitude and the period of the propagating weak shock waves emanating from the trajectory. Physically, the wavelength of the near-field, acoustic frequency shock wave generated by the equivalent explosion source is about 2.81 times the line source relaxation radius, $R_0(z)$. To understand the ray theory limit of possible propagation paths, the associated acoustic characteristic velocity, $K(z)$, the Snell's Law constant of the motion (by analogy with ray optics) for spherical or cylindrical geometry at each source height must be computed. In a perfectly stratified (range independent medium), steady state fluid, both $K(z)$ and the heading of the wave normal are constants of the wave motion. The characteristic velocity, $K(z)$, of a point source and a line source at any height depends on $c_s(z)$, on the elevation angle of the wave normal, $\Theta(z)$, on the horizontal wind speed at each altitude, $V_H(z)$ and on the vector heading azimuth of the wave, $\Phi(z)$, relative to the prevailing vector wind direction, $\Psi(z)$. For a perfectly stratified, steady state atmosphere these can be expressed through the relationships:
Point source:

$$K(z) = c_s(z)/\cos\Theta + V_H \cos[\Phi(z) - \Psi(z)]. \tag{52}$$

Line source; if $V(z) \gg c_s(z)$:

$$K(z) = \Delta\ (c_s(z)/\cos\Theta) + V_H \cos[\Phi(z) - \Psi(z)], \tag{53}$$

where

$$\Delta = [\cos^2\Theta + (1 - 2\,\delta\Phi/\pi)^2 \sin^2\Theta]^{1/2}. \tag{54}$$

The characteristic velocity of a line source (Equation (53)) is far more complicated since the source in this case is highly directional. If the refracted signal is of sufficient amplitude or if the shock wave rise time is short enough, it will also be heard on the ground as a boom or as a series of booms if fragmentation has occurred along the flight path. Audibility of multiple booms can also be influenced by turbulent eddies within the atmospheric boundary layer and by reflection effects from topography, etc.

For an elevated point source it is also possible to estimate the distance scale over which sounds can be recorded within the direct zone of 'audibility' near the source. This distance can be expressed analytically using standard acoustical analysis, with T_0, the surface temperature, z_s, the source altitude and Γ, the mean atmospheric temperature lapse rate between the source altitude and the ground (Fleagle and Businger, 1980) in the form:

$$D = 2\ (T_0 z_s/\Gamma)^{1/2}. \tag{55}$$

Using $T_0 = 300$ K, $\Gamma = 6.5$ K km^{-1} (temperature decreasing with increasing height) and $z_s = 20$ km produces $D = 60.8$ km. Using a reasonable range of lapse rates and source altitudes, D values from 25–110 km are obtained using (55). Beyond this horizontal range, sounds will not reach the surface directly except through diffraction or scattering effects. They will be received again some 200 km downwind in the next zone of 'audibility', however, etc.

In Great Britain in 1969 the sounds from a meteorite in flight were fortuitously recorded on a tape recorder by Miss Eileen M. Brown in Northern Ireland. This is the famous Boveedy-Sprucefield fireball and meteorite, most of which fell into the Irish Sea. Miss Brown was out recording bird calls in her backyard near sunset. She did not see the fireball herself due to clouds, but numerous others saw and photographed the event (Millman, 1970). The fundamental reason the tape was thought to be unusual was that her dog barked fiercely after the multiple sounds arrived and her dog had never ever responded in this fashion to thunder which the sounds somewhat resembled. Fortunately, the famous meteor astronomer Dr Ernst J. Öpik of the Armagh Observatory was nearby and Miss Brown brought the tape to him and asked for his advice on the source of the signals!

More recently audible acoustic records have also been recorded for very bright bolides on security video cameras which also had audio capability. These bolides had stellar magnitudes ranging from -12 to -15 and occurred over southern Spain

at 23:59:36 UT on November 17, 1995 (personal communication with Marc de Lignie and H. Betlem, 1995 and with P. Spurny, 1996, 1997) and over southeastern Colorado at 09:18 UT on November 21, 1995 (ReVelle and Whitaker, 1996a).

3.6.2. *Electrophonic Sounds: 'Abnormal Sounds'*

In addition to the normal hypersonic boom reports from bolides, historically there have been reports of sounds accompanying the flight of very bright bolides, i.e., with nearly instantaneous transmission properties. In fact in some cases it was the sound heard indoors that alerted the observer's to the presence of the fireball which they suddenly saw when they went outdoors! For many years these sounds were dismissed as being an aberration, because a correct understanding of some of the necessary physics during the entry of large fireballs was not properly understood until about 1980. Keay, Bronshten and others have formulated theories of how sounds are heard simultaneously with the flight of bolides. Unlike ordinary acoustical waves which travel at the about the local effective sound speed and which arrive with delays of a few minutes from source altitudes of 20 to 30 km, electrophonic sounds must travel at nearly the speed of light.

The theory presently accepted predicts that only very bright fireballs can produce such electrophonic sounds. These fireballs penetrate deeply enough into the atmosphere to enter a continuum flow regime and produce a turbulent wake behind the fireball. The action of the turbulent wake in twisting or winding up the geomagnetic field lines and their subsequent relaxation back to an equilibrium state is the physical mechanism for the generation of these reported sounds whose intensity is a function of a critical magnetic Reynolds number ($\gg 10$). After propagation as a VLF (very low frequency) electromagnetic wave through the atmosphere, the signals can become transduced at the ear of the observer by various nearby metal objects. Not all observer's are of equal ability in hearing the clicking sounds that are commonly reported. Keay has continued to publish renewed efforts at bringing together observations and theory in this field, which is very much in its infancy (Keay, 1980a,b, 1992, 1993). Additional perspectives are also given in Bronshten (1983). There have also been recent attempts by P. Brown and colleagues to record these signals during the Perseid meteor shower in Europe in 1993. Some very suggestive evidence of the electrophonic emission from a bright bolide was obtained, but further corroborative evidence is needed to fully validate the association of these signals with the fireball in question.

3.7. METEOR SOUNDS: THEORETICAL UNDERSTANDING OF METEOR SOUND PROPAGATION

3.7.1. *Zones of 'Audibility' and Silence: Anomalous Propagation*

An appreciation of the complexities of sound propagation in the atmosphere was not possible until the turn of the century when during the funeral of Queen Victoria cannon fire was heard by the mourner's in distinct elliptical bands surrounding the explosions with zones of 'audibility' and of silence at ranges of the order of 200 - 300 km surrounding a ground level source. In other words, audible sounds were heard quite near the cannons, out as far as perhaps 30–50 km and then not heard again until about 200 km downwind from the source, etc. The modern acoustical explanation of these zones is that for a perfectly stratified, steady state atmosphere, the combined vertical atmospheric structure of air temperature (or $c_s(z)$) and horizontal winds refracted the sound downward toward the ground. This is a direct application of using Snell's Law of acoustics, i.e., linear, small amplitude theory. Two recent excellent reviews of acoustical/infrasonic propagation are provided in Kulichkov (1992) and in Embleton (1996).

Very far from the source this geometrical acoustics, ray theory approach breaks down in favor of a waveguide mode description for the propagation of acoustic-gravity waves (see below) launched from a bolide. For a uniform waveguide, this limiting regime is measured by a horizontal scale $= 2H^2/\lambda$ (Weston and Rowlands, 1979), where H is the vertical duct thickness and λ is the wavelength of the waves. For a typical stratospheric vertical dimension of 50 km and a wavelength of 1 km (wave frequency of about 0.33 Hz or a period of about 3.0 s), a horizontal scale beyond about 5000 km is best described in terms of waveguide modal analysis rather than in terms of ray theory. The ray description can also be modified due to weakly nonlinear effects due to the presence of caustics where a significant number of rays intersect as at the boundary near an acoustic shadow zone. Within the shadow zone, low frequency acoustic energy can exist due primarily to diffraction effects (Cox, 1958).

For meteors there are at least two major differences expected compared with signals from very low altitude point explosive sources. The first is that the altitude of the source changes the potential propagation paths with respect to a ground based observer (possible wave ducting heights). Secondly, for a truly line source geometry, the available wave normal paths that can reach a given level are far more restrictive, especially for a very elevated source (ReVelle, 1976). The observed zones of 'audibility' and of silence are determined to be about 200 km apart downwind (or about 300 km upwind) however, as was the case for Queen Victoria's funeral and as documented for meteor's long ago by Ceplecha for the case of Příbram, which fell in 1959.

TABLE XII
Ducted paths

Letter designation of type of return	Signal velocity km s^{-1}	Horizontal trace velocity km s^{-1}	Name of ducted return or of the wave type
L	0.33–0.34	0.34 horizontal arrivals	Lamb wave arrivals
T	0.30–0.32	0.32–0.34	tropospheric returns
S	0.28–0.31	0.34–0.45	stratospheric returns
Th	0.22–0.24	0.45–1.1 generally steep arrivals	thermospheric returns

3.7.2. *Observations of Infrasound from Meteors at Long Ranges*
In this section we will summarize the observations of meteors made using infrasonic microbarographs at large horizontal distances away from the source. Infrasound is the term describing the highest frequency part of the spectrum of linearized acoustic-gravity waves that can exist in an isothermal atmosphere (Fleagle and Businger, 1980), i.e., for angular frequencies $\gg$ the acoustic waveguide cut-off frequency (about 2.1×10^{-2} Hz).

The available ducted paths, i.e., the possible acoustic phases between the source and the observer are given in Table XII as follow from ReVelle and Whitaker (1996b). In addition to the listing in Table XII, for low altitude sources there are also additional types of local acoustical returns, both downwind and upwind of the source, within the planetary boundary layer as well (due to a combination of an elevated temperature inversion level near the ground and also due to elevated regions of wind shear at night (nocturnal low-level jets, etc.).

The theoretical foundation for these acoustical phases is based on the mean structure of the atmosphere. This can be categorized as having a semi-permanent inversion of temperature (or of sound speed ignoring mean molecular weight variation effects) at the base of the thermosphere ($z > 100$ km) and a temperature maximum at the stratopause (about 50 km). The upper duct height (**Th** type returns) is often enhanced by the strong winds at these heights whereas the lower duct height (**S** type returns) is only defensible using ray theory in the downwind direction. Thus, it is the unique presence of winds at stratospheric heights which makes this lower duct possible. Ducting is also possible between the stratopause and the mesospause for signals from elevated sources as well. If range dependent atmospheric behavior is evident, this duct can also carry signals which can subsequently leak downward into the lower atmosphere which can provide **S** type ducted returns at the ground.

ReVelle (1997) has provided a comprehensive summary of all the long range infrasonic observations available from observed meteor-fireball explosions at relatively low altitudes and has given the empirical relations determined by the US Air Force (AFTAC, Air Force Technical Applications Center, Patrick Air Force Base, Florida) relating the observed signal period at maximum amplitude to the source kinetic energy. All of these bolide signals are **S** type ducted returns which for long distance propagation are the most repeatable and reliable. In other cases, as listed in ReVelle (1997), the **Th** returns are also available from bolide explosions as well. For **S** type returns, source energies from 1.6×10^{-5} kt to 1.1 Mt were calculated for 16 meteor-fireball events. The steady state influx rate for these bodies, which is also in rough agreement with other estimates, was also calculated. A thorough discussion of the meteor-fireball line source problem and earlier NOAA (National Oceanographic and Atmospheric Administration) and USGS (United States Geological Survey) observations are also given in ReVelle (1976). The AFTAC relations have indicated a correlation between the observed acoustic period at maximum signal amplitude to the source energy to about the 0.25–0.30 power as indicated below.

AFTAC point source: semi-empirical curve fit

$$\log(E_s/2) = 3.34\ \log(P) - 2.58, \quad E_s/2 \leq 100 \text{ kt}, \tag{56}$$

$$\log(E_s/2) = 4.14\ \log(P) - 3.61, \quad E_s/2 > 40 \text{ kt}. \tag{57}$$

The acoustic wave period range of interest for the original AFTAC data ranged from 2.5 to 36 s.

The fall of the St. Robert Meteorite (Brown et al., 1996; Hildebrand et al., 1997), has provided an impetus to the author to provide additional ways of evaluating the source energies of meteors from the measurement of their amplitude as a function of range, etc. The St. Robert event, the earlier events considered in ReVelle (1976, 1997) and the more recent events in Colorado and California (ReVelle and Whitaker, 1996a; ReVelle et al., 1997) have now resulted in four approaches, one based on a semi-empirical relation developed at Los Alamos for near-surface point source explosions which also accounts for the effects of the stratospheric winds on the observed signal amplitude. The second approach makes use of the acoustic efficiency concept for near-surface point source explosions as discussed earlier, but which combines both amplitude and wave period as well as the total signal duration. A preliminary analysis has now been completed to better define this factor numerically from all the earlier AFTAC meteor-fireball infrasonic recordings (ReVelle and Whitaker, 1995). These first two point source relations used, with R, the horizontal range, E_s, source energy, V_H, the horizontal wind speed at 50 km, ε_{ac}, the acoustic efficiency, Δ, a ground reflection effect propagation factor, Δ_p, the positive phase acoustic amplitude, ρ, the air density at the observation height,

and τ_D, the time duration of the acoustic signals can be written as:
Near-surface ANFO (ammonimum nitrate-fuel oil) point source:

$$E_s = (\Delta p/2.35 \times 10^4)^{1.47} 10^{0.02 V_H} R^2. \tag{58}$$

Acoustic efficiency for a near-surface point source:

$$E_s = 2\pi R^2/(\varepsilon_{ac}\Delta) \int_0^{\tau_D} (\Delta p/(\rho c_s))\, \mathrm{d}t. \tag{59}$$

In Equation (58) we have assumed that the source is not directly at the surface, otherwise this relation must be multiplied by a factor of $\frac{1}{2}$ before its evaluation. Equation (59) actually applies strictly to a low level source with a $c_s(z)$ profile increasing with increasing height (a temperature inversion situation). To evaluate (59), the acoustic efficiency must be assumed or evaluated by other means and the complete pressure signal time series of the arrival must be integrated over the duration of the wavetrain. In both of these expressions significant corrections for air density stratification for sources at heights exceeding about two pressure scale heights must also be made. This amplitude correction factor accounts for the conservation of the wave energy density as the acoustic signal propagates vertically in a stratified medium. Its incorporation involves a multiplication of the amplitude by the ratio of the density at the source altitude to that at the surface to the $\frac{1}{2}$ power (for details see ReVelle, 1976). In addition, there are two other relations available (ReVelle, 1976) that are useful for the estimation of the bolide source energy as a function of the total slant range R', amplitude, Δp, wave period, τ_G , etc. These were developed for a windless, hydrostatic, isothermal model atmosphere since the full expressions involving wave amplitude and period decouple to simple algebraic expressions for this limiting case. These are respectively:
Line source: linear wave propagation (ReVelle et al., 1997): wave period method

$$E_s[J] = 0.161\,(\pi/6)\,(\rho_m c_s^7/V)\,(\tau_G^4/R'). \tag{60}$$

Line source: weak shock propagation (ReVelle and Whitaker, 1996): wave period and amplitude method

$$E_s[J] = 11.5\,\pi \rho_m R'^3 (\Delta p_{o-p}/(p_z p_g)^{1/2})^4 c_s^3/V. \tag{61}$$

Equation (60) is the analog of the expressions (56) and (57) for a point source explosion and assumes that ultimately linear wave propagation can occur for signals observed at great range on the ground for bolide sources at sufficiently great altitude. In contrast, Equation (61) assumes that weak shock propagation dominates the propagation of the line source signal as it travels away from the source. This is limited to a region however where the distortion distance exceeds the distance that the wave has left to travel before it is observed (for full details see ReVelle, 1976). There is a also specific modal solution called the fundamental mode or the

Lamb (edge) wave which is vertically evanescent (non-propagating), which has commonly been detected and has been used previously to interpret observations from low altitude explosions ($z_s/H_p < 2$, with H_p the pressure scale height). E_s estimates made using these horizontally propagating surface waves have been quite useful for understanding large sources at long range. The equation connecting E_s to Lamb wave period and amplitude is given in ReVelle (1997). It shows a proportionality between E_s and Lamb wave amplitude, Lamb wave period to the $\frac{3}{2}$ power and to the horizontal source-observer range on a spherical earth to the $\frac{1}{2}$ power (for a ducted cylindrically wave). For example, for the Tunguska bolide of 30 June, 1908 using Equation (52), we find $E_s = 10$ MT and this is also very close to the value we obtain using the Pierce-Posey Lamb wave equation as well (developed for point sources).

Postscript: as of this writing a new bolide was observed over El Paso, Texas at about 12:47 p.m. MST on 9 October, 1997. This object penetrated very deeply into the atmosphere and consequently generated significant sonic booms that were detected infrasonically at the CTBT (Comprehensive Test Ban Treaty) detection arrays in Los Alamos and in Lajitas, Texas. Seismic recording were also made at two stations in the vicinity of El Paso and at Lajitas, Texas as well. In addition, several videos of the ensuing dust cloud were also readily available. It is anticipated that meteorites will be recovered from this event which is likely to become one of the best documented cases available. The DoD (Department of Defense) announced on 20 October, 1997 that its satellite sensors had also detected this event. Our preliminary infrasonic analysis using the above equations gives an upper limit to the bolide source energy of about 490 tons (TNT equivalent), but with a rather large uncertainty to the true lower limit to the source energy.

3.8. PRE- AND POST-ABLATION REGIMES

3.8.1. *Preheating*

The preheating part of the atmospheric trajectory can be described by partial differential equation expressing the flow of energy from the meteoroid surface inside and outside. The energy input originates from the air atoms and molecules hitting the gas-cap-unprotected meteoroid surface directly.

The surface temperature at which ablation begins should fall somewhere between the melting and the boiling points for the body. Our task is to determine at what height this temperature is reached for a homogeneous sphere with radius r_0, density δ, specific heat c, and heat conductivity λ, assuming black-body radiation. We will assume a randomly oriented, rapidly rotating meteoroid whose kinetic energy is converted to heat uniformly distributed on its surface. Then the following differential equation of heat conduction applies ($\tau(r, t)$ is the temperature relative to T_0, as function of time t and distance from the center of the body r; T_0 is the absolute temperature of the meteoroid outside the atmosphere; σ is Stefan-Boltzman constant; Λ is the heat transfer coefficient; v is the meteor velocity; ϱ is

the air density; ϱ_B is the air density at which the meteoroid attains temperature τ_B at surface; b is the air density gradient; z_R is the zenith distance of the radiant; τ_0 is the temperature at the meteoroid center, when the surface temperature is τ_B):

$$\frac{\partial \tau}{\partial t} - \frac{2\beta^2}{r}\frac{\partial \tau}{\partial r} - \beta^2 \frac{\partial^2 \tau}{\partial r^2} = 0, \tag{62}$$

where

$$\beta^2 = \frac{\lambda}{\delta c} \tag{63}$$

and

$$\tau = \tau(r, t) = T - T_0. \tag{64}$$

The initial condition can be written

$$\tau(r, -\infty) = 0. \tag{65}$$

The boundary conditions are

$$\tau(0, t) = \text{finite value} \tag{66}$$

and

$$\lambda \left(\frac{\partial \tau}{\partial r}\right)_{r=r_0} + \sigma(\tau + T_0)^4 - \sigma T_0^4 = \frac{\Lambda \varrho v^3}{8}. \tag{67}$$

Equations (62) and (65) assume a more suitable form under the following transformation

$$u = \tau r. \tag{68}$$

Then

$$\frac{\partial u}{\partial t} - \beta^2 \frac{\partial^2 u}{\partial r^2} = 0 \tag{69}$$

and

$$u(r, -\infty) = 0 \tag{70}$$

with the relative temperature of the meteoroid surface τ_B at the time $t = 0$. We search for a point on a meteoroid trajectory (given by air density, i.e., height), where the surface temperature reaches the 'ablation' temperature, i.e., the temperature at

TABLE XIII

Material and other constants for two meteoroid models used in computations of theoretical beginning heights

Quantity	Stone	Porous body	Unit
Bulk density δ	3500	1000	kg m^{-3}
Thermal conductivity λ	3.5	0.2	m kg s^{-3} K^{-1}
Specific heat c	1000	1000	m^2 s^{-2} K^{-1}
Heat transfer coeff. Λ	1.0	1.0	–
Drag coefficient Γ	0.46	0.46	–
Boiling point T_B	2180	2180	K
Ambient temperature T_0	280	280	K

TABLE XIV

Theoretical beginning heights h_B (km), where temperature attains T_B. Radiation, heat conduction and deceleration considered simultaneously in numerical solutions. Material and other constants are in the preceding table

Model	cos z	v_∞	r (cm)								
		(km s^{-1})	10	3	1	0.3	0.1	0.03	0.01	0.003	0.001
Stone	1	15	78.1	78.2	78.4	79.3	82.0	86.9	89.1	89.1	–
		30	87.7	87.8	87.9	88.5	90.5	95.5	99.7	101.1	101.3
		60	97.2	97.3	97.4	97.9	99.6	105.0	111.1	114.0	114.7
	0.3	15	81.2	81.7	82.0	83.6	87.3	89.3	88.9	–	–
		30	90.7	90.9	91.2	92.3	95.8	100.0	100.9	100.9	100.3
		60	100.6	100.9	101.1	102.2	105.6	111.7	113.8	114.6	114.8
Porous	1	15	86.9	86.9	87.0	87.2	87.9	89.1	89.0	–	–
body		30	97.1	97.1	97.2	97.4	98.0	100.0	101.0	101.4	101.5
		60	108.5	108.5	108.6	108.9	109.6	112.0	114.0	115.0	116.3
	0.3	15	88.3	88.4	88.5	88.8	89.2	88.7	–	–	–
		30	98.9	99.0	99.1	99.3	100.2	100.9	101.0	99.8	–
		60	111.0	111.0	111.2	111.5	112.6	114.0	114.6	114.9	115.6

which ablation starts. This temperature is somewhere between 2200 K and 2600 K depending on the meteoroid material.

The problem was not solved until now in explicit analytical form. The numerical results can be seen in Table XIV with meteoroid material defined in Table XIII. But if we omit the radiation term in Equation (67), which we can do for bodies larger than 1 mm, the problem becomes linear and the solution is then

$$\varrho_B = \frac{8\lambda\tau_B}{\Lambda v^3}\left[\frac{Q}{\beta}\coth\left(\frac{r_0 Q}{\beta}\right) - \frac{1}{r_0}\right], \tag{71}$$

with $Q = \sqrt{bv\cos z_R}$ and the temperature in the center of the body is given by

$$\tau_0 = \frac{\Lambda v^3 r_0^2 Q \varrho_B}{8\lambda\left[r_0 Q\cosh\left(\frac{r_0 Q}{\beta}\right) - \beta\sinh\left(\frac{r_0 Q}{\beta}\right)\right]}. \tag{72}$$

The theoretically computed points of onset of the ablation correspond roughly to the observed beginning heights for meteors photographed with classical small cameras, i.e., they correspond to sudden increase of brightness by about 3 stellar magnitudes at onset of the ablation (at +4 to +1 magnitude) for meteors of maximum magnitude in the range from –2 to –8 or so. Brighter objects are also photographically recorded before the onset of severe ablation in this sense.

3.8.2. *Dark-Flight and Impact*

If a fireball penetrates very deep into the atmosphere, the computed velocities and decelerations at the end of the luminous trajectory may yield a non-zero mass of the body. In such a case a meteorite fall is predicted to follow the fireball and we are interested in predicting the meteorite impact point from the data on the luminous trajectory of the fireball. After terminating the luminous trajectory, the body continues in its flight without emitting light in a 'dark-flight trajectory'. The last measured velocity and deceleration at the terminal point, the position of the terminal point and the direction of flight completely define the solution of this problem. One of the complications in the computations of the dark flight lies in the poorly known wind field. The main uncertainty originates from the unknown shape of the body, which we have to assume to be symmetrical. The equations of motion of a non-ablating body can be written as

$$\frac{\mathrm{d}v_l}{\mathrm{d}h} = -\Gamma S\varrho v(V_l + v_l)/v_h, \tag{73}$$

$$\frac{\mathrm{d}v_h}{\mathrm{d}h} = (-\Gamma S\varrho v v_h - g)/v_h, \tag{74}$$

$$\frac{\mathrm{d}v_x}{\mathrm{d}h} = \Gamma S\varrho v(V_x + v_x)/v_h, \tag{75}$$

where v, the velocity of a meteoroid is composed of 3 perpendicular components: the vertical plane containing the fireball trajectory contains the horizontal component of the velocity, v_l; the same vertical plane contains the vertical velocity component, $v_h = \mathrm{d}h/\mathrm{d}t$; the horizontal direction perpendicular to the vertical plane containing the fireball trajectory contains the other horizontal component of velocity, v_x (perpendicular to the fireball trajectory in horizontal direction). The sign of the velocity components are chosen so that $v_l > 0$ in the direction of the meteoroid flight, so that $v_h > 0$ up (in the real problem of the meteoroid motion $v_h < 0$ always), and so that $v_x > 0$ to the right hand side viewing along the meteor motion. The other symbols are: V_l, V_x the wind velocity components, $V_l > 0$ *against* the meteoroid motion, $V_x > 0$ *against* the positive direction of v_x; Γ the drag coefficient as function of Mach number $\Gamma = \Gamma(M)$ (and thus function of v and the air temperature); $S = m/s$ the ratio of meteoroid mass, m, and meteoroid head cross-section, s; ϱ the air density.

The solution of differential Equations (73), (74), (75) can be performed numerically starting from the terminal point and going to lower and lower heights until the surface of the Earth is reached (e.g., the Runge–Kutta method of integration can be used). The integration step $\mathrm{d}h = 0.01$ km is of enough precision, but higher up in the atmosphere even bigger steps do not decrease the accuracy of computations. At each integration step, the velocity of the meteoroid is computed from

$$v^2 = v_h^2 + (v_l + V_l)^2 + (v_x + V_x)^2. \tag{76}$$

The initial values of v_l, v_h, v_x for integration of systems (73), (74), (75), and (76) are given by

$$v_l = \quad v_T \sin z_R, \tag{77}$$

$$v_H = -v_T \cos z_R, \tag{78}$$

$$v_x = \qquad 0, \tag{79}$$

where v_T is the velocity at the terminal point of the luminous trajectory of the fireball computed from the measured lengths along the fireball trajectory and z_R is the zenith distance against the direction of flight at the terminal point (zenith distance of the radiant). The initial value of ΓS is given by the drag equation written for the terminal point of the luminous trajectory. This initial value of ΓS is completely given by the observations: implicitly it contains the unknown mass, shape, density and drag coefficient of the meteoroid. Thus the *relative change of* ΓS during the decreasing velocity is the only necessary assumption for solving (73)–(76)y. We change Γ as function of Mach number, M, for a symmetrical shape and assume

S constant (it means no change in the shape and orientation of the flight position takes place).

$$(\Gamma S)_T = -\frac{1}{\varrho_T v_T^2}\left(\frac{\mathrm{d}v}{\mathrm{d}t}\right)_T, \tag{80}$$

where v_T and $(\mathrm{d}v/\mathrm{d}t)_T$ are the velocity and deceleration observed at the terminal point of the fireball luminous trajectory and ϱ_T is the air density at the terminal height h_T. The air densities for low penetrating fireballs are usually available from meteorological aeronomical measurements, or higher up (between 30 to 40 km) they can be extrapolated from them with the standard relative change taken from CIRA 1972 atmosphere (month and geographic latitude averages). The wind direction and velocity are given from aeronomical data and we usually take the closest values in time and location of the fireball and interpolate (if the locations are not separated by singularities in meteorological situation). From aerological measurements, we can determine at each integration step for the particular height:

$$T = T(^\circ\mathrm{C}) + 273.15, \tag{81}$$

$$\rho = 3.483676 \times 10^{-4} P/T \ \mathrm{g\,cm^{-3}}, \tag{82}$$

$$c = 0.0200468\sqrt{T} \ \mathrm{km\ s^{-1}}, \tag{83}$$

where temperature, T, is the absolute temperature, P the air pressure in millibars (hectopascals), ρ the air density in $\mathrm{g\,cm^{-3}}$ ($\mathrm{Mg\,m^{-3}}$), and c is the velocity of sound.

We are also interested in the total length of the dark flight from the terminal point of the luminous trajectory to the impact point. More details on computation of dark flights can be found in Ceplecha (1987a). It is worth mentioning that all these computations are independent of the meteoroid mass.

4. Radio Wave Scattering from Meteor Trails

4.1. UNDERDENSE AND OVERDENSE TRAILS

At heights below 95 km a meteor trail can be considered as a slightly tapered circular cylinder of ionization, highly linear when first formed, and extending over a height range of 10 to 15 km. The same picture applies initially to trails formed above 95 km, but during the subsequent diffusion of the ionization the magnetic field of the Earth modifies the trajectories of the electrons, and the cross-section of the trails becomes oblate. In general, meteor trails are formed in an atmosphere that is in horizontal motion with speeds of the order of 100 $\mathrm{m\ s^{-1}}$ and subject to wind shears that are typically 5 $\mathrm{m\ s^{-1}\ km^{-1}}$.

The radio reflection coefficient of any section of the ionized column depends on the volume number density of the electrons. If secondary scatter is insignificant

the radio wave penetrates the plasma essentially unchanged, and the total scattered radiation is the sum of the contributions from individual electrons. Such meteor trails are classified as *underdense*. This condition applies to trails with line densities less than 10^{13} electrons per meter (radio magnitude +7.5).

If the electron density in the trail is sufficiently large, say 10^{15} electrons per meter, secondary scattering between electrons is important and the dielectric constant of the plasma becomes negative. The wave disturbance within the trail now becomes evanescent, and the meteor trail is said to be *overdense*. For such trails with a Gaussian distribution of ionization it is always possible to determine a critical radius within which the dielectric constant is negative. Thus an overdense trail can be modeled as a metallic cylinder which expands as the trail diffuses, and then suddenly vanishes when the electron concentration falls below the critical value.

It is conventional to define the transition from the underdense to the overdense condition as occurring when the evanescent wave amplitude is reduced to $1/e$ at the trail axis. The effective radius of the trail is then $\lambda/2\pi$. For the idealized case of a uniform cylinder of ionization whose electron density has just reached the critical value N_c, the line density is given by $q = \pi r^2 N_c = 1/4\pi\lambda^2 N_c$. But $N_c = 1.11 \times 10^{15}/\lambda^2$. Thus the transition line density is independent of wavelength, and the transitional value of q is about 10^{14} electrons per meter. This result is essentially unchanged when the argument is extended to a cylinder with a Gaussian radial distribution of ionization density (McKinley, 1961).

The reflection coefficient for an underdense trail also depends on the orientation of the electric vector relative to the trail axis. Theory and observation indicate an enhancement of the transverse reflection coefficient by a factor of about 2 compared to the case when the electric vector is aligned parallel to the trail axis (i.e., longitudinal reflection coefficient).

4.2. BACKSCATTERING FROM AN UNDERDENSE METEOR TRAIL

4.2.1. *Idealized Case*

Consider a trail of uniform ionization whose diameter is small compared to the wavelength and where the effect of diffusion during the formation period of the trail can be ignored. It is also assumed that the trail is underdense, so that secondary radiative and absorptive effects can be neglected.

At a point on a trail distance R from a radio transmitter, the power flux of the incident wave is $\Phi_i = P_T G_T/(4\pi R^2)$ watts m^{-2}, where P_T is the transmitted power and G_T is the antenna gain relative to an isotropic radiator, in the direction of the trail element. The scattering cross-section of a free electron is $\sigma_e = 4\pi r_e^2 \sin^2\gamma$, where r_e is the classical electron radius and γ is the angle between the electric vector of the incident wave and the line of sight of the receiver. For the case of backscatter $\gamma = \pi/2$ and $\sigma_e = 1.0 \times 10^{-28}$ m^2. Thus the power flux at the receiving antenna of radiation scattered from the single electron is $\Phi_e = \Phi_i\ \sigma_e/(4\pi R^2) = \Phi_i (r_e/R)^2$.

In a trail whose diameter is small compared to the wavelength all electrons can be assumed to be on the axis, and thus all those in a line element ds scatter in phase. In order to sum the resultant returned radiation at the receiving antenna an electric field $\mathbf{E}_e$ is associated with each scalar quantity Φ_e, such that the maximum amplitude of the field E_0, is given by $E_0 = (2Z_0\Phi_e)^{1/2}$ where Z_0 is the wave impedance of free space (120π). Moreover, each field vector has a phase delay of $2kR$ radians, relative to the transmitted radiation, where $k = 2\pi/\lambda$. If the trail has a line density of q electrons per meter, the instantaneous amplitude of the field due to the q ds electrons in the trail element ds is given by $(2Z_0\Phi_e)^{1/2} \exp j\,(\omega t - 2kR)\, q$ ds. Hence the amplitude E_R, of the field at the receiving antenna due to scattering from the whole trail is given by

$$E_R = (2Z_0\Phi_e)^{1/2} q \int \exp j\,(\omega t - 2kR)\,\mathrm{d}s, \tag{84}$$

where the integral is taken over the length of the trail.

In general the change in range is small compared to the orthogonal distance R_0 to the trail, so that the approximation $R \cong R_0 + s^2/(2R_0)$ can apply, where s is the distance along the trail from the orthogonal point ('t_0 point') to ds. With the substitution $\pi x^2/2 = ks^2/R_0$, the phase factor becomes $\omega t - \pi x^2/2 - 2kR_0$, and $\mathrm{d}s = (R_0\lambda/4)^{1/2}\mathrm{d}x$. Thus the expression for E_R becomes

$$E_R = (R_0\lambda/4)^{1/2}(2Z_0\Phi_e)^{1/2} \exp j(\omega t - 2kR_0)\, q \int \exp j(-\pi x^2/2)\,\mathrm{d}x,$$

$$E_R = (R_0\lambda/4)^{1/2}(2Z_0\Phi_e)^{1/2} \exp j(\omega t - 2kR_0)\, q\, (C - jS), \tag{85}$$

where C and S are the Fresnel integrals,

$$C = \int \cos(\pi x^2/2)\,\mathrm{d}x \quad \text{and} \quad S = \int \sin(\pi x^2/2)\,\mathrm{d}x. \tag{86}$$

The maximum amplitude of the oscillatory field is

$$(E_R)_0 = (R_0\lambda/4)^{1/2}(2Z_0\Phi_e)^{1/2}\, q\, (C^2 + S^2)^{1/2}, \tag{87}$$

and the power flux is given by

$$\Phi_R = (E_R)_0^2/2\,Z_0 = \Phi_e(R_0\lambda/4)\, q^2\, (C^2 + S^2). \tag{88}$$

If the receiving antenna has a gain of G_R, the effective absorbing area is $G_R\lambda^2/4\pi$ when the antenna is matched to the receiver. Thus the power delivered to the receiver by scattering from the whole trail is

$$\begin{aligned} P_R &= \Phi_e(G_R\lambda^3 R_0/16\pi)q^2(C^2 + S^2) \\ &= \Phi_i G_R\lambda^3/(16\pi R_0)q^2 r_e^2\, (C^2 + S^2), \end{aligned} \tag{89}$$

where the orthogonal range R_0 can be used in place of all R, with negligible error. Whence, on substituting for Φ_i the received power is

$$P_R = P_T G_T G_R \lambda^3 q^2 r_e^2 (C^2 + S^2)/(64\pi^2 R_0^3). \quad (90)$$

If the extremities of the trail are several Fresnel zones either side of the t_0 point the value of $C^2 + S^2$ is close to 2 and the received power is given in watts by

$$P_R = P_T G_T G_R \lambda^3 q^2 r_e^2/(32\pi^2 R_0^3) = 2.51 \times 10^{-32} P_T G_T G_R \lambda^3 q^2/R_0^3). \quad (91)$$

Expression (91) gives the power of the echo once the whole trail is formed. During the formative stages the value of C^2+S^2 grows steadily until after the meteoroid passes the t_0 point, and then oscillates to produce amplitude fluctuations that are the analogue of the optical Fresnel diffraction at a straight edge. The intensity and phase variations for the echo from this idealized trail are shown in Figure 7 (curve A), where $x = 2Vt/(\lambda R_0)^{1/2}$ and the origin of time is the t_0 point. The speed of the meteoroid may be determined from the amplitude ('Fresnel') oscillations or the phase variation prior to the t_0 point.

The power of the echo illustrated in Figure 7 shows its most rapid build up as x changes from –1 to +1, which is equivalent to a portion of the trail of length $(\lambda R_0)^{1/2}$ about the t_0 point. While this region is slightly less than the central Fresnel zone, scattering from the electrons in this portion of the trail contributes over 90% of the received echo power. However, it is the scattering from regions outside this zone that is often the most useful for making measurements of significance to meteor astronomy. Typical scattering zone lengths for a meteor at a range of 140 km are 900 m at 50 MHz, 1200 m at 30 MHz and 2500 m at 6 MHz.

4.2.2. *Actual Trail*

As has already been discussed meteor trails are formed with a finite radius and commence diffusing immediately. Further, the ionization along the trail is distributed in an approximate parabolic manner over a height range of 10 to 15 km. Also some degree of plasma resonance may occur in the case of scattering when the polarization of the incident wave is transverse to the trail axis. In order to include all these factors in the analysis of backscattering from meteor trails it is more appropriate to discuss the scattering in terms of the *reflection coefficient* of any segment of the trail.

By employing wave matching techniques, complex backscatter reflection coefficients have been calculated for columns of meteoric ionization possessing a Gaussian radial profile of electron density (Poulter and Baggaley, 1977, 1978). For the case where the electric wave vector is parallel to the axis of the trail the plane wave solution gives the magnitude of the reflected field E_r, at a large distance R, as $E_r = g_\parallel (\pi k R/2)^{-1/2} E_i$, where E_i is the incident field strength at the trail and $g_\parallel$ is the reflection coefficient. Taking into account the fact that meteor trails are observed with spherical waves, the ratio of the power flux Φ_R at the receiving antenna,

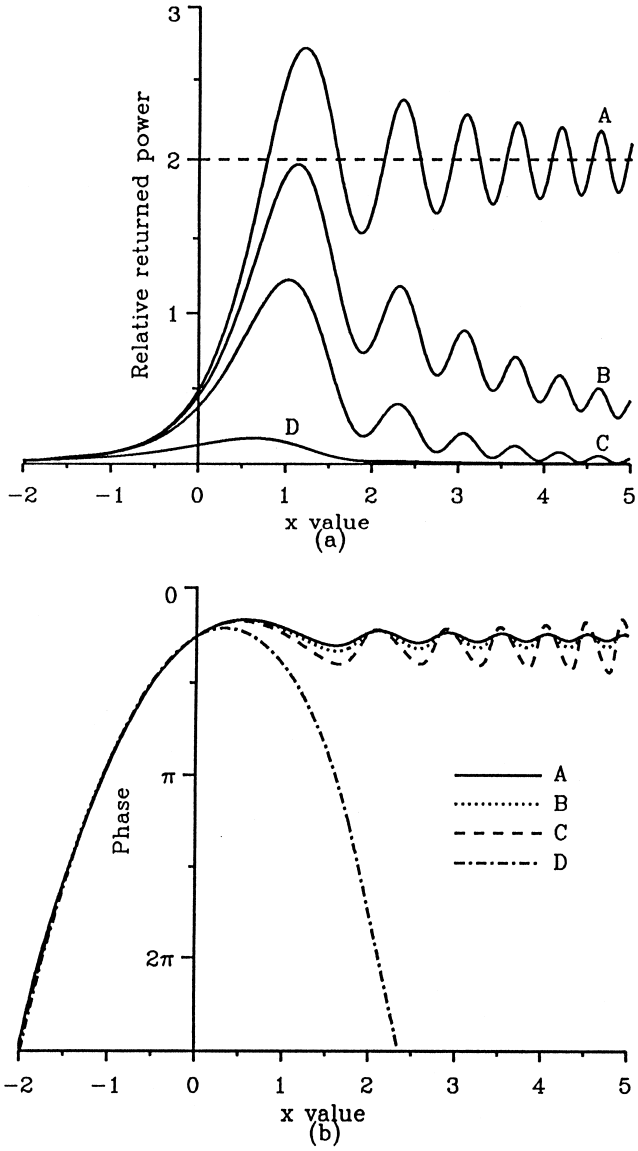

Figure 7. Predicted behavior of the power and phase of the radar echo from an underdense trail. Curve A is based on Equation (85) with $x = 2Vt/(\lambda R_0)^{1/2}$. Curves B, C, and D show the effect of including an increasing degree of diffusion of the trail.

to the incident flux Φ_i at the trail, at range R, is given by $\Phi_R = g_\parallel^2(\pi k R)^{-1}\Phi_i$ and the power in watts delivered to the receiver is given by

$$P_R = g_\parallel^2 P_T G_T G_R \lambda^3/(32\pi^4 R_0^3) \tag{92}$$

(Kaiser and Closs, 1952; Eshelman, 1955). A similar expression applies for the case when the electric wave vector is transverse to the axis of the trail, with calculated values of $g_\perp$ replacing $g_\parallel$. A comparison of this expression for the received power to that given above for an idealized trail shows that for such trails (strictly underdense) the parallel reflection coefficient $g_\parallel$ is given by $q\pi r_e$.

To examine the subsequent temporal variation of the reflection coefficient of a segment of the trail, two cases are identified: underdense trails occurring *below* and *above* 95 km.

4.2.3. *Underdense Trails Below 95 km*

For any line segment on an actual trail of line density q, that is in the process of diffusing from some initial radius r_0, the radial distribution of the ionization is usually assumed to be Gaussian and given by the expression (45). In the case of underdense trails the reflection coefficient then has the simple form

$$g_\parallel = q\pi r_e \exp(-k^2a^2) = 8.85 \times 10^{-15} q \exp(-k^2a^2), \tag{93}$$

where $a^2 = 4Dt + r_0^2$, $k = 2\pi/\lambda$ and q is electrons per meter (Poulter and Baggaley, 1978). In fact this exponential decay in the amplitude of the echo from an underdense trail can be derived by summing the contributions across the trail from the spatially distributed electrons (McKinley, 1961). The time constant for the decay of this type of echo is $(4k^2D)^{-1}$, and measurements of echo decay time constants have been used by many observers to indirectly determine the value of the diffusion coefficient for a given height in the atmosphere where the trail is observed to occur. The chief feature of such studies is the large dispersion in the inferred values of D, a characteristic that has, as yet, not been adequately addressed (Elford, 1993).

Jones (1995) has shown that the initial radial distribution of ionization in a meteor trail is far from Gaussian, and that the expression for $n(r, t)$ given in Equation (45) only holds when $4Dt \gg r_0^2$. Nevertheless, Jones also finds that for underdense trails the radar echo decays exponentially independent of the form of the initial radial distribution of ionization, so that in the case of parallel polarization the time constant $(4k^2D)^{-1}$ holds at all times during the lifetime of the echo. The predicted behavior of echoes under these conditions is shown in Figure 7 for three values of the diffusion coefficient (curves B, C, D). A remarkable feature of the plots is the great similarity in the phase-time curves prior to the t_0 point, a characteristic that is the basis of an accurate method for measuring meteor velocities.

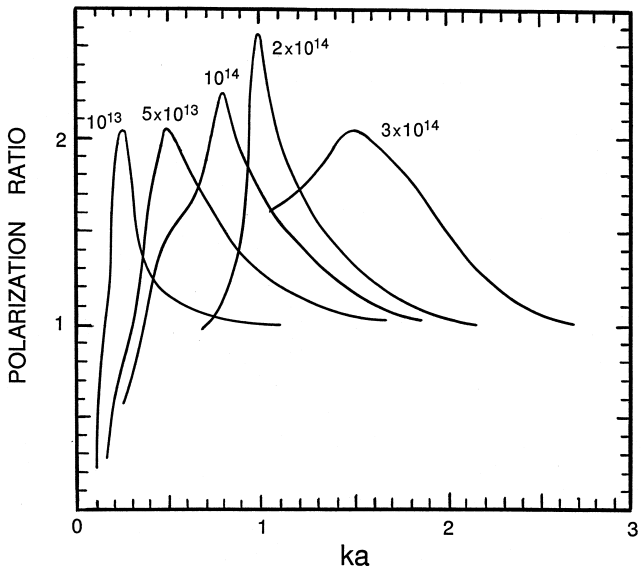

Figure 8. The polarization ratio $g_\perp/g_\parallel$ for underdense and transition trails as a function of ka where $(ka)^2 = 4k^2Dt + (kr_0)^2$ (after Poulter and Baggaley, 1977).

When the electric vector is *transverse* to the trail axis the separation of the ions and the electrons under the action of the field causes radial polarization and some degree of resonant oscillation in the column of ionization. The wave matching technique employed by Poulter and Baggaley (1977) predicts that for underdense trails the ratio $g_\perp/g_\parallel$ can reach a maximum of about 2 soon after formation of the trails. However for underdense trails the condition for resonance is short lived, the ratio $g_\perp/g_\parallel$ tending to unity as the trail diffuses and the density gradient of the ionization decreases (see Figure 8). For trails with line densities less than 10^{12} m^{-1} resonance is not significant and it can be assumed that at all times $g_\perp = g_\parallel$.

4.2.4. *Underdense Trails above 95 km*

At heights above 95 km the Earth's magnetic field significantly affects the motion of the electrons in a trail, and the diffusion becomes anisotropic. An appropriate coordinate system is shown in Figure 9, where the trail defines the Z-axis, and the ZX-plane is defined by the trail and the direction of the magnetic field. For backscatter, the vector **k** defines the wave-vector of the radiation incident on the trail in the specular mode.

As the trail diffuses the cross-section becomes increasingly more elliptical, and in the XY-plane the distribution of electron density is given by

$$n(x, y, t) = \frac{q \exp(-x^2/a_x^2 - y^2/a_y^2)}{\pi a_x a_y}, \tag{94}$$

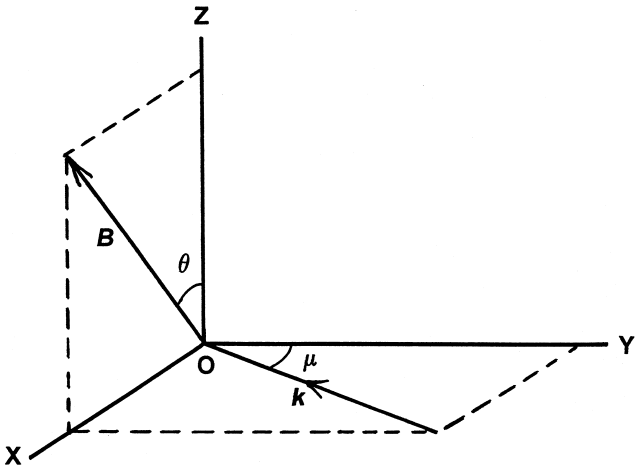

Figure 9. Coordinate system used to describe the effect of the Earth's magnetic field on the diffusion of trails occurring above 95 km. The trail lies along OZ, the angle between the magnetic field and the trail is θ, and the wave vector **k** for backscattering makes an angle μ with the OY axis.

where $a_x^2 = 4D_x t + r_0^2$ and $a_y^2 = 4D_y t + r_0^2$, and D_x and D_y are the diffusion coefficients along the OX and OY directions respectively (Jones, 1991). Values of D_x and D_y are given in Figure 6 as a function of height for several values of the angle θ between the trail and the magnetic field direction.

Equation (94) implies that the initial electron distribution ($t = 0$) has a Gaussian profile with circular symmetry, given by

$$n(x, y, 0) = \frac{q \exp(-r^2/r_0^2)}{\pi r_0^2}, \tag{95}$$

where $r^2 = x^2 + y^2$. As already discussed, Jones has shown that the initial ionization distribution is not Gaussian but is characterized by a high density core. However for underdense trails the backscatter observations can be well approximated by assuming a Gaussian distribution with an effective initial radius $r_{0(\text{eff})}$. Values of $r_{0(\text{eff})}$ are given in Table IX. Schematic contour plots of $n(x, y, t) =$ constant, at successive equal intervals of time are given in Figure 10.

The amplitude of the scattered wave is proportional to the Fourier transform of the distribution of the ion density n, and is given by (Jones, 1995)

$$a(\mu) = a_0 \exp(-4k^2 D_{\text{eff}}\, t), \tag{96}$$

where the wave-vector **k** has direction cosines $(\sin\mu, \cos\mu, 0)$, a_0 is the echo amplitude associated with the initial distribution (assumed to be circularly symmetric), and

$$D_{\text{eff}} = D_x \sin^2\mu + D_y \cos^2\mu. \tag{97}$$

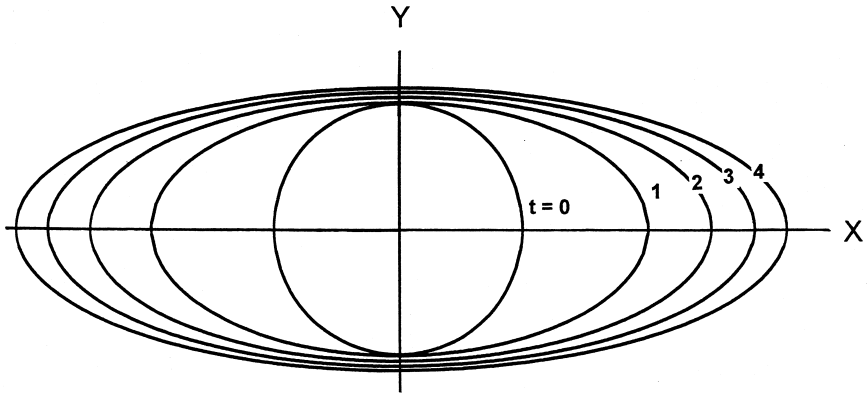

Figure 10. Section of a trail at 105 km at four successive equal intervals of time after the trail has formed at $t = 0$. Contour plots are curves of constant electron density. The Earth's magnetic field lies in the plane containing the axis of the trail and the major axis of the ellipse. Diffusion in the direction of the major axis is unaffected by the field; diffusion in the direction of the minor axis is severely inhibited. The angle between the field and the trail axis is 50°.

TABLE XV

Values of effective diffusion coefficient (m^2 s^{-1}). For $\theta < 5°$ D_{eff} becomes independent of μ and its value approaches D_{eff} ($\theta = 90°$, $\mu = 0°$)

θ	10°			50°			90°		
μ	0°	30°	90°	0°	30°	90°	0°	30°	90°
Height									
90 km	2.1	2.1	2.1	2.0	2.1	2.1	1.9	2.0	2.1
100 km	15.0	15.5	17.0	4.8	7.8	17.0	3.2	6.6	17.0
110 km	43.6	68.3	142	3.2	37.9	142	1.9	37.0	142
120 km	41.5	254	890	2.2	224	890	1.3	223	890

Values of D_{eff} are given in Table XV for a range of values of height, and angles θ and μ. A feature of the Table is the fact that all echoes, other than those observed in the plane containing the trail and the magnetic field ($\mu = 90°$), decay less rapidly than expected in the absence of the field. Such behavior has been observed in medium frequency observations of meteors (Brown, 1976). When the direction in which echoes are observed is orthogonal to the magnetic field (i.e., $\mu \to 0°$) and when $\theta \geq 40°$, the values of D_{eff} are similar (within a factor of 2) at all heights above 90 km; echoes observed under these conditions will decay far less rapidly than expected in the absence of the field.

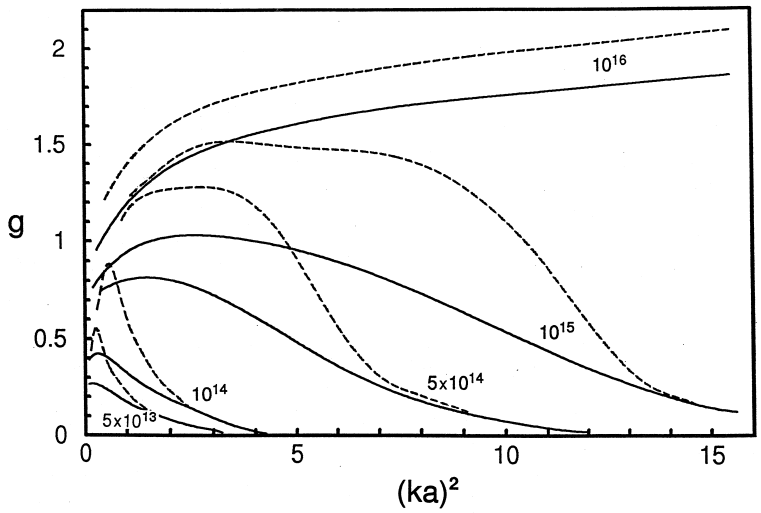

Figure 11. Reflection coefficients for parallel (full-line) and transverse (dashed-line) polarizations.

4.3. BACKSCATTERING FROM OVERDENSE TRAILS

4.3.1. *Overdense Trails below 95 km*

For overdense trails ($q > 5 \times 10^{14}$ m^{-1}) and for transition-type trails (10^{13} m$^{-1} < q < 5 \times 10^{14}$ m^{-1}) the full wave analysis of Poulter and Baggaley predicts reflection coefficients as shown in Figure 11. For overdense trails the reflection can be considered as taking place at the surface of the cylinder within which the dielectric constant is negative. The phase behavior of the reflected wave shown in Figure 12 indicates that for trails with line densities $> 10^{16}$ m^{-1} the metallic cylinder model holds well, while echoes from trails with line densities between 10^{14} and 10^{16} m^{-1} exhibit both overdense and underdense types of behavior. Inspection of the reflection coefficient plots for parallel polarization suggests that the changeover from overdense to underdense behavior can be considered as occurring at $g_{\parallel} = 0.45$. Then the duration of the overdense echo can be defined as the value of $(ka)^2$ when $g_{\parallel} = 0.45$. This gives a duration (in seconds) close to that given by an expression derived by McKinley (1961),

$$T_{ov} \cong 7 \times 10^{-17} \lambda^2 q D^{-1} - r_0^2 (4D)^{-1} \tag{98}$$

for D in m^2 s^{-1}, λ and r_0 in m, and q electrons m^{-1}. Except for trails at great heights the second term is usually much smaller than the first and can often be neglected. In these situations the duration of the overdense echo can be considered as proportional to the line density q. In those cases where the second term cannot be ignored the choice of a value for r_0 needs to take into account the possibility of an initial high density core as suggested by Jones (1995).

From a comparison of the maximum amplitudes of the overdense echoes in Figure 11 the reflection coefficient $(g_{\parallel})_{ov} \cong 7.5 \times 10^{-5} q^{0.275}$. This gives an echo

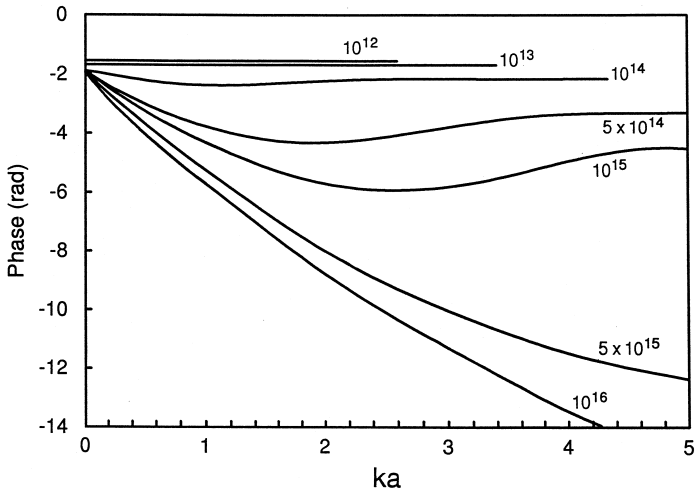

Figure 12. Phase angle (radians) of the reflected wave for parallel polarization.

power from overdense trails $\propto q^{0.55}$ over a range of line densities from 10^{14} to 10^{16} m^{-1}, which differs only marginally from the $q^{0.50}$ dependence based on the metallic cylinder model usually found in most discussions of meteor echoes (McKinley, 1961; Hughes, 1978). The full expression for the received echo power in watts from an overdense trail is

$$P_R = (g_\parallel)^2_{ov} P_T G_T G_R \lambda^3/(32\pi^4 R_0^3) = 1.8 \times 10^{-12} P_T G_T G_R (\lambda/R_0)^3 q^{0.55}. \quad (99)$$

The reflection coefficients for overdense trails under conditions of transverse polarization are also shown in Figure 11. In contrast to the transient resonant behavior of echoes from underdense trails, overdense trails exhibit resonant behavior during most of their life with a maximum polarization ratio that is close to 2. Transition-type echoes may also show resonance effects at wavelengths sufficiently long for the trail to have an overdense core for a significant time.

4.3.2. *Overdense Trails above 95 km*

As in the case of overdense trails occurring below 95 km the reflection is considered as taking place at the surface of a cylinder within which the dielectric constant is negative. However, due to the effect of the magnetic field the surfaces have elliptical cross-section with the major axis lying in the plane containing the axis of the trail and the direction of the magnetic field. The behavior of the surfaces of critical density as time elapses can be seen by reference to Figure 10 and noting the position of the curves of constant electron density at successive intervals of time. The position of the initial radius circle is indicative – its actual value must be determined by numerical analysis (Jones, 1995).

For those situations where the initial radius can be ignored ($4Dt \gg r_0^2$), the duration T, of the echo is given by

$$T/T_0 = D/(D_x\, D_y)^{1/2}, \tag{100}$$

where T_0 and D are the duration and diffusion coefficient if the field was zero, and D_x and D_y are as defined in the previous section (Jones, 1991).

4.3.3. *Duration of Overdense Echoes*

A radar echo from an overdense trail will endure as long as the electron concentration near the column axis exceeds the critical density for the radio wavelength being used. A comprehensive survey of the various processes of depletion of meteoric ionization has been given by Baggaley (1980), who has shown that the depletion is controlled by ambipolar diffusion above 93 km and by chemical destruction below 93 km. The chief chemical process is the reaction of meteoric ions with ozone to form oxide ions which rapidly recombine dissociatively with the free electrons. Jones et al. (1990) have shown that the duration distribution of overdense echoes at a given height has a 'characteristic time' corresponding to the change over from 'diffusion-limited' durations to 'chemistry-limited' durations. From the known rate-constants for the production of oxide ions, values of the 'characteristic times' can be converted to ozone concentrations. Thus, by observing the duration distributions at a number of heights, a profile of the ozone concentration between 80 and 100 km can be determined.

4.4. Attenuation Factors for Echoes from Underdense Trails

The factors which determine the amplitude of a radar echo from an underdense trail during the formation and initial evolution of the trail are well known and have already been alluded to in the earlier discussion on initial radius and diffusion of the ionization. It is now necessary to clearly identify the factors and quantify their effects as a function of velocity and height. The attenuation factors derived in what follows apply to the amplitude of the echo.

4.4.1. *Initial Radius Factor*

As already discussed the reflection coefficient for a segment of an underdense trail is given: $g = q\pi r_e \exp(-k^2a^2)$ where $a^2 = 4Dt + r_0^2$, and D and r_0 are the diffusion coefficient and initial radius appropriate to the height of the segment. (It is assumed that for the trails being considered here $g_\perp = g_\parallel = g$).

However, Jones (1995) has shown that the initial radius is far from Gaussian, and the reflection coefficient should be expressed as $g = q\pi r_e \alpha_r \exp(-4k^2Dt)$ where α_r is an attenuation factor dependent on the atmospheric number density n_a, the velocity V of the meteoroid, and the radio wavelength λ. Jones (1995) calculated a generalized form for α_r in terms of a parameter $\kappa = 4\pi V^{0.8}/(Cn_a\lambda)$, where C is 5.6×10^{-19} when V is in km s^{-1} and n_a and λ are in M.K.S. units. The

graphical form for α_r is given in Jones' paper. A suitable computation function for α_r ($\kappa \leq 8$) is

$$\alpha_r = \exp(-y^2) \tag{101}$$

and

$$y = a_0 + a_1\kappa + a_2\kappa^2 + a_3\kappa^3, \tag{102}$$

where $a_0 = 0.0292$, $a_1 = 0.8225$, $a_2 = -0.1374$, $a_3 = 0.0091$. Jones shows that the rms initial radius, $r_i = 1.593v^{0.8}/(Cn_a)$.

4.4.2. *Finite Velocity Factor*

Due to the finite velocity of the meteoroid, the trail is diffusing while the central Fresnel zone is being formed and the reflection coefficient of trail segments decreases with increasing distance back from the head of the trail (Kaiser, 1953). Peregudov (1958) has shown that the attenuation α_v due to this effect can be well approximated by the expression

$$\alpha_v = [1 - \exp(-\Delta)]\Delta^{-1}, \tag{103}$$

where $\Delta = 2k^2 D (2R\lambda)^{1/2} V^{-1}$, R is the range (m) and V the meteoroid speed (m s^{-1}). A comparison of the results of this attenuation expression with the results of a detailed integration along a diffusing trail at a zenith angle of 45° shows that the approximation is improved if the value of Δ in the expression is multiplied by a factor of 1.18.

4.4.3. *Pulse Repetition Rate Factor*

When the interpulse period of a meteor radar is comparable or longer than the decay time of the echo due to radial diffusion of the trail ionization, it is possible for a trail formed just after the passage of a transmitted pulse not to be detected by the subsequent pulse. The effect is significant when a radar is being used to determine the meteor flux. The echo rate reduction factor η, is given by

$$\eta = [1 - \exp(-w_1)]w_1^{-1}, \tag{104}$$

where $w_1 = 4(s-1)k^2 D p^{-1}$, s is the mass index of the meteoroids, $k = 2\pi/\lambda$, D is the diffusion coefficient, and p is the pulse repetition frequency in Hz. It is also useful to generate an average attenuation factor α_p due to the finite pulse repetition rate by determining the average amplitude of an exponential echo over one interpulse period. The expression for α_p is

$$\alpha_p = [1 - \exp(-w_2)]w_2^{-1}, \tag{105}$$

where $w_2 = 4k^2 D p^{-1}$, and w_2 is identical with w_1 when $s = 2$.

The above analysis can be extended to cases where the meteor echo recognition criterion is, say, n pulses above a limiting signal level. The expression for η then becomes

$$\eta = [1 - \exp(-w_1)][w_1 \exp w_1(n-1)]^{-1} \tag{106}$$

with a similar expression for α_p.

4.4.4. *Ionospheric Effects*

The ionosphere below a meteor trail acts as a doubly refracting medium for the passage of radio waves involved in the detection of meteors. For day-time conditions at frequencies less than about 10 MHz the ordinary and extraordinary waves may become manifest as two pulses with different amounts of retardation and absorption. For frequencies greater than about 15 MHz the phase difference between the ordinary and the extraordinary waves within the pulse produces Faraday rotation of the plane of polarization.

The amount of Faraday rotation to be expected on linearly polarized signals reflected from meteor trails depends on the integrated ionization over the propagation paths, the orientation of the path to the magnetic field and the radio frequency (Budden, 1985). An estimate of the effect can be determined by assuming a quasi-longitudinal approximation to the estimation of the ionospheric refractive index. Then the Faraday rotation Ω, between the ground and a meteor trail is given by

$$\Omega = 2.36 \times 10^4 f^{-2} \int_{\text{path}} B \cos\chi \; N(s) \, \mathrm{d}s \qquad \text{(radians)}, \tag{107}$$

where f is the wave frequency (Hz), B is the local geomagnetic field (Wb m^{-2}), χ is the angle between the wave propagation direction and the direction of B, N is the electron density (m^{-3}) and ds is a path element [m]. For backscatter the total rotation is 2Ω, and if the transmitting and receiving antennas have common linear polarizations, the amplitude of the echo is reduced by a factor α_F given by $\alpha_F = \cos(2\Omega)$. In general, calculations of Faraday rotation in the ionosphere need to be based on the full Appleton–Hartee expressions for the refractive index, including losses due to collisions (Budden, 1985).

For radars operating in the frequency range 20–40 MHz the amount of Faraday rotation of signals reflected from a meteor can exceed 90° during daytime. The most dramatic effect is on the amplitude of the echoes received from some specific height ranges. This will manifest itself directly as a height selection effect dependent on the elevation and azimuth of the reflection point, the time of the day, the dip angle of the magnetic field, and the solar activity. The effect of Faraday rotation on meteor echoes at 30 MHz during daytime is shown in Figure 13. As Faraday rotation is essentially an effect on linearly polarized signals, studies using circularly polarized transmissions are to a large extent immune to this effect. However, the use of, e.g., horizontal crossed dipoles fed in quadrature will only ensure

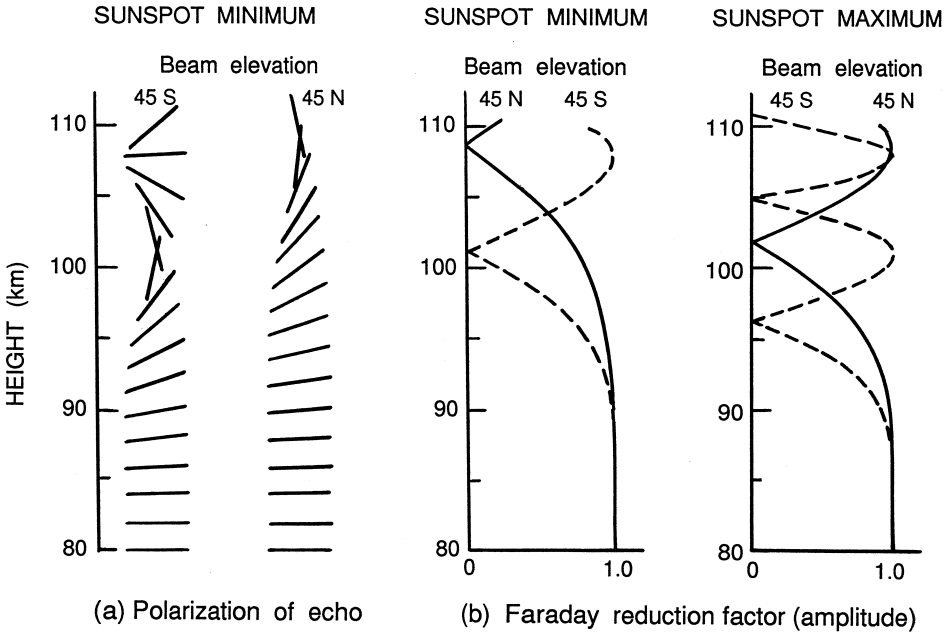

Figure 13. Effect of Faraday rotation in the ionosphere on meteor echoes observed at midday in medium latitudes (S. hemisphere). (a) Total rotation of the plane of polarization of echoes reflected from given heights. (b) Faraday reduction factor α_F, as a function of the height of a meteor.

circular polarization close to the zenith; at elevations of 45° the radiation exhibits significant elliptical polarization.

4.5. METEOR ECHO RATES AND THE RESPONSE FUNCTION

The measurement of meteor echo rates over long periods of observation has been a major feature of radar meteor studies. The basic parameters recorded for each echo are range and time of occurrence together with one or more of the amplitude, duration, phase and direction of arrival of the echo. To interpret meteor echo rates in terms of the flux of meteors entering the atmosphere, it is necessary to determine the fraction of the incident population detectable by the radar.

A meteor trail formed within the radiation pattern of a radar system will be detected if the orientation of the trail satisfies the geometrical condition of specular reflection, and if the echo power and duration exceed the threshold detection levels of the system. For the majority of meteor radars the number of echoes from underdense trails greatly exceeds that from overdense trails, so that the echo amplitude can be assumed to be proportional to the electron line density at the reflection point modified by the attenuation factors discussed in the previous section.

To make the connection between the observed line density and the original mass of the ablated meteoroid recourse must be made to the discussion and data given in Section 3.5, where it was shown that, over a wide mass range, meteoroids of a given

velocity tend to produce trails at the same height. Typically, the trails detected by radar extend over a height range of 10 to 15 km and the ionization distribution along the trail is well approximated by a parabolic function of the density of the atmosphere about the height of maximum ionization.

For meteors of the same velocity the maximum value of the line density $q_{\max}$ can be written as $q_{\max} \sim m \cos \chi$, where m is the initial mass of the meteoroid and χ is the zenith angle of the trail. At any position on the trail where the height is h, it is assumed that the line density q can be written as

$$q = Q(h) q_{\max}, \tag{108}$$

where $Q(h)$ describes the parabolic behavior of q as function of the density of the atmosphere. It is convenient to define a zenithal line density q_z as $q_z = q_{\max} / \cos \chi$.

Further, to interpret the echo rates it is necessary to assume a mass distribution for those meteoroids generating the majority of the trails detected by radar. For this purpose it is generally accepted that the flux of meteoroids with masses in excess of any value, m, is well described by a simple power law m^c, where the value of c lies in the range $-1.3 < c < -0.7$. Thus the flux of meteoroids $N(q_z)$ that produce trails with zenithal line densities greater than q_z can be expressed as a simple power law of the form

$$N(q_z) = K q_z^c = K (q_{\max} \sec \chi)^c. \tag{109}$$

At a height h where the line density is given by expression (108), the flux of meteors with line density $\geq q$ can be written as

$$N^*(q) = K [q \sec \chi / Q(h)]^c. \tag{110}$$

If the parameters of the meteor radar system are known with sufficient accuracy, the theoretical echo rate for a point source radiant of unit strength can be determined for all positions of the radiant in elevation and azimuth. The result of such a calculation is a description of the response of the radar system to a radiant in any position in the sky, and is appropriately called the *'response function'* of the system.

The calculation of the response function is based on the fact that, for almost all meteor radars, scattering from trails occurs specularly, so that the echoing points for meteors from a point radiant all lie in an 'echo plane' passing through the station and normal to the radiant direction. The geometry for a simple monostatic backscatter system is shown in Figure 14, where the radiant is at an elevation θ_r and azimuth angle ϕ_r, as seen from the radar site, and all possible reflection points **P** lie in the echo plane **ABCD**. All meteors with the same velocity are assumed to have the same height limits and thus all occur within the strip formed by the intersection of the echo plane and these height limits.

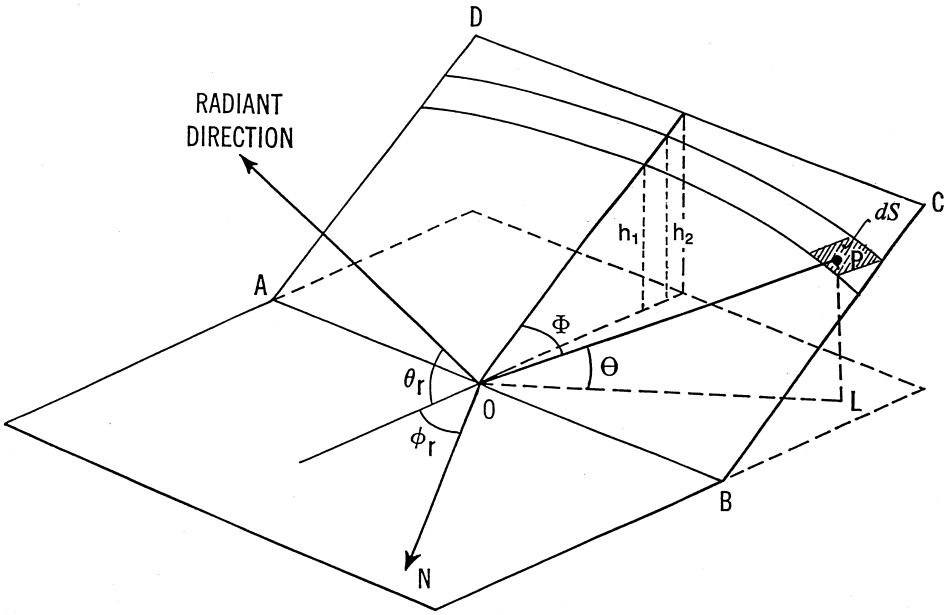

Figure 14. Geometry of the echo plane. The radiant direction is defined by the elevation angle θ_r and azimuth angle ϕ_r relative to the radar site at **O**. The reflection point **P** on the meteor trail in the echo plane **ABCD** is at elevation Θ and echo-plane azimuth Φ. Meteors of a given velocity have beginning and end heights h_2 and h_1, respectively.

Point **P** is within an area dS in the echo plane, which is at a range R, elevation angle Θ, height h, and echo plane azimuth angle Φ as measured in that plane. For the following analysis $\cos\chi$ can be approximated by $\sin\theta_r$ with negligible error, so that the meteor flux associated with a minimum line density q can be written as $N^*(q) = K[q \operatorname{cosec}\theta_r / Q(h)]^c$. The total echo rate n, is found by integrating over the echo-plane strip:

$$n(\theta_r, \phi_r) = \int\int K[q \operatorname{cosec}\theta_r / Q(h)]^c \, \mathrm{d}S, \tag{111}$$

where dS can be written $\mathrm{d}S = R\,\mathrm{d}R\,\mathrm{d}\Phi = F(h, \Theta)\,\mathrm{d}h\,\mathrm{d}\Phi$. For underdense trails, the minimum detectable line density q, is given by Equation (91):

$$q = 6.31 \times 10^{15} (R/\lambda)^{3/2} P_R^{1/2} (P_T\, G_T\, G_R)^{-1/2} \eta^{-1}, \tag{112}$$

where R is the range, λ is the wavelength, P_T is the transmitted power, G_T and G_R are the power gains of the transmitting and receiving antennas, respectively, with respect to an isotropic radiator, and P_R is the minimum detectable echo power for the system.

The factor η is the fractional reduction in the received echo amplitude due to (i) the finite initial diameter of the trail, (ii) diffusion during the formation of the

trail, (iii) diffusion during the interpulse period, (iv) the Faraday effect. These four attenuation factors have been discussed in the preceding section, where they were given the symbols $\alpha_r, \alpha_v, \alpha_p, \alpha_F$ respectively, and appropriate expressions for each were written down. Thus $\eta = \alpha_r \alpha_v \alpha_p \alpha_F$. All four factors are height dependent, whilst the Faraday factor α_F is also dependent on the time of the observation.

By substituting Equation (112) in (111) and carrying out the numerical integration for every position of the echo plane defined by a grid of radiant points (θ_r, ϕ_r), the *response function* of the system can be tabulated as an array and hence interpolated to give a contour representation of the function (Elford et al., 1994). The response function of a narrow beam radar is shown in Figure 17. The expected echo rate from a meteor shower with a given radiant can be readily predicted using the response function. The expected sporadic echo rate can also be estimated by convolving the response function with the sporadic radiant density distribution in the ecliptic coordinate system. Conversely, echo rate data associated with meteor showers can be interpreted in terms of the coordinates of the shower radiants.

In general, for a given radar system, response functions need to be calculated for a range of velocities from 10 to 70 km s^{-1}. If sporadic meteors are being observed the overall response function will be some weighted mean dependent on the velocity distribution (Taylor, 1995, 1996). The effect of Faraday rotation can be assessed by comparing the response functions calculated for diurnally changing ionospheric conditions.

4.6. METEOR VELOCITIES

The first technique used to measure meteor speeds with a radar was the range-time method by Hey and Stewart (1947). These measurements made use of the head echo, the speed being obtainable because of the later occurrence of a body echo, indicative of a meteor trajectory that crossed the radar beam at right angles. This method was soon superseded by the amplitude-time method, suggested by Herlofson (1948), which exploits the Fresnel diffraction characteristics of a specular echo (Ellyett and Davies, 1948; McKinley, 1961). Baggaley et al. (1994) employed a time-of-flight method for finding meteor speeds, as part of their AMOR system for measuring meteoroid orbits.

4.6.1. *Fresnel Amplitude-Time Method*

The theoretical behavior of the amplitude fluctuations of meteor echoes depicted in Figure 7 indicates that the spacing between the maxima, and the spacing between the minima are not grossly sensitive to the rate of decay of the echoes. Thus measurements of the times of occurrence of the maxima and minima together with the range, allow a determination of the speed of the meteoroid just after it has passed the t_0 point (McKinley, 1961). An improvement in precision and yield is obtained by using continuous-wave radars with the transmitter and receivers separated by 10–30 km. These radars combine the weak ground wave with the signal returned

from a meteor trail so that the phase information inherent in the received signal prior to the meteoroid reaching the specular point radio appears as amplitude fluctuations (McKinley, 1951, 1961; Mainstone, 1960). This type of measurement has the added advantage that unwanted phase effects due to the action of atmospheric winds on the trails can be measured and allowed for (Nilsson, 1964).

4.6.2. *Fresnel Phase-Time Method*

The theoretical behavior of the amplitude and phase of a radar echo from an underdense trail during the formative stages was already analyzed and depicted in Figure 7. Of particular interest here is the phase behavior of the echo prior to the t_0 point. It is clear that the phase-time curve is remarkably insensitive to the diffusion, even when the diffusion is so rapid that it has inhibited any post-t_0 Fresnel oscillations (curve D in Figure 7).

Recent developments in VHF radars make it possible to measure both phase and amplitude of the received signal. In these systems the receivers have dual channels, producing separate in-phase (p) and quadrature (q) output signals from which the amplitude A, and phase ϕ, are formed by the standard expressions $A^2 = p^2 + q^2$, and $\phi = \arctan(q/p)$. Typical systems have pulse repetition frequencies as high as 2000 Hz and narrow steerable beams. Although developed primarily for measuring winds in the troposphere, they are readily adapted for measuring winds in the lower thermosphere by observing drifts of meteors (Avery et al., 1990; Nakamura et al., 1991).

Figure 7(b) shows that the phase of the signal reflected by a meteor has a one-to-one correspondence with the x-value in Fresnel diffraction, where $x = 2Vt/(\lambda R)^{1/2}$ and the symbols have their usual meanings (see Section 4.2). Thus phase-time meteor data give $x(t)$ and hence the velocity V of the meteoroid (Elford et al., 1995). An example of a typical meteor echo obtained with the Adelaide VHF radar, operating on 54 MHz and at a pulse repetition frequency of 1024 Hz, is shown in Figure 15. The raw data in the left-hand panels shows (a) the exponential decay of the amplitude with only one Fresnel oscillation readily distinguished, and (b) the phase variation with time due to the action of the wind on the trail. To determine the $x(t)$ record from the phase-time data, the effect of the wind-induced phase shift is first removed from the whole of the record. The phase is then accumulated by removing all the 2π jumps, giving the result in panel (d). A fit of the theoretical curve to the phase-time record between 460 and 530 time units gave a velocity of 27.5 km s^{-1} with an uncertainty of less than 1%. The coherence in the phase record at low signal to noise in the amplitude record is a remarkable feature of this technique and is exhibited in all echoes. As a result about 70% of the echoes detected give a reliable velocity measurement. This is about 7 times the yield from the post-t_0 Fresnel oscillations. For those echoes exhibiting such amplitude oscillations a comparison of the pre- and post-t_0 velocities gives reliable deceleration measurements.

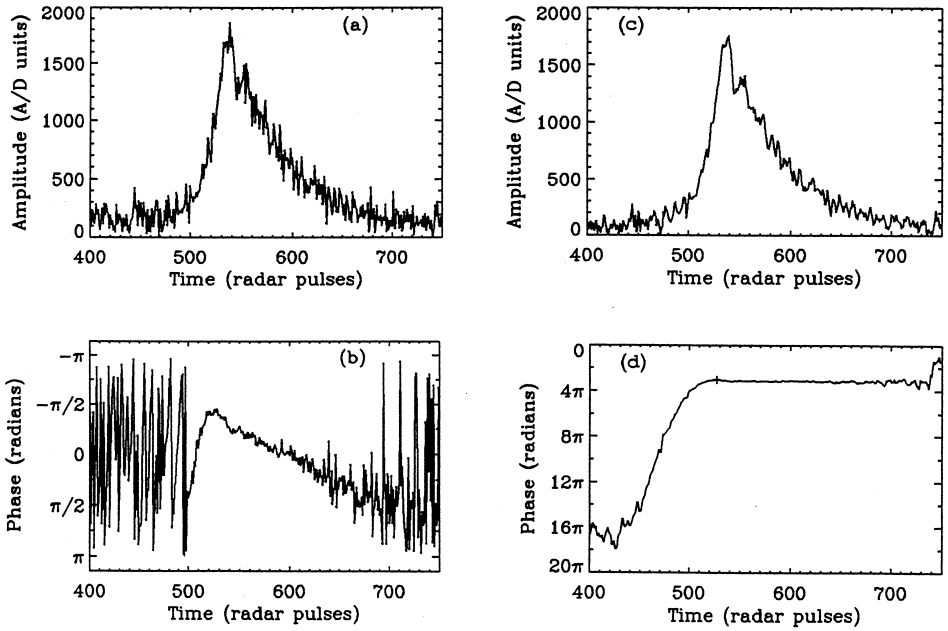

Figure 15. Meteor echo observed by the Adelaide VHF radar at a range of 110 km and at an elevation of 60°. The echo has a duration of about 1.2 seconds. The left-hand panels (a) and (b) show the raw data; the phase change between 540 and 670 time units is due to the bodily motion of the trail. The right-hand panels (c) and (d) show the effect of two-point smoothing and the effect of accumulating the phase (removing the 2π jumps) and removing the wind induced phase drift from the whole of the record.

4.6.3. *Pseudo Head-Echo Phase-Time Method*

At heights where the radius of a diffusing meteor trail exceeds $\lambda/2\pi$ the scattered radar signal is significantly attenuated and the effective scattering length of the trail can become too short to produce any Fresnel oscillations in the amplitude of the signal. Such a situation has already been described in Figure 7 (curve D), where the phase varies with time as if the meteor were a 'moving-ball target'. This situation has been analyzed in detail by Eshelman (1960). For the purposes of velocity measurement the phase behavior can be considered as a parabolic function of time about the t_0 point. This is analogous to the range behavior of the rare large head echoes described by McKinley (1961). Examples of these pseudo head-echoes and the associated estimates of velocity are given by Elford et al. (1995) and Cervera et al. (1997).

4.6.4. *'Down the Beam' Phase-Time Method*

The observation of meteors with narrow-beam (2–3°) VHF radars has revealed the presence of a new type of meteor echo that appears at consecutive decreasing range intervals in rapid succession (Taylor et al., 1996a). Such echoes are interpreted as being produced by meteoroids moving through the beam at a small angle to the

beam axis, and the time intervals between the appearance of the echoes at the given ranges give the line-of-sight velocities of the meteoroid. The precision of the line-of-sight speed measurement can be greatly improved by exploiting the observed phase changes between the returned pulses. Although the meteoroid moves a distance equivalent to many wavelengths between radar pulses, the integer number of phase cycles can be determined by comparison with the velocity inferred by the change in range. Assuming that the deceleration of the meteoroid at the commencement of the trail can be neglected, the total phase-time record then gives the speed of the meteoroid along its trajectory, and also the angle between the trajectory and the axis of the radar beam. The observations give velocities of remarkable precision and make possible measurements of the terminal deceleration (Taylor et al., 1996a).

4.6.5. *Time-of-Flight Method*

As part of the Advanced Meteor Orbit Radar (AMOR), Baggaley et al. (1994) developed a method of determining meteor velocities by equipping three sites 8–11 km apart with antennas that produce parallel fan-shaped beams, and measuring the time of flight between points on a trail where specular reflections occur for each of the sites. The reference points are the times of maximum gradients at the leading edge of each echo profile, and the overall velocity uncertainty is $\approx 3\%$.

4.7. METEOR HEIGHTS AND POSITION OF TRAILS

The simplest method for measuring the height of the reflection point on a trail is to use a narrow beam and measure the range of the echo. In fact, this method has only become available since the inception of VHF radars with steerable narrow beams ($\sim$2–3° wide). The more common technique is to use a combination of radar range together with a measurement of the direction of the reflection point by phase comparisons of signals received on closely spaced antennas. Height accuracies of 1–2 km are achieved using these methods. Typical height profiles of sporadic meteors using these techniques are shown in Figure 16. The observations leading to these profiles were all made at the same site (Adelaide, 35° S) and the results provide a self evident example of the gross effect of the 'height ceiling' associated with underdense echoes (McKinley, 1961; Steel and Elford, 1991; Elford, 1993).

The theoretical height distribution shown in Figure 16(a) was calculated by an extension of the response function analysis discussed earlier, and includes the attenuation factors due to the initial radius, and the diffusion of the trail during formation and during the interpulse period. The effect of Faraday rotation was not included as it is minimal at heights below 100 km at 54 MHz. The close similarity of the observed and predicted height distributions confirms that the attenuation factors are a good representation of the conditions applying in meteor trails in this region of the atmosphere.

To assess the effects of the attenuation factors at other frequencies, the product of the factors, given by η in Equation (112), was calculated as a function of height

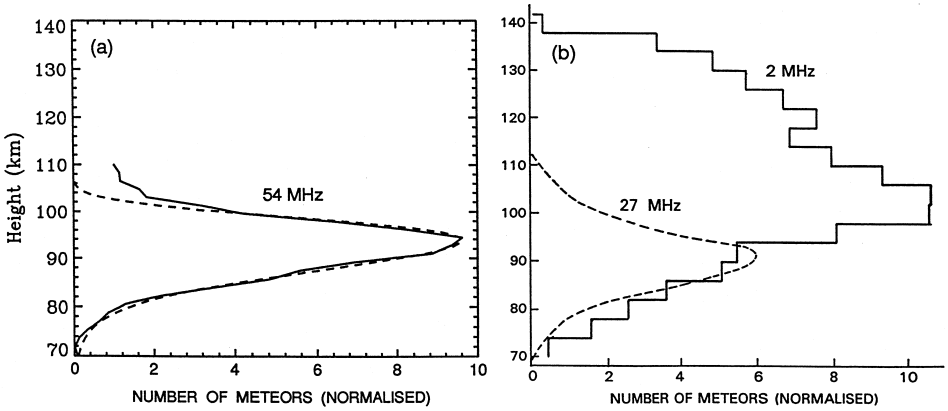

Figure 16. Height profiles of underdense sporadic meteors observed at the same site on three different radio frequencies. (a) full line: meteors detected in a pencil beam inclined at 30° to the zenith; dashed line: theoretical profile based on the response function of the system. (b) heights determined from measurements of range and angle of arrival of echo.

over a range of frequencies, and the heights noted where the values of the attenuation were 0.5 and 0.05. The results are given in Table XVI. In the calculation no allowance was made for the effect of Faraday rotation so that the results should be considered as indicative of night-time only. Above a height of 95 km the Earth's magnetic field causes the diffusion of the ionization to be anisotropic as already discussed and thus some mean value for the effective diffusion coefficient D_{eff}, was selected by setting θ and μ (Table XV) to about 45°. The values of the pulse repetition frequency given in Table XVI are typical of modern meteor radars. The heights where the attenuation is 0.05, called H_5 in the table, can be considered as the 'height ceiling' for radars operating at the frequencies listed.

As the 'height ceiling' for a 2 MHz radar exceeds the observational limit of the system (140 km) that gave rise to the height distribution given in Figure 16(b), the possibility of meteors occurring above this level cannot be excluded. If such meteors do exist their detection by radar will probably depend on the development of low-frequency high-power narrow-beam systems capable of detecting pseudo-head echoes of the type described in Section 4.6.3.

In some situations knowledge of the meteor height is required as part of other geophysical measurements such as wind drifts from observations of the doppler-shift of the meteor echo. While many meteor radar systems developed for these studies use range and direction of arrival to determine the heights, a significant number of systems infer heights from the decay time-constant of the amplitude-time profile of the echo. This procedure assumes a one-to-one correspondence between the time constant and the height. Many studies have now shown that this assumption is subject to a large uncertainty; the standard deviation of heights inferred from the decay time-constant is about 6 km. Significant contributors to this uncertainty include, (a) the combination of wind shear and variable ionization

TABLE XVI

Heights (H_{50} and H_5) where echo amplitudes attenuated by factors of 0.5 and 0.05, respectively

V (km s^{-1})		20		40		60	
Freq. (MHz)	Prf (Hz)	H_{50} (km)	H_5 (km)	H_{50} (km)	H_5 (km)	H_{50} (km)	H_5 (km)
50	1000	95	107	93	105	90	103
40	700	97	108	96	108	94	106
30	400	100	112	100	111	98	110
20	200	104	116	105	117	104	117
10	100	110	122	113	124	113	125
5	50	116	130	119	133	120	135
2	50	125	>140	124	>140	132	>140

along the trail, (b) the effect of the Earth's magnetic field at heights above 95 km, and (c) the fact that many measurements of amplitude decays include echoes from trails with line densities greater than 10^{13} m^{-1} (i.e., not strictly underdense). One further factor that could influence the decay time of a meteor echo is the presence of any external electric field. Such fields always accelerate the diffusion, and at high latitudes the external electric field can have sufficiently large values for the decay of meteor echoes to be significantly modified.

4.8. METEOR RADIANTS AND METEOROID ORBITS

4.8.1. *Meteor Shower Radiant*

Radar echoes from meteors that are members of a shower cause an increase of the echo rate above the sporadic background for a limited time on any one day. The situation is readily analyzed by the use of the response function of the radar, and an example is given in Figure 17 for a narrow beam system. In these cases the detection of the shower is analogous to the problem of detecting a radio pulse above a radio noise background. If a wider beam is used, say 10°, directed at low elevation, a shower becomes manifest as a characteristic temporal change in the ranges of the echoes. By using two antennas directed to azimuths symmetric about the east-west direction Aspinall et al. (1951) showed that the times of occurrence of shower meteor activity in each beam enabled the shower radiant to be determined. This technique has been exploited by many workers to detect showers and measure their radiants using a single station system (Weiss, 1955; Ellyett and Keay, 1956; Plavcová and Šimek, 1960; Belkovich and Pupyshev, 1968; Poole and Kaiser, 1972; Hughes, 1972). Further discrimination is possible by counting only those

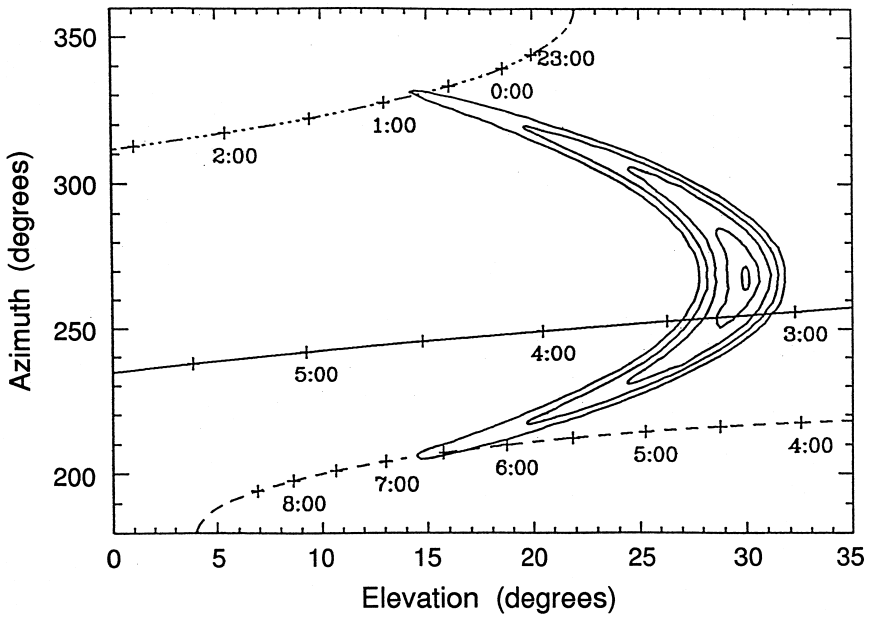

Figure 17. Response function of a 54 MHz radar with a narrow beam tilted 30° east of the zenith. Contours are at 20, 40, 60, 80, and 95% of the peak value. The other curves show the positions (and time) of three meteor radiants at declinations of +33° (top), −28° (center) and −59° (bottom).

echoes that occur in a limited range interval centered on the most probable range (Keay, 1957). Cervera et al. (1997) has shown that by including measurements of velocity using the phase-time method (Elford et al., 1995) weak showers can be identified in the rate data and their radiants measured.

4.8.2. *Distribution of Radiants*

When the direction of the reflection point is known, wide aperture radars can be used to determine the radiants of showers using a geometric procedure developed by Elford (Weiss, 1955), and Jones and Morton (1977), and applied as a technique for 'imaging radiant distributions' by Morton and Jones (1982), and Poole and Roux (1989). The latter authors have emphasized the importance of using an all-sky radar for this work, and Figure 18 shows an example of the radiant distributions obtained by these authors.

In principle the radar data could be deconvolved to determine the general radiant activity distribution over the sky (Jones, 1977), but this procedure requires the development of appropriate fast computational algorithms. In order to describe the radiant distributions in terms of a given limiting electron line density, corrections need to be applied for the antenna polar diagram and the various selectivity effects discussed in Section 4.4. As all these factors are included in the system response function, and as the direction of each reflection point is known, each observation can be weighted according to the reciprocal of the appropriate value of the response

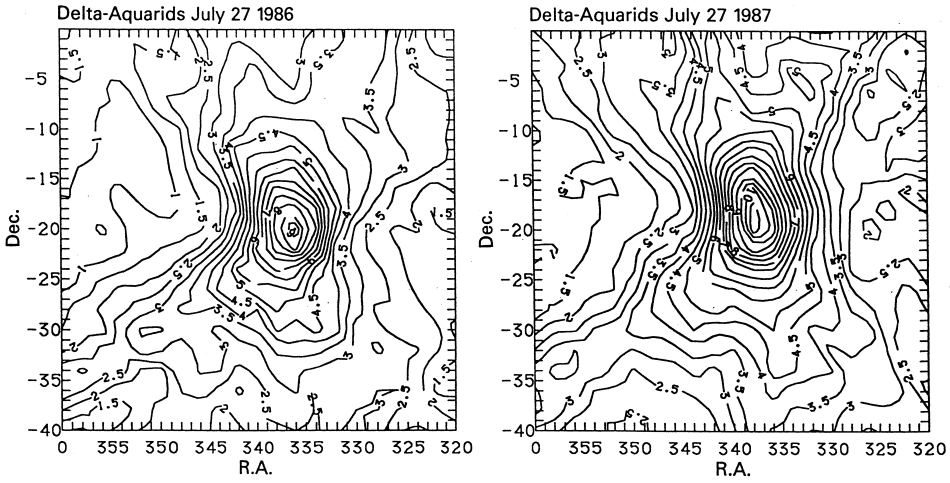

Figure 18. Radiant activity in the vicinity of the δ-Aquarid shower radiant in 1986 and 1987 deduced from measurements of the direction of radar reflection points, using the meteor radar at Grahamstown, South Africa. Contours are hourly rate of echoes attributed to radiants at the positions specified. The hour-glass shape of the distributions is an artifact of the slight anisotropy in the system. The resolution is $\sim 2^\circ$ (after Poole and Roux, 1989).

function. The final step, to present the distributions in terms of a given limiting mass requires knowledge of the velocity of each meteor, and the meteoroid ionizing efficiency.

4.8.3. *Individual Radiants and Orbits*

Radiants of individual radar meteors can be determined by using three or more closely spaced receivers (4–15 km separation) as first suggested by T.R. Kaiser (Gill and Davies, 1956). Most systems make use of the time difference between the commencement of the echo at each receiving site together with the velocity of the meteoroid deduced from the Fresnel oscillations. These measurements together with the time of observation are sufficient to determine the radiant of the meteor and the orbit of the meteoroid. The majority of the observations have been carried out with pulse transmissions (Davies and Gill, 1960; Kashcheev and Lebedinets, 1967; Lebedinets, 1968; Fedynski, 1975, 1977; Kashcheev and Tchakuk, 1980; Lebedinets et al., 1982). The Harvard Radio Meteor System, developed and operated in the 1960s, extended orbits measurements to trails with a limiting magnitude of $+12$. Further, the system was phase coherent so that the motion of the reflection points due to winds could be measured, and the observations of meteoroid speed and trail orientation corrected appropriately (Cook et al., 1972; Sekanina, 1976).

Nilsson (1964) and Gartrell and Elford (1975) used CW systems with the transmitter separated 20–30 km from the three or more receiving sites. The velocity was determined from the pre-t_0 diffraction fluctuations as discussed in Section 4.6, and corrections applied for the effect of winds. Oblique scatter CW observations over

an extended path were used by Andrianov et al. (1968) to determine radiants and velocities, the obliquity of the path increasing the effective 'height ceiling' from about 108 to 120 km.

The installation of the Advanced Meteor Orbit Radar (AMOR) near Christchurch, New Zealand in the early 1990s has revolutionized the collection of meteoroid orbit data (Baggaley et al., 1994). With a magnitude limit of about +13, the system is capable of yielding 1500 orbits per day. AMOR has two distinctive features (a) south and north directed fan-shaped beams, narrow in azimuth (transmitting $\pm 0.7^\circ$, receiving $\pm 1.6^\circ$) and broad in elevation permitting a large declination response, and (b) meteor speed measurements based on the time of flight between points on the trails where specular reflections occur for each of three sites separated by 8–11 km. In addition 10–15% of the echoes yield speeds from the Fresnel diffraction pattern analysis, which enable decelerations to be determined for 5–10% of the observations. Almost 1% of the meteoroids have atmospheric speeds measured in excess of 100 km s^{-1}. Taylor et al. (1996b) have shown that these meteoroids are interstellar, identifying two galactic sources and tentatively suggesting a third.

The correction of the distributions of radar meteor orbit data for selectivity effects has also been discussed by Lebedinets (1968) and by Cook et al. (1972). These authors differed markedly on the extent of the correction due to the initial radius of a trail. It is generally agreed that this is still the factor of greatest uncertainty.

4.9. NON-SPECULAR ECHOES

Although the majority of radar meteor echoes are scattered from trails under the specular condition, the occurence of long enduring echoes exhibiting deep fading indicates the presence of multiple scattering regions. In some cases such echoes are due to the action of winds distorting an essentially smooth trail; in other cases the distribution of ionization along the trail is sufficiently irregular that the scattering can be considered to occur from a few regions where the ionization is most intense.

A special case of non-specular echoes is the 'head echo' which shows a change in range consistent with scattering from ionization close to the head of the trail (McIntosh, 1962, 1963; McKinley, 1961). Zhou et al. (1995) have reported that this type of echo has been observed with the 430 MHz Arecibo incoherent scatter radar over a height range of 80 to 120 km. The 'down the beam' echoes observed with narrow-beam VHF radars are further examples of head echoes (Taylor et al., 1996a).

By sampling the amplitude of VHF 'down the beam' head echoes in successive range bins, an amplitude-time profile of the echo can be determined and related to the distribution of ionization along the trail. An example of such an observation is shown in Figure 19, where the meteor shows a terminal flare, probably due to severe fragmentation (Taylor and Elford, 1998). Some 'down the beam' echoes show a regular beat pattern, which is interpreted as the combination of echoes from two regions of ionization separated by a few meters along a common trajectory. Taylor

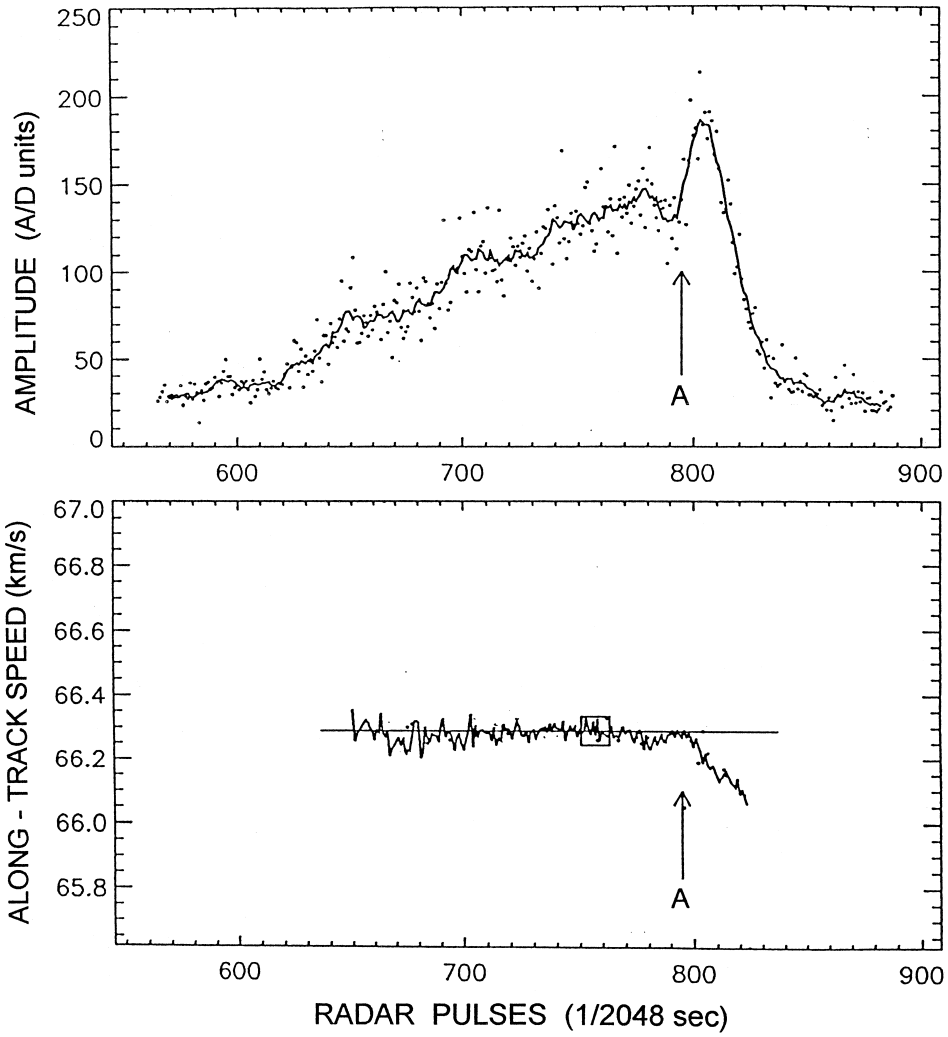

Figure 19. Amplitude of a meteor radar echo (top), and the speed of the ablating meteoroid determined from a 'head echo' observed using a narrow beam VHF radar. The meteoroid entered the beam at 21° to the beam axis and during the time interval 600–750 units moved at constant speed. The particle then underwent a catastrophic event at A and burnt out. The associated 'flare' in amplitude and the large deceleration suggest major fragmentation into many particles.

and Elford suggest that this is evidence for gross fragmentation of a meteoroid into two parts of relatively similar mass.

As the head echo from a meteor occurs over a significant change in height, such echoes observed in daytime are likely to show amplitude variations that are a result of the change in the degree of Faraday rotation of the received signal as the meteoroid descends in the atmosphere (see Section 4.4.4). In this context it should

be noted that a striking change in the amplitude profile of head echoes at sunrise has been reported by McIntosh (1963).

4.10. FORWARD SCATTER FROM METEOR TRAILS

Radio propagation over distances of the order of 2000 km are possible by forward scattering from meteors. The geometry of forward-scatter is described by McKinley (1961) and a full-wave treatment of the situation for both underdense and overdense trails has been presented by Jones and Jones (1990, 1991).

From the astronomical point of view the most significant feature of meteor forward scatter is that for underdense trails the effects of the initial radius and diffusion on the scattered signal are similar to the backscatter case but with the wavelength λ being replaced by a term $\lambda \sec\phi$, where 2ϕ is the forward scattering angle at the reflection point on the trail. As $\sec\phi$ is typically about 3, the decay time constant is increased by a factor of 9 over that expected for backscatter at the same wavelength. Thus forward scatter has the potential to explore populations of meteors that are inaccessible to backscatter systems on the same wavelength.

Jones and Jones (1991) showed that for forward scatter from overdense trails the duration of the echo is given by an expression similar to that for backscatter but with the wavelength λ being replaced by the term $\lambda\,\mathrm{cosec}(\theta)$, where θ is the oblique angle, i.e., of the trail at the reflection point on the trail.

Notwithstanding the advantages of forward scatter, the interpretation of the observations are complicated by a number of geometrical and propagation factors that do not occur with back scatter observations (Baggaley, 1979).

5. Composition and Structure of Meteoroids

5.1. METEORITES – SAMPLES OF METEOROIDS IN LABORATORIES

If a meteoroid is sufficiently large and its velocity low, a substantial rest mass lands onto the Earth's surface. If recovered, it is called a *meteorite*. These masses of interplanetary origin (sometimes with interstellar inclusions) form a unique opportunity to study the high strength populations of meteoroids in laboratories. This way only populations of type I and partly also of type II can be directly studied giving enormous amount of information incomparable to the indirect methods possible for meteoroids as described in Section 5.2.1 and Table XVII. Precise orbits of meteorites based on photographic or videorecords from at least two different stations are quite rare: there are only four cases so far documented (Příbram, Lost City, Innisfree, and Peekskill). All four of these orbits are asteroidal and of Apollo type.

Also the friable part of the interplanetary matter is accesible to direct laboratory measurements thanks to collections of dust grains in the upper atmosphere. Larger

chunks of friable meteoroids never reach the Earth's surface, except they are very large and give origin to an explosive impact crater.

5.2. MECHANICAL PROPERTIES

5.2.1. *Meteoroid Polulations*

Different meteoroid populations were first recognized independently by Jacchia (1958) and Ceplecha (1958). The differences in beginning heights proved to be the most important tool for recognition of different meteoroid populations among Super-Schmidt and small-camera meteors when and if the right dependence on velocity was considered (Ceplecha, 1967a, 1968, 1988). This was also expanded to faint TV meteors (Hawkes et al., 1984; Jones et al., 1985). Two main discrete levels of meteor beginning heights were found. They are separated by 10 km difference. The lower level was denoted A, the higher was denoted C (Table XVII). The C-group of meteoroids was recognized to contain two populations of orbits: one with ecliptically-concentrated short-period orbits was denoted C1 and the other with random orbital inclinations of long-period orbits was denoted C2. Classical meteor showers with known parent comets are of type C1 or C2; thus the cometary origin of meteoroids of the whole C-group is quite convincing.

In addition, two smaller groups were found among Super-Schmidt, small-camera and TV meteors. The intermediate group B has typical orbits with small perihelion distances and aphelion close to Jupiter. The other smaller group was originally referred to as a group 'above C' accounting for very high beginning heights. Today the notation D is used for this group. The Draconid meteor shower is a typical member of this group. It contains extremely friable meteoroids with the lowest known densities of all types of solid cometary material coming to the Earth (Ceplecha, 1968).

Details on these four populations of big meteoroids can be found elsewhere (Ceplecha and McCrosky, 1976; Ceplecha, 1977, 1983, 1985, 1994a; Sekanina, 1983; Wetherill and ReVelle, 1981a,b). Four independent methods gave results differing in details, but the existence of four groups of fireballs according to various ablation abilities of their bodies, as found originally by Ceplecha and McCrosky (1976), has been confirmed. A brief summary of the fireball groups follows. Group I fireballs are of the smallest ablation ability and of the greatest bulk density. Among them are the *Příbram, Lost City* and *Innisfree* meteorite falls. Group I was proposed to be connected with ordinary chondrites *before* the Innisfree meteorite fall. Group II fireballs belong to meteoroids of somewhat lower density and greater ablation ability than the group I meteoroids. It is proposed that the group II fireballs belong to carbonaceous bodies, which mostly disintegrate in the atmosphere and only the most compact members of their population can reach the ground as carbonaceous chondrites of CI and CM types. This meteoric material may be both of asteroidal and cometary origin. Wetherill and ReVelle (1981b) prefer rather the cometary source. The average ablation coefficient of the type I fireball is 0.014 s^2 km^{-2},

while the same value for the type II fireball is 0.042 s^2 km^{-2} (based on individual determinations of total ablation coefficient from the most precise photographic records of fireballs).

Group IIIA contains bodies with a high ablation ability and small bulk density less than 1000 kg m^{-3}. The cometary origin of these meteoroids is evident, because cometary shower meteors belong to this group. Also the two systems of orbits, i.e., the short-period ecliptically-concentrated system and the long-period randomly-inclined system (IIIAi) exist among fireballs of group IIIA, in complete analogy to cometary orbits. In addition a third system or subgroup among these IIIA fireballs, denoted C3, has short-period but randomly-inclined orbits. This C3 system forms only 4% of all fireballs, but becomes the most important for meteoroids with masses below 10^{-6} kg (Hawkes et al., 1984; Jones et al., 1985). The mass-selective ejection-velocities from long-period comets is suspected to be the main reason for existence of such a system of orbits of cometary meteoroids.

The fourth group of fireballs was denoted IIIB. Bodies of this group have the highest known ablation ability and the smallest bulk density of several hundreds of kg m^{-3}. Fireballs of the Draconid meteor shower belong to this group. The cometary origin is also evident. It is rather surprising that this group contains relatively more bodies among fireballs than among fainter meteors. Evidently more cometary material comes to the Earth in meter and ten meter size ranges than estimated before photographic observations on fireballs became available.

Table XVII contains a survey of all meteoroid populations as delineated among bodies observed by different technics. Also iron meteoroids are presented as a separate population recently recognized by ReVelle and Ceplecha (1994) in PN fireball data. The whole range covers masses from 2×10^{-8} kg to 2×10^{3} kg. Table XVII contains the fraction of bodies of the given group among all observed meteor bodies. 'Characteristic' orbits are also given for each group, but these values are maxima (and sometimes medians) of very broad irregular statistical distributions. *It is not possible to separate these populations using the orbital elements alone.* The average value of the bulk density of the bodies, ϱ_m, and the average value of the ablation coefficient σ, are given for each group. The proposed probable 'composition and structure' of the groups, as given in the last column of Table XVII, is established on many facts: values of the bulk densities and of the ablation coefficients, the direct identification of 3 photographic meteorite falls with group I fireballs, the detailed study by Wetherill and ReVelle (1981a) on the relation of ordinary chondrites to fireballs, the study by the same authors (1981b) of the cometary origin of some fireballs, the classification of shower meteors with known parent comets as C and IIIA groups, the classification of Giaccobinids (γ Draconids) as D and IIIB groups, the spectral records containing the radiation of CN for the group II, IIIA and IIIB bodies, but not containing CN radiation for the group I fireballs. Parent bodies of group I are evidently asteroids, the most important of them having orbits probably close to the 3:1 Kirkwood gap (Wetherill, 1985). Parent bodies of group II and group A are perhaps partly asteroids and partly

TABLE XVII

Survey of meteoroid populations among photographic and television meteors. a is the semi-major axis, e is the eccentricity, i is the inclination, ρ_M is the meteoroid bulk density in (1000 kg m^{-3}), σ is the ablation coefficient in (s^2 km^{-2}), % obs is the relative observed number of meteors in percent, ast.met. means 'asteroidal meteors'

	Television cameras				Super-Schmidt				Small cameras				Fireball networks					Properties of the meteoroid material		
mass range	b) from 2×10^{-8} to 5×10^{-6} kg				b) from 5×10^{-7} to 10^{-3} kg				b) from 10^{-4} to 0.5 kg				b) from 0.1 to 2×10^{3} kg							
group	% obs	characteristic orbit			% obs	characteristic orbit			% obs	characteristic orbit			group	% obs	characteristic orbit			ρ_M	σ	assumed composition parent bodies
		a	e	i		a	e	i		a	e	i			a	e	i			
													irons	3	1.8	0.5	6°	7.8	≈ 0.07	iron meteorites asteroids
ast. met.	<1	a) 0.7	a) 0.39	a) 18°	1	2.4	0.64	15°	5	2.5	0.64	10°	I	29	2.4	0.68	6°	3.7	0.014	ordinary chondrites asteroids
A	27	1.6	0.55	14°	50	2.3	0.61	1°	39	2.5	0.64	4°	II	33	2.3	0.61	5°	2.0	0.042	carbonaceous chondrites comets, asteroids
B	2	2.1	0.95	29°	3	2.4	0.92	5°	5	2.5	0.90	6°	–	–	–	–	–	1.0	0.08	dense cometary material inner parts of comets
c) C1	21	1.7	0.63	16°	7	2.2	0.80	6°	11	2.5	0.80	5°	c) IIIA	11	2.4	0.82	4°	0.75	0.10	regular cometary material short period comets
C2	18	≈∞	0.99	ran- dom	32	≈∞	0.99	ran- dom	21	≈∞	0.99	ran- dom	IIIAi	11	≈∞	0.99	ran- dom	0.75	0.10	regular cometary material long period comets
c) C3	28	1.3	0.60	ran- dom	6	1.9	0.72	ran- dom	9	2.1	0.77	ran- dom	c) C3	4	2.7	0.67	ran- dom	0.75	0.10	regular cometary material long period comets ?
D	3	2.6	0.66	18°	1	3.3	0.70	25°	10	3.1	0.77	10°	IIIB	9	3.0	0.70	13°	0.27	0.21	soft cometary material short period comets of Giacobini-Zinner type

a) only one meteor No. 811104060 recognized as "asteroidal"; its elements are given.

b) total mass range: individual groups differ due to different distribution of velocities.

c) C3 corrected for random i (instead of $i > 35°$) by adding the correspondiong part of C1 (IIIA) to C3.

comets (Wetherill and ReVelle, 1981b); comets may be their primary source. All the rest of the bodies (B, C, D, IIIA, IIIB) are clearly of cometary origin.

The characteristic orbits for the individual groups show the most systematic difference in eccentricities: ordinary chondrites and carbonaceous chondrites have the characteristic orbit with the smallest eccentricity, 0.6. The Draconid type of material has a somewhat higher eccentricity, 0.7. The regular cometary material with ecliptic concentration even higher, 0.8, followed by the dense cometary material of the B-group, 0.9, and by the cometary material with randomly inclined long-period orbits whose eccentricity approaches 1. This holds for bodies above 0.1 gram. Smaller meteoroids in groups A, C1, C3 and D have distinctly smaller eccentricities and also the semimajor axes of these small meteoroids are shorter. Meteoroids smaller than 0.1 g frequently have semimajor axes between 0.5 and 1. A.U., which is quite an exception for larger bodies. This is probably due to the radiation forces (Gustafson and Adolfsson, 1995).

5.2.2. *Fragmentation Classes and Strength Categories*

When the gross-fragmentation model was applied to the most precise photographic records of Prairie Network fireballs (with precision of the solution for one measured distance along the trajectory $\varepsilon_l < \pm 30$ m), three different fragmentation classes of meteoroid interaction with the atmosphere were revealed (Ceplecha et al., 1993):

NF $\equiv$ without gross-fragmentation (fireballs, which yielded only the single-body solution).

1F $\equiv$ with one point of sudden overwhelming fragmentation (fireballs, which yielded solution for one fragmentation point).

MF $\equiv$ with many points (at least two) of comparable amount of fragmentation (fireballs, which yielded no single-body solution and also no solution with one gross-fragmentation point: they can be solved for partial parts of their trajectories containing just one gross-fragmentation point).

For all these classes including NF, continuous fragmentation can be estimated from the value of the resulting ablation coefficient. From 80 records of PN fireballs with the most precise values of the measured distances and heights, 21 proved to be NF class, 19 cases 1F, 11 cases MF and 29 cases could not be classified due to still low precision. This classification reflects the ability of meteoroids to withstand fragmentation and their ability to be then crushed in the atmosphere suddenly at a point. The classification of meteoroids according to their ablation ability (with the continuous fragmentation included) into groups (types) I, II, IIIA, and IIIB (see Section 5.2.1), and the classification into NF, 1F, and MF classes as defined in this section, they both form two dimensional diagnostic in some extent separating the influence of composition of the body from the influence of its structure.

The dynamic pressure $p = \rho v^2$ at the fragmentation points of the 1F and MF cases can be also computed. Histogram of them is in Figure 20. Preference of some pressure values is evident. Thus also several strength categories of meteoroids can

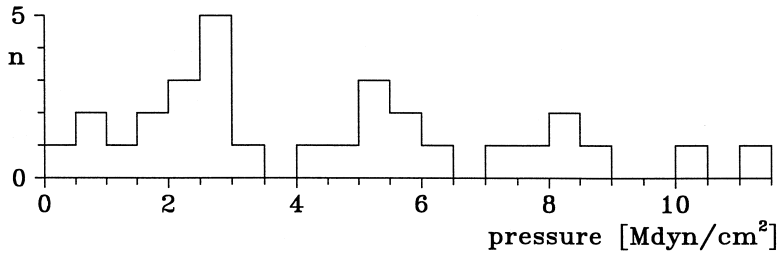

Figure 20. Histogram of dynamic pressure at fragmentation points of 1F and MF fireballs.

TABLE XVIII
Definition of strength categories

Strength category	Interval of p (MPa)	Average p (MPa)
a	$p < 0.14$	0.08
b	$0.14 \leq p < 0.39$	0.25
c	$0.39 \leq p < 0.67$	0.53
d	$0.67 \leq p < 0.97$	0.80
e	$0.97 \leq p < 1.20$	1.10

be defined at prevailing values of pressures, where meteoroid gross-fragmentation takes place (Table XVIII). More precise photographic records are needed to be sure of such a classification according to meteoroid strength (Ceplecha, 1994a).

The maximum dynamic pressure acting on the NF (no fragmentation) fireballs is mostly below 1.2 MPa with the exception of very strong bodies. The largest pressure among 21 studied fireballs of class NF was found for PN 39935A, which survived 5 MPa. About one half of the type I gross-fragmentation is realized at several points for one fireball. Type II fireballs with gross-fragmentation have usually only one fragmentation point.

The gross-fragmentation process is more frequent for stronger types of fireballs. For group I, there are almost twice as many 1F+MF classes as NF classes, whereas for group II, these two categories occur at almost equal rates. And the only IIIB type, which gave enough precise solution, was of NF class. But the ablation in both single-body and the fragmentation model already contains also the continuous fragmentation. Thus the studied meteoroid of the IIIB type (PN 39973) fragmented very smoothly and continuously without sudden gross-fragmentation. The maximum pressure it suffered was only 0.0088 MPa at the terminal height of 75 km with terminal velocity of 15.5 ± 0.3 km s^{-1}. Other extreme belonging to the NF class is the already mentioned meteoroid PN 39935A. Its very low ablation coefficient of

0.0010 ± 0.0005 guarantees that continuous fragmentation was almost completely absent.

Another parameter determined in the gross-fragmentation model is the amount of fragmented mass, m_f, relatively to the mass immediately before gross-fragmentation. This amount of fragmentation for 1F class is typically 60%, which corresponds to breaking the body into approximately two halves with some accompanying small fragments. Also values between 95% and 99% are quite frequent corresponding to nearly complete disruption of the body. The MF class shows only a marginal preference for values of 65% mass stripped of the main body. Thus a typical sudden fragmentation for almost half of all fragmented meteoroids is equivalent to stripping away slightly more than half of the mass.

5.2.3. *Non-Existent Average Meteoroid*

The old interpretation of Super-Schmidt meteors by Verniani (1965, 1967) assigned very low bulk densities to all meteoroids. Although his results which were based on the simple equalization of photometric and dynamic masses in Hoppe's theory (single-body theory) have been critically rejected many times, we can still hear or read the following universal statement: 'all meteoroids are low-density friable fluffy particles of cometary origin'. This is evidently a false statement and the reason mostly lies in Verniani's 'double biased' statistical treatment of the data. Most of the Super-Schmidt meteors were published by McCrosky and Posen (1961) without any selection at all. This material contains 50% of the A-type bodies and 45% of the C-type bodies. Jacchia and Whipple (1961) were interested in precise data on initial velocities, on orbits and thus on good atmospheric trajectories: they chose the longer trajectories for this purpose. Their selection of 413 Super-Schmidt meteors contains 32% of the A-type bodies and 62% of the C-type bodies. Verniani (1967) in his final analysis used 189 'best' meteors selected from Jacchia's and Whipple's 413: among other criteria for his rather narrow selection he used the 'regular' statistical distribution of the ratio of dynamic to photometric mass, expressed as $\log(\tau_0/\varrho_m^2)$. This selection worked exactly in the same way as Jacchia's and Whipple's selection. Among the 189 meteors of Verniani's selection from Jacchia's and Whipple's selection of 413 meteors there remained only 20% of the A-type bodies and 75% of the C-type bodies. Verniani actually recognized these 20% of meteors as bodies of densities higher that the rest, but he then used an average dependence of his $\log(\tau_0/\varrho_m^2)$ on $\log v$ (an incorrect exponent resulted, because of two superposed statistical distributions) thus smoothing these 20% into the overwhelming rest of 75% of the C-bodies. His statement that all meteoroids are low-density friable bodies of cometary origin should be attributed, as a first approximation, only to the C-type bodies. Also the absolute values of the bulk densities of 'all meteors' of Verniani are too low due to the above mentioned smoothing over two different statistical distributions and due to the applied but uncalibrated equivalence of photometric and dynamic mass.

5.3. CHEMICAL COMPOSITION

Besides the mechanical properties, chemical composition of meteoroids is the second most important parameter for classification of meteoroids and for relating them to other objects of the solar system. In fact, chemical composition is well known for meteorites and we will primarily compare meteoroids observed as meteors with meteorites. On the contrary, meteors can enlarge our knowledge on the composition of comets and asteroids, if origin of a corresponding meteor is established on the basis of the orbit or the mechanical properties. For comets, only volatiles can be usually observed spectroscopically in comae. The ratios of heavier elements could be determined only for few comets approaching closely the Sun and from in situ mass spectroscopy at comet Halley. For asteroids, the chemical composition has been only roughly estimated by the comparison of their reflectance spectra with those of known materials.

Two approaches have been used to derive meteoroid chemical composition from meteor spectra. The first is based on laboratory experiments. Savage and Boitnott (1973) simulated the meteor conditions and measured the brightness of the major emissions of Na, Ca, Mg, and Fe in the spectrum. The results are applicable to faint meteors under free molecular flow. They were used by Millman (1972) to derive the ratios of the above four elements in Giacobinid meteors. The derived average ratios are in good agreement with the composition of ordinary chondrites (see Table XIX).

The second approach is the physical interpretation of spectra of bright fireballs with sufficient number of lines. As described in Section 3.3, different authors started from different assumptions when interpreting the spectra. Harvey (1973c) and Nagasawa (1978) assumed optically thin radiation, Ceplecha (1964, 1965) constructed the emission curve of growth, and Borovička (1993) computed meteor synthetic spectra. Their results summarized in Table XIX differ due to the methods used rather than to real differences among the meteors studied. In the next we follow in detail the most extensive computation so far available done by Borovička (1993), who analyzed a fireball spectrum at 43 points along the trajectory.

The main spectral component (see Section 3.3) is much more suitable for abundance determinations. The intercombination lines are to be excluded from the analysis in some cases, but for other lines, thermal equilibrium is a good assumption. The results from a synthetic spectrum fitting are the temperature, T, the column abundances of the atoms observed in the spectrum, N_j, and the visible cross-section of the radiating volume, P. The total abundances of atoms are simply PN_j. However, these relate only to neutral atoms visible in the spectrum. To obtain the elemental abundances, the Saha equation is to be used to compute the ionization degree of different elements. The temperature is known but the density of free electrons must be estimated. This can be done using the known area P and assuming some simple geometrical form of the radiating volume (Borovička, 1993). So, the representative values of elemental abundances in the radiating gas can be derived

TABLE XIX

Relative abundances by mass (Fe = 100) in several types of meteorites and in the radiating gas of fireballs as determined by various authors

Meteorites		Na	Mg	Al	Si	Ca	Ti	Cr	Mn	Co	Ni
CI chondrites		2.6	52	4.6	56	4.9	0.23	1.4	1.0	0.26	5.8
H chondrites		2.3	51	4.4	61	4.5	0.21	1.0	0.9	0.33	5.9
L chondrites		3.2	69	5.9	86	6.3	0.34	1.4	1.1	0.26	5.1
Eucrites		2	30	50	170	50	2.5	2	2.5	0.004	0.001
Diogenites		0.02	120	5	180	7	0.8	4	2	0.08	0.2
Aubrites		20	1500	20	1600	40	2	3	7		4
Fireball:											
S 6[a]	[1]	0.07	50	0.04	$\leq$16	6.5[b]		0.02	4	5	10
S 526[a]	[2]	0.3	500	0.02		0.15		0.05	0.14	6	50
Draconids[c]	[3]	4.2	48			4.3					
#56	[4]	0.4	1100			0.09				1000	
#59	[4]	10^{-6}	350			0.08			0.02	500	
sporadic	[5]	9	130			1.1		0.2	1.8		15
Taurid	[5]	4	150			1.5		0.04	0.04		12
Geminid	[5]	4	190			1.3		0.04	0.04		13
Perseid	[5]	1.1	220			4		0.1	0.04		
Čechtice	[6]										
max		7.5	100	0.25	200	0.8	0.12	0.9	1.2	0.3	6[d]
min		1.5	60	0.02		0.07	0.01	0.2	0.3		2[d]
Šumava	[7]	5	60	0.13		0.8		0.4	1		
Benešov	[7]										
upper		1	80			0.2[e]	0.03	0.4	0.3		5
lower		4	160			9	0.07	0.5	0.6		
Two Perseids	[8]	4	90		110[f]	4		0.7	1.3		

Notes: (a) ratios of neutral atoms; (b) including ionized calcium; (c) an average of 10 meteors, based on radiative efficiencies; (d) the original values of Borovička (1993) were reconsidered using better values of oscillator strengths for Ni I; (e) 0.02 at 78 km; (f) from the second spectrum.

References: [1] Ceplecha (1964), [2] Ceplecha (1965), [3] Millman (1972), [4] Nagasawa (1978), [5] Harvey (1973c), [6] Borovička (1993), [7] Borovička and Spurný (1996), [8] Borovička and Betlem (1997).

from a high quality meteor spectrum under the simplified assumption of constant temperature, density and simple geometry of the radiating volume. The precision is not high and values better than within a factor of two cannot be expected. Of course, only the elements observable in the spectrum can be analyzed.

The results of all authors are summarized in Table XIX and compared with the composition of stony meteorites (as compiled from meteorite literature). The mass abundances relative to iron are given. Iron is used as a reference element because it exhibits numerous lines in meteor spectra and is the most important element for the determination of temperature. For the Čechtice fireball analyzed by Borovička (1993), the lowest and highest values found along the trajectory are given. In some cases (e.g., for Mg) the variations represent simply the scatter of the measurements, but some variations are very large and certainly real. This is demonstrated in Figure 21 for Ca, Ti, and Al. Their variations are correlated. The maxima were reached in the periods of enhanced temperature but the maxima are still lower than the expected values for chondrites. The abundances of other elements are approximately consistent with chondritic composition, at least at some part of the trajectory.

No stony meteorites with such low content of Ca, Al, and Ti relative to Fe are known. This and the variations along the trajectory suggest that the composition of the radiating gas does not directly reflect the composition of the meteoroid, i.e., not all ablated mass is evaporated completely. Calcium, aluminium and titanium belong to the most refractory elements, which are the most difficult to melt and evaporate. The volatility index given by Kargel and Lewis (1993) reflects this property.

So, the depletion of Ca, Al, and Ti is a demonstration of incomplete evaporation of meteoritic material. This incompleteness varies in different meteors and in single meteor during the flight. This is most clearly demonstrated in the Benešov fireball, where the calcium abundance varies from almost zero at the beginning to the chondritic values at the end (Borovička and Spurný, 1996). In Table XIX the average abundances in the upper (height 63–71 km) and lower (height 21–25 km) part of the Benešov trajectory are given. Fast cometary Perseid meteors show (after correcting for severe ionization) chondritic abundance of calcium at high altitudes (Borovička and Betlem, 1997). The effect of incomplete evaporation reflects the varying condition of ablation and could be used in future for studying the ablation process. On the other hand, this effect complicates the determination of the chemical composition of the meteoroid itself. Before the ablation process is better understood, we have to assume that the incomplete evaporation is nearly the same for meteors of comparable velocity, brightness and height, and keep in mind that the abundances of refractory elements in meteoroids can be determined with low degree of reliability.

The meteors given in Table XIX are the only ones to date with detailed abundance computations. In addition, Borovička and Zamorano (1995) estimated the lithium relative abundance of Li/Fe $= 2 \times 10^{-6}$ (by mass) in one fireball, which

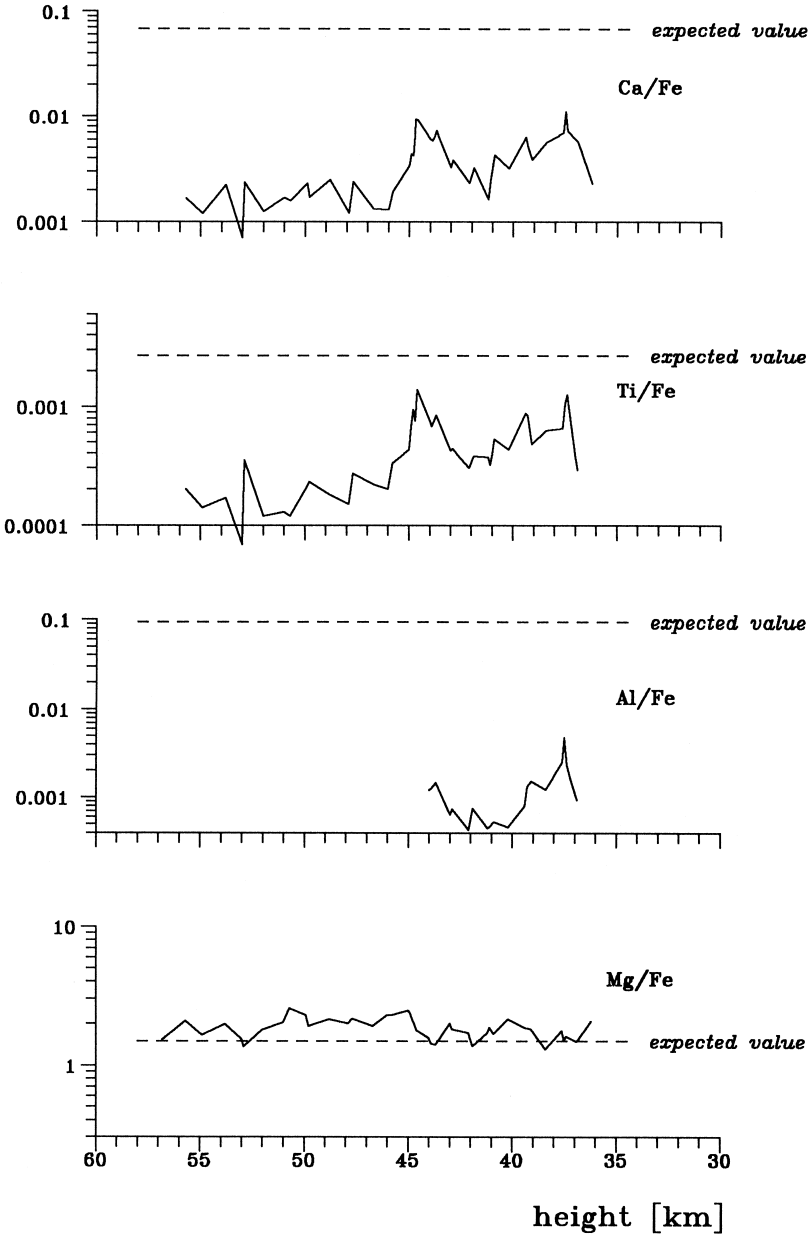

Figure 21. The relative abundances of calcium, titanium, aluminum, and magnesium relative to iron in the Čechtice fireball as a function of the fireball height above surface. The values expected for chondritic composition are shown. Ca, Ti, and Al were vaporized incompletely. According to Borovička (1993).

is less than the chondritic value (8×10^{-6}). More spectra analyzed by a uniform method would be needed to make some definite conclusions. However, the detailed analysis is applicable only to rich and well calibrated spectra of bright fireballs. To make use also of medium quality spectra and spectra of fainter meteors, simpler comparative and statistical studies are useful. Borovička (1994c) compared 53 meteor spectra from the Ondřejov archives. 51 of them were found 'normal', i.e., consistent with chondritic composition. One was an iron meteoroid described already by Ceplecha (1967b). The last one was found to have significantly lower content of Na and higher content of Mg, Cr, and Si, which is consistent with the composition of diogenites. The orbit of this body placed it into 3:1 resonance with Jupiter, confirming the scenario of diogenites (and related types howardites and eucrites) being fragments of asteroid Vesta delivered to Earth via the 3:1 resonance (Binzel and Xu, 1993). This is the only reliably known orbit of an achondrite meteoroid. Although Meisel et al. (1995) claimed to have observed an aubrite meteoroid, the re-evaluation of their published spectrum led to the conclusion that there is in fact *absolutely no evidence* for the aubrite composition.

An overview of several hundreds of meteor spectra was presented by Harvey (1973b). Again, more than 95% of them are consistent with normal chondritic composition. About 2% are iron meteoroids, while about 1% show deficiency of iron and may be related to aubrites (orbits are not available). Some spectra are deficient in sodium (diogenites?). One spectrum showed no atomic emission, only continuum at 3600–4000 Å. An iron meteoroid spectrum was observed also by Halliday (1960b).

The statistics of meteorite falls show 84% of various types of chondrites, 8% achondrites, 7% irons and 1% stony-irons. The above results for meteors demonstrate that we are able to identify irons and achondrites in meteor spectra but chondrites are not distinguished from cometary meteoroids which have no meteorite analog. At least to the first approximation, cometary meteoroids have the same elemental ratios for elements observable in the meteor main spectral component. This is an expected result because both chondrites and comets are believed to represent undifferentiated material with the abundances of heavier elements the same as in the primordial solar nebula. Large differences could be expected in light volatile elements, H, C, and N. Hydrogen is observable in the second spectral component. However, this component is very faint in slow meteors, which excludes them from the hydrogen analysis. Moreover, the second spectrum is not very suitable for abundance analysis. Nevertheless, Borovička and Betlem (1997) were able to conclude that the hydrogen abundance relative to iron is not higher in Perseid meteors than in carbonaceous chondrites. This somewhat surprising result can be explained by loss of volatile material during the long period meteoroids spent orbiting the Sun. Atomic carbon is never observable. However, the carbon bearing molecules observed in some spectra, especially C_2 and CN, offer some possibility to evaluate carbon content. Nitrogen cannot be evaluated because most of nitrogen in the radiating gas is of atmospheric origin.

Summary: Cometary meteoroids cannot be easily distinguished from chondrites, especially carbonaceous chondrites, on the basis of their spectra. The abundance of hydrogen and carbon is difficult to obtain. The cometary origin is better recognized from the ablation ability (see Section 5.2) or from the membership in a particular cometary shower. On the other hand, a detailed chemical analysis of a large number of meteor spectra has not yet been done and the existence of some minor chemical differences cannot be excluded also for well observable elements. The observation of meteor spectra in the far ultraviolet realized from outside the Earth's atmosphere (satellites) would offer the possibility of recording more chemical elements.

6. Meteoroids in the Solar System

The space among the planets is filled with an extended cloud of tiny particles – meteoroids – orbiting about the Sun and concentrated predominantly toward the ecliptic. The meteoroid population has several sources from which it is continuously being fed and subjected to a variety of dissipative forces. The evolution of the complex has been modeled over a large time span in various studies considering gravitation, radiation effects and collisions controlling dynamics and spatial distribution of the meteoroid complex. The observational evidence is in favour of a present steady-state nature of the complex, may be a quasi-steady state of sources replenished from the outskirts of the solar system once a while.

The results obtained by detectors on spacecrafts and combined with the interplanetary flux near the Earth indicate the existence of more distinct populations among meteoroids. However, the following paragraphs discuss the meteoroid population known from the Earth-bound observations consisting of the two well known components, shower and sporadic, and their influx onto the Earth including potential hazard. Decaying comets releasing dust through sublimation processes and asteroids freeing dust by collisional processes are considered as the main sources of this complex.

6.1. METEOR SHOWERS AND METEOROID STREAMS

The meteoroid influx onto the Earth consists of the shower and sporadic component. A meteor shower is observed when the Earth passes through a meteoroid stream which is a family of particles moving in orbits that are either similar to that of the parent body or at least can be traced back by integration to the parent. The meteor shower appears if one node of the meteoroid stream is near the orbiting Earth. The ability to recognize meteor shower members depends on the experience of the observer and on level of the shower activity. Practically on each day the Earth meets one or few meteoroid streams.

Actually it was great meteor showers at the beginning of the 19th century, namely Leonids 1799, Lyrids 1803 and Leonids 1833 which initiated the study of

meteor astronomy. Various showers of 'shooting stars' observed occasionally had attracted little attention until some spectacular meteor storm appeared. On November 13, 1833 a great storm of meteors was seen in the Northern America. Meteors fell as thickly as snowflakes and the phenomenon alarmed many people. It was for the first time that some observers realized that the meteors appeared to radiate from one point in the sky, in the constellation of Leo, and thus the radiant of a meteor shower was discovered. In 1834 Olmsted and Twining suggested that the Leonid shower was caused by a cloud of particles which the Earth met each November. In 1834 Locke pointed out that the August meteors, known as the burning tears of St. Lawrence, had also a point of radiation in the constellation of Perseus and the Perseid shower was shown to be periodic by Quetelet in 1836. The idea that meteors and comets were closely connected was first suggested by Kirkwood in 1861: '*May not our periodic meteors be debris of ancient but now disintegrated comets, whose matter has become distributed round their orbits ?*'

The first identification of a comet–meteoroid stream relationship was made by Schiaparelli, who at the end of 1866 announced that the Perseid stream moves in the same orbit as comet 1862 III (Swift-Tuttle). Soon followed other suggestions of similar relationships by Leverrier and Peters between the Leonids and comet 1866 I (Tempel-Tuttle), confirmed independently by Schiaparelli, and also by Weiss between the Lyrids and comet 1861 I (Thatcher), and between the Andromedids and comet Biela.

A significant role in establishing a relationship between meteoroid streams and comets played comet Biela discovered by Wilhelm von Biela in 1826 (period of revolution 6.6 years). The comet was observed also at its following returns. However, in 1846, it split into two parts. At the next return in 1852, the two comets were separated from each other by about 2 million kilometers. This was the last time that comet Biela was observed. In November 1872 a strong meteor shower (Andromedids) in the same orbit as comet Biela was observed and this phenomenon repeated also in 1885. These events, more than any others, strongly supported the idea that a meteor stream is generically related to a comet being a result of a comet's gradual desintegration. The history of the early period of meteor astronomy is described in details in earlier publications or recent reviews on meteoroid streams (e.g., Olivier, 1925; Porter, 1952; Kronk, 1988; Steel, 1994; Williams, 1993, 1995).

6.2. METEOR SHOWER OBSERVATIONS

6.2.1. *Activity*

The structure of a meteoroid stream can be studied by the meteor shower which is observed in the atmosphere when the Earth passes through the stream. The standard methods of obtaining observational data on meteoroid streams are based on visual, telescopic, photographic, TV or radar techniques. The observational methods applied in meteor research are summarized and discussed in Section 2. Visual observations are the simplest ones; their accuracy strongly depends on the

experience and ability of the observers. If the observations are systematic they may provide a rather complete information on the shower activity: maximum, period of activity, profile of the activity curve and magnitude or mass distribution of the particles.

The magnitude distribution is represented by the population index (magnitude function), r, defined as the ratio between the number n of meteors with magnitude $m + 1$ and the number with magnitude m

$$r = n_{m+1}/n_m. \tag{113}$$

The mass distribution exponent s is determined from the assumption that the number of particles having masses between M and $M+\mathrm{d}M$ is given by

$$\mathrm{d}N \approx M^{-s}\, \mathrm{d}M. \tag{114}$$

The mass exponent has been derived in radio observations from the observed distribution of the echo durations. The relation between both indexes is

$$s = 1 + 2.5\, \log_{10}\, r. \tag{115}$$

The population index and the mass exponent are important parameters for studies of meteoroid streams. As the indexes describe the internal structure of individual streams their values are constant only over a limited range of the magnitudes and masses and to a certain degree vary from stream to stream.

According to the activity, the showers are divided into the *major* and *minor* meteor showers. There are also rare *temporary* showers having a not regular annual activity, sometimes low, sometimes high. Some showers are known to exhibit occasional intense outbursts or enhancements in their activity and some annual showers exhibit significant variations in the activity too, reflecting the structure of the meteoroid stream. With the advent of radio techniques into meteor science in the 1940s, the daytime meteor showers have been also observed.

The duration of a meteor shower provides information on the profile across the stream, derived from the variation of the meteor counts and mass distribution in successive hours or days. The study of the above quantities in successive years provides information about the structure of the stream along its orbit. Profiles of the Perseid activity along the Earth's path through the stream based on long-term radar observations have been made among others by Lindblad and Šimek (1986) and by Šimek and McIntosh (1986). Similar analyses for the Geminids were performed by Šimek and McIntosh (1989), for the Lyrids by Porubčan, Šimek and McIntosh (1989) and for the Quadrantids by Šimek and McIntosh (1991). There is observational evidence that, if the activity from year to year is relatively constant, as, e.g., in the Geminids, then the duration of the stream is longer, while high activity outbursts are narrow and their occurrence variable, e.g., in the Leonids. The Perseids show an interesting compound variation with regular displays and an additional narrow peak being noted first visually in 1988 and evident in a few following years. This apparently can be explained so that the peak is associated with

the recent perihelion passage of the stream's parent comet Swift-Tuttle in 1992 (Wu and Williams, 1993). The Lyrids is another stream that exhibits outbursts (Lindblad and Porubčan, 1992), but their explanation is more complex as the orbital period of both the stream and its parent comet Thatcher is the order of a few hundred years. One possibility may be a disintegration of a secondary body in the orbit far beyond the parent comet (Porubčan et al., 1992).

In the past two centuries, 36 outbursts of 17 meteor showers have been reported including the recent 1995 α Monocerotids outburst on November 22. These events occur rather frequently, what is well documented by the fact that in the twelve years from 1982 to 1993, 12 meteor outbursts have been recorded (Jenniskens, 1995). A meteor outburst is here defined as an enhancement of a meteor shower activity that stands out significantly above the random variation of a standard activity.

6.2.2. *Shower Radiant*

A meteor shower is named after the constellation in which its radiant lies, and defined as an area in the sky from where the shower meteors appear to radiate. The position of a meteor shower radiant is determined by orbits of the meteoroid stream members and the orbit of the Earth. A theoretical shower radiant is obtained assuming that the orbital parameters of the stream or those of the parent comet are known. The most frequently applied method for calculating the theoretical radiants was described by Porter (1952) involving a determination of the closest approach distance (between the orbits of the supposed stream parent body and that of the Earth) and a parallel shift of the velocity vector. A better method involving adjustments of the orbit to get a node at 1 AU either by the variation of the perihelion distance or the argument of perihelion and inclination was presented by Hasegawa (1990) and Hasegawa et al. (1992). Svoreň et al. (1994) discussed various methods for the derivation of the theoretical radiant and recommended optimum ones depending on the type of the orbit. However, a determination of an accurate theoretical radiant should involve a numerical integration of the potential parent body orbit.

From visual observation a shower meteor is defined by the position of the shower radiant and the angular velocity of the meteor. For the major meteor showers, e.g., the Perseids, Geminids or Quadrantids with the maximum hourly counts of meteors of several dozens, there is no problem with the identification of the shower meteors. However, when the hourly rates are of about 5 or less it is not so apparent whether it is a particular shower or just a chance alignment, particularly for the radiants near the ecliptic, where sporadic meteors are a serious problem in recognizing a definite shower.

6.2.3. *Meteor Orbits*

All the present knowledge on the structure of meteoroid streams and sporadic population is based on precise photographic and television orbits and on a statistically significant sample of radio orbits accumulated over the past decades. A record of about 6000 optical orbits and 62000 radar orbits generally available is archived at

the IAU Meteor Data Center in Lund (Linblad, 1991; Lindblad and Steel, 1994). Most of the orbits were obtained in the 1960s and 1970s, but still represent our best knowledge on the orbital distribution of meteoroids in the size range approx. from 100 μ m to 0.1 m. A comprehensive statistical analysis including mutual comparisons of all the orbital surveys available from the observational programs carried out chiefly in the USA, Canada, the former Soviet Union, Europe and Japan has recently been made by Steel (1996). Using this statistical material on meteor orbits one must be aware of large differences in quality of these data. Moreover, no standard deviations of the individual values are given. A new and very effective radio system providing about 1500 radio orbits daily was introduced at the University of Canterbury in New Zealand (Baggaley et al., 1994) rendering about 500 000 new meteor orbits by now.

The catalogued meteoroid orbits have been used in various searches for meteoroid streams mostly applying the D-criterion derived by Southworth and Hawkins (1963). Though various modifications of D, as well as some new criteria for a stream-membership have been suggested, the Southworth–Hawkins D–criterion is still the most applied criterion in stream searches and is formulated by the relation

$$D^2 = (e_2 - e_1)^2 + (q_2 - q_1)^2 + [2\ \sin(I/2)]^2 + [(e_1 + e_2)\ \sin(P/2)]^2, \quad (116)$$

where

$$[2\ \sin(I/2)]^2 = [2\ \sin[(i_2 - i_1)/2]]^2 + \sin\ i_1\ \sin\ i_2[2\ \sin[(\Omega_2 - \Omega_1)/2]]^2, \quad (116)$$

$$P = \omega_2 - \omega_1 + 2\ \arcsin[\cos[(i_2 + i_1)/2]\ \sin[(\Omega_2 - \Omega_1)/2]\ \sec(I/2)], \quad (117)$$

and e, q, i, ω, Ω are the orbital elements.

So far, the most commonly used list of meteor showers is that compiled by Cook (1973) and summarizing basic data on 58 meteor showers. However, more of the mean orbits listed in the catalogue are based on a small number of individual orbits available at that time – e.g., the 'mean orbit' of the η Aquarids is represented by one photographic orbit only – (Lindblad et al., 1994), thus the list desires inevitable revision including new observational data. Jenniskens (1984) published also a critical list of meteor streams. International Meteor Organization regularly issues a working list of visual meteor showers. An updated list of meteor showers is being prepared by Lindblad and Porubčan (1998).

6.2.4. *Selection Effects*

The observation of a meteor stream is subject to various selection effects discussed in detail by Kresák (1968) and Hughes (1986). Among them the most important is the condition that only those streams can be observed which have perihelia inside the Earth's orbit and at least some part with nodes near 1 AU. There is also a higher probability to recognize wider streams as are the Perseids or Geminids

and the streams with low inclination, that is close to the ecliptic (inclination near 0° or 180°). The geocentric radiant position of the shower is important, too, and strongly influences the observed activity of the shower. A daytime stream having its radiant approximately in the solar direction cannot be observed visually at all. The geographic position of the observing place also influences the observed shower activity. The shower displays in full activity only when its radiant passes near the zenith. The geometry of the intersection between the stream and the Earth causes another important selection effect. As the geocentric velocities of meteoroids lie approximately in the range 12 to 72 km s^{-1}, the shower meteors have encounter velocities dispersed over a range with the ratio 1 to 6, and the kinetic energy per unit mass of the incident meteoroid varies over the range of 1 to 36. As both the meteor luminosity and electron line density are directly proportional to the kinetic energy, the streams with high geocentric velocities, with the radiants near the apex (e.g., the Leonids, Orionids, Perseid) are greatly favored over the streams with low geocentric velocities. We can detect much lower mass meteoroids in these streams than we could in minor streams of low geocentric velocity. Kresák (1968) discussed also importance of an additional selection effect regarding the size of the radiant area. This area increases considerably for radiants at an elongation from the apex over 90° which makes a separation of a shower member from the sporadic still more difficult. Due to this effect the retrograde streams are greatly favored over the streams from the direction of the antiapex. E.g., the motion of the Earth reduces the size of the apparent radiant area of the Leonids (retrograde orbit, elongation of the geocentric radiant 10°) to 34% of the true radiant area and that of the Draconids (direct orbit, elongation 100^o) increases to 240%.

6.2.5. *Meteor Storms*

Meteor storms rank among the most impressive phenomena observed in the night sky and many accounts of them are recorded in ancient chronicles (e.g., Imoto and Hasegawa, 1958; Hasegawa, 1993). These records are extraordinary valuable as they provide the best possibility to check models of dynamical evolution of meteoroid streams. Recently, the origin and structure of dense meteoroid streams producing meteor storms were discussed in more details by Kresák (1993a,b) and Jenniskens (1995). There is no generally accepted dividing line between meteor storms (short-duration 0.01 to 0.10 day, intensive bursts in a shower activity) and standard meteor showers which are much more frequent.

Table XX lists the most intensive meteor storms recorded during the last 200 years (Kresák, 1993a). The selection of the storms in Table XX was made adopting two criteria: the reduced maximum zenith hourly rate, Z, and the ratio of the actual stream density to the mean density of the sporadic background, D. This ratio D is related to Z by the approximate formula $D \approx 100\ Z\ V_G^{-1}\ V_E^{-2}$, where V_G and V_E are the unperturbed geocentric and encounter velocity, respectively ($V_E^2 \approx V_G^2 +$ 124 $km^2\ s^{-2}$, it holds exactly at a point 6 429 km from the Earth center). The limiting value of Z applied for Table XX was one meteor per second observed

TABLE XX

The most intensive meteor storms recorded during the last 200 years

Storm	Year	$\Delta t/P$	Z	D
Leonids	1799	−0.010	30 000	8
	1832	−0.005	20 000	6
	1833	+0.026	100 000	30
	1866	+0.025	6 000	
	1867	+0.055	5 000	
	1965	+0.016	5 000	
	1966	+0.046	150 000	40
Andromedids	1872	+0.036	8 000	120
	1885	−0.012	15 000	230
	1892	+0.048		15
Draconids	1933	+0.033	20 000	180
	1946	+0.007	7 000	60
	1985	+0.011		7

at the time of maximum, i.e., $Z = 3\,600$. For a comparison, Jenniskens (1995) presents substantially different values of Z, especially for the returns of Leonids, e.g., for the 1966 peak, 15 000 only.

All meteor storms listed in Table XX have their origin in only three comets: P/Tempel–Tuttle (revolution period of $P = 33$ yr) – Leonids, P/Biela ($P = 6.6$ yr) – Andromedids and P/Giacobini–Zinner ($P = 6.5$ yr) – Draconids. It is evident that the retrograde motion of the parent comet of the Leonids ($V_G \approx 70$ km s^{-1}) in comparison to the Andromedids and Draconids (geocentric velocity ≈ 16 and ≈ 21, respectively), was responsible for the strongest meteor storms. Table XX lists also the ratio of the time lapsed between the passage of the Earth and comet through the node in which the storm occurred, Δt, to the revolution period of the comet, P.

Meteor storms are very rare events, and their quantitative evaluation relies on old observations. For the Leonids, observations of storms go back until at least 902 AD (33 apparitions of the comet). Sometimes however it is very difficult to derive the real meteor counts from the original records and normalize them to standard observing conditions.

Meteor storms recorded in the last two centuries and cometary dust trails detected by the IRAS were compared with the spatial distribution, orbital evolution and relative production of all known periodic comets (Kresák, 1993b). The parents

TABLE XXI
Predictions of increased shower activity

Date	Shower	δ	M	Best conditions (Z)
Kresák (1993a):				
1998 Apr. 23.50	Puppids	−44	27	Australia
1998 Oct. 8.70	Draconids	+54	17	E. Europe, W. Asia
1998 Nov. 17.35	Leonids	+22	28	E. America (10 000)
1999 Nov. 17.60	Leonids	+22	9	N. Pacific (100 000)
2000 Nov. 16.85	Leonids	+22	20	C. Asia (1 000)
Yeomans et al. (1996):				
1998 Nov. 17.82	Leonids	+22	28	Japan, Asia
1999 Nov. 18.08	Leonids	+22	10	Europe, N. Africa

of the dust trails are mainly comets of Jupiter family situated on both sides of the 2:1 resonance gap, which were not subject to closer encounters with Jupiter for several revolutions. The survival times of the compact dust streams are typically about 60 years, with the ejection velocities of the meteoroids being up to 5 m s^{-1} and the solar radiation pressure to solar gravity ratio, β, of about 10^{-3}. Every active comet produces a compact dust trail of limited lifetime, stretching predominantly behind it.

Studies of the long-term integration of the motion of periodic comets provides a possibility to investigate the evolution and occurrence of meteor storms. From the computation by Carusi et al. (1985), Kresák (1993a) has concluded that for all the comets of Jupiter family there was not a single meteor storm to be expected in the 17th century and two in the 18th century (but not observed). In the 19th and 20th century the number of potential storms increases. Predictions until 2000 including temporary showers with $Z \approx 100$ are summarized in Table XXI, where δ is the radiant declination and M the age of the Moon. Yeomans et al. (1996) integrated the orbit of the Leonid parent comet (55P/Tempel–Tuttle) back for two millennia. From their result it is evident (Figure 22) that the Leonids could not be observed prior to the eighth century as the comet's descending node was well outside the Earth's orbit. Their prediction of the expected Leonid storms in 1998 and 1999 is also included in Table XXI. In 1998–1999 the Earth will pass nearly three times as far from the comet's orbit as in 1966 and more than six times further than in 1833. Consequently, they expect rather low rates resembling those in 1886–1888 ($\approx$ 5000) or in 1931–1932 ($\approx$ 200).

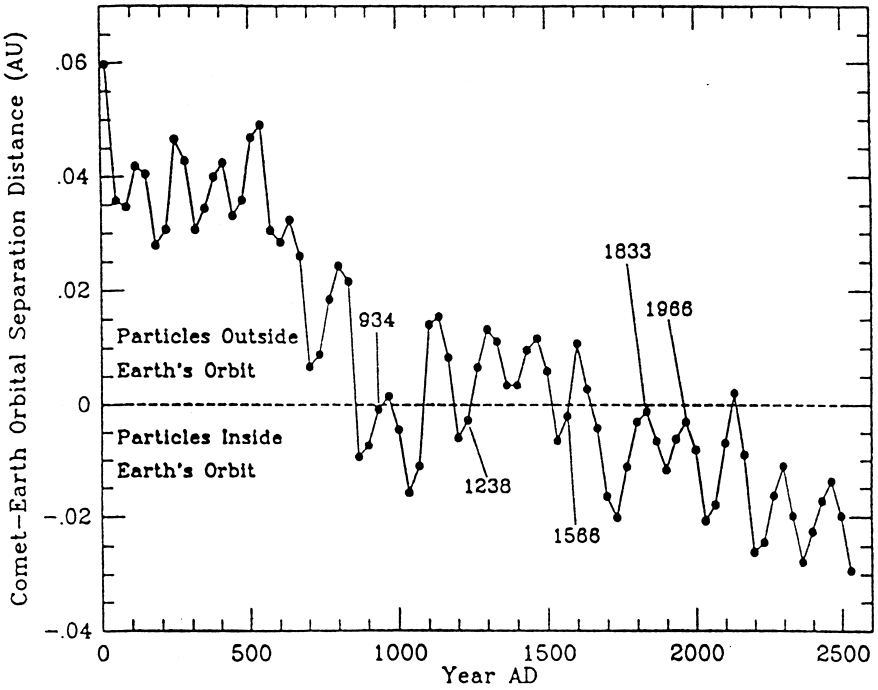

Figure 22. Minimum distances between comet 55P/Tempel-Tuttle and Earth orbits at the time of the comet's passage through its descending node (Yeomans et al., 1996).

6.2.6. *Major Meteor Showers*

Table XXII lists basic parameters of major meteor showers: period of activity, maximum (date and solar longitude), duration defined as the width of the rate profile at one-quarter of the maximum, radiant, approximate local time of the radiant transit, geocentric velocity and orbital elements. The activity of the major meteor showers obtained from visual observations coordinated by the IMO has been recently summarized and discussed by Jenniskens (1994).

Quadrantids are known only from the beginning of the nineteenth century as a shower with a narrow and sharp maximum. There was no parent body of the stream known for a long time. McIntosh (1990) following the orbital evolution of comet 96P/Machholz suggested its association with the Quadrantids. Babadzhanov and Obrubov (1992b) have concluded that the comet is parent body of eight meteoroid streams including the Quadrantids.

Lyrids are a meteor shower of moderate activity exhibiting semi-regularly impressive activity bursts through which the Lyrids can be traced back for about 2 000 years. These exceptional bursts consist predominantly of faint visual meteors and precede the main Lyrid maximum (Lindblad and Porubčan, 1992). The period of the bursts was modeled and discussed in more analyses (Guth, 1947; Emelyanenko, 1990; Arter and Williams, 1997). The parent comet of the stream is C/1861 G1

(Thatcher). It is a comet with the longest period of revolution (415 years) having a known meteoroid stream.

η Aquarids (May) and *Orionids* (October) are two streams with the same parent body, the comet 1P/Halley. The η Aquarids are almost unknown in northern hemisphere, nevertheless both showers rank among regular annual major meteor showers of higher activity. A new model of the Halley meteoroid stream explaining satisfactorily all observed features of both the showers was suggested by McIntosh and Hajduk (1983).

Northern and *Southern δ Aquarids* and *α Capricornids* belong to regular annual meteor shower of moderate activity with flat maxima. The Northern and Southern δ Aquarids are members of the complex of meteoroid streams associated with comet 96P/Machholz (Babadzhanov and Obrubov, 1992b) and the parent of the α Capricornids is the short-period comet 45P/Honda-Mrkos-Pajdušáková.

Perseids similarly as the Lyrids can be traced back far in historical records. However, the Perseids with their regular high activity displays are one of the most intensively observed and studied meteor showers. Almost 18% of all meteor orbits available from precise photographic surveys belong to the Perseids. The zenithal hourly rates observed in 1991–1993, i.e., at the return of the parent comet of the stream 109P/Swift-Tuttle, rose up to about 300 (Brown and Rendtel, 1996). Brown and Jones (1998) have modeled the formation and evolution of the Perseids considering all known features of the stream and their results are well consistent with the observations. They estimate the age of the core population of the stream to about 25 000 years and the total age of the stream of the order of 10^5 years.

Northern and *Southern Taurids* are due to their low rates better known from photographic than from visual observations. Their parent body is 2P/Encke. However, there are also suggestions that the Taurids may have originated from more than one body (as first suggested by Whipple and Hamid, 1952). The Taurids form actually a large meteor complex consisting of four meteoroid streams at least: the Northern and Southern Taurids observed in autumn and the daytime β Taurids and ζ Perseids known from radio observations (June–July). There are also indications that some additional streams preceding and following the activity of the Taurids may belong to the Taurid meteor complex (Štohl and Porubčan, 1992).

Leonids rank among meteor showers with the most variable activity with magnificent displays approximately every 33 years (see Section 6.2.5), and with a low activity in between. A long-term activity of the shower monitored by the meteor radars at Springhill and Ondřejov (1964–1995) was analyzed by Brown et al. (1997). At present, there has been organized an international observing campaign (International Leonid Watch coordinated by the IMO) for a complex study of the stream and exceptional displays expected in 1998 and 1999. The first observations of an enhanced activity in 1994 was published by Jenniskens (1996a,b).

Geminids are regular and high activity meteor shower moving in an orbit outside the region of known short-period comets. The discovery of a potential parent body, asteroid 3200 Phaethon, moving in the orbit of the stream and following suggestion

TABLE XXII
Major meteor showers

Shower	Period of activity	Maximum		Duration	Radiant		Transit	V_g	q	a	e	i	ω	Ω
		Date	Sun		α	δ	(LT)	(km s^{-1})	(AU)	(AU)		(°)	(°)	(°)
Quadrantids	Jan. 1–5	Jan. 4	283.3	0.5	231	49	08:30	41	0.98	3.0	0.66	72	170	283
Lyrids	Apr. 17–26	Apr. 22	32.2	2	272	33	04:05	47	0.92	48	0.98	80	214	32
η Aquarids	Apr. 21–May 25	May 6	45.5	10	337	−2	07:30	66	0.57	9.2	0.94	164	96	44
S δ Aquarids	July 12–Aug. 19	July 28	126	(10)	339	−16	02:15	41	0.09	2.7	0.97	25	149	310
α Capricornids	July 3–Aug. 15	July 30	127	(20)	306	−10	23:55	22	0.60	2.5	0.76	7	267	127
N δ Aquarids	July 15–Aug. 25	Aug. 9	136	(20)	342	−1	01:40	39	0.10	2.3	0.96	20	328	139
Perseids	July 23–Aug. 27	Aug. 12	139.9	4	46	58	05:45	59	0.95	24	0.96	113	150	139
Orionids	Oct. 2–Nov. 7	Oct. 22	208.4	10	94	16	04:15	67	0.58	17	0.97	164	81	28
S Taurids	Sep. 25–Nov. 23	Nov. 3	220		51	14	00:35	28	0.38	2.2	0.81	5	112	42
N Taurids	Oct. 9–Nov. 27	Nov. 13	230		59	22	00:25	29	0.36	2.2	0.83	4	295	226
Leonids	Nov. 14–21	Nov. 17	235.2	2	153	22	06:25	71	0.98	15	0.93	162	172	235
Geminids	Dec. 4–17	Dec. 14	262.0	3	112	33	01:55	35	0.14	1.3	0.89	24	325	261
Ursids	Dec. 18–26	Dec. 22	270.9	2	217	76	08:25	33	0.93	5.8	0.84	53	208	268

of their mutual association (Whipple, 1983) have initiated an extensive discussion on their possible generic relation (e.g., Hunt et al., 1986).

Ursids are known since the discovery of the shower at the Skalnate Pleso Observatory in 1945. The shower is of a lower activity, but a sudden burst in activity of the shower was observed in 1986. Though comet 8P/Tuttle has been considered for the parent of the stream for a longer time, Babadzhanov and Obrubov (1992b) conclude that the stream is a part of the meteoroid stream originated in comet 96P/Machholz.

6.3. THE FORMATION AND EVOLUTION OF METEOROID STREAMS

The concepts for the formation and evolutionary processes of meteoroid streams were proposed over a long time, but there have been more reviews on this topic published in the last few years (McIntosh, 1991; Babadzhanov and Obrubov, 1992a; Williams 1993, 1995; Steel, 1994). It is generally accepted that particles are ejected from the cometary nucleus and consequently form a meteoroid stream. However, there are also more studies dealing with meteoroid streams of probable asteroidal origin.

6.3.1. *Ejection from a Comet*

The formation of a meteoroid stream from a cometary nucleus has already been studied by Whipple (1950, 1951) and Plavec (1957). When nearing the Sun the cometary material begins to sublimate and the meteoroids embedded in the icy matrix of the nucleus are ejected by the outflow gases. For the ejection velocity of dust particles or of meteoroids, V (in cm s^{-1}), Whipple derived a formula which is still considered a classical one and is frequently used in the form

$$V^2 = 656R[1/(nb\rho r^{2.25}) - 0.013R], \tag{118}$$

where R is the radius of the comet in km, n the fraction of solar radiation used for sublimation, r the distance of the comet from the Sun in AU, b the meteoroid radius and ρ its density in units of 1000 kg m^{-3}.

More modifications of this formula have been used (Hughes, 1977; Gustafson, 1989; Williams, 1992; Jones, 1995), however their final results do not differ significantly and are more or less consistent. The ejection velocities are in the range from ten to hundred of meters per second, i. e. significantly less then the orbital velocity of the comet. Thus the meteoroids are confined to move in orbits similar to the cometary orbit, but with small differences in each of the orbital elements. A change in the semimajor axis means a change in the period of revolution so that the dust particles slowly spread about the orbit and finally form a continuous envelope. At least three stages in a meteoroid stream can be recognized: a cloud or thin filament, a narrow ring along the whole orbit, and a wide and diffuse stream.

There were some attempts to derive the ejection velocities for different meteoroid streams from the orbital elements of precise photographic orbits listed in

the Lund Catalogue. Kresák (1992) has argued that this is essentially impossible due to original dispersion velocities being masked completely by the much larger measuring errors, and also by the accumulated effects of planetary perturbations for all permanent meteor showers. Brown and Jones (1998) in their analysis of the Perseid meteoroid stream evolution arrived at consistent results.

6.3.2. *Ejection from an Asteroid*

Following Williams (1993), in the case of a formation of a stream from an asteroid, unless it is an inactive comet, a collision is required to eject the meteoroids from the parent. A collision case can occur at any place in the orbit, but near the aphelion it is more probable. Again the ejection velocity of particles (unlikely to exceed 200 $\mathrm{m\,s^{-1}}$) is smaller than the orbital velocity of the potential parent and the orbits of individual meteoroids will be again similar to that of the asteroid, but with a greater spread. A cometary stream would be denser and more confined in space. The cometary ejection can take place at each perihelion passage, while collisions among asteroids are not so frequent phenomena. While the cometary origin of meteoroid streams is taken for granted, the asteroidal origin is still not being proved. The most prospective generic relation seems to be between the Geminids and asteroid 3200 Phaethon, suggested by Whipple (1983). Hunt et al. (1986) have modeled the stream formation by a collision between two rocks in order to explain the Geminids, but immersed into difficulties in explaining the observed distribution of aphelion distances being characteristic for a cometary meteoroid stream. Investigating the Geminid fireballs from the viewpoint of composition, Halliday (1988) also concluded that the Geminid meteoroids are not tough enough and that they have too low density to associate them with meteorites or normal asteroids. However, from their study of several Geminids with the most precise photographic data available, Ceplecha and McCrosky (1992) concluded in contrast that the density of Geminid meteoroids is between 3000–4000 $\mathrm{kg\,m^{-3}}$.

The analyses dealing with an asteroid – meteoroid stream relationship made so far are based on the orbital similarity only, thus a real relationship still has to be proved. Nevertheless, there have been published more papers discussing this topic and suggesting various associations between the Earth-crossing asteroids and meteor showers on the basis either radar or photographic observational data (e.g., Sekanina, 1973, 1976; Drummond, 1982; Babadzhanov and Obrubov, 1983; Olsson-Steel, 1988; Hasegawa et al., 1992; Štohl and Porubčan, 1993; Babadzhanov, 1996).

6.3.3. *Catastrophic Break-up*

A meteoroid stream can be formed also by a catastrophic break up of the parent body as indicated by comet Biela and the strong meteor showers observed in 1872, 1885, 1892 and 1899. A splitting of cometary nuclei is a rather frequently observed phenomenon which may result in a more rapid disintegration of the individual parts of the original nucleus and formation of meteoroid streams. Another interesting

information was reported by Bosler and Roure in 1937, where they showed that the Leonids orbit and comet Biela were separated only 0.0265 AU in 1846, and suggested that a collision between the comet nucleus and the dense part of the Leonids might be the cause of the Biela disintegration. Babadzhanov et al. (1991) re-analyzed the situation following the orbital evolution by numerical integration. They confirmed that the separation between comet Biela and the Leonid stream was only 0.026 AU in 1846 and the closest approach occurred on 21 November, 1832 at a distance of 0.002 AU. The fact that comet Biela may passed through the densest region of the Leonid stream does not mean that the event is responsible for the comet break up, but the possibility is rather intriguing (Williams, 1993). Another stream of particular interest that may be related to a catastrophic episode is the Taurid meteor complex (Steel et al., 1991).

6.3.4. *Stream Evolution*

As mentioned above, meteoroids are released from their parent bodies with relatively low speeds, however, these may be accelerated by other forces soon after the release and may lead to evolution of the stream which means also a change in the structure of the observed meteor shower. Immediately after the release, the dust particles are subjected to radiation pressure effects and the Poynting–Robertson drag which are important for smaller particles (lifetime of a particle depends on both the size and composition). Equations governing the motion under the Poynting-Robertson drag were derived by Wyatt and Whipple (1950) and the effect is discussed in detail by Burns et al. (1979). Kresák (1976) has shown the importance of the direct radiation pressure which increases the semimajor axis of the orbit and so the period of revolution of meteoroids. This size-dependent effect causes a greater spread of meteoroids around the common orbit and leads to a longer lifetime. Gustafson and Adolfsson (1996) analyzing radiation pressure correction to meteor orbits conclude that the effect is negligible for fireballs, of the order of the measurement errors ($\approx$ 1%) for photographic meteors and substantially larger than the errors ($\approx$ 10%) for radar meteors.

The meteoroids after their release from the parent body are also subject to gravitational perturbations due to the planets. The importance of this effect is known since the early attempts to follow the orbital evolution of meteoroid streams. A meteoroid stream can be represented by a large number of test particles and its evolution under the influence of gravitational and radiation forces can be followed by numerical integration of the equations of motion of each individual particle. The use of direct numerical integration is now widespread, being used for the study of particular meteoroid streams and for meteoroid stream evolution in general.

Babadzhanov and Obrubov in their study from 1989 stated that secular perturbations are constrained by two integrals of motion

$$(1 - e^2)\ \cos^2\ i = C_1 \tag{119}$$

$$e^2\ (0.4 - \sin^2\ i\ \sin^2\ \omega) = C_2, \tag{120}$$

where C_1, C_2 are constants determined from the observed orbital elements. The first integral follows from the Tisserand criterion assuming a = constant, and the second was developed by authors referenced by Babadzhanov and Obrubov (1989). Since meteors can be observed only if they have nodes at the Earth's orbit, a third relation is valid

$$a\,(1-e^2) = 1 \pm e\,\cos\omega. \tag{121}$$

Applying this procedure for simulation the orbital evolution of the meteoroid streams related to parent bodies, Babadzhanov and Obrubov obtained a series of multiple related meteoroid streams, e.g., four meteoroid streams including the Geminids are theoretically related with 3200 Phaethon. P/Machholz may produce eight meteoroid streams consisting of six known streams: Quadrantids, Ursids, N and S δ Aquarids, Daytime Arietids and α Cetids (Babadzhanov and Obrubov, 1992b).

6.4. SPORADIC METEORS

6.4.1. *Population of Sporadic Meteors*

The sporadic component of the meteoroid influx constitutes a major part of the whole complex of the interplanetary bodies. Only about one quarter of visually observable meteors are in showers. The rest consists of meteors from the general random background, called *sporadic* meteors, not belonging to any recognized shower. It is also possible that some sporadic meteors are actually members of very dispersed minor showers with large radiant areas and low hourly rates, influenced by selection effects described in the preceding section. In such a case the shower members are difficult to recognize from the sporadic background. Some of the catalogued minor streams are unrealistic because their identification is based only on a chance resemblance of several sporadic orbits. The frequency of such cases primarily depends on the distribution of orbits within the sporadic background and this circumstance affects all identification criteria. Meteor showers are dominant only among meteors of medium brightnesses and sizes, a result issuing from studies of various data sets and techniques (Table XXIII). They become less significant among smaller particles, which is demonstrated also by larger values of the mass distribution exponent, s, in radio observations, or by the magnitude function, r, in visual observations, obtained for sporadic meteors ($s \approx 2, r \approx 3$), with respect to the shower meteors ($s \approx 1.5, r \approx 2.5$). Moreover, showers are less significant also among very bright meteors, which is also to be expected as, e.g., there are no meteorites known to be of cometary origin so far. Originally stream meteoroids spread into sporadic background may be the reason for a small bump on the flux curve (Figure 26) of sporadic meteoroids for this limited mass range mainly of grams and tenths of grams (Ceplecha, 1992). Table XXIII comprises meteoroid masses in the range 10^2–10^{-9} kg. Though the results may be influenced by various selection effects and individual criteria applied for the stream membership, the

TABLE XXIII
Relative number of sporadic meteors N_{sp}

m_{lim}	N_{sp} (%)	N	Method	References
-7^m	85	230	Photogr.	McCrosky et al. (1976)
-3^m	54	1 028	Photogr.	Porubčan and Gavajdová (1994)
0^m	40	144	Photogr.	Whipple (1954)
0^m	35	413	Photogr.	Jacchia and Whipple (1961)
0^m–4^m	45	1 827	Photogr.	Lindblad (1974)
4^m	64	359	Photogr.	Southworth and Hawkins (1963)
7^m	71	1 900	Radio	Nilsson (1964)
7^m	72	12 500	Radio	Kashcheev et al. (1967)
7^m	72	16 800	Radio	Lebedinets et al. (1973)
8^m	78	4 500	Radio	Babadzhanov et al. (1974)
13^m	85	39 000	Radio	Sekanina (1973, 1976)

tendency for the sporadic meteors to dominate the meteoric complex seems to be conclusive.

Practically, all the basic information on the population of sporadic meteors was obtained thank to various radar and photographic surveys over the past few decades, and can be found in more survey papers (e.g., Davies, 1957; Kashcheev et al., 1967; Lebedinets et al., 1973; Štohl, 1983, 1986; Olsson-Steel, 1986; Jones and Brown, 1994). Studies of the sporadic background meteoroid orbits reveal also distinct differences between various sporadic populations (e.g., Hughes, 1978; Kashcheev and Tkachuk, 1979; Ceplecha, 1988; Divine, 1993). Photographic meteoroids exhibit a strong preponderance of orbits similar to the orbits of short period comets, with small direct orbits ($a < 4$ AU), low inclination ($i < 30°$) and high eccentricities ($e > 0.7$). Radio meteoroids down to 7^m exhibit a large number of both direct and retrograde orbits with high inclinations ($30° < i < 165°$) and small eccentricities ($e < 0.7$). For still fainter radio meteors the relative number of orbits with high inclinations is still higher.

6.4.2. *Variations of Sporadic Meteors and Radiant Distribution*
From the first systematic visual observations it became evident that sporadic meteors exhibit diurnal and seasonal variations in their activity. The diurnal variation observed already Brandes in 1825 and Schiaparelli in 1866 attempted to explain the variations as an effect of geometry, where sporadic radiants were initially distributed isotropicly, but appear to be concentrated about the apex of the Earth because of the Earth's orbital motion. As a result of the apex position, higher counts of sporadic meteors will be recorded in the morning hours and smaller in the evening hours. Normally the ratio is in the range 3 to 5 and one would expect the greatest

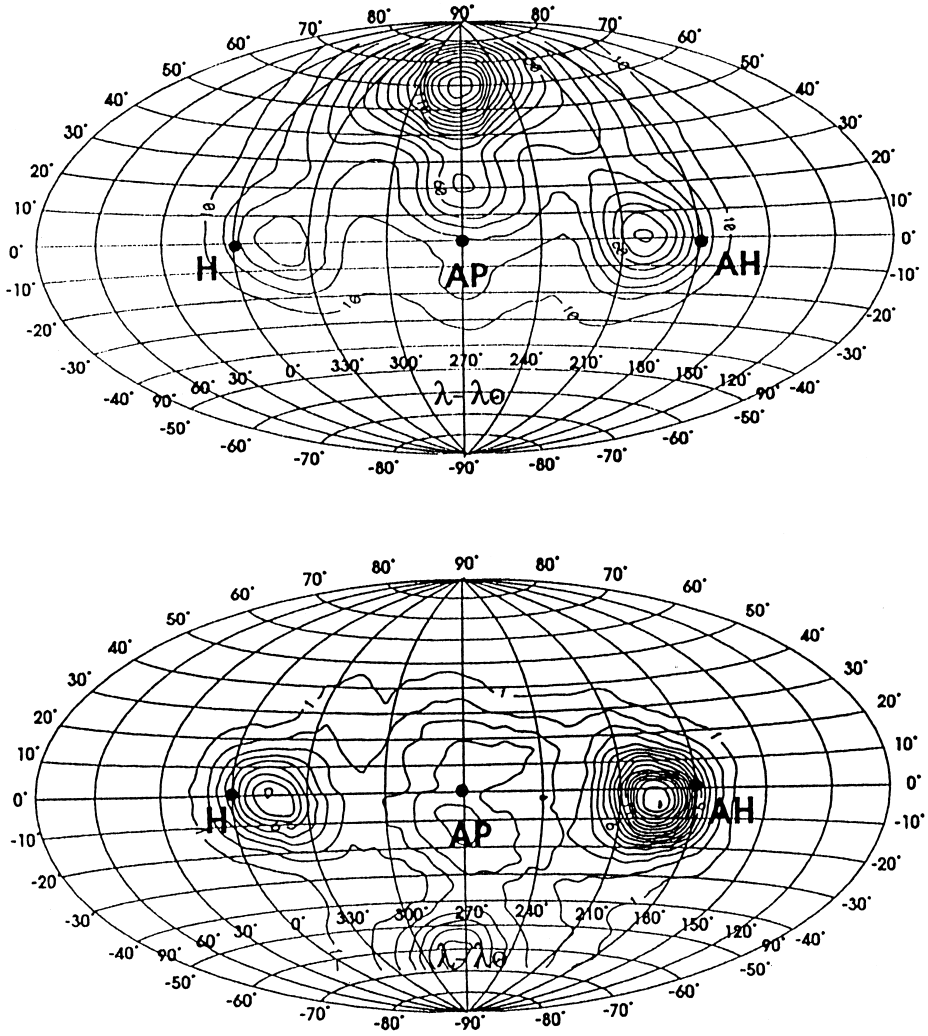

Figure 23. Contours of apparent density of meteor radiants from the combined Harvard (upper plot) and Adelaide (lower plot) radio surveys (Jones and Brown, 1994). **H** denotes the position of the Sun, **AP** the Earth's apex and **AH** the antihelion point.

daily variation at the equator and the least one at either pole (McKinley, 1961). In the course of the year, the apex is at the greater elevations for the northern hemisphere in autumn, which should result in higher sporadic meteor counts observed there in autumn with respect to spring. Reliable results concerning the variations and distributions of apparent (geocentric) and true (heliocentric) radiants could be obtained only after radio methods were introduced into meteor observations, enabling whole day monitoring of the sky, independently of weather or moonshine.

TABLE XXIV

Means and widths (to half-maximum) of the radiant distributions of the diffuse sporadic sources (Jones and Brown, 1994)

Source	Long. (°)	Lat. (°)	Radius (°)
Antihelion	198	0	18
Helion	342	1	16
North toroidal	271	58	19
South toroidal	274	−60	16
North apex	271	19	21
South apex	273	−11	?

As summarized by Štohl (1986), the diurnal variation of sporadic meteor rates shows three maxima, at about 2, 6, and 10 LT. The maxima correspond to three concentrations of the geocentric radiants in the ecliptic found by Hawkins (1956) from Jodrell Bank radar observations: the *apex* source (AP) – in the direction of the Earth's apex, the *helion* (HE) and *antihelion* (AH) sources – located symmetrically on each side from the apex at a distance of about 60°–70°, and moreover there are two additional concentrations located at ecliptical latitudes of about ±60° – the *toroidal* sources. Jones and Brown (1993, 1994) analyzing data from six major surveys of orbits of radar meteoroids found that the apex source appears to be split into northern and southern components. The splitting was previously noted also by Elford and Hawkins (1964).The mean values of the locations of all the sources are given in Table XXIV and activity contours for the Harvard and Adelaide radio surveys presented by Jones and Brown (1994) are depicted in Figure 23.

The relative strengths of individual sources differ greatly and depend on individual surveys. This is to be expected due to various selection effects, location, antenna systems and instrumental limitations. Considering the radiant distribution from various data sets, one can conclude that for meteors from 0^m to about 6^m–8^m, the strength of the helion and antihelion sources is about twice the strength of the apex source. For faint meteors down to about 12^m, the strength of the apex source overruns the helion and antihelion sources as evident from Kharkov radio data (Tkachuk, 1978) (Figure 24). The helion and antihelion sources are populated by low inclination, prograde eccentric orbits which are essentially identical to short period comets and may also have an asteroidal component (Jones and Brown, 1993).

The seasonal variation of sporadic meteors in the strength of the apparent maxima of the helion and antihelion sources shows asymmetric features during certain periods. The radio data of the meteor hourly rates from the southern and northern

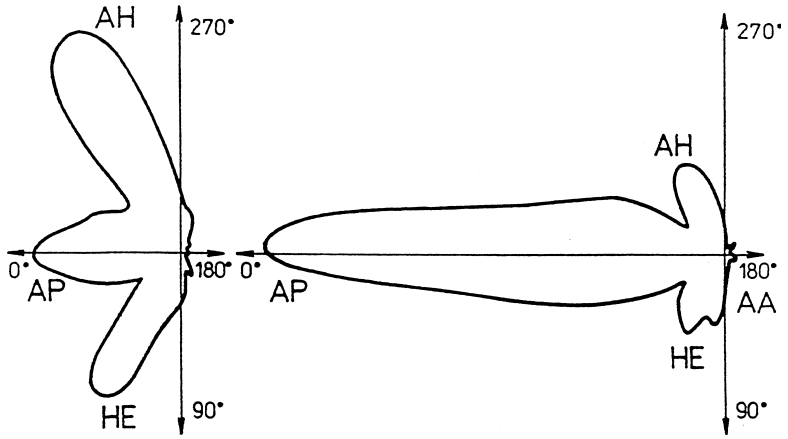

Figure 24. Distribution of the apparent sporadic radiants along the ecliptical longitude (0° is direction to the apex) from the radio observations at Jodrell Bank (left) (Davies, 1957) and Kharkov (right) (Tkachuk, 1978). **AP, HE, AH,** and **AA** denote directions to the apex, helion, antihelion, and antiapex, respectively.

hemispheres (Christchurch: Keay, 1963; Ottawa: Štohl, 1968) revealed a strong maximum of the helion source in April–June, a maximum of the antihelion source in April–July and especially in October–December.

Štohl (1983, 1986) analyzing the activity of the helion and antihelion sources noted that the observed seasonal variations rather agree with strong concentrations of similar orbits in some preferential directions, which may be interpreted as very broad and diffuse *'sporadic meteoroid streams'* to be observed twice a year as a twin meteor shower. This scheme confirms the two maxima of the activity of the antihelion (October–December) and helion (April–June) sources derived from the observed hourly rates. The approximate dates of the maxima of activity of the sources provide the longitude of perihelion of the 'sporadic meteoroid stream' of about 140°. Taking into account the mean orbits of the 'sporadic stream' for the helion and antihelion sources, Štohl has suggested that the stream is closely related to several daytime (helion) and nighttime (antihelion) showers possibly associated with comet Encke.

6.4.3. *Sources of Sporadic Meteors*

Sporadic meteoroids may originate in a number of different sources. They can be a result of gradual evolution and diffusion of meteoroid streams under the radiation and perturbation effects, collisions between the stream and dust cloud particles, particles evolved from the asteroidal belt or from meteorite streams. Further, meteors from the marginal regions of meteoroid streams and from streams in direct orbits with low geocentric velocities (diffuse, large radiant areas) may be observed as sporadic. It is still not clear if the origin of the sporadic complex is predominantly cometary or asteroidal, though Olsson-Steel (1986) noted that the

streams with orbits similar to short period comets ($a < 5$, $e > 0.7$, low inclination) are a major source of the sporadic meteoroid complex, as a result of planetary encounters, particularly with Jupiter. One should be also aware of the fact that for different size ranges, the ratio of meteoroids of asteroidal origin to cometary origin differs by a great extent (Ceplecha, 1988).

6.5. INTERSTELLAR METEOROIDS

Öpik (1941), based largely on an analysis of visual observations conducted using the rocking mirror method during the Arizona observational campaign, claimed that as many as 70% of the meteors were in heliocentric hyperbolic orbits, some at several times the parabolic velocity limit. In later papers Öpik (1956) down-scaled the claim to approximately 3% of meteors in hyperbolic orbits. McKinley (1961) reviewed the Ottawa radar results with respect to hyperbolic meteor velocities: only about 0.3% of the detected meteors were more than one standard deviation above the parabolic limit, and none more than two standard deviations above the limit. The Jodrell Bank radio observations produced similar results. However, it can validly be claimed that one should really perform individual orbit calculations, and not simply look at gross velocity distributions, and furthermore that these traditional radar observations are strongly biased against high velocity meteors due to the rapid diffusion of the electron column at great heights (and consequent destructive interference of the radio echo components – the already mentioned radio echo ceiling effect). Štohl (1970) reviewed available data from small camera and Super Schmidt photographic results, finding that the percentage of meteors in hyperbolic orbits range from about 2 to 24% in the 8 different studies. However, when the data are divided into categories according to the precision of the orbital determinations, only 0 to 2% of the most precise orbits are hyperbolic. More recently Hajduková (1993, 1994) analyzed the photographic meteor orbits collected in the IAU Meteor Data Center. Although 12% of the orbits are hyperbolic (347 from the collection of 2910 meteor orbits), when only the most precise data is examined the proportion shrinks considerably. She reaches the conclusion, considering probably velocities of interstellar material, that not more than 0.02% (for unbiased mass interval) of photographic meteors are of interstellar origin.

Woodworth and Hawkes (1996) summarized the evidence for hyperbolic orbits in television data. In the first multistation television meteor study (Hawkes et al., 1984) 5 (from the sample of 77) meteors are in hyperbolic orbits ($e > 1$), but if we apply the two standard deviation confidence criterion, only one of these is hyperbolic. A much larger sampling of slightly fainter television meteors is provided in the studies by Jones and Sarma (1985), and in the last section they discuss the issue of hyperbolic meteors. They find that 26 (i.e. 6%) of the orbits are hyperbolic if a 95% confidence interval is employed. However, when they examine more carefully the probable systematic errors in velocities due to the difficulty in defining a unique fiducial point, they come to the conclusion that only 8 of the meteors (1.7% of the

sample) are hyperbolic. Ueda and Fujiwara (1995) have provided an analysis of 265 doubly observed television meteors. If we apply the 95% criterion then it is found that 29 meteors (10.9% of the sample are hyperbolic). The natural question to ask is why the significant difference in the fraction of hyperbolic meteors observed in the three studies (1.3% in the Hawkes et al., 1984 study; 1.7% in the Jones and Sarma, 1985 study; and 8.9% in the Ueda and Fujiwara study). However, the differences are not so marked if one is reminded of the fact that Jones and Sarma (1985) first found nearly 6% at the 95% confidence level, but after consideration of systematic velocity error effects they reduced the number to 1.7%. One must be cautious of correlations between errors which can underestimate the standard error predicted from the true value. It is likely that the real percentage of hyperbolic meteors in the Ueda and Fujiwara study is only of the order of few percent as well.

In summary, it would seem that at most approximately 2% of faint television meteors are hyperbolic. However almost all of these occur at geocentric velocities of less than 80 km s^{-1}, and there does not seem to be the strongly hyperbolic excess which has been claimed as detected by the southern hemisphere radar (Baggaley et al., 1993a, 1994). There seems to be no consistent picture regarding the months when hyperbolic orbit dust is most likely to be encountered by mid-north latitude observatories. No southern hemisphere low light level television observations have been conducted.

6.6. METEOROID INFLUX ONTO THE EARTH

In the past many authors estimated the total interplanetary matter arriving on the Earth by extrapolating results from a limited size-range by assuming a power law size distribution with a constant exponent. Namely visual observations of meteors and also the observations by radar occupy very narrow size-range and such an extrapolation cannot yield a good estimation of the total influx. In this section we attempt to estimate the total influx of bodies onto the Earth from 10^{-21} kg to 10^{15} kg by combining results of different methods and authors (Table XXV). Results published by Ceplecha (1992) are updated by using the new mass scale for 100 kg bodies as resulting from detailed analysis of the photographic records of the Lost City fireball and meteorite fall (Ceplecha, 1996a).

The resulting cumulative number fluxes of interplanetary bodies onto the Earth derived from data of Table XXV are given in Figure 25 and in Table XXVI. Fluxes across this vast range of masses cannot be expressed by a simple power law, which suggests several interlaced populations of different origin, as was already demonstrated for meteoroids entering the atmosphere as sporadic meteors with masses from 10^{-6} to 2×10^3 kg. Incremental fluxes derived from Table XXVI are given in Figure 26. There are three mass ranges with unstable populations: $\log m = (-9.5, -6), (-4, -2.5)$ and $(5, 9)$. The first region corresponds to the situation where the losses of particles caused by Poynting-Robertson effect outweigh the collisional gains of particles from bigger bodies (Grün et al., 1985; Leinert and

TABLE XXV
Sources of observational flux-data on Earth-crossing interplanetary bodies

Mass range (kg) from	to	Method	Author
10^{-21}	10^{-9}	lunar microcraters space probes	Grün et al. (1985)
10^{-16}	6×10^{-10}	space probes	Naumann (1966) Hoffman et al. (1975a,b) Grün and Zook (1980)
3×10^{-9}	3×10^{-6}	radar meteors	Elford et al. (1964) Verniani and Hawkins (1965)
10^{-6}	10^{4}	photographic and television meteors	Ceplecha (1988, 1996a, 1997)
8×10^{5}	10^{15}	asteroid discoveries by Spacewatch	Rabinowitz (1993, 1994, 1996) Rabinowitz et al. (1993)
10^{12}	10^{15}	photographic Earth-crossing asteroids	Shoemaker et al. (1990)

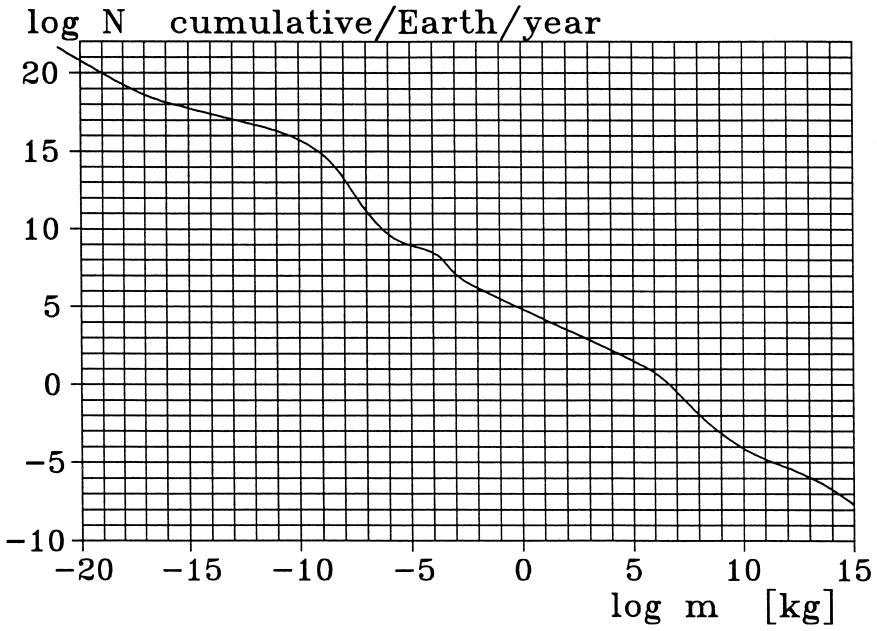

Figure 25. Logarithm (base 10) of the cumulative number, N, of interplanetary bodies with mass equal or greater than m coming to the entire Earth's surface per year is plotted against logarithm of the mass m.

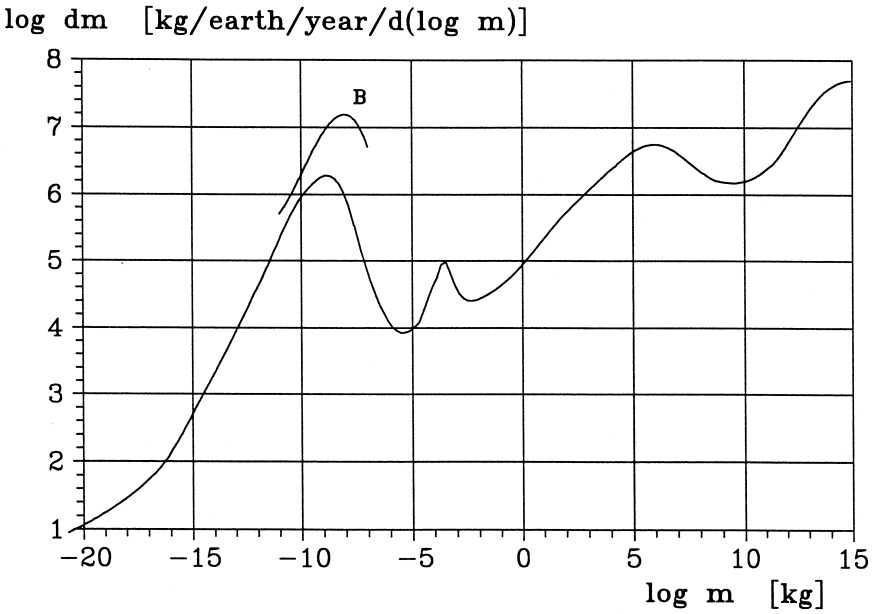

Figure 26. Increment of mass, $\log \mathrm{d}m$, per one order of mass per the entire Earth's surface per year is plotted against the logarithm of mass, $\log m$. The dust range contains also new measurements by Love and Brownlee (1993) denoted **B**.

Grün, 1988). The second region at $\log m = -3$ corresponds to the mass range where meteor showers are the most distinct phenomena (see Section 6.4.1): perhaps a good part of sporadic meteors in this mass range originate from shower meteors perturbed and spread to such an extent that they cannot be distinguished from the sporadic background. The third region corresponds perhaps to a majority of small cometary fragments (small inactive comets) (Ceplecha, 1992; Ceplecha et al., 1997) as already proposed by Kresák (1978) to explain the comet discovery statistics. Perhaps comets need to have masses of at least 10^9 kg to be active.

The total mass influx of all interplanetary bodies to the Earth across the mass range 10^{-21} kg to 10^{15} kg is 1.3×10^8 kg per year for the entire Earth surface. This value is one order of magnitude higher than those derived from extrapolations of fluxes of small bodies (e. g. Hughes, 1978). But one should be aware that this flux is mostly due to very large bodies: one body of 10^{14} kg to 10^{15} kg coming at an average interval of 10^7 to 10^8 years. Masses less than 10^{-7} kg contribute to the influx by 4×10^6 kg per year per Earth's surface; masses between 10^{-7} kg and 10^2 kg contribute by 0.8×10^6 kg; masses between 10^2 kg and 10^9 kg contribute by 20×10^6 kg; masses between 10^9 kg and 10^{15} kg contribute by 100×10^6 kg per year per Earth's surface.

We see that the mass influx in perspective of a human life span is significantly lower then the total influx. If one takes 100 years as a period for averaging, one has to omit all bodies with masses over 10^8 kg and the total influx becomes 2.4×10^7 kg

TABLE XXVI

Cumulative numbers N (all bodies with masses larger than the given mass m) of interplanetary bodies coming to the entire Earth's surface per year

log m kg	log N	log m kg	log N	log m kg	log N	log m kg	log N	log m kg	log N	log m kg	log N
15.0	−7.71	9.0	−3.18	3.0	2.85	−3.0	7.10	−9.0	14.85	−15.0	17.77
14.8	−7.49	8.8	−2.97	2.8	2.99	−3.2	7.38	−9.2	15.06	−15.2	17.84
14.6	−7.29	8.6	−2.77	2.6	3.13	−3.4	7.71	−9.4	15.26	−15.4	17.92
14.4	−7.09	8.4	−2.55	2.4	3.27	−3.6	8.05	−9.6	15.43	−15.6	17.99
14.2	−6.90	8.2	−2.33	2.2	3.40	−3.8	8.30	−9.8	15.59	−15.8	18.07
14.0	−6.72	8.0	−2.09	2.0	3.54	−4.0	8.46	−10.0	15.74	−16.0	18.15
13.8	−6.55	7.8	−1.85	1.8	3.67	−4.2	8.59	−10.2	15.87	−16.2	18.23
13.6	−6.38	7.6	−1.61	1.6	3.80	−4.4	8.70	−10.4	16.00	−16.4	18.32
13.4	−6.23	7.4	−1.36	1.4	3.93	−4.6	8.78	−10.6	16.11	−16.6	18.42
13.2	−6.08	7.2	−1.10	1.2	4.06	−4.8	8.86	−10.8	16.22	−16.8	18.52
13.0	−5.94	7.0	−0.85	1.0	4.18	−5.0	8.95	−11.0	16.31	−17.0	18.63
12.8	−5.81	6.8	−0.60	0.8	4.31	−5.2	9.05	−11.2	16.40	−17.2	18.74
12.6	−5.69	6.6	−0.36	0.6	4.43	−5.4	9.16	−11.4	16.48	−17.4	18.86
12.4	−5.57	6.4	−0.12	0.4	4.55	−5.6	9.30	−11.6	16.56	−17.6	18.99
12.2	−5.46	6.2	0.12	0.2	4.67	−5.8	9.46	−11.8	16.63	−17.8	19.12
12.0	−5.35	6.0	0.34	0.0	4.79	−6.0	9.65	−12.0	16.70	−18.0	19.26
11.8	−5.24	5.8	0.56	−0.2	4.91	−6.2	9.89	−12.2	16.77	−18.2	19.40
11.6	−5.14	5.6	0.76	−0.4	5.04	−6.4	10.16	−12.4	16.84	−18.4	19.54
11.4	−5.03	5.4	0.96	−0.6	5.17	−6.6	10.47	−12.6	16.91	−18.6	19.69
11.2	−4.92	5.2	1.15	−0.8	5.30	−6.8	10.80	−12.8	16.98	−18.8	19.84
11.0	−4.79	5.0	1.33	−1.0	5.43	−7.0	11.16	−13.0	17.05	−19.0	20.00
10.8	−4.67	4.8	1.50	−1.2	5.57	−7.2	11.55	−13.2	17.12	−19.2	20.15
10.6	−4.53	4.6	1.66	−1.4	5.71	−7.4	11.96	−13.4	17.19	−19.4	20.31
10.4	−4.39	4.4	1.82	−1.6	5.86	−7.6	12.38	−13.6	17.26	−19.6	20.47
10.2	−4.24	4.2	1.98	−1.8	6.01	−7.8	12.82	−13.8	17.33	−19.8	20.63
10.0	−4.08	4.0	2.13	−2.0	6.17	−8.0	13.25	−14.0	17.40	−20.0	20.79
9.8	−3.91	3.8	2.28	−2.2	6.33	−8.2	13.65	−14.2	17.47	−20.2	20.95
9.6	−3.74	3.6	2.42	−2.4	6.50	−8.4	14.00	−14.4	17.54	−20.4	21.12
9.4	−3.56	3.4	2.56	−2.6	6.68	−8.6	14.32	−14.6	17.62	−20.6	21.28
9.2	−3.37	3.2	2.71	−2.8	6.88	−8.8	14.60	−14.8	17.69	−20.8	21.45

per year per Earth. The interplanetary dust component of the influx is 4×10^6 kg per year per Earth, i.e., about 17% of the influx originates in the interplanetary dust and 83% in bodies mostly inside a mass range of 10^5 kg to 10^8 kg (10 to 100 m sizes). We see that these large bodies form the most important source of mass influx onto the Earth from the perspective of human life span. Because most of this incoming mass is converted to small dust grains (due to fragmentation and ablation), these bodies are also the most important source of meteoric dust in the middle atmosphere (Ceplecha, 1976). This situation would change, if one assumes that the significantly larger dust fluxes resulting from the Long Duration Exposure Facility (Love and Brownlee, 1993) are real. Then the original dust component of the influx would be about $3\times$ larger than the flux from the 10 to 100 m size bodies.

The size range of visual meteors is located in a minimum of incremental flux. The flux of visual sporadic meteors is the least important component from the point of view of the total influx. However, we should take into consideration also the flux of stream meteoroids seen as meteor showers. There are periods of time with much increased activity called meteoroid storms increasing the flux by a factor of up to 10^5 on a time scale of hours (see Section 6.2.5). A flux increase of $1000\times$ or higher is already the most efficient source of Earth influx for a short period of tens of minutes up to few hours. These bodies are the real danger for human activity in the near Earth space and on the surface of Moon.

Atmospheric penetration of meter and ten meter size bodies is regularly and globally observed by satellites (Tagliaferri et al., 1994; McCord et al., 1995). Bodies of 10 and 100 m sizes imperil the Earth's biosphere on a time scale of hundreds and thousands of years. A good example from this century is the Tunguska body explosion. An atmospheric explosion of a body of about $5\times$ larger size over ocean waters would give rise to an enormous tsunami wave already endangering coastal ranges. Bodies in the size range of 10 and 100 meters are the least known bodies of the solar system. Their exploration is of prime importance. Satellite systems should be improved to be able to yield precise data on trajectories, velocities and orbits, and also on spectral radiation at penetration of these bodies into the Earth's atmosphere. This can help to reveal composition and structure of these bodies, as well as new insights into the atmospheric interaction processes for such large bodies. Also observing these bodies in interplanetary space by systems of sensitive telescopes using reflected sun light, either from ground or from space stations, can help to place these bodies in their planetary context.

Acknowledgements

This work has been supported by Contracts 205/94/1862 and 205/97/0700 of the Grant Agency of the Czech Republic and by the Sandia National Laboratories Contract AJ-4706.

References

Adolfsson, L.: 1998, 'Rotation of Meteors: Lost City', *Icarus* (submitted).

Allen, C. W.: 1973, *Astrophysical Quantities*, 3rd ed., Athlone Press, London.

Arlt, R.: 1995, 'The New Working List of Visual Showers, *WGN: J. Int. Met. Org.* **23**, 105–109.

Arter, T. R. and Williams, I. P.: 1997, 'Periodic Behaviour of the April Lyrids', *Monthly Notices Roy. Astron. Soc.* **286**, 163–172.

Andrianov, N. S., Kurganov, R. A., Nasirov, A. M., and Sidorov, V. V.: 1968, in L. Krešak and P. M. Millman (eds.), 'Oblique Scattering Method for Measuring Individual Radiants and Meteor Velocities', *Physics and Dynamics of Meteors*, D. Reidel Publ. Co., Dordrecht, Holland, pp. 14–26.

Aspinall, A., Clegg, J. A., and Hawkins, G. S.: 1951, 'A Radio Echo Apparatus for the Delineation of Meteor Radiants', *Phil. Mag.* **42**, 504–515.

Avery, S. K., Avery, J. P., Valentic, S. E., Palo, S. E., Leary, M. J., and Obert, R. L.: 1990, 'A New Meteor Echo Detection and Collection System: Christmas Island Mesospheric Wind Measurements', *Radio Sci.* **25**, 657–669.

Ayers, W. G., McCrosky, R. E., and Shao, C.-Y.: 1970, 'Photographic Observations of 10 Artificial Meteors', *Smithsonian Astrophys. Obs. Spec. Rep.* **317**, 1–40.

Babadzhanov, P. B.: 1996, 'Meteor Showers of Asteroids Approaching the Earth', *Astron. Vestnik* **30**, 442–453.

Babadzhanov, P. B. and Getman, V. S.: 1980, in I. Halliday and B. A. McIntosh (eds.), 'Orbit, Chemical Composition and Atmospheric Fragmentation of a Meteoroid from Instantaneous Photographs', *Solid Particles in the Solar System.*, D. Reidel Publ. Co., Dordrecht, Holland, pp. 111–115.

Babadzhanov, P. B. and Obrubov, Yu. V.: 1983, in C.-I. Lagerkvist and H. Rickman (eds.), 'Secular Perturbations of Apollo, Amor, Aten Asteroid Orbits and Theoretical Radiants of Meteor Showers Probably Associated with Them', *in Asteroids, Comets, Meteors*, Astron. Obs. Univ., Uppsala, pp. 411–417.

Babadzhanov, P. B. and Obrubov, Yu. V.: 1992a, 'Evolution of Short-Period Meteor Streams', *Cel. Mech. Dynam. Astron.* **54**, 111–127.

Babadzhanov, P. B. and Obrubov, Yu. V.: 1992b, in A. W. Harris and T. Bowel (eds.), 'P/Machholz and Quadrantid Meteoroid Stream. Orbital Evolution and Relationship', *in Asteroids, Comets, Meteors 1991*, LPI, Houston, pp. 27–31.

Babadzhanov, P. B., Demochko, N. K., Kashcheev, B. L., Novoselova, N. V., and Fedynskij, V. V.: 1974, 'The Number of Meteors in the Southern and Northern Celestial Hemisphere on the Basis of Radar Observations at the Equator', *Astron. Vestnik* **8**, 154–157 (in Russian), and *Bull. Astron. Inst. Czech.* **34**, 195–212.

Babadzhanov, P. B., Wu, Z., Williams, I. P., and Hughes, D. W.: 1991, 'The Leonids, Comet Biela and Biela's Associated Meteoroid Stream', *Monthly Notices Roy. Astron. Soc.* **253**, 69–74.

Baggaley, W. J.: 1970, 'The Determination of the Initial Radii of Meteor Trains', *Monthly Notices Roy. Astron. Soc.* **147**, 231–243.

Baggaley, W. J.: 1979, 'D-Region Absorption and Forward-Scatter Radio-Meteor Data', *J. Atmospheric Terrest. Phys.* **41**, 671–676.

Baggaley, W. J.: 1980, in I. Halliday and B. A. McIntosh (eds.), 'Meteors and Atmospheres', *Solid Particles in the Solar System*, D. Reidel Publ. Co., Dordrecht, Holland, pp. 85–100.

Baggaley, W. J.: 1981, 'Single Wavelength Measurements of the Initial Radii of Radio Meteor Ionization Columns', *Bull. Astron. Inst. Czech.* **32**, 345–348.

Baggaley, W. J. and Fisher, G. W.: 1980, 'Measurements of the Initial Radii of the Ionization Columns of Bright Meteors', *Planetary Space Sci.* **28**, 575–580.

Baggaley, W. J. and Webb, T. H.: 1977, 'The Thermalization of Meteoric Ionization', *J. Atmospheric Terrest. Phys.* **39**, 1399–1403.

Baggaley, W. J., Taylor, A. D., and Steel, D. I.: 1993a, in J. Štohl and I. P. Williams (eds.), 'The Influx of Meteoroids with Hyperbolic Heliocentric Orbits', *Meteoroids and Their Parent Bodies*, Polygrafia SAV, Bratislava, pp. 53–56.

Baggaley, W. J., Taylor, A. D., and Steel, D. I.: 1993b, in J. Štohl and I. P. Williams (eds.), 'The Southern Hemisphere Meteor Orbit Radar Facility: AMOR', *Meteoroids and Their Parent Bodies*, Polygrafia SAV, Bratislava, pp. 245–248.

Baggaley, W. J., Bennett, R. G. T., Taylor, A. D., and Steel, D. I.: 1994, 'The Advanced Meteor Orbit Radar Facility: AMOR', *Quant. J. Roy. Astron. Soc.* **35**, 293–320.

Baldwin, B. and Sheaffer, Y,: 1971, 'Ablation and Breakup of Large Meteoroids during Atmospheric Entry', *J. Geophys. Res.* **76**, 4653–4668.

Bayrachenko, I. V.: 1965, 'Measurements of the Initial Radii of Ionized Meteor Trails from Simultaneous Observations of Radio Meteors on two Wavelengths', *Geomagn. Aeron.* **5**, 353.

Beech, M., Brown, P., and Jones, J.: 1995, 'VLF Detection of Fireballs', *Earth, Moon, Planets* **68**, 181–188.

Belkovich, O. I. and Pupyshev, J. A.: 1968, L. Kresák and P. M. Millman (eds.), 'The Variation of Sporadic Meteor Radiant Density and the Mass Law Exponent over the Celestial Sphere', *Physics and Dynamics of Meteors*, D. Reidel Publ. Co., Dordrecht, Holland, pp. 373–381.

Bessel, M. S.: 1990, 'UBVRI Passbands', *Publ. Astron. Soc. Pacific* **102**, 1181–1199.

Binzel, R. P. and Xu, S.: 1993, 'Chips off of Asteroid 4 Vesta: Evidence for the Parent Body of Basaltic Achondrite Meteorites', *Science* **260**, 186–191.

Borovička, J.: 1993, 'A Fireball Spectrum Analysis', *Astron. Astrophys.* **279**, 627–645.

Borovička, J.: 1994a, 'Line Identifications in a Fireball Spectrum', *Astron. Astrophys. Suppl. Ser.* **103**, 83–96.

Borovička, J.: 1994b, 'Two Components in Meteor Spectra', *Planetary Space Sci.* **42**, 145–150.

Borovička, J.: 1994c, in Y. Kozai, R. P. Binzel, and T. Hirayama (eds.), 'Meteor Spectra – Possible Link between Meteorite Classes and Asteroid Families', '*75 Years of Hirayama Asteroid Families*', *ASP Conf. Series* **63**, 186–191.

Borovička, J. and Boček, J.: 1996, 'Television Spectra of Meteors', *Earth, Moon, Planets* **71**, 237–244.

Borovička, J. and Spurný, P.: 1996, 'Radiation Study of Two Very Bright Terrestrial Bolides', *Icarus* **121**, 484–510.

Borovička, J. and Zamorano, J.: 1995, 'The Spectrum of Fireball Light Taken with a 2-m Telescope', *Earth, Moon, Planets* **68**, 217–222.

Borovička, J., Zimnikoval, P., Škvarka, J., Rajchl, J., and Spurný, P.: 1996, 'The Identification of Nebular Lines in Spectra of Meteor Trains', *Astron. Astrophys.* **306**, 995–998.

Bronshten, V. A.: 1983, *Physics of Meteor Phenomena*, D. Reidel Publ. Co., Dordrecht, Holland, 356 pp.

Bronshten, V. A.: 1993a, 'Entry of Large Meteoroids into the Atmosphere', *Solar System Res.* **27**, 80–95.

Bronshten, V. A.: 1993b, 'On Some Attempts to Critique the Physical Theory of Meteors', *Astron. Vestnik* **27**, 97–111 (in Russian).

Bronshten, V. A. and Zotkin, I. T.: 1995, 'Tunguska Meteorite: Fragment of a Comet or an Asteroid?', *Solar System Res.* **29**, 241–245.

Brown, N.: 1976, 'Radio Echoes from Meteor Trains at a Radio Frequency of 1.98 MHz', *J. Atmospheric Terrest. Phys.* **38**, 83–87.

Brown, P. and Jones, J.: 1998, 'Simulation of the Formation and Evolution of the Perseid Meteoroid Stream', *Icarus*, submitted.

Brown, P. and Rendtel, J.: 1996, 'The Perseid Meteoroid Stream: Characterization of Recent Activity from Visual Observation', *Icarus* **124**, 414–428.

Brown, P., Ceplecha, Z., Hawkes, R. L., Wetherill, G., Beech, M., and Mossman, K.: 1994, 'The Orbit and Atmospheric Trajectory of the Peekskill Meteorite from Videorecords', *Nature* **367**, 624–626.

Brown, P., Hildebrand, A. R., Green, D. W. E., Page, D., Jacobs C., ReVelle, D. O., Tagliaferri, E., Wacker, J., and Wetmiller, B.: 1996, 'The Fall of the St. Robert Meteorite', *Meteorit. Planetary Sci.* **31**, 502–517 (also LA-UR-96-8, Los Alamos National Labs., U.S.A.).

Brown, P, Šimek, M., and Jones J.: 1997, 'Radar Observations of the Leonids 1964–1995', *Astron. Astrophys.* **322**, 687–695.

Budden, K. G.: 1985, *The Propagation of Radio Waves*, Cambridge University Press, Cambridge.

Burns, J. A., Lamy, P. L., and Soter, S.: 1979, 'Radiation Forces on Small Particles in the Solar System', *Icarus* **40**, 1–48.

Carusi, A., Kresák, L'., Perozzi, E., and Valsecchi, G. B.: 1985, *Long-Term Evolution of Short-Periods*, Hilger, Bristol.

Ceplecha, Z.: 1957, 'Photographic Geminids 1955', *Bull. Astron. Inst. Czech.* **8**, 51–61.

Ceplecha, Z.: 1958, 'On the Composition of Meteors', *Bull. Astron. Inst. Czech.* **9**, 154–159.

Ceplecha, Z.: 1959, 'On the Color Index of Meteors', *Bull. Astron. Inst. Czech.* **10**, 39.

Ceplecha, Z.: 1961a, 'Multiple Fall of Příbram Meteorites Photographed: Double-Station Photographs of the Fireball and Their Relations to the Found Meteorites', *Bull. Astron. Inst. Czech.* **12**, 21–47.

Ceplecha, Z.: 1961b, 'Determination of Wavelengths in Meteor Spectra by Using a Diffraction Grating', *Bull. Astron. Inst. Czech.* **12**, 246–250.

Ceplecha, Z.: 1964, 'Study of a Bright Meteor Flare by Means of Emission Curve of Growth', *Bull. Astron. Inst. Czech.* **15**, 102–112.

Ceplecha, Z.: 1965, 'Complete Data on Bright Meteor 32281', *Bull. Astron. Inst. Czech.* **16**, 88–101.

Ceplecha, Z.: 1967a, 'Classification of Meteor Orbits', *Smithsonian Contr. Astrophys.* **11**, 35–60.

Ceplecha, Z.: 1967b, 'Spectroscopic Analysis of Iron Meteoroid Radiation', *Bull. Astron. Inst. Czech.* **18**, 303–310.

Ceplecha, Z.: 1968, 'Discrete Levels of Meteor Beginning Heights', *Smithsonian Astrophys. Obs. Spec. Rep.* **279**, 1–54.

Ceplecha, Z.: 1971, 'Spectral Data on Terminal Flare and Wake of Double-Station Meteor No. 38421 (Ondřejov, April 21, 1963)', *Bull. Astron. Inst. Czech.* **22**, 219–304.

Ceplecha, Z.: 1973, in C. L. Hemenway, P. M. Millman, and A. F. Cook (eds.), 'Evidence from Spectra of Bright Fireballs', *Evolutionary and Physical Properties of Meteoroids*, *NASA SP* **319**, 89–102.

Ceplecha, Z.: 1976, in H. Elssäser and H. Fechtig (eds.), 'Fireballs as an Atmospheric Source of Meteoric Dust', *IAU Colloq.* **31**, *Lecture Notes in Physics* **48**, 385–388.

Ceplecha, Z.: 1977, in A. H. Delsemme (ed.), 'Meteoroid Populations and Orbits', *Comets, Asteroids, Meteorites: Interrelations, Evolution and Origins*, University Press, Toledo, pp. 143–152.

Ceplecha, Z.: 1979, 'Earth-Grazing Fireballs (The Daylight Fireball of August 10, 1972)', *Bull. Astron. Inst. Czech.* **30**, 349–356.

Ceplecha, Z.: 1980, in I. Halliday and B. A. McIntosh (eds.), 'Observational and Theoretical Aspects of Fireballs', *Solid Particles in the Solar System*, D. Reidel Publ. Co., Dordrecht, Holland, pp. 171–183.

Ceplecha, Z.: 1983, in C. I. Lagerkvist and H. Rickman (eds.), 'New Aspects in Classification of Meteoroids', *Asteroids, Comets, Meteors*, Astron. Obs. University, Uppsala, pp. 435–438.

Ceplecha, Z.: 1985, 'Fireball Information on Meteoroids and Meteorites', *Bull. Astron. Inst. Czech.* **36**, 237–241.

Ceplecha, Z.: 1986, in C.-I. Lagerkvist, B. A. Lindblad, H. Lundsted, and H. Rickman (eds.), 'Photographic Fireball Networks', *Asteroids, Comets, Meteors II*, Astron. Obs. University, Uppsala, pp. 575–582.

Ceplecha, Z.: 1987a, 'Geometric, Dynamic, Orbital, and Photometric Data on Meteoroids from Photographic Fireball Networks', *Bull. Astron. Inst. Czech.* **38**, 222–234.
Ceplecha, Z.: 1987b, in J. Kleczek (ed.), 'Atmospheric Trajectory of a Meteoroid', *Exercises in Astronomy*, D. Reidel Publ. Co., Dordrecht, Holland, pp. 57–63.
Ceplecha, Z.: 1988, 'Earth's Influx of Different Populations of Sporadic Meteoroids from Photographic and Television Data', *Bull. Astron. Inst. Czech.* **39**, 221–236.
Ceplecha, Z.: 1992, 'Influx of Interplanetary Bodies onto Earth', *Astron. Astrophys.* **263**, 361–366.
Ceplecha, Z.: 1994a, in A. Milani, M. DiMartino, and A. Celino (eds.), 'Meteoroid Properties from Photographic Records of Meteors and Fireballs', 'Asteroid, Comets, Meteors 1993', *IAU Symp.* **160**, 343–356.
Ceplecha, Z.: 1994b, 'Earth-Grazing Daylight Fireball of August 10, 1972', *Astron. Astrophys.* **283**, 287–288.
Ceplecha, Z.: 1996a, 'Luminous Efficiency Based on Photographic Observations of the Lost City Fireball and Implications for the Influx of Interplanetary Bodies onto Earth', *Astron. Astrophys.* **311**, 329–332.
Ceplecha, Z.: 1997, 'Influx of Large Meteoroids onto Earth', *Proc. SPIE* **3116**, 134–143.
Ceplecha, Z. and Borovička, J.: 1992, in D. Benest and C. Froeschle (eds.), 'Meteors', *Interrelations between Physics and Dynamics for Minor Bodies in the Solar System*, Frontières, Gif-sur-Yvette, pp. 309–367.
Ceplecha, Z. and McCrosky, R. E.: 1976, 'Fireball end Heights: a Diagnostic for the Structure of Meteoric Material', *J. Geophys. Res.* **81**, 6257–6275.
Ceplecha, Z. and McCrosky, R. E.: 1992, in A. W. Harris and E. Bowell (eds.), 'Fragmentation of Meteoroids and Bulk Density of Geminids from Photographic Fireball Records', *Asteroids, Comets, Meteors '96*, LPI, Houston, pp. 109–112.
Ceplecha, Z. and McCrosky, R. E.: 1997, 'Prairie Network Fireballs: Data on Height, Distance, and Brightness for Each Measured Time-Mark', *Meteorit. Planetary Sci.* **32**, A157–A158.
Ceplecha, Z. and Rajchl, J.: 1963, 'The Meteor Spectrum with Dispersion from 11 to 38 Å/mm', *Bull. Astron. Inst. Czech.* **14**, 29–49.
Ceplecha, Z. and Rajchl, J.: 1965, 'Program of Fireball Photography in Czechoslovakia', *Bull. Astron. Inst. Czech.* **16**, 15–22.
Ceplecha, Z., Jacobs, C., and Zaffery C.: 1997, in J. L. Remo (ed.), 'Correlation of Ground- and Space-Based Bolides', 'Near-Earth Objects. The United Nations International Conference', *Ann. New York Acad. Sci.* **822**, 145–154.
Ceplecha, Z., Spalding, R. E., Jacobs, C., and Tagliaferri, E.: 1996, 'Luminous Efficiencies of Bolides', *Proc. SPIE* **2813**, 46–56.
Ceplecha, Z., Spurný, P., Borovička, J., and Keclíková, J.: 1993, 'Atmospheric Fragmentation of Meteoroids', *Astron. Astrophys.* **279**, 615–626.
Cervera, M. A., Elford, W. G., and Steel, D. I.: 1997, 'A New Method for the Measurement of Meteor Speeds: the Pre-t_0 Phase Technique', *Radio Sci.* **32**, 805–816.
Clegg, J. A.: 1948, 'Determination of Meteor Radiants by Observation of Radio Echoes from Meteor Trails', *Phil. Mag.* **39**, 577–594.
Cook, A. F.: 1973, 'Working List of Meteor Streams', *NASA SP* **319**, 183–191.
Cook, A. F., Halliday, I., and Millman, P. M.: 1971, 'Photometric Analysis of Spectrograms of Two Perseid Meteors', *Can. J. Phys.* **49**, 1738–1749.
Cook, A. F., Flannery, M. R., Levy II, H., McCrosky, R. B., Sekanina, Z., Shao, C.-Y., Southworth, R. B., and Williams, J. T.: 1972, *Meteor Research Programs*, NASA CR-2109, Washington, pp. 1–166.
Cook, A. F., Hemenway, C. L., Millman P. M., and Swider, A.: 1973, in C. L. Hemenway, P. M. Millman, and A. F. Cook (eds.), 'An Unusual Meteor Spectrum', 'Evolutionary and Physical Properties of Meteoroids', *NASA SP* **319**, 153–159.
Cox, E. F.: 1958, 'Sound Propagation in Air', *Handbuch der Physik* **48**, 455–478.

Davies, J. G.: 1957, 'Radio Observation of Meteors', *Adv. Electronics Electron Phys.* **9**, 95–128.
Davies, J. G. and Gill, J. C.: 1960, 'Radio Echo Measurements of the Orbits of Faint Sporadic Meteors', *Monthly Notices Roy. Astron. Soc.* **121**, 437–462.
Davis, J., Greenhow, J. S., and Hall, J. E.: 1959, 'The Effect of Attachment on Radio Echo Observations of Meteors', *Proc. Roy. Soc.* **A253**, 130–139.
de Lignie, M., Jobse, K., and Schievink, R.: 1993, in D. Ocenas and P. Zimnikoval (eds.), 'Double-Station LLLTV Observations of the Geminid Meteor Stream', *Proceedings International Meteor Conference 1992*, IMO Publication, Antwerp, pp. 59–62.
Delsemme, A. H.: 1976, 'Can Comets be the Only Source of Interplantary Dust?', *Lecture Notes in Physics* **48**, 481–484.
Divine, N.: 1993, 'Five Populations of Interplanetary Meteoroids', *J. Geophys. Res.* **98**, 17 029–17 048.
Drummond, J. D.: 1982, 'Theoretical Meteor Radiants of Apollo, Amor and Aten Asteroids', *Icarus* **49**, 143–153.
Elford, W. G.: 1993, in J. Stohl and I. P. Williams (eds.), 'Radar Observations of Meteors', *Meteoroids and Their Parent Bodies*, Polygrafia SAV, Bratislava, pp. 235–244.
Elford, W. G. and Hawkins, G. S.: 1964, 'Meteor Echo Rates and the Flux of Sporadic Meteors', *Radio Meteor Project Res. Rep.* **9**, Harvard and Smithsonian Obs., Cambridge.
Elford, W. G., Hawkins, G. S., and Southworth, R. B.: 1964, 'The Distribution of Sporadic Meteor Radiants', *Radio Meteor Project Res. Rep.* **11**, 1–19, Harvard and Smithsonian Obs., Cambridge.
Elford, W. G., Cervera, M. A., and Steel, D. I.: 1994, 'Single Station Identification of Radar Meteor Shower Activity: the June Librids in 1992', *Monthly Notices Roy. Astron. Soc.* **270**, 401–408.
Elford, W. G., Cervera, M. A., and Steel, D. I.: 1995, 'Meteor Velocities: a New Look at an Old Problem', *Earth, Moon, Planets* **68**, 257–266.
Ellyett, C. D. and Davies, J. G.: 1948, 'Velocity of Meteors Measured by Diffraction of Radio Waves from Trails During Formation', *Nature* **161**, 596–597.
Ellyett, C. D. and Keay, C. S. L.: 1956, 'Radio Echo Observations of Meteor Activity in the Southern Hemisphere', *Australian J. Phys.* **9**, 471–480.
Embleton, T. F. W.: 1996, 'Tutorial on Sound Propagation Outdoors', *J. Acous. Soc. Am.* **100**, 31–48.
Emelyanenko, V. V.: 1990, 'Dynamics of the Lyrid Meteor Streams', *Astron. Vestnik* **24**, 308–313 (in Russian).
Eshelman, V. R.: 1955, 'Theory of Radio Reflections from Electron-Ion Clouds', *Inst. Radio Engrs. Trans. AP* **3**, 32–39.
Eshelman, V. R.: 1960, in D. H. Menzel (ed.), 'Meteor Scatter', *The Radio Noise Spectrum*, University Press, Harvard, Ch. 4.
Fedynski, V. V.: 1975, *Meteor Orbits and Rates from Equatorial Survey*, Vol. 1, World Data Center B, Moscow.
Fedynski, V. V.: 1977, *Meteor Orbits and Rates from Equatorial Survey*, Vol. 2, World Data Center B, Mosccow.
Fleagle, R. G. and Businger, J. A.: 1980, *An Introduction to Atmospheric Physics*, 2nd ed., Academic Press, New York, pp. 1–432.
Fleming, D. E. B., Hawkes, R. L., and Jones, J.: 1993, in J. Stohl and I. P. Williams (eds.), 'Light Curves of Faint Television Meteors', *Meteoroids and Their Parent Bodies*, Polygrafia SAV, Bratislava, pp. 261–265.
Forsyth, P. A., Vogan, E. L., Hansen, D. R., and Hines, C. O.: 1957, 'The Principles of JANET – a Meteor-Burst Communication System', *Proc. IRE* **45**, 1642–1657.
Friichtenicht, J. F., Slattery, J. C., and Tagliaferri, E.: 1968, 'A Laboratory Measurement of Meteor Luminous Efficiency', *Astrophys. J.* **151**, 747–758.
Gartrell, G. and Elford, W. G.: 1975, 'Southern Hemisphere Meteor Stream Determinations', *Australian J. Phys.* **28**, 591–620.

Gill, J. C. and Davies, J. G.: 1956, 'A Radio Echo Method of Meteor Orbit Determination', *Monthly Notices Roy. Astron. Soc.* **116**, 105–113.
Graf, Th., Marti, K., Xue, S., Herzog, G. F., Klein, J., Koslowski, V. T., Andrews, H. R., Cornett, R. J. J., Davies, W. G., Greiner, B. F., Imahori, Y., McKay, J. W., Milton, G. M., Milton, C. D., Metzler, K., Jull, A. J. T., Wacker, J. F., Herd, R., and Brown, P.: 1994, 'Size and Exposure History of the Peekskill Meteoroid', *Meteoritics* **29**, 469–470.
Greenhow, J. S.: 1952, 'A Radio-Method for the Investigation of Atmospheric Winds at Altitudes of 80 to 100 km', *J. Atmospheric Terrest. Phys.* **2**, 282–291.
Grün, E. and Zook, H. A.: 1980, in I. Halliday and B. A. McIntosh (eds.), 'Dynamics of Micrometeoroids in the Inner Solar System', *Solid Particles in the Solar System*, D. Reidel Publ. Co., Dordrecht, Holland, pp. 293–298.
Grün, E., Zook, H. A., Fechtig, H., and Giese, R. H.: 1985, 'Collisional Balance of the Meteoric Complex', *Icarus* **62**, 244–272.
Gustafson, B. A. S.: 1989, 'Comet Ejection and Dynamics of Nonspherical Dust Particles and Meteoroids', *Astrophys. J.* **337**, 945–949.
Gustafson, B. A. S. and Adolfsson, L. G.: 1996, 'Radiation Pressure Correction to Meteor Orbits', *Earth, Moon, Planets*, **72**, 327-332.
Guth, V.: 1947, 'On the Periodicity of the Lyrids', *Bull. Astron. Inst. Czech.* **1**, 1–4.
Hajdukova, M.: 1993, in J. Stohl and I. P. Williams (eds.), 'On the Hyperbolic and Interstellar Meteor Orbits', *Meteoroids and Their Parent Bodies*, Polygrafia SAV, Bratislava, pp. 61–64.
Hajduková, M.: 1994, 'On the Frequency of Interstellar Meteoroids', *Astron. Astrophys.* **288**, 330–334.
Halliday, I.: 1958, 'Meteor Spectroscopy with Transmission Diffraction Gratings', *J. Roy. Astron. Soc. Can.* **52**, 169–179.
Halliday, I.: 1960a, 'Auroral Green Line in Meteor Wakes', *Astrophys. J.* **131**, 25–33.
Halliday, I.: 1960b, 'The Spectrum of an Asteroidal Meteor Fragment', *Astrophys. J.* **132**, 482–485.
Halliday, I.: 1961, 'A Study of Spectral Line Identifications in Perseid Meteor Spectra', *Publ. Dominion Obs. Ottawa* **25**, 3–16.
Halliday, I.: 1968, in L'. Kresák and P. M. Millman (eds.), 'The Influence of Exposure Duration and Trail Orientation on Photographic Meteor Spectra', *Physics and Dynamics of Meteors*, D. Reidel Publ. Co., Dordrecht, Holland, pp. 91–104.
Halliday, I.: 1969, 'A Study of Ultraviolet Meteor Spectra', *Publ. Dominion Obs. Ottawa* **25**, 315–322.
Halliday, I.: 1988, 'Geminid Fireballs and the Peculiar Asteroid 3200 Phaethon', *Icarus* **76**, 279–294.
Halliday, I., Blackwell, A. T., and Griffin, A. A.: 1978, 'The Innisfree Meteorite and the Canadian Camera Network', *J. Roy. Astron. Soc. Can.* **72**, 15–39.
Halliday, I., Griffin, A. A., and Blackwell, A. T.: 1981, 'The Innisfree Meteorite Fall', *Meteoritics* **16**, 153–170.
Halliday, I., Blackwell, A. T., and Griffin, A. A.: 1984, 'The Frequency of Meteorite Falls on the Earth', *Science* **223**, 1405–1407.
Hapgood, M., Rothwell, P., and Royvrik, O.: 1982, 'Two-Station Television Observations of Perseid Meteors', *Monthly Notices Roy. Astron. Soc.* **201**, 569–577.
Harvey, G. A.: 1971, 'The Calcium H- and K-Line Anomaly in Meteor Spectra', *Astrophys. J.* **165**, 669–671.
Harvey, G. A.: 1973a, in C. L. Hemenway, P. M. Millman, and A. F. Cook (eds.), 'Spectral Analysis of Four Meteors', *Evolutionary and Physical Properties of Meteoroids*, *NASA SP* **319**, 103–129.
Harvey, G. A.: 1973b, in C. L. Hemenway, P. M. Millman, and A. F. Cook (eds.), 'NASA-LRC Faint Meteor Spectra', *Evolutionary and physical properties of meteoroids*, *NASA SP* **319**, 131–139.
Harvey, G. A.: 1973c, 'Elemental Abundance Determinations for Meteors by Spectroscopy', *J. Geophys. Res.* **78**, 3913–3926.
Harvey, G. A.: 1977, 'Air Radiation in Photographic Meteor Spectra', *J. Geophys. Res.* **82**, 15–22.

Hasegawa, I.: 1990, 'Predictions of a Meteor Radiant Point Associated with a Comet', *Publ. Astron. Soc. Japan* **42**, 175–186.
Hasegawa, I.: 1993, in J. Štohl and I. P. Williams (eds.), 'Historical Records of Meteor Showers', *Meteoroids and Their Parent Bodies*, Polygrafia SAV, Bratislava, pp. 209-223.
Hasegawa, I., Ueyama, Y., and Ohtsuka, K.: 1992, 'Prediction of the Meteor Radiant Point Associated with and Earth Approaching Minor Planet', *Publ. Astron. Soc. Japan* **44**, 45–54.
Hawkes, R. L.: 1993, in J. Štohl and I. P. Williams (eds.), 'Television Meteors', *Meteoroids and Their Parent Bodies*, Polygrafia SAV, Bratislava, pp. 227–234.
Hawkes, R. L. and Fleming, D. E. B.: 1995, 'TVZHR Profile of the 1991 Perseid Shower', *Earth, Moon, Planets* **68**, 303–310.
Hawkes, R. L. and Jones, J.: 1975, 'A Quantitive Model for the Ablation of Dustball Meteors', *Monthly Notices Roy. Astron. Soc.* **173**, 339–356.
Hawkes, R. L. and Jones, J.: 1986, 'Electro-Optical Meteor Observation Techniques and Results', *Quart. J. Roy. Astron. Soc.* **27**, 569–589.
Hawkes, R. L., Jones, J., and Ceplecha, Z.: 1984, 'The Populations and Orbits of Double-Station TV Meteors', *Bull. Astron. Inst. Czech.* **35**, 46–64.
Hawkes, R. L., Mason, K. I., Fleming, D. E. B., and Stultz, C. T.: 1993, in D. Ocenas and P. Zimnikoval (eds.), 'Analysis Procedures for Two Station Television Meteors', *Proceedings International Meteor Conference 1992*, IMO Publication, Antwerp, pp. 28–43.
Hawkins, G.S.: 1956, 'A Radio Echo Survey of Sporadic Meteor Radiants', *Monthly Notices Roy. Astron. Soc.* **116**, 92–104.
Hemenway, C. L., Swider, A., and Bowman, C.: 1971, 'Meteor Spectroscopy Using an Image Orthicon', *Can. J. Phys.* **49**, 1361–1364.
Herlofson, N.: 1948, 'The Theory of Meteor Ionization', *Rep. Prog. Phys.* **11**, 444–454.
Hey, J. S. and Stewart, G. S.: 1947, 'Radar Observations of Meteors', *Proc. Phys. Soc.* **59**, 858–883.
Hey, J. S., Parsons, S. J., and Stewart, G. S.: 1947, 'Radar Observations of the Giacobinid Meteor Shower', *Monthly Notices Roy. Astron. Soc.* **107**, 176–183.
Hildebrand, A. R., Brown, P., Wacker, J., Wetmiller, B., Page, D., Green, D. W. E., Jacobs, C., ReVelle, D. O., and Tagliaferri, E.: 1997, 'The St.-Robert Bolide of June 14, 1994', *J. Roy. Astron. Soc. Can.* **91**, 261–275.
Hills, J. G. and Goda, M. P.: 1993, 'The Fragmentation of Small Asteroids in the Atmosphere', *Astron. J.* **105**, 1114–1144.
Hoffmann, H. J., Fechtig, H., Grün, E., and Kissel, J.: 1975a, 'First Results of the Micrometeoroid Experiment S215 on HEOS 2 Satellite', *Planetary Space Sci.* **23**, 215–224.
Hoffmann, H. J., Fechtig, H., Grün, E., and Kissel, J.: 1975b, 'Temporal Fluctuations and Anisotropy of the Micrometeoroid Flux in the Earth-Moon System', *Planetary Space Sci.* **23**, 985–991.
Holton, J. R.: 1990, *An Introduction to Atmospheric Dynamics*, 3rd ed., Academic Press, New York, pp. 1–488.
Hoppe, J.: 1937, 'Die physikalische Vorgänge beim Eindringen meteorischer Körper in die Erdatmosphäre', *Astronomische Nachrichten* **262**, 169–198.
Hughes, D. W.: 1972, 'A Radar Determination of the Right Ascension and Declination of the Quadrantid Meteor Stream', *Monthly Notices Roy. Astron. Soc.* **155**, 395–402.
Hughes, D. W.: 1977, *Space Res.* **17**, 565.
Hughes, D. W.: 1978, in J. A. M. McDonnell (ed.), 'Meteors', *Cosmic Dust*, John Willey, Chichester, pp. 123–186.
Hughes, D. W.: 1986, in C.-I. Lagerkvist, B. A. Lindblad, H. Lundstedt, and H. Rickman (eds.), 'The Relation between Comets and Meteoroid Streams', *Asteroids, Comets, Meteors II*, Astron. Obs. University, Uppsala, pp. 503–519.
Humboldt, A.: 1802, *Relat. Hist.* **1**, 519.

Hunt, J., Fox, K., and Williams, I. P.: 1986, in C.-I. Lagerkvist, B.A. Lindblad, H. Lundstedt, and H. Rickman (eds.), 'Asteroidal Origin of the Geminid Meteor Stream', *Asteroids, Comets, Meteors II*, Astron. Obs. University, Uppsala, pp. 549–553.

Imoto, S. and Hasegawa, I.: 1958, 'Historical Records of Meteor Showers in China, Korea, and Japan', *Smithsonian Contr. Astrophys.* **2**, 131–144.

Jacchia L.G.: 1958, 'On Two Parameter Used in the Physical Theory of Meteors', *Smithsonian Contr. Astrpophys.* **2**, 181–187.

Jacchia, L. G. and Whipple, F. L.: 1961, 'Precision Orbits of 413 Photographic Meteors', *Smithsonian Contr. Astrophys.* **4**, 97–129.

Jacchia, L. G., Verniani, F., and Briggs, R. E.: 1965, 'An Analysis of the Atmospheric Trajectories of 413 Precisely Reduced Photographic Meteors', *Smithsonian Astrophys. Obs. Spec. Rep.* **175**.

Jenniskens, P.: 1984, 'Meteor Stream Activity', *Astrophys. J.* **287**, 990–1013.

Jenniskens, P.: 1994, 'Meteor Stream Activity I. The Annual Streams', *Astron. Astrophys.* **287**, 990–1013.

Jenniskens, P.: 1995, 'Meteor Stream Activity. II. Meteor Outbursts', *Astron. Astrophys.* **295**, 206–235.

Jenniskens, P.: 1996a, 'Meteor Stream Activity. III. Measurement of the First Series of Leonid Outbursts', *Meteoritics Planetary Sci.* **31**, 177–184.

Jenniskens, P.: 1996b, 'The First in a New Series of Leonid Outbursts', *IAU Colloq.* **150**; 'Physics, Chemistry, and Dynamics of Interplanetary Dust', *ASP Conf. Ser.* **104**, 117–120.

Jones, J.: 1977, 'Meteor Radiant Distribution Using Spherical Harmonic Analysis', *Bull. Astron. Inst. Czech.* **28**, 272–277.

Jones, J.: 1995, 'The Ejection of Meteoroids from Comets', *Monthly Notices Roy. Astron. Soc.* **275**, 773–780.

Jones, J. and Brown, P.: 1993, 'Sporadic Meteor Radiant Distributions: Orbital Survey Results', *Monthly Notices Roy. Astron. Soc.* **265**, 524–532.

Jones, J. and Brown, P.: 1994, 'The Radiant Distribution of Sporadic Meteors', *Planetary Space Sci.* **42**, 123–213.

Jones, J. and Jones, W.: 1991, 'Oblique-Scatter of Radio Waves from Meteor Trains: Full-Wave Calculations', *Planetary Space Sci.* **39**, 1289–1296.

Jones, J. and Kaiser, T. R.: 1966, 'The Effects of Thermal Radiation, Conduction and Meteoroid Heat Capacity on Meteoric Ablation', *Monthly Notices Roy. Astron. Soc.* **133**, 411–420.

Jones, J. and Morton, J. D.: 1977, 'The Determination of Meteor Stream Radiants from Single Station Observations', *Bull. Astron. Inst. Czech.* **28**, 267–272.

Jones, J. and Sarma, T.: 1985, 'Double-Station Observations of 454 TV Meteors II: Orbits', *Bull. Astron. Inst. Czech.* **36**, 103–115.

Jones, J. and Webster, A. R.: 1991, 'Visual and Radar Studies of Meteor Head Echoes', *Planetary Space Sci.* **39**, 873–878.

Jones, J., Sarma, T., and Ceplecha, Z.: 1985, 'Double-Station Observations of 454 TV Meteors III: Populations', *Bull. Astron. Inst. Czech.* **36**, 116–122.

Jones, J., McIntosh, B. A., and Šimek, M.: 1990, 'Ozone and the Duration of Overdense Radio Meteors', *J. Atmospheric Terrest. Phys.* **52**, 253–258.

Jones, W.: 1991, 'Theory of Diffusion of Meteor Trains in the Geomagnetic Field', *Planetary Space Sci.* **39**, 1283–1288.

Jones, W.: 1995, 'Theory of the Initial Radius of Meteor Trains', *Monthly Notices Roy. Astron. Soc.* **275**, 812–818.

Jones, W.: 1997, 'Theoretical and Observational Determinations of the Ionization Coefficient of Meteors', *Monthly Notices Roy. Astron. Soc.* **288**, 995–1003.

Jones, W. and Jones, J.: 1990, 'Oblique-Scattering of Radio Waves from Meteor Trains: Theory', *Planetary Space Sci.* **38**, 55–66.

Kaiser, T. R.: 1953, 'Radio Echo Studies of Meteor Ionization', *Phil. Mag. Suppl.* **2**, 495–544.

Kaiser, T. R.: 1955a, 'The Interpretation of Radio Echoes from Meteor Trails', *Spec. Suppl. J. Atmospheric Terrest. Phys.* **2**, 55–64.
Kaiser, T. R.: 1955b, 'The Incident Flux of Meteors and the Total Meteoric Ionization', *Spec. Suppl. J. Atmospheric Terrest. Phys.* **2**, 119–130.
Kaiser, T. R. and Closs, R. L.: 1952, 'Theory of Radio Reflections from Meteor Trails: I', *Phil. Mag.* **43**, 1–32.
Kaiser, T. R., Pickering, W. M., and Watkins, C. D.: 1969, 'Ambipolar Diffusion and Motion of Ion Clouds in the Earth's Magnetic Field', *Planetary Space Sci.* **17**, 519–552.
Kargel, J. S. and Lewis, J. S.: 1993, 'The Composition and Early Evolution of Earth', *Icarus* **105**, 1–25.
Kashcheev, B. L. and Lebedinets, V. N.: 1963, 'The Initial Radius of Ionized Meteor Trails', *Smithsonian Contr. Astrophys.* **7**, 19–22.
Kashcheev, B. L. and Lebedinets, V. N.: 1967, 'Radar Studies of Meteors', *Smithsonian Contr. Astrophys.* **11**, 183–199.
Kashcheev, B. L. and Tkachuk, A. A.: 1979, 'Raspredelenije orbit sporadicheskich meteorov po radionabljudenijam', *Meteor. Issled.* **6**, 41–49 (in Russian).
Kashcheev, B. L. and Tkachuk, A. A.: 1980, in *Results of Radar Observations of Faint Meteors: Catalogue of Meteor Orbits to +12m*, World Data Center B, Moscow.
Kashcheev, B. L., Lebedinets, V. N., and Lagutin, M. F.: 1967, *Meteoric Phenomena in the Earth's Atmosphere*, Nauka, Moscow, p. 260.
Keay, C. S. L.: 1957, 'Meteor Radiant Determination from High Echo-Rate Observations', *Australian J. Phys.* **10**, 471–482.
Keay, C. S. L.: 1963, 'The Annual Variation in the Radiant Distribution of Sporadic Meteors', *J. Atmospheric Terrest. Phys.* **25**, 507–513.
Keay, C. S. L.: 1980a, 'Anomalous Sounds from the Entry of Meteor-Fireballs', *Science* **210**, 11–15.
Keay, C. S. L.: 1980b, 'Audible Sounds Excited by Aurorae and Meteor-Fireballs', *J. Roy. Astron. Soc. Can.* **74**, 253–260.
Keay, C. S. L.: 1992, 'Electrophonic Sounds from Large Meteor-Fireballs', *Meteoritics* **27**, 144–148.
Keay, C. S. L.: 1993, in J. Štohl and I. P. Williams (eds.), 'Electrophonic Meteor-Fireballs Require Further Study', *Meteoroids and Their Parent Bodies*, Polygrafia SAV, Bratislava, pp. 315–318.
Kresák, Ľ.: 1968, in P. M. Millman and L. Kresák (eds.), 'Structure and Evolution of Meteor Streams', *Physics and Dynamics of Meteors*, D. Reidel Publ. Co., Dordrecht, Holland, pp. 391–403.
Kresák, Ľ.: 1976, 'Orbital Evolution of the Dust Streams Released from Comets', *Bull. Astron. Inst. Czech.* **27**, 35–46.
Kresák, Ľ.: 1978, 'The Comet and Asteroid Population of the Earth's Environment', *Bull. Astron. Inst. Czech.* **29**, 114–135.
Kresák, Ľ.: 1992, 'On the Ejection and Dispersion Velocities of Meteor Particles', *Contr. Astron. Obs. Skalnate Pleso* **22**, 123–130.
Kresák, Ľ.: 1993a, in J. Štohl and I. P. Williams (eds.), 'Meteor Storms', *Meteoroids and Their Parent Bodies*, Polygrafia SAV, Bratislava, pp. 147–156.
Kresák, Ľ.: 1993b, 'Cometary Dust Trails and Meteor Storms', *Astron. Astrophys.* **279**, 646–660.
Kronk, G. W.: 1988, *Meteor Showers. A Descriptive Catalog*, Enslow Publ., Hillside, p. 291.
Kulichkov, S. N.: 1992, 'Long-Range Propagation of Sound in the Atmosphere, A Review', *Izv. Atmospheric Ocean. Phys.* **28**, 253–269 (English translation).
Lebedinets, V. N.: 1968, in Ľ. Kresák and P. M. Millman (eds.), 'Radar Meteor Orbits', *Physics and Dynamics of Meteors*, D. Reidel Publ. Co., Dordrecht, Holland, pp. 241–264.
Lebedinets, V. N., Korpusov, V. N., and Sosnova, A. K.: 1973, 'Radar Studies of Meteoric Clusters', *Astron. Vestnik* **7**, 16–20 (in Russian).
Lebedinets, V. N., Korpusov, V. N., and Manokhina, A. V.: 1981, *Radio Meteor Investigations in Obnisk: Catalogue of Orbits* **1**, World Data Center B, Moscow.

Lebedinets, V. N., Korpusov, V. N., and Manokhina, A. V.: 1982, *Radio Meteor Investigations in Obnisk: Catalogue of Orbits* **2**, World Data Center B, Moscow.

Leinert, C. and Grün E.: 1989, in R. Schwenn and E. March (eds.), 'Interplanetary Dust', *Physics of the Inner Heliosphere*, Springer-Verlag, Heidelberg, pp. 207–260.

Levin (Lewin) B. J.: 1961, 'Physikalische Theorie der Meteore und die Meteorische Substanz im Sonnensystem', *Scientia Astronomica* **4**, Akademie Verlag, Berlin, pp. 1–330.

Lindblad, B. A.: 1974, in C. Cristescu, W. J. Klepczynski, and B. Milet (eds.), 'The System of Short Period Meteor Streams', *Asteroids, Comets, Meteoric Matter*, Bucuresti, pp. 269–281.

Lindblad, B. A.: 1991, in A. C. Levasseur-Regourd and H. Hasegawa (eds.), 'The IAU Meteor Data Center in Lund', *Origin and Evolution of Interplanetary Dust*, Kluwer Academic Publishers, Dordrecht, Holland, pp. 311-314.

Lindblad, B. A. and Porubčan, V.: 1992, in A. W. Harris and E. Bowell (eds.), 'Activity of the Lyrid Meteor Stream', *Asteroids, Comets, Meteors 1991*, LPI Press, Huston, pp. 367–371.

Lindblad, B. A. and Šimek, M.: 1986, in C.-I. Lagerkvist, B. A. Lindblad, H. Lundstead, and H. Rickman (eds.), 'The Activity Curve of the Perseid Meteor Stream from Onsala Radar Observations 1953–78', *Asteroids, Comets, Meteors II*, University Reprocentralen HSC, Uppsala, pp. 537–540.

Lindblad, B. A. and Steel, D.: 1994, in A. Milani, M. DiMartino, and A. Cellino (eds.), 'Meteoroid Orbits Available from the IAU Meteor Data Center', *in Asteroids, Comets, Meteors 1993*, Kluwer Academic Publishers, Dordrecht, Holland, pp. 497–501.

Lindblad, B. A., Ohtsuka, K., and Shirakawa, K.: 1994, 'The Orbit of the Eta Aquarid Meteor Stream', *Planetary Space Sci.* **42**, 113–116.

Lovell, A. C. B.: 1954, *Meteor Astronomy*, University Press, Oxford, pp. 21–30.

Love, S. G. and Brownlee, D. E.: 1991, 'Heating and Thermal Transformation of Micrometeoroids Entering the Earth's Atmosphere', *Icarus* **89**, 26–43.

Love, S. G. and Brownlee, D. E.: 1993, 'A Direct Measurement of the Terrestrial Mass Accretion Rate of Cosmic Dust', *Science* **262**, 550–553.

Mainstone, J. S.: 1960, 'The Calculation of Meteor Velocities from Continuous-Wave Radio Diffraction Effects from Trails', *Monthly Notices Roy. Astron. Soc.* **120**, 517–529.

Manning, L. A.: 1948, *J. Appl. Phys.* **19**, 689.

Manning, L. A., Villard, O. G., and Peterson, A. M.: 1949, 'Radio Doppler Investigation of Meteoric Heights and Velocities', *J. Appl. Phys.* **20**, 475–479.

Mason, E. A. and McDaniel, E. W.: 1988, *Transport Properties of Ions in Gases*, Wiley, London.

Massey, H. S. W. and Sida, D. W.: 1955, 'Collision Processes in Meteor Trails', *Phil. Mag.* **46**, 190–198.

Massey, H. S. W.: 1982, in H. S. W. Massey and D. R. Bates (eds.), 'Meteor Ionization', *Appl. Atomic Collision Phys.* **1**, Academic Press, New York, pp. 135–148.

McCord, T. B., Morris, J., Persing, D., Tagliaferri, E., Jacobs, C., Spalding, R. E., Grady, L., and Schmidt, R.: 1995, 'Detection of a Meteoroid Entry into the Earth's Atmosphere on February 1, 1994', *J. Geophys. Res.* **100**, 3245–3249.

McCrosky, R. E. and Posen, A.: 1961, 'Orbital Elements of Photographic Meteors', *Smithsonian Contr. Astrophys.* **4**, 15–84.

McCrosky, R. E. and Soberman, R. K.: 1963, 'Results from an Artificial Iron Meteoroid at 10 km/s', *Smithsonian Contr. Astrophys.* **7**, 199–208.

McCrosky, R. E., Posen, A., Schwartz, G., and Shao, C.-Y.: 1971, 'Lost City Meteorite – Its Recovery and a Comparison with Other Fireballs', *J. Geophys. Res.* **76**, 4090–4108.

McCrosky, R. E., Shao, C.-Y., and Posen, A.: 1976, 'Prairie Network Fireball Data I: Summary and Orbits', *Center Astrophys. Prepr. Ser.* **665**.

McCrosky, R. E., Shao, C.-Y., and Posen, A.: 1977, 'Prairie Network Fireball Data II: Trajectories and Light Curves', *Center Astrophys. Prepr. Ser.* **721**.

McIntosh, B. A.: 1962, 'The Meteoric Head Echo', *J. Atmospheric Terrest. Phys.* **24**, 311–315.

McIntosh, B. A.: 1963, 'Experimental Study of the Amplitude of Radar Meteor-Head Echoes', *Can. J. Phys.* **41**, 355–371.
McIntosh, B. A.: 1970, 'On the End Point of Fireballs', *J. Roy. Astron. Soc. Can.* **64**, 267–281.
McIntosh, B. A.: 1990, 'Comet P/Machholz and the Quadrantid Meteor Stream', *Icarus* **86**, 299.
McIntosh, B. A.: 1991, in R. L. Newburn, J. M. Neugebauer, and J. Rahe (eds.), 'Debris from Comets: the Evolution of Meteor Streams', *The Post Halley Era*, Kluwer Academic Publishers, Dordrecht, Holland, pp. 557–591.
McIntosh, B. A. and Hajduk, A.: 1983, 'Comet Halley Meteor Stream: a New Model', *Monthly Notices Roy. Astron. Soc.* **205**, 931–943.
McKinley, D. W. R.: 1951, 'Meteor Velocities Determined by Radio Observations', *Astrophys. J.* **113**, 225–267.
McKinley, D. W. R.: 1961, *Meteor Science and Engineering*, McGraw Hill, New York, pp. 1–309.
McKinley, D. W. R. and Millman, P. M.: 1949, 'Determination and Elements of Meteor Paths from Radar Observations', *Can. J. Res.* **31**, 171–181.
Meisel, D. D., Getman, V. S., Mathews, J. D., Jacobs, S. C., and Roper, R. G.: 1995, 'Bolide AIDA: Death of an Aubrite Meteoroid', *Icarus* **116**, 227–254.
Millman, P. M.: 1970, 'Meteor News', *J. Roy. Astron. Soc. Can.* **64**, 57–59.
Millman, P. M.: 1972, 'Giacobinid Meteor Spectra', *J. Roy. Astron. Soc. Can.* **66**, 201–211.
Millman, P. M.: 1980, in I. Halliday and B. A. McIntosh (eds.), 'One Hundred and Fifteen Years of Meteor Spectroscopy', *IAU Symp.* **90**, 121–128.
Millman, P. M. and Clifton, K. S.: 1975, 'SEC Vidicon Spectra of Geminid Meteors, 1972', *Can. J. Phys.* **53**, 1939–1947.
Millman, P. M. and Clifton, K. S.: 1979, 'Video Techniques in Comet-Debris Studies', *Sky Telesc.* **57**, 21–23.
Millman, P. M. and Halliday, I.: 1961, 'The Near-Infrared Spectrum of Meteors', *Planetary Space Sci.* **5**, 137–140.
Millman, P. M. and McKinley, D. W. R.: 1963, in B. M. Middlehurst and G. P. Kuiper (eds.), 'Meteors', *The Moon, Meteorites, and Comets*, University Press, Chicago, pp. 674–773.
Millman, P. M., Cook, A. F., and Hemenway, C. L.: 1971, 'Spectroscopy of Perseid Meteors with an Image Orthicon', *Can. J. Phys.* **49**, 1365–1373.
Moore, C. E.: 1945, 'A Multiplet Table of Astrophysical Interest', *Contr. Princeton Univ. Obs.* **20**.
Morton, J. D. and Jones, J.: 1982, 'A Method for Imaging Radio Meteor Radiant Distributions', *Monthly Notices Roy. Astron. Soc.* **198**, 737–746.
Mukhamednazarov, S. and Mal'tseva, N. V.: 1989, 'Study of Television Spectrograms of Meteors', *Solar Sys. Res.* **23**, 179–183.
Nagasawa, K.: 1978, 'Analysis of Spectra of Leonid Meteors', *Ann. Tokyo Astron. Obs., 2nd ser.* **16**, 157–187.
Nakamura, T., Tsuda, T., Tsutaumi, T., Kita, K., Uehara, T., Kato, S., and Fukao, S.: 1991, 'Meteor Wind Observations with the MU Radar', *Radio Sci.* **26**, 857–869.
Nauman, R. J.: 1966, 'The Near Earth Meteoroid Environment', *NASA TND* **3717**.
Nemtchinov, I. V., Popova, O. P., Shuvalov, V. V., and Svetsov, V. V.: 1994, 'Radiation Emitted During the Flight of Asteroids and Comets through the Atmosphere', *Planetary Space Sci.* **42**, 491–506.
Nemtchinov, I. V., Popova, O. P., Svetsov, V. V., and Shuvalov, V. V.: 1995, 'On Photometric Masses and Radiation Sizes of Large Meteoroids', *Astron. Vestnik* **29**, 155–173.
Nilsson, C. S.: 1964, 'A Southern Hemisphere Radio Survey of Meteor Streams', *Australian J. Phys.* **17**, 205–256.
Olivier, C. P.: 1925, *Meteors*, Williams and Wilkins, Baltimore, p. 276.
Olsson-Steel, D.: 1986, 'The Origin of the Sporadic Meteoroid Complex', *Monthly Notices Roy. Astron. Soc.* **219**, 47–73.

Olsson-Steel, D.: 1988, 'Identification of Meteoroid Streams from Apollo Asteroids in the Radar Orbit Surveys', *Icarus* **75**, 64–94.
Öpik, E. J.: 1933, 'Atomic Collisions and Radiation of Meteors', *Acta Comment. Univ. Tartu* **26**, 1–39.
Öpik, E. J.: 1937, 'Basis of the Physical Theory of Meteors', *Acta Comment. Univ. Tartu* **33**, 1–66.
Öpik, E.J.: 1941, 'Observations of Meteor Velocities 1931–1938', *Publ. Astron. Obs. Tartu* **30**.
Öpik, E. J.: 1955, 'Meteor Radiation. Ionization and Atomic Luminous Efficiency', *Proc. Roy. Soc.* **A230**, 463–501.
Öpik, E. J.: 1956, 'Concluding Remarks from the Arizona Expedition for the Study of Meteors', *Irish Astron. J.* **4**, 49–59.
Öpik, E. J.: 1958, *Physics of Meteor Flight in the Atmosphere*, Interscience, New York, pp. 1–179.
Öpik, E. J.: 1963, 'Tables of Meteor Luminosities', *Irish Astron. J.* **6**, 3–11 and 93–112.
Öpik, E. J.: 1970, 'The Sonic Boom of the Boveedy Meteorite', *Irish Astron. J.* **9**, 308–310.
Park, F. R. and McIntosh, B. A.: 1967, 'A Bright Fireball Observed Photographically, by Radar and Visually'. *J. Roy. Astron. Soc. Can.* **61**, 25–39.
Pecina, P. and Ceplecha, Z.: 1983, 'New Aspects in Single-Body Meteor Physics', *Bull. Astron. Inst. Czech.* **34**, 102–121.
Pecina, P. and Ceplecha, Z.: 1984, 'Importance of Atmospheric Models for Interpretations of Photographic Fireball Data', *Bull. Astron. Inst. Czech.* **35**, 120–123.
Peregudov, F. I.: 1958, 'On the Effect of Meteor Velocities on the Hour Number in Radio-Echo Detection of Meteors', *Soviet Astron.* **2**, 833–838.
Piers, P. A. and Hawkes, R. L.: 1993, 'An Unusual Meteor Cluster Observed by Image-Intensified Video', *WGN: J. Int. Met. Org.* **21**, 168–174.
Plavcová, Z. and Šimek, M.: 1960, 'Meteor Radar of the Ondřejov Observatory', *Bull. Astron. Inst. Czech.* **11**, 228–231.
Plavec, M.: 1957, 'On the Origin and Early Stages of the Meteor Streams', *Publ. Astron. Inst. Czech. Acad. Sci.* **30**.
Poole, L. and Kaiser, T. R.: 1972, 'The Detection of Shower Structure in Sporadic Meteor Background', *Monthly Notices Roy. Astron. Soc.* **156**, 283–290.
Poole, L. M. G. and Roux, D. G.: 1989, 'Meteor Radiant Mapping with an All-Sky Radar', *Monthly Notices Roy. Astron. Soc.* **236**, 645–652.
Porter, J. G.: 1952, *Comets and Meteor Streams*, Chapman and Hall, London, p. 123.
Porubčan, V. and Gavajdová, M.: 1994, 'A Search for Fireball Streams Among Photographic Meteors', *Planetary Space Sci.* **42**, 151-155.
Porubčan, V., Štohl, J., and Svoreň, J.: 1982, 'On the Origin of the 1982 Lyrids Burst', *Contr. Astron. Obs. Skalnaté Pleso* **22**, 25–31.
Porubčan, V., Šimek, M., and McIntosh, B. A.: 1989, 'Lyrid Meteor Stream: Long-Term Activity Profile', *Bull. Astron. Inst. Czech.* **40**, 298–302.
Poulter, E. M. and Baggaley, W. J.: 1977, 'Radiowave Scattering from Meteoric Ionization', *J. Atmospheric Terrest. Phys.* **39**, 757–768.
Poulter, E. M. and Baggaley, W. J.: 1978, 'The Application of Radio-Wave Scattering Theory to Radio-Meteor Observations', *Planetary Space Sci.* **26**, 969–977.
Pravec, P.: 1992, 'Telescopic Observations of the 1991 Perseids in Czechoslovakia', *WGN: J. Int. Met. Org.* **20**, 46–49.
Pravec, P. and Boček, J.: 1992, 'Precision of Telescopic Meteor Recordings', *WGN: J. Int. Met. Org.* **20**, 70–83.
Rabinowitz D. L.: 1993, 'The Size Distribution of the Earth-Approaching Asteroids', *Astrophys. J.* **407**, 412–427.
Rabinowitz, D. L.: 1994, 'The Size and Shape of the Near-Earth Asteroid Belt', *Icarus* **111**, 364–377.

Rabinowitz, D. L.: 1996, in T. W. Rettig and J. M. Hahn (eds.), 'Observations Constraining the Origins of Earth-Approaching Asteroids', 'Completing the Inventory of the Solar System', *ASP Conf. Ser.* **107**, 13–28.

Rabinowitz, D. L., Gehrels, T., Scotti, J. V., McMillan, R. S., Perry, M. L., Winslewski, W., Larson, S. M., Howel, E. S., and Mueller, B. E. A.: 1993, 'Evidence for a Near-Earth Asteroid Belt', *Nature* **363**, 704–706.

ReVelle, D. O.: 1975, 'Studies of Sounds from Meteors', *Sky Telesc.* **49**, 87–91.

ReVelle, D. O.: 1976, 'On Meteor-Generated Infrasound', *J. Geophys. Res.* **81**, 1217–1230.

ReVelle, D. O.: 1979, 'A Quasi-Simple Ablation Model for Large Meteorite Entry: Theory versus Observations', *J. Atmospheric Terrest. Phys.* **41**, 453–473.

ReVelle, D. O.: 1980a, in I. Halliday and B. A. McIntosh (eds.), 'Interaction of Large Bodies with the Earth's Atmosphere', *Solid Particles in the Solar System*, D. Reidel Publ. Co., Dordrecht, Holland, pp. 185–198.

ReVelle, D. O.: 1980b, 'A Predictive Macroscopic Integral Radiation Efficiency Model', *J. Geophys. Res.* **85**, 1803–1808.

ReVelle D. O.: 1983, 'The Role of Porosity in Modeling the Dynamics, Ablation, and Luminosity of Fireballs', *Meteoritics* **18**, 386.

ReVelle, D. O.: 1993, in J. Štohl and I. P. Williams (eds.), 'The Meteoroid/Atmosphere Interaction Spectrum', *Meteoroids and Their Parent Bodies*, Polygrafia SAV, Bratislava, pp. 343–346.

ReVelle, D. O.: 1995, 'Historical Detection of Atmospheric Impacts by Large Bolides Using Acoustic-Gravity Waves', *LA-UR-95-1263*, National Laboratory, Los Alamos, pp. 1–26.

ReVelle, D. O.: 1997, in J. Remo (ed.), 'Historical Detection of Atmospheric Impacts by Large Bolides Using Acoustic-Gravity Waves', 'Near-Earth Objects', *Ann. New York Acad. Sci.* **822**, 284–302 (also available as *LA-UR-95-1263*, National Laboratory, Los Alamos, p. 26).

ReVelle, D. O. and Ceplecha, Z.: 1994, 'Analysis of Identified Iron Meteoroids: Possible Relations with M-type Earth-crossing Asteroids?', *Astron. Astrophys.* **292**, 330–336.

ReVelle, D. O. and Rajan R. S.: 1979, 'On the Luminous Efficiency of Meteoritic Fireballs', *J. Geophys. Res.* **84**, 6255–6262.

ReVelle, D. O. and Whitaker, R. W.: 1995, in M. Boslough (ed.), 'Acoustic Efficiency Analysis Using Infrasound from NEOs', *Proceedings of Comet Day II*, Space96, Albuquerque, New Mexico (June 1–6, 1996) (also available as *LA-UR-95-4121*, National Laboratory, Los Alamos, 9 pp.).

ReVelle, D. O. and Whitaker, R. W.: 1996a, 'Detection of Large Meteoroid/NEO Flux Using Infrasound: Recent Detection of the November 21, 1995 Colorado Fireball', *Proc. SPIE* **2813**, 57–68 (also available as *LA-UR-96-2236*, National Laboratory, Los Alamos, p. 12).

ReVelle, D. O. and Whitaker, R. W.: 1996b, in D. Juve, H. E. Bass, and K. Attenborough (eds.), 'Lamb Waves from Airborne Explosion Sources: Viscous Effects and Comparisons to Ducted Acoustic Arrivals', *Proceedings of the 7th Symposium on Long-Range Sound Propagation*, Ecole Centrale de Lyon, Ecully, France, pp. 323–337 (also available as *LA-UR-96-3594*, National Laboratory, Los Alamos, p. 15).

ReVelle, D. O., Whitaker, R. W., and Armstrong, W. T.: 1997, 'Infrasonic Observations of Bolides on October 4, 1996', *Proc. SPIE* **3116**, 156–167 (also available as *LA-UR-97-2481*, National Laboratory, Los Alamos, p. 12).

Robertson, M. C. and Hawkes, R. L.: 1992, in A. W. Harris and E. Bowell (eds.), 'Wake in Faint Television Meteors', *Asteroids, Comets, Meteors 1991*, LPI, Huston, pp. 517–520.

Sarma, T. and Jones, J.: 1985, 'Double Station Observations of 454 TV meteors: I. Trajectories', *Bull. Astron. Inst. Czech.* **36**, 9–24.

Savage, H. F. and Boitnott, C. A.: 1973, in C. L. Hemenway, P. M. Millman, and A. F. Cook (eds.), 'Laboratory Determinations of the Luminous Efficiency of Meteor Constituents', 'Evolutionary and Physical Properties of Meteoroids', *NASA SP* **319**, 83–87.

Schafer, J. P. and Goodall, W. M.: 1932, 'Observations of the Kennelly-Heaviside Layer During the Leonid Meteor Shower of November 1931', *Proc. IRE* **20**, 1941–1945.

Schneider, W.: 1974, 'Radiation Gas Dynamics of Planetary Entry', *Astron. Acta* **18**, 193–213.
Sekanina, Z.: 1973, 'Statistical Model of Meteor Stream III', *Icarus* **18**, 253–284.
Sekanina, Z.: 1976, 'Statistical Model of Meteor Stream IV', *Icarus* **27**, 265–321.
Sekanina Z.: 1983, 'The Tunguska Event: No Cometary Signature in Evidence', *Astron. J.* **88**, 1382–1484.
Shadbolt, L. and Hawkes, R. L.: 1995, 'Absence of Wake in Faint Television Meteors', *Earth, Moon, Planets* **68**, 493–502.
Shoemaker, E. M., Wolfe, R. F., and Shoemaker, C. S.: 1990, in V. L. Sharpton and P. D. Ward (eds.), 'Asteroid and Comet Flux in the Neighborhood of Earth', *Global Catastrophes in Earth History*, Geological Soc. of America, pp. 155–170.
Sida, D. W.: 1969, 'The Production of Ions and Electrons by Meteoric Processes', *Monthly Notices Roy Astron. Soc.* **143**, 37–47.
Šimek M. and McIntosh, B. A.: 1986, 'Perseid Meteor Stream: Mean Flux Curve from Radar Observations', *Bull. Astron. Inst. Czech.* **37**, 146–155.
Šimek M. and McIntosh, B. A.: 1989, 'Geminid Meteor Stream: Activity as a Function of Particle Size', *Bull. Astron. Inst. Czech.* **40**, 288–298.
Šimek, M. and McIntosh, B. A.: 1991, 'Cross Section of the Quadrantid Meteor Stream', *Bull. Astron. Inst. Czech.* **42**, 124–132.
Skellett, A. M.: 1931, 'The Effect of Meteors on Radio Transmission through the Kennelly-Heaviside Layer', *Phys. Rev.* **37**, 1668.
Skellett, A. M.: 1935, 'The Ionizing Effects of Meteors', *Proc. IRE* **23**, 132–149.
Southworth, R. B. and Hawkins, G. S.: 1963, 'Statistics of Meteor Streams', *Smithsonian Contr. Astrophys.* **7**, 261–285.
Spurný, P.: 1997, 'Photographic Monitoring of Fireballs in Central Europe', *Proc. SPIE* **3116**, 144–155.
Stauffer, J. and Spinrad, H.: 1978, 'The Spectrum of a Bright Meteor Obtained with the Wampler Scanner', *Publ. Astron. Soc. Pacific* **90**, 222–225.
Steel, D. I.: 1994, in A. Milani, M. DiMartino, and A. Cellino (eds.), 'Meteoroid Streams', *Asteroids, Comets, Meteors 1993*, Kluwer Academic Publishers, Dordrecht, Holland, pp. 111–126.
Steel, D. I.: 1996, 'Meteoroid Orbits', *Space Sci. Rev.* **78**, 507–553.
Steel, D. I. and Elford, W. G.: 1991, 'The Height Distribution of Radio Meteors: Comparison of Observations at Different Frequencies on the Basis of Standard Echo Theory', *J. Atmospheric Terrest. Phys.* **53**, 409–417.
Steel, D. I., Asher, D. J., and Clube, S. V. M.: 1991, 'The Structure and Evolution of the Taurid Complex', *Monthly Notices Roy. Astron. Soc.* **251**, 632–648.
Štohl, J.: 1968, in P. M. Millman and L'.Kresák (eds.), 'Seasonal Variation of the Radiant Distribution of Meteors', *Physics and Dynamics of Meteors*, D. Reidel Publ. Co., Dordrecht, Holland, pp. 298-303.
Štohl, J.: 1970, 'On the Problem of Hyperbolic Meteors', *Bull. Astron. Inst. Czech.* **21**, 10–17.
Štohl, J.: 1983, in C.-I. Lagerkvist and H. Rickman (eds.), 'On the Distribution of Sporadic Meteor Orbits', *Asteroids, Comets, Meteors*, Astron. Obs. University, Uppsala, pp. 419–424.
Štohl, J.: 1986, in C.-I. Lagerkvist, B. A. Lindblad, H. Lundstedt, and H. Rickman (eds.), 'The Distribution of Sporadic Meteor Radiants and Orbits', *Asteroids, Comets, Meteors*, Astron. Obs. University, Uppsala, pp. 565–574.
Štohl, J. and Porubčan, V.: 1992, in E. Ferraz-Mello (ed.), 'Dynamical Aspects of the Taurid Meteor Complex', *Chaos, Resonance and Collective Phenomena in the Solar System*, Kluwer Academic Publishers, Dordrecht, Holland, pp. 315–324.
Štohl, J. and Porubčan, V.: 1993, in J. Štohl and I. P. Williams (eds.), 'Meteor Streams of Asteroidal Origin', *Meteoroids and Their Parent Bodies*, Polygrafia SAV, Bratislava, pp. 41–47.
Suzuki, K., Akebo, T., Suzuki, S., Yoshida, T., and Ohtsuka, K.: 1993, 'Orbits of TV η–Aquarid Meteors Obtained in 1988', *WGN: J. Int. Met. Org.* **21**, 214–215.

Svoreň, J., Neslušan, L., and Porubčan, V.: 1994, 'Applicability of Meteor Radiant Determination Methods Depending on Orbit Type', *Contr. Astron. Obs. Skalnaté Pleso* **24**, 5–18.

Tagliaferri, E., Spalding, R., Jacobs, C., Worden, S. P., and Erlich, A.: 1994, in T. Gehrels (ed.), 'Detection of Meteoroid Impacts by Optical Sensors in Earth Orbit', *Hazards Due to Comets and Asteroids*, University of Arizona Press, Tucson, pp. 199–220.

Taylor, A. D.: 1995, 'The Harvard Radio Meteor Project: Meteor Velocity Distribution Reappraised', *Icarus* **116**, 154–158.

Taylor, A. D.: 1996, 'Earth Encounter Velocities for Interplanetary Meteoroids', *Adv. Space Res.* **17**, 205–209.

Taylor, A. D. and Elford, W. G.: 1998, 'Aspects of the Terrestrial Influx of Small Meteoroids', *IAU Meeting 1997*, Kyoto, Japan (in press).

Taylor, A. D., Baggaley, W. J., Bennett, R. G. T., and Steel, D. I.: 1994, 'Radar Measurements of Very High Velocity Meteors with AMOR', *Planetary Space Sci.* **42**, 135–140.

Taylor, A. D., Cervera, M. A., Elford, W. G., and Steel, D. I.: 1996a, in Bo A. Gustafson and M. Hanner (eds.), 'A New Technique for Radar Meteor Speed Determination: Inter-Pulse Phase Changes from Head Echoes', *IAU Colloq.* **150**; 'Physics, Chemistry, and Dynamics of Interplanetary Dust', *ASP Conf. Ser.* **104**, 75–78.

Taylor, A. D., Baggaley, W. J., and Steel, D. I.: 1996b, 'Discovery of Interstellar Dust Entering the Earth's Atmosphere', *Nature* **380**, 323–325.

Tkachuk, A. A.: 1978, 'Raspredelenije plotnosti sporadicheskich meteornych tel', *Meteorn. Issled.* **5**, 67–73 (in Russian).

Ueda, M. and Fujiwara, Y.: 1993, 'TV Observations of the 1991 Geminid Meteor Shower', *WGN: J. Int. Met. Org.* **21**, 215–217.

Ueda, M. and Fujiwara, Y.: 1995, 'Television Meteor Radiant Mapping', *Earth, Moon, Planets* **68**, 585–603.

Verniani, F.: 1965, 'On Luminous Efficiency of Meteors', *Smithsonian Contr. Astrophys.* **8**, 141–171.

Verniani, F.: 1967, 'Meteor Masses and Luminosity', *Smithsonian Contr. Astrophys.* **10**, 181–195.

Verniani, F. and Hawkins, G. S.: 1965, 'Masses, Magnitudes, and Densities of 320 Radio Meteors', *Radio Meteor Project* **12**, 1–35, Harvard and Smithsonian Obs., Cambridge.

Weiss, A. A.: 1955, 'Radio Echo Observations of Meteors in the Southern Hemisphere', *Australian J. Phys.* **8**, 148–166.

Weston, D. E. and Rowlands, P. B.: 1979, 'Guided Acoustic Waves in the Ocean', *Rep. Prog. Phys.* **42**, 347–387.

Wetherill, G. W.: 1985, 'Asteroidal Source of Ordinary Chondrites', *Meteoritics* **20**, 1–22.

Wetherill, G. W. and ReVelle, D. O.: 1981a, 'Which Fireballs Are Meteorites? A Study of the Prairie Network Photographic Meteor Data', *Icarus* **48**, 308–328.

Wetherill, G. W. and ReVelle, D. O.: 1981b, in L. Wilkening (ed.), 'Relationship between Comets, Large Meteors and Meteorites', *Comets*, University of Arizona Press, Tucson, pp. 297–319.

Whipple, F. L.: 1938, 'Photographic Meteor Studies I', *Proc. Amer. Phil. Soc.* **79**, 499–548.

Whipple, F. L.: 1950, 'A Comet Model I', *Astrophys. J.* **111**, 375–394.

Whipple, F. L.: 1951, 'A Comet Model II', *Astrophys. J.* **113**, 464–474.

Whipple, F. L.: 1954, 'Photographic Meteor Orbits and Their Distribution in Space', *Astron. J.* **59**, 201–217.

Whipple, F. L.: 1983, *IAU Circ.* **3881**.

Whipple, F. L. and Hamid, S. E.: 1952, 'On the Origin of the Taurid Meteor Streams', Harvard Reprint 321, p. 30.

Whipple, F. L. and Jacchia, L. G.: 1957, 'Reduction Methods for Photographic Meteor Trails', *Smithsonian Contr. Astrophys.* **1**, 183–206.

Williams, I. P.: 1992, in E. Ferraz-Mello (ed.), *Chaos, Resonance and Collective Phenomena in the Solar System*, Kluwer Acadmic Publishers, Dordrecht, Holland, p. 299.

Williams, I. P.: 1993, in J. Štohl and I. P. Williams (eds.), 'The Dynamics of Meteoroid Streams', *Meteoroids and Their Parent Bodies*, Polygrafia SAV, Bratislava, pp. 31–40.

Williams, I. P.: 1995, 'Meteoroid Streams and the Sporadic Background', *Earth, Moon, Planets* **68**, 1–12.

Woodworth, S. and Hawkes, R. L.: 1996, in Bo A. Gustafson and M. Hanner (eds.), 'Optical Search for High Meteors in Hyperbolic Orbits', *IAU Symp.* **150**; 'Physics, Chemistry, and Dynamics of Interplanetary Dust', *ASP Conf. Ser.* **104**, 83–86.

Wu, Z. and Williams, I. P.: 1993, 'The Perseid Meteor Shower at the Current Time', *Monthly Notices Roy. Astron. Soc.* **264**, 980–990.

Wyatt, S. P. and Whipple, F. L.: 1950, 'The Poynting-Robertson Effect on Meteor Orbits', *Astrophys. J.* **111**, 134–141.

Wylie, C. C.: 1932, 'Sounds from Meteors', *Pop. Astron.* **40**, 289–294.

Yeomans, D. K., Kevin, K. Y., and Weissman, P. R.: 1996, 'The Impending Appearance of Comet Tempel-Tuttle and the Leonid Meteors', *Icarus* **124**, 407–413.

Zhou, Q., Tepley, C. A., and Sulzer, M. P.: 1995, 'Meteor Observations by the Arecibo 430 MHz Incoherent Scatter Radar – I. Results from Time-Integrated Observations', *J. Atmospheric Terrest. Phys.* **57**, 421–431.

Znojil, V., Grygar, J., Mikulášek, Z., Šimek, M., and Šulc, M.: 1980, 'The Relation between Meteor Optical Brightness and the Properties of the Ionized Trail I', *Bull. Astron. Inst. Czech.* **31**, 14–25.

Znojil, V., Šimek, M., Grygar, J., and Hollan, J.: 1981, 'The Relation between Meteor Optical Brightness and the Properties of the Ionized Trail II', *Bull. Astron. Inst. Czech.* **32**, 1–19.

Znojil, V., Hollan, J., and Šimek, M.: 1987, 'The Relation between Meteor Optical Brightness and the Properties of the Ionized Trail III', *Bull. Astron. Inst. Czech.* **36**, 44–56.